The development of novel PVA hydrogel for biomedical and drug delivery applications

A thesis submitted to complete a degree of

PhD in Polymer Engineering

by

Bor Shin Chee

Based on the research carried out under the supervision

of

Dr. Michael Nugent

Submitted to the Athlone Institute of Technology,08/2021

Declaration

I hereby declare that this thesis submitted to the higher education and training awards council for doctoral degree of Science by research, is a result of my own work and has not in the same or altered form, been presented to this institute or any other institute in support for any degree, other than for which I am now a candidate. The contents in literature review contained works that I have published in my book chapters. The work discussed in Chapter 3 has been published with myself as the primary author of the paper. Chapter 4 is a joint research with Federal University of Parana which also been published, I and another author contributed equally to this paper. The work in Chapter 5 is published in the Materials Today Chemistry journal with myself as the primary author. Furthermore, the work in Chapter 6 is under correction and will be ready to submit to journal in August 2021.

Bor Shin Chee

Acknowledgements

This thesis would never have been possible without the guidance and support of many people. I would exclusively like to thank Athlone Institute of Technology by awarding me the AIT President Seed Fund and AIT Presidents Doctoral Scholarship in order to financially support me on completing my PhD.

I would like to acknowledge my supervisor, Dr. Michael Nugent for his guidance, support and time throughout the duration of this project. Your expertise on hydrogels and polymer characterisation was invaluable in framing the research questions and methodologies. Also, your valuable feedback given for the papers, book chapter and conference presentations has made a great support to me.

A special thanks to my colleagues, in particularly Gabriel Gotten de lima, Viviane Seba, Bruno Leandro Pereira, Luiza Steffens Reinhardt, Tielidy Angelina Moraes de Lima, Lynn Louis and Jeferson Henn for their wonderful collaboration. I am very appreciative for all the time they spent to support me in completing this thesis.

I would also like to thank Dr. Declan Devine, Dr. Sean Lyons, Dr Noel Gately, Dr. Neil Rowan, Dr. Cao Zhi, Mr. Alan Murphy, the CISD and APT staffs as well as the research hub officers for their technical supports and trainings throughout the research project.

Table of Contents

List of figures

Abstract

Aim and objectives

Chapter 1: Literature review

Chapter 2: Materials and methods

Chapter 3: The synthesis and characterisation of non-orientated and orientated physically crosslinked Polyvinyl alcohol hydrogels

Chapter 4: Synthesis and characterisation of cryogenic Polyvinyl alcohol spheres

Chapter 5: Synthesis and characterisation of electrospun Polyvinyl alcohol/Polyacrylics acid bilayer nanofibres

Chapter 6: Synthesis and characterisation of freeze-thawed electrospun Polyvinyl alcohol nanofibres

List of tables

Chapter 1: Literature review

Chapter 2: Materials and methods

Chapter 3: The synthesis and characterisation of non-orientated and orientated physically crosslinked Polyvinyl alcohol hydrogels

Chapter 4: Synthesis and characterisation of cryogenic Polyvinyl alcohol spheres

Chapter 5: Synthesis and characterisation of electrospun Polyvinyl alcohol nanofibres

Chapter 6: Synthesis and characterisation of freeze-thawed electrospun Polyvinyl alcohol nanofibres

List of appendixes

Abbreviations

Abbreviation	Full form
AcOEt	Ethyl acetate
Al	Aluminium
ANOVA	Analysis of variance
API	Active pharmaceutical ingredient
ATCC	American Type Culture Collection
Au	Gold
Be	Berry number
BMP	Bone morphogenetic protein
C	Carbon
Ca	Calcium
CAF	Caffeine
CDI	Coefficient of drug interaction
CIP	Ciprofloxacin
CLA	Clarithromycin
CO_2	Carbon dioxide
DMA	Dynamic mechanical analysis
DMEM	Dulbecco's Modified Eagle Medium
DMSO	Dimethyl sulfoxide
DOX	Doxorubicin Hydrochloride
EDTA	Trypsin-ethylenediaminetetraacetic acid
EDX	Energy dispersive X-ray
EWC	Equilibrium water content
F/T	Freeze-thawing
FBS	Fetal bovine serum
FTIR	Fourier transform infrared spectroscopy
G'	Storage modulus
G"	Loss modulus
GA	Glutaraldehyde
Gly	Glycerol
h	Hours
HAp	Hydroxyapatite
HCl	Hydrochloric acid

HIPS	High impact polystyrene
ISO	International Organization for Standardization
min	Minutes
MTT	3-(4,5-Dimethylthiazol-2-yl)-2,5-Diphenyltetrazolium Bromide
MW	Molecular weight
n	The number of repeating monomer units
Na	Sodium
NaCl	Sodium Chloride
NaOH	Sodium Hydroxide
NIH	National Institutes of Health
O	Oxygen
OD	Optical density
OH	Hydroxyl group
P	Phosphorus
PAA	Poly (acrylic acid)
PBS	Phosphate-buffered saline
PCL	Polycaprolactone
PDGF	Platelet-derived growth factor
PHEMA	Poly (2, -hydroxyethyl methacrylate)
PLA	Poly (D, L-lactide)
PLGA	Poly (lactic-co-glycolic acid)
PNIPAAm	Poly (N-isopropyl acrylamide)
PVA	Polyvinyl alcohol
RT	Room temperature
SC	Solvent casting
SEM	Scanning electron microscope
Si	Silicon
Tg	Glass transition temperature
Tm	Melting temperature
VEGF	Vascular endothelial growth factor
XRD	X-ray Diffraction

Abstract

Hydrogels have been used widely in biomaterial applications, mainly due to their low interfacial tension, useful swelling properties and high lubricity. In addition to their promising biocompatibility characteristics, certain hydrogels are desirable in the biomedical field due to their sensitivity to the physiological or biological environment where they are used. There are many current applications for hydrogels, and this includes 8,000 different kinds of medical devices and 40,000 different pharmaceutical preparations. This research aims to develop and characterise the physically cross-linked PVA hydrogels with different sizes range from centi- to micro- to nano- meter in macroscopic, microscopic and nanoscopic viewpoint for drug delivery applications **(Figure 1)**. Freeze-thawing and thermal annealing were the physical crosslinking methods used to prepare the PVA hydrogels. Water-soluble drugs (i.e. caffeine, doxorubicin hydrochloride, propolis extract) and poorly water-soluble drugs (i.e. ciprofloxacin, clarithromycin) were incorporated into these PVA hydrogels to study their drug release kinetics.

In the macro point of view, although freeze-thawed hydrogels have been deeply studied in the literature, uniaxial stretching hydrogels in between freeze-thawing cycles could further improve its mechanical properties. It suggested that the orientated PVA hydrogel provided an immediate full caffeine release in 15-20 min. Furthermore, PVA hydrogel was made into spheres to increase its surface area. The PVA spheres provide an immediate full ciprofloxacin or caffeine release within 60 min. Both orientated PVA hydrogels and PVA spheres followed Hixson-Crowell release kinetics and were found to be non-toxic to NIH 3T3 fibroblast cells.

The field of biomedical applications for hydrogels required the development of nanostructures with specific controlled diameter and mechanical properties. Nanofibres were ideal candidates for these advanced requirements, and one of the easiest techniques that can produce nanostructured materials in fibrous form was the electrospinning process. Electrospinning demonstrated extreme versatility, allowing the use of different polymers for tailoring properties and applications. The thermal annealed PVA/PAA bilayer nanofibres gave a dual drug delivery of clarithromycin and doxorubicin hydrochloride for osteosarcoma treatment. The U2OS osteosarcoma cells viability was effectively decreased with the combination of both drugs. Furthermore, the freeze-thawed PVA+propolis nanofibres showed a bi-phasic drug release with an initial burst drug release in first 30 min and followed by a much slower release for 8 h.

Finally, all these novel hydrogels have the potential to be produced as new commercialise products in biomedical area mainly in drug delivery applications because of their tunable hydrogel preparation process, intrinsic biocompatible and non-toxic characteristics.

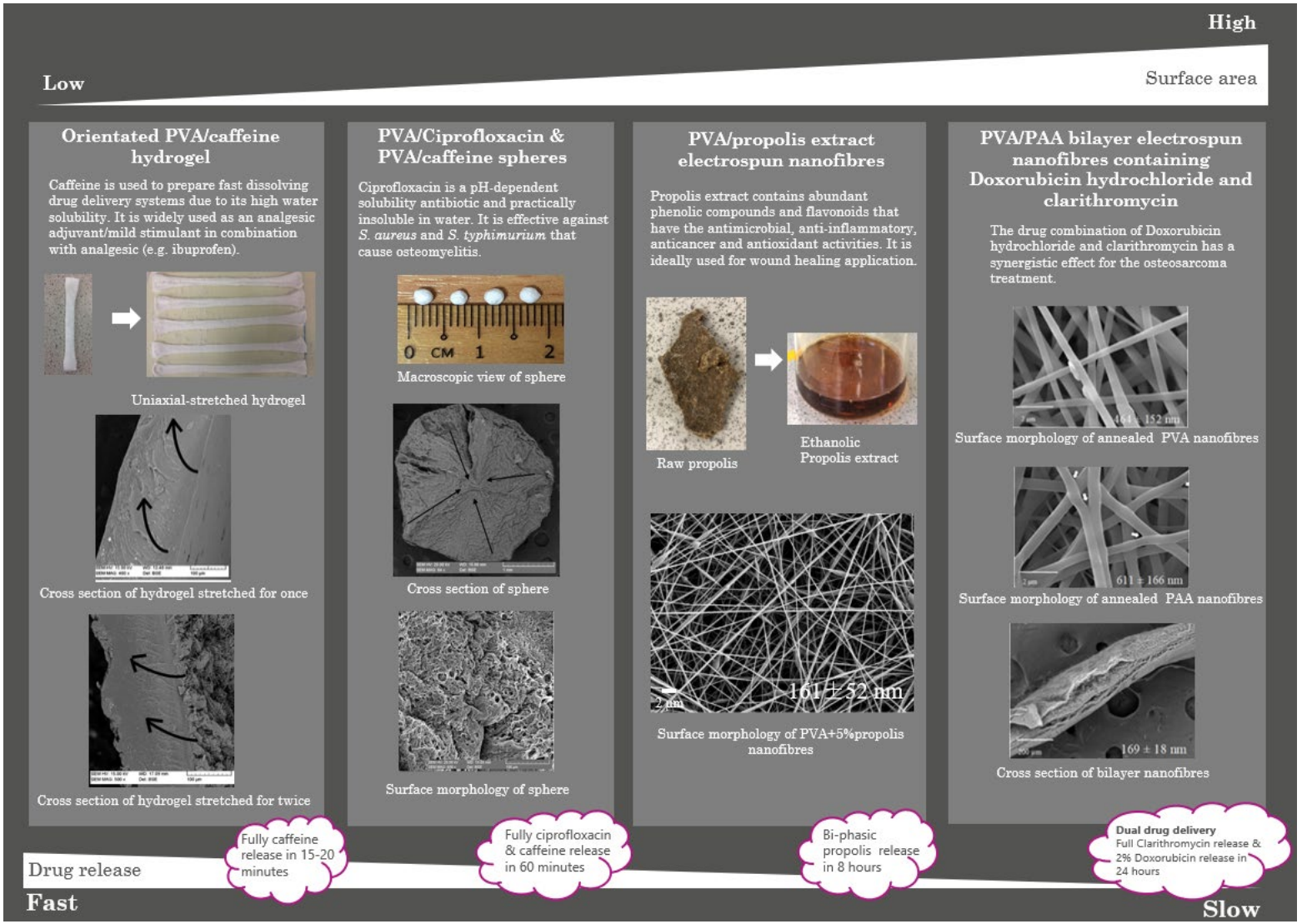

Figure 1: Schematic diagram of the work detailed in this project.

Aim and objectives

The project mainly aims to develop novel PVA hydrogels from centi- to micro- to nano- meter. It also aims to incorporate an active pharmaceutical ingredient (API) into these novel polymer matrices to study their drug delivery system. It is believed that by decreasing the surface area of the systems, the drug can have a better encapsulation and further improve its drug delivery mechanism. By making these modifications, prepared hydrogels could be used for drug delivery and tissue engineering in the field of biomedical application.

The objectives of the study are listed as follow:

(i) To prepare (a) the PVA hydrogels with repeated F/T cycles and uniaxial orientation cycles, (b) the PVA sphere with repeated F/T cycles, (c) the thermal annealed PVA/PAA bilayer electrospun nanofibres and (d) the F/T PVA electrospun nanofibres.

(ii) To characterise the mechanical and chemical properties of the (a), (b), (c) and (d) PVA hydrogel samples.

(iii) To evaluate the *in vitro* drug delivery of (a), (b), (c) and (d) PVA hydrogel samples by incorporating different drugs which included caffeine, ciprofloxacin, doxorubicin hydrochloride, clarithromycin and propolis extract.

(iv) To evaluate the cell viability on (a), (b) and (c) PVA hydrogel samples in accordance with ISO 10993-5:2009.

The detail of the project is illustrated using a flowchart.

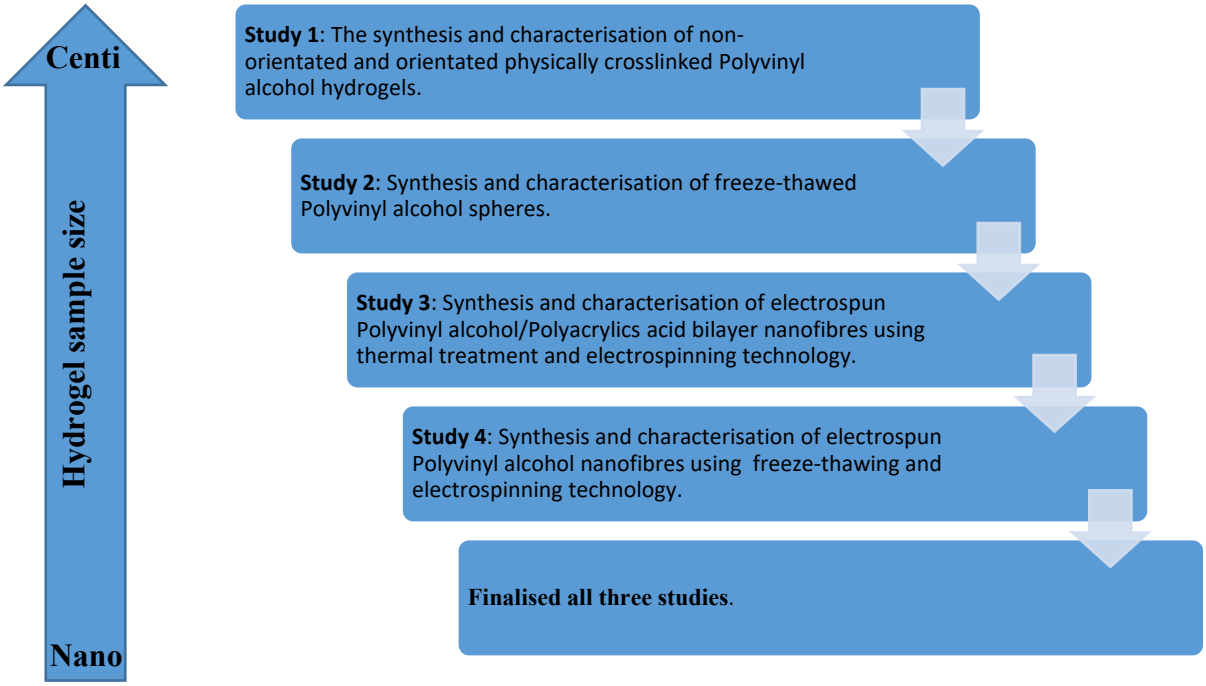

Figure 2: The milestone of the project.

Chapter 1
Literature review

1.1 PVA

PVA is a synthetic polymer that commonly composed by vinyl acetate monomer. Vinyl alcohol is not the precursor of PVA because vinyl alcohol itself is an unstable liquid compound. Thus, the PVA is produced by carrying out the following two steps (**Figure 1.1**) : (1) free radical vinyl polymerisation of vinyl acetate monomer, (2) hydrolysis (methanolysis) of polyvinyl acetate using an alcohol, methanol with an alkaline catalyst, sodium hydroxide [1].

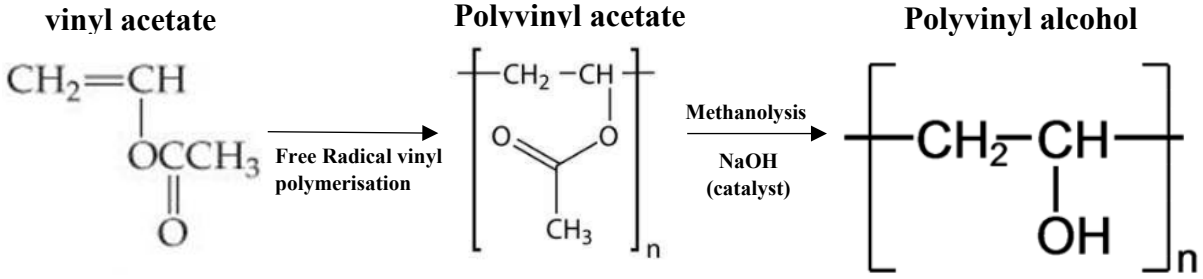

Figure 1.1: Production of PVA.

Different molecular weight (MW), degree of polymerisation and degree of hydrolysis can produce different properties of PVA in physical properties, chemical properties, gelation time, the density of crystallites and solubility [2], [3].

1.1.1 PVA molecular weight

The increase in PVA MW commonly translates to have longer polymer chains. PVA with higher MW improves the mechanical properties of polymer materials in term of tensile strength, Young's modulus and elongation at break [4]. The MW is closely related to PVA solution concentration. Higher mechanical properties can be obtained by increasing the PVA solution concentration with MW parameter kept constant. For example, 10% w/v PVA has better mechanical properties than 5% w/v PVA at the same MW because the PVA with higher concentration increases the viscosity and creates a more compact network [5]. MW can also vary the specific functional uses of PVA, namely solubility in water, degree of swelling, crystallisation, etc. [6].

1.1.2 Degree of polymerisation

The degree of polymerisation is a fundamental characteristic that determines the physical properties of polymer materials. It is depending on the number of repeating monomer units, in a polymer chain. For example, PVA is composed of repeating units $[CH_2CH(OH)]_n$ where "n" is an integer number that indicates the degree of polymerization. The chemical structure of PVA occurred in head-to-tail configuration is shown in **Figure 1.2** [7].

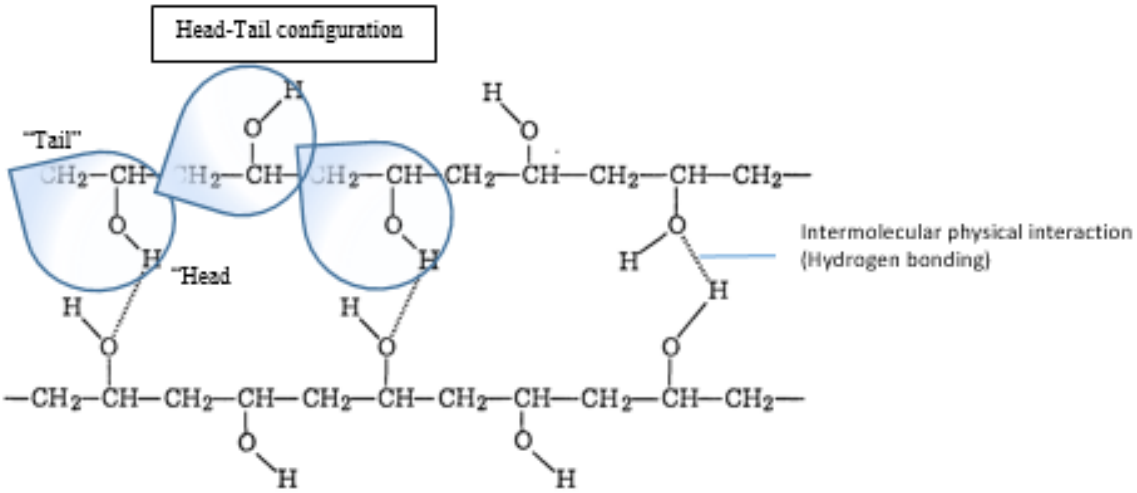

Figure 1.2: Schematic chemical structure of highly hydrolysed (>98%) PVA [8].

PVA can form highly swollen gels due to its polymer backbone chemistry [9]. The network of polymer chains contains a large number of hydrophilic side chains of hydroxyl groups [-OH] that responsible for trapping water without dissolving in the polymer matrix [9], [10]. In addition, the [-OH] groups also help to form strong hydrogen bonds between hydroxyl groups of the neighbouring chain in highly hydrolysed (>98%) PVA [11].

1.1.3 Degree of hydrolysis

The degree of hydrolysis is explained as the mole% of the residual acetate groups (1-x) over the hydroxyl groups (x) along the PVA chain [12]. It was classified into two categories: partially hydrolysed and fully hydrolysed PVA [13]. The lower the degree of hydrolysis, the higher the number of acetate groups contained in the polymer chain, the lower the number of hydrogen bonding formation. Therefore, in **Figure 1.3** shows that PVA with a low degree of hydrolysis (<88%) results in a larger interchain separation distance that weakens the intermolecular hydrogen bonding interactions between nearby hydroxyl groups due to bulky

acetate groups [11], [12]. Therefore, partially hydrolysed PVA is more soluble in water when compared to fully hydrolysed PVA.

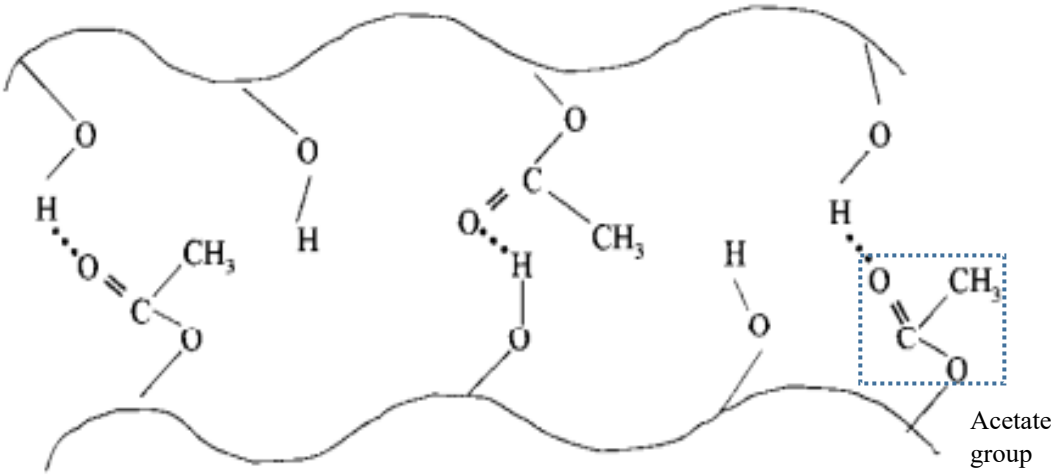

Figure 1.3: Schematic chemical structure of low degree hydrolysed (<88%) PVA [2]**.**

PVA with a high degree of hydrolysis in the range of 98% and 99% has a smaller PVA interchain separation distance and stronger hydrogen bonding because it has a lower number of acetate groups. The strength of intermolecular physical interactions (hydrogen bonds) can cause a competition between polymer–solvent and polymer–polymer interactions during the physical formation of PVA hydrogel [12], [14]. If under the condition where there is a PVA with a higher degree of hydrolysis and a good solvent, the polymer–solvent interaction will become stronger [15]. Whereas, the fully hydrolysed PVA has the greater extent of hydrogen bonding than the partially hydrolysed PVA. It causes a lower solubility or insoluble in water. Dissolution will only occur when PVA is heated at the temperature above 85°C to break up the strong H-bonding [16]. Moreover, the influence of degree in hydrolysis increases with increasing rigidness of the hydrogel.

1.2 PVA hydrogel

As a biomaterial, PVA hydrogel plays a major role in the biomedical application. PVA is a hydrophilic polymer that capable of trapping water and offers the possibility of attaching drugs, small molecules and cells [17]. In addition, PVA hydrogel has great biocompatibility and is biodegradable. Hence it has a great potential to produce as a product for wound dressing, tissue regeneration and drug delivery system [12].

1.2.1 Chemically and physically cross-linked hydrogel

The linear PVA polymer chains in an aqueous PVA solution can be either chemically cross-linked **(Figure 1.4a)** or physically cross-linked **(Figure 1.4b)** in order to form a PVA hydrogel [18], [19]. The chemical crosslinked hydrogel is prepared by polymerization of PVA monomers in the presence of a crosslinker. While the physically crosslinked hydrogel is formed without a chemical reaction. The differences between chemically cross-linked and physically cross-linked hydrogels are further illustrated in **Table 1.1** [20], [21]. In this project, the crystallisation method called freeze-thawing technique was used to produce the physically cross-linked hydrogels.

Table 1.1: Chemically cross-linked hydrogels and physically cross-linked hydrogels.

Chemically cross-linked hydrogels	**Physically cross-linked hydrogels**
Polymer chains are covalently cross-linked by molecular bond	Polymer chains are non-covalently cross-linked by molecular entanglements and secondary forces including ionic, H-bonding or hydrophobic forces.
"Permanent" hydrogel Good mechanical stability	"Reversible" hydrogel Low mechanical strength
Not influenced by external factors, such as pH, temperature or mechanical strains.	Influence by environmental conditions, such as pH, temperature and the ionic strength of a solution Will degrades, disintegrates and eventually dissolves
Chemical crosslinking methods by: a. radical polymerization b. chemical reaction of complementary groups c. high energy irradiation d. using enzymes	Physical crosslinking methods by: a. ionic interactions b. crystallisation c. hydrogen bonds d. protein interactions e. using amphiphilic block and graft copolymers

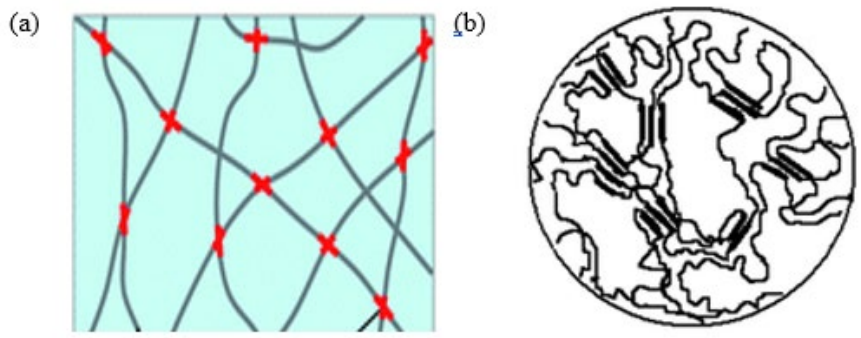

Figure 1.4: Schematics of polymer hydrogels. (a) Chemically cross-linked gel by free-radical polymerization [22] **(b) Physically cross-linked gel by repeated freeze and thaw** [14]**.**

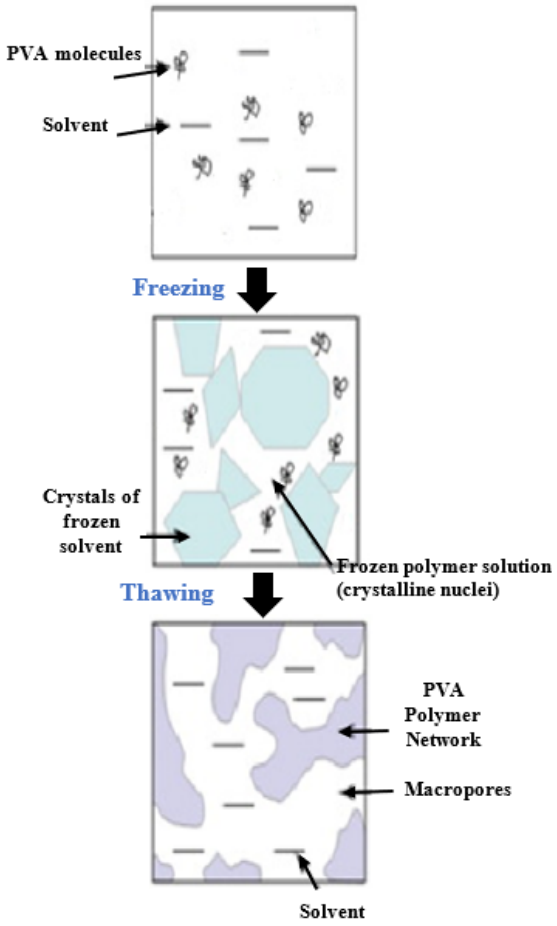

Figure 1.5: Schematic diagram of a freeze-thawing process in PVA hydrogel [23]. When the PVA solution was frozen, the PVA molecules induce the formation of small crystalline. In the meantime, the formation of ice crystals also occured. A macroporous hydrogel is then formed after the frozen solvent is completely thawed.

1.2.2 The synthesis of PVA hydrogel by Freeze-Thaw technique

The freeze-thaw technique is a cryogenic route [24], which considered as the physical crosslinking method by crystallisation. It is being widely used and first discovered by Peppas in the year 1975 for various pharmaceutical and medical applications. The freeze-thaw technique is a simple way to induce good elastic, stronger and high dimensional stability hydrogels due to the formation of hydrogen bonds which act as physical crosslinking sites in the PVA polymer network during crystallisation [14], [25]. The crystallisation process of PVA molecules can eventually induce the formation of small crystalline nuclei [24], [26]–[28] during the freezing step **(Figure 1.5)**. In the meantime, the formation of ice crystals provides a mechanism for the development of side-by-side polymer chains associations. Subsequently, a macroporous hydrogel is formed after the frozen solvent is completely thawed [23].

The major limitations of soft, biocompatible hydrogels are their relatively poor mechanical properties and low elastic modulus compared with those polymers that are solid and less biocompatible (e.g. metals, alloys) in term of mechanical beghaviour [9]. For instance, the 'gripping' of PVA hydrogels for tensile testing can be problematic as they are soft and difficult to handle. Moreover, the elastic modulus of PVA hydrogels are generally in kiloPascals, the tensile testing equipment might not be sensitive enough to determine the elastic modulus as they are optimised for the range of Mega to GigaPascals [9]. Thus, high mechanical and tensile strength hydrogel is investigated by varying the number of freezing and thawing cycles which assist to intensify existing crystals within the PVA structure [29]. In addition, the benefit of using F/T technique is these hydrogels will not manifest chemical residual due to the absence of crosslinking agents, especially emulsifier involved in the formation of hydrogel [19]. The hydrogels also give a high water content and elastic mechanical character after several F/T cycles [30].

There are two methods to go through the freezing process: fast freezing methods such as dipping in liquid nitrogen and low freezing methods such as putting in an extremely low-temperature freezer. The different rate of freezing and rate of thawing can produce different size of ice crystals. For example, fast freezing generates small and discrete ice crystals matrix structure which prevent network stabilisation, whereas slow freezing gives sufficient time to form large, contiguous ice crystals and hydrogen bonds [14], [31].

1.2.3 The crystalline effect on freeze-thawed hydrogel

The strength of PVA hydrogels is determined by their crystalline effect, particularly on crystallisation [32]. Crystallisation is the primary mechanism accountable for the mechanical properties during a freeze-thawing process [33]. The crystalline portion is dependent on the numbers of [-OH] groups and hydrogen bonds from the PVA precursor [12]. **Figure 1.*6*** shown that during the unidirectional freezing process, the water within the hydrogel freezes and forcing the PVA chains into close contact with each other, thus decreasing the distance between the PVA interchains, assisting the formation of crystallites and hydrogen bonding [32], [33].

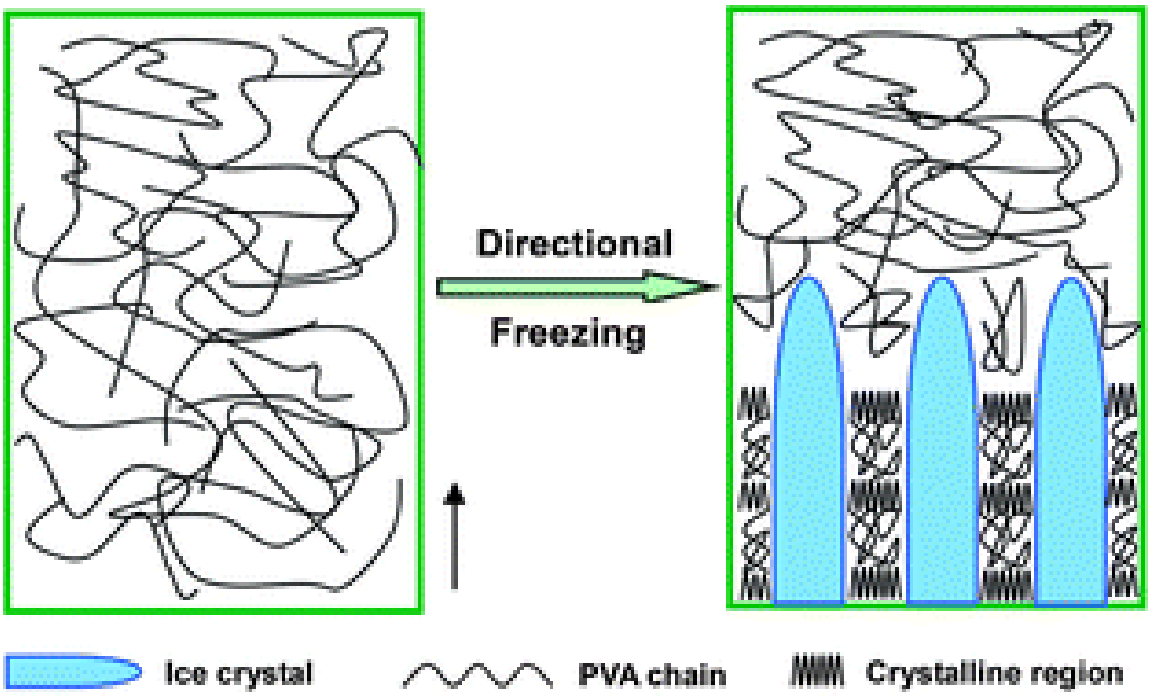

Figure 1.6: The formation of directionally arranged crystalline regions in Directional Freezing–Thawing (DFT) technique PVA hydrogels [32]**.**

The crystallinity and mechanical properties have influenced by the amount of freeze-thawed cycles. An increase of the number of F/T cycles can assist to intensify existing crystals within the PVA network structure and resulting in the formation of a more ordered and homogeneous PVA hydrogel structure. It is a fact that the amount of F/T cycles is proportional to the degree of crystallinity, but up to a limiting value, which arises from the increase of C-C stretching during the process [14]. In FTIR analysis, an absorption peak at 1141 cm^{-1} can determine a crystalline effect that takes place in the hydrogel [27]. By observing the opaque nature of hydrogel during thawing also able to determine the presence or absence of crystallisation [14].

Ricciardi *et al*. have stated if a hydrogel reaches a high level of crystallinity, it would lose its elasticity and become rigid and breakable, whereas if the hydrogel has a low level of crystallinity, it is poorly coherent [34]. Thus, the number of F/T cycles should be considered to achieve the desired hydrogel, whether a viscoelastic or non-elastic hydrogel needed.

Further research found that mechanical strength of hydrogel also determined by the additional mechanisms, called phase separation and PVA densification during the freeze-thaw process, which ease the development of PVA crystalline regions and continue to exist after thawing [33]. However, this only occurred significantly after the third freeze-thaw cycles when crystallisation reaches the plateau level, particularly through at least six cycles [14], [33]. In addition, the combination of PVA hydrogel with other types of polymers and chemical such as Poly (acrylic acid) (PAA), NaOH, HCl, NaCl and DMSO can increase the mechanical strength of hydrogel than those containing only water [27], [28], [35].

1.3 Morphology of hydrogel and orientated hydrogel

Hydrogel structures had reported having three different type of networks: fibrillar network [30], irregular porous network [18] and honeycomb-like structure [25]. Hydrogel prepared using F/T method have a highly porous fibrillar structure (**Figure 1.*7***) on the surface via scanning electron microscopy (SEM). The size of ice crystals produced in the polymer-depleted pockets increased through repeated freezing steps. Water act as a porogen in polymer solution. During the thawing steps, the ice crystals melt and leave the porous structure of the hydrogel keep intact [34]. The repeated F/T cycles can increase the stability of the network structure and become denser because of an increase in polymer chains entanglement [30].

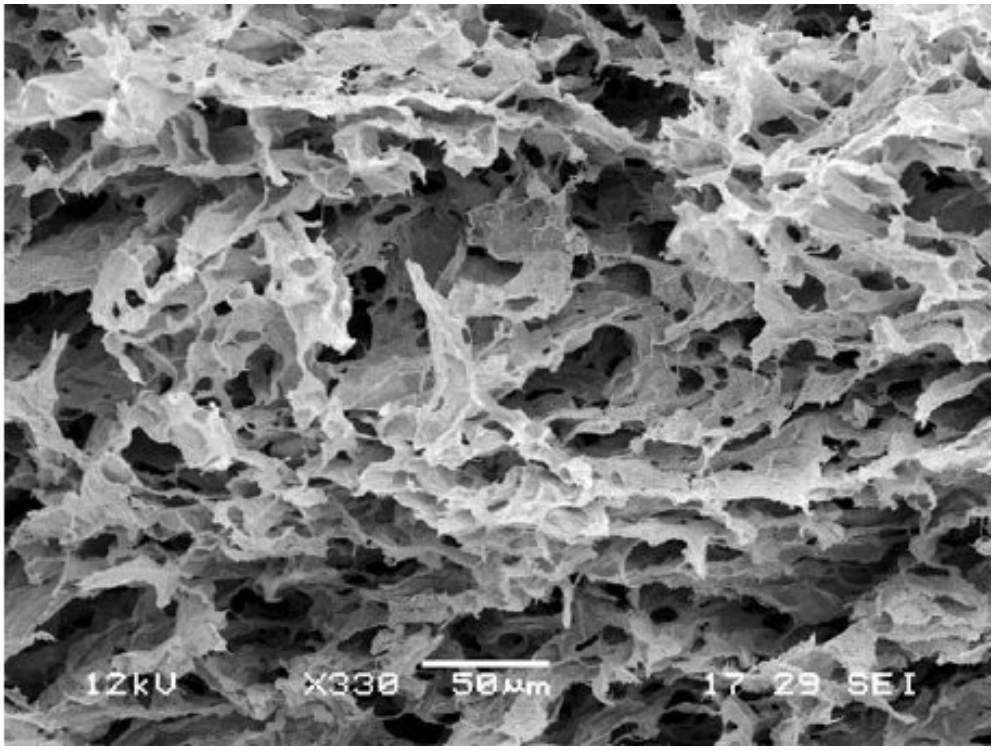

Figure 1.7: SEM image of a pure PVA hydrogel underwent eight F/T cycles [36]**.**

An additional mechanical stretching applies to the hydrogel can induce a uniaxial polymer chain alignment. The research group of Choi visualised a linear pattern in the direction of stretching of the hydrogel and a randomly arranged structure on the control hydrogel (**Figure 1.*8***) [37]. In addition, the orientated hydrogel showed the improvement of the mechanical property. In the studies of alginate hydrogel microfibres, the stretched alginate hydrogel can lift up a 10 g metal pillar but the typical hydrogel of the same composition cannot withstand such manipulation, this indicated the enhancement of tensile strength of the hydrogel was attributed to the applied stretching [38]. Moreover, the influence of polymer chains alignment on the orientated hydrogel increase with increasing cell adhesion and proliferation on or within the orientated polymer matrix. The research group of Wang has investigated that the growth of cells is aligned almost perpendicularly to the stretching direction [39].

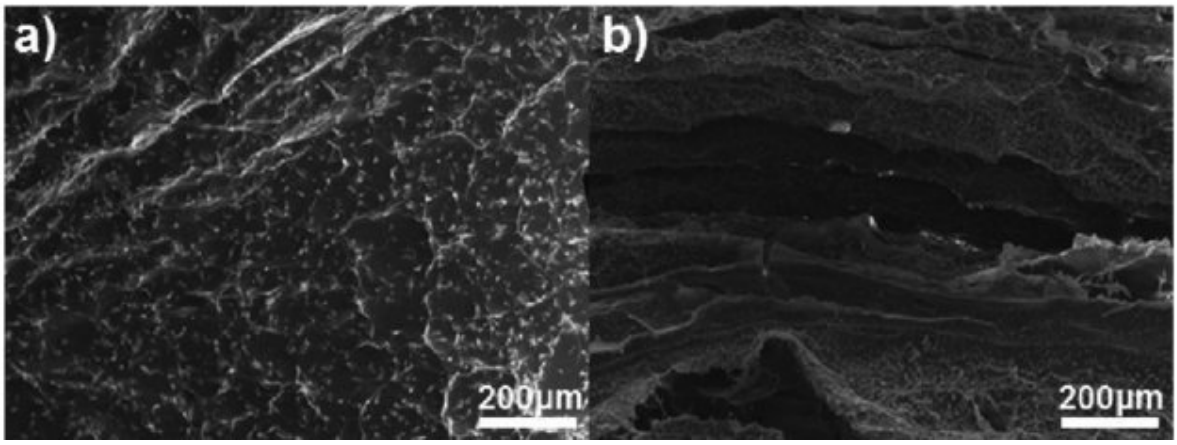

Figure 1.8: SEM of Ba-alginate/PAM hybrid hydrogel prepared (a) without stretching and (b) with stretching to 300% of its initial length [37]**.**

1.4 PVA hydrogels for drug delivery

Some drugs are difficult to absorb by the body via oral and parental administration because they may be easily digested in the gastrointestinal tract, are poorly water-soluble and have short biological half-life after injection. Thus the development of viable hydrogel drug delivery system can solve the above problems by injecting the drugs into the gels or apply on the desired part of the body either as an implant or biomedical dressing to sustain and control the continuous drug delivery temporally and spatially with a high oxygen permeability and low protein adsorption [10], [19], [40].

Moreover, there are difficulties related to drug dissolution in water. As some of the drugs are thermo-, light- or pH-sensitive and may affect the efficiency of drug delivery system. Therefore, these types of drugs are encouraged to incorporate with a stimuli-sensitive or smart hydrogel for controlled delivery of drugs. For example, a pH-responsive polymer PAA is mixed with PVA to produce a promising hydrogel that can delivery API dependent on the environmental pH and ionic strength to a particular location in the body [41].

In the study, the degree of drug release is controlled by the numbers of F/T cycles, which is closely linked with the degree of PVA hydrogel physically cross-linking [19], [26]. The repeated F/T cycles will increase the formation of crystallites and super-molecular structure; consequently, give a denser crosslinking structure of hydrogel, and resulting in a decrease of hydrogel matrix permeability to release the drug from a hydrogel. By varying the numbers of F/T cycles, different rate of drug release from hydrogel can be achieved [19].

PVA hydrogels that have been undergone several F/T cycles show significant improvement in the long-term stability, high tensile strength, high elastic mechanical character and demonstrate a high degree of swelling in water [26], [30]. In addition, these physically crosslinked gels do not involve any chemical crosslinking agents or emulsifying process that are toxic and affect the integrity of the biological samples to be entrapped [21]. They are non-irritating, non-carcinogenic and acceptable in the body [32]. Therefore, the characteristic stated above make PVA hydrogel served as an ideal and desirable biomaterial to use as a controlled drug delivery system. PVA hydrogel is able to use for implantable devices as membranes or coatings; for pharmaceutical applications as dissolution and binding agents in tablets and as matrices for cell immobilization [42].

1.5 Electrospinning

As in numerous technologies, hydrogels technology is being informed by nanotechnology. "Nano" comes from the Greek Nanos, meaning extremely small. Nanotechnology is the science of changing properties of materials at the molecular and atomic level [43]. The drive for materials with specific sizes and geometry has made an enormous impact on biomedical applications in terms of nanotechnology. The integration of nanotechnology into biomedical applications is called "nanomedicine". One area of particular interest is electrospinning. It is one of the foremost nanotechnology applications to fabricate materials with sizes in the nanometer range. It is regarded as a versatile, inexpensive and simple methodology with positive outcomes for constructing of very compact and high-performance nanomaterials. It has widespread applications in nanomedicine and the potential to solve unmet medical needs in the future.

The incorporation of the electrospinning technology with the biocompatibility and controlled biodegradable rate of hydrogels have driven the research of electrospun hydrogel composites for successful tissue engineering. These electrospun hydrogels are beneficial because they are having a hydrophilic polymeric network that is capable of trapping a large amount of water or biological fluid without dissolving in the polymer matrix and consequently giving a moist environment for cell seeding, migration and proliferation of cells. In addition, the electrospun hydrogels as drug loaded nanostructures pose great advantages in drug delivery system. The high drug encapsulation efficacy of the nanofibres prevents drug degradation and controls the

drug release rate into the human body either in a controlled way or fast dissolving rate. Moreover, in the medical diagnostic and therapeutic field, the surface area of electrospun nanofibres acts as an ultrasensitive biosensor to provide many highly specific binding sites for the detection of cancer cells [44], [45]. Besides the nanosized therapeutic agents encapsulated-polymer is able to circulate in the bloodstream and allow them to reach the target site [46].

1.5.1 General principles of electrospinning

Attributed to the protein adsorption and cells adhesion have been significantly improved in nanomaterials, there is an increasing recognition that a nano-sized biomaterial is very likely to be more bioactive than a micro-sized one [47]. Undeniably, the most applicable and controllable nano-sized biomaterial production method is electrospinning. This method allows the fabrication of filament-forming, super lightweight polymers, electrospun nanofibres from solutions and melts (polymer or polymer mixed) in the presence of an electric field. It is one of the few techniques used to create composite materials made up of two or more different materials [48]. The first development of electrostatic attraction of a fluid was investigated in the seventeenth century by the physician, William Gilbert [49]. After a duration of time of dramatic growth, the first patent for electrospun nanofibres was issued in the year 1902 by William James Morton titled ‘Method of Dispersing Fluid’ [50].

An electrospinning apparatus setup (**Figure 1.*9***) comprises of three main parts: a high voltage generator, a syringe pump and a collector plate. Initially, a syringe pump containing polymer solution with a metal needle tip is connected to the positive electrode of the power supply generator, while the grounded electrode is connected to a collector plate on the opposite end. Subsequently, a high voltage is applied in the system to create an electric field between the tip of the needle and the collector plate, which helps to cross-link the polymer chains during the electrospinning process. The polymer solution acts as a charged carrier transferring the electricity over to the side of the collector with no charge and this can result in a potential voltage difference between the polymer solution and the collection plate [51]. When the relatively weak surface tension of the charged solution droplet is overwhelmed by a strong electrostatic force, the droplet is distorted and forms a conical shape known as a Taylor cone. The distortion is continued and leads to an electrically charged jet ejection which draws the aligned thin polymer fibres to accelerate toward the collector [52]–[55]. In the electrospinning process, the solvent evaporates and leaves the dry nanofibres deposited on the collector [51].

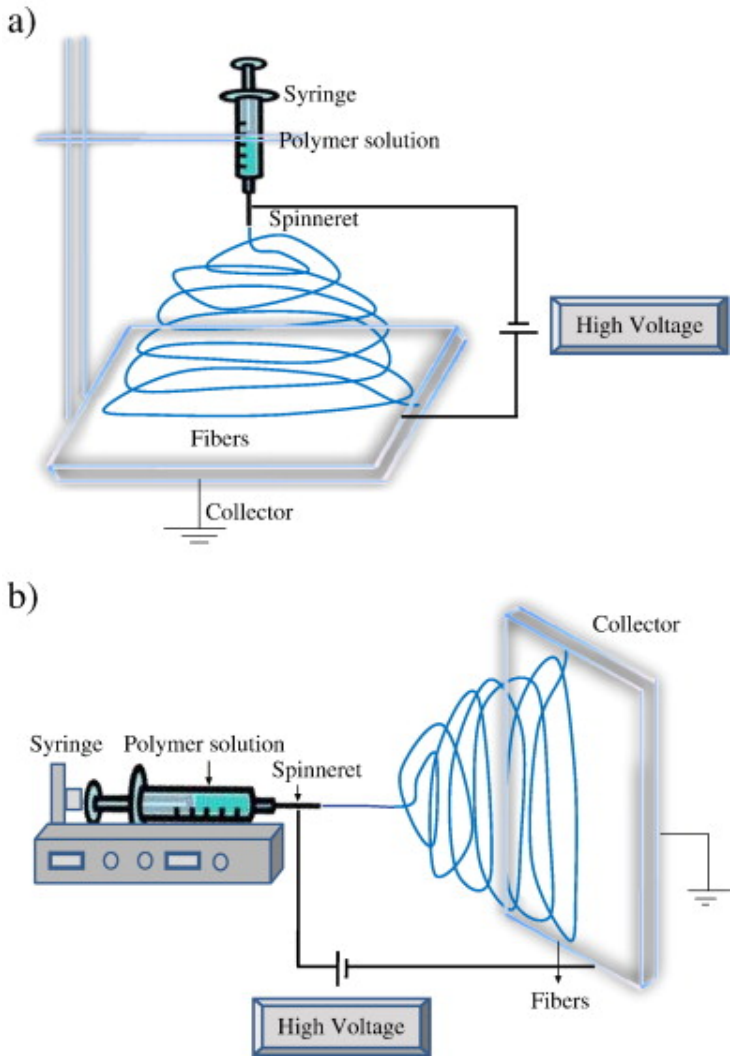

Figure 1.9: Schematic diagram of setting up of electrospinning apparatus (a) vertical set up and (b) horizontal set up of electrospinning apparatus [56]**.**

There are a number of conventional techniques available for the fabrication of nanofibres for use in tissue engineering, including electrospinning [57], rotary jet spinning [58], self-assembly [59], sol–gel methods [60], phase separation [61], melt-blow [62], melt spinning [63] and template synthesis [39]. Out of all of these methods, electrospinning tends to have the most remarkable effects in relation to the size and shape of fibres, which is similar to the extracellular matrix (ECM). Unlike the use of mechanical forces to draw nanofibres via conventional spinning processes (i.e. melt spinning) [52], the electrostatic force acts as a driving mechanism in electrospinning to produce nanofibres which have a uniform, non-beaded and ultrafine morphologies (**Figure 1.*10***) [55], [64].

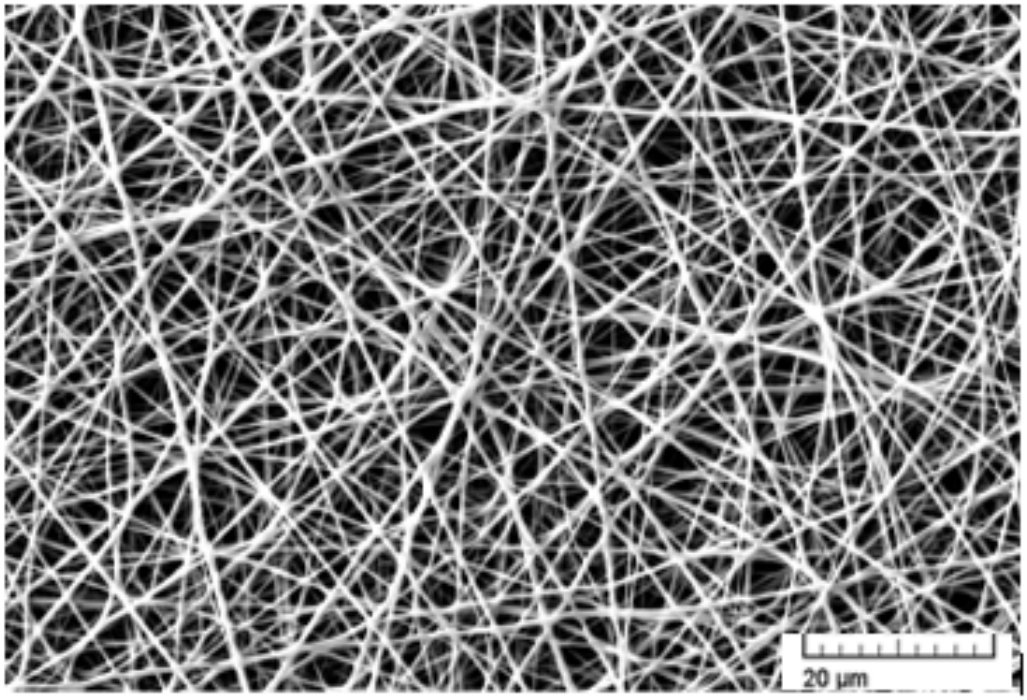

Figure 1.10: Scanning Electron Microscopy (SEM) photograph of PVA electrospun nanofibres at 2.00 KX magnification [65]**.**

1.5.2 The impact of various parameters on the electrospinning process for nanofibre morphology

Many experiments have been done to determine the effects of various parameters on morphological structures and diameters of electrospun nanofibres. The polymer solution parameters, processing parameters, and ambient parameters (**Figure 1.11**) are three main groups of factors that can affect the nanofibre morphology such as the diameter of the nanofibre and the shape (i.e., bead, non-bead, flat) of the nanofibre [66]. Through appropriate adjustment of different variables from those parameters, different surface morphology of nanofibres can be generated [52], [64], [67], [68], as illustrated in **Figure 1.12**. However, not all the variables listed in **Figure 1.11** are fundamental control parameters nor are they independent of each other. For example, applied voltage, target distance and electric field are all interconnected [69]. The fact that one variable can influence one or more parameters, it is ideal to change the setting of one variable at a time.

Figure 1.11: Polymer solution, electrospinning process and ambient parameters that affect the characteristics of electrospun nanofibres.

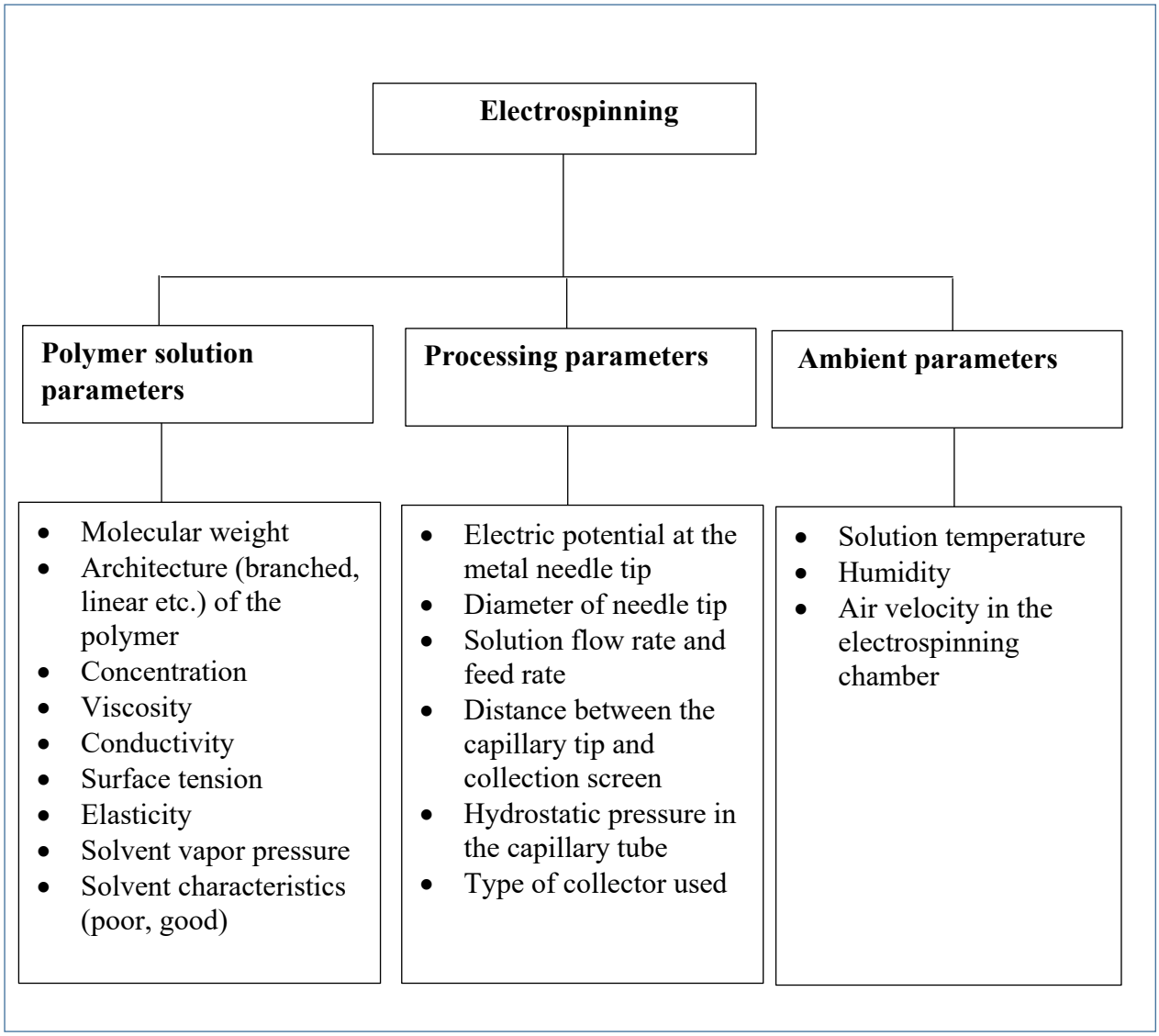

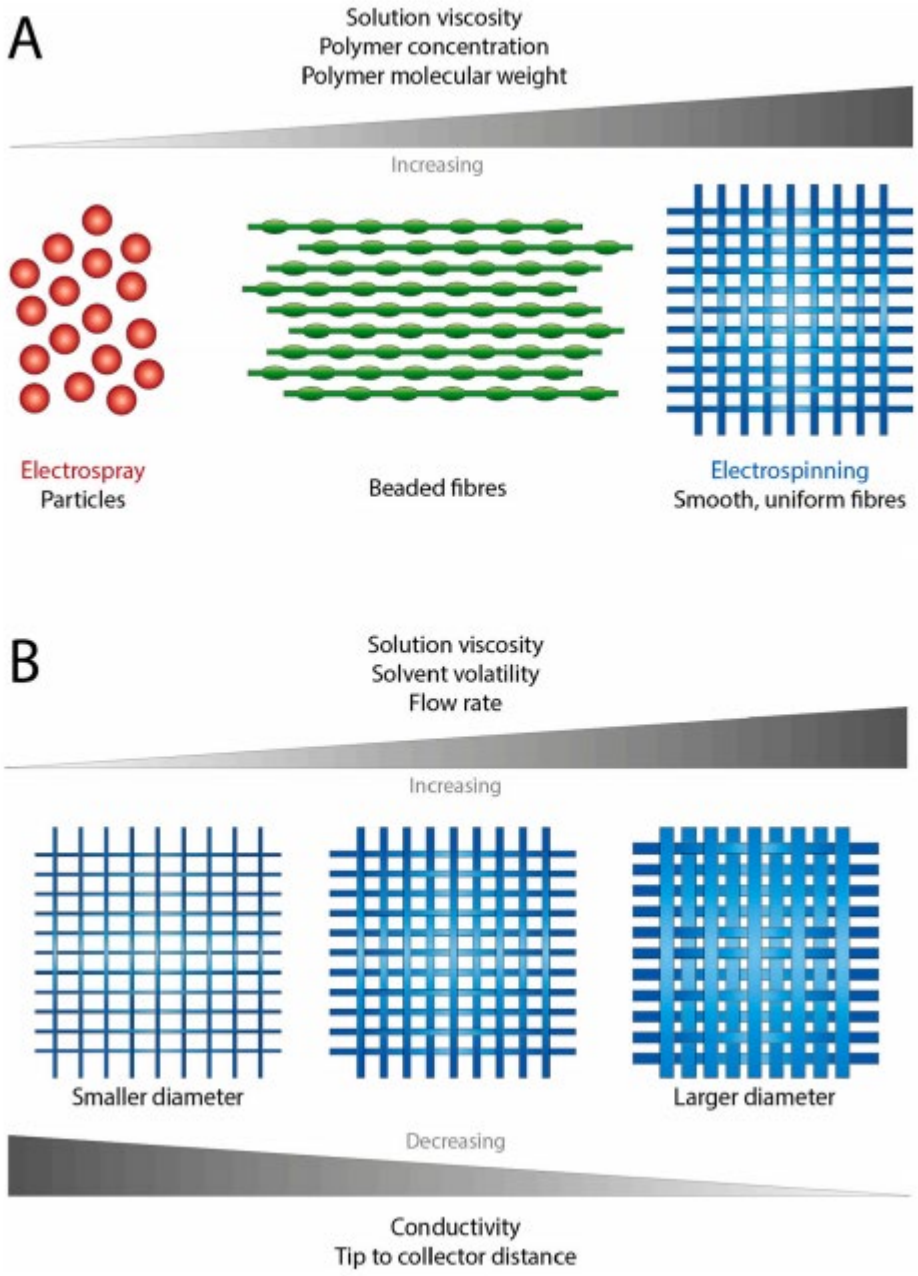

Figure 1.12: The effect of (A) solution parameters and (B) solution and processing parameters on the surface morphology of electrospun nanofibres during electrospinning [70]**.**

1.5.2.1 Polymer solution parameters

Chain entanglement is considered to be one of many parameters that can significantly influence fibre formation during polymer electrospinning [69] and it can be varied depending on both fundamental variables: the polymer MW and concentration. The chain entanglement plays a major role in stabilising the fibrous structure. If the chain entanglements in the solution are insufficient to stabilise the solution jet, only beads will form during electrospinning [71]. The

establishment of the optimum ranges for concentration and MW is desirable to ensure stable nanofibre formation. It is well known for a given MW, the entanglement density varies exponentially with concentration [72]. Alternatively, the same result is achieved at a fixed polymer concentration by increasing MW [69]. It is also known that the polymer concentration and MW may have a significant effect on electrical conductivity and on fibres diameter [68].

Furthermore, both the increase of polymer concentration and MW also result in a corresponding increase in solution viscosity, [η] [73]. The Mark-Houwink-Sakurada equation is relating the intrinsic viscosity to the MW of a linear polymer,

$$[\eta] = KM^{a} \quad (1)$$

where the empirical constants K and a depending on the polymer, solvent and temperature [74]. For example, Tacx et al. have obtained the Mark–Houwink relationship for PVA in different solvent and temperature. There were [η] = 1.51×10^{-4} M $^{0.804}$ for PVA in DMSO at 65°C, [η] =3.54×10^{-4} M $^{0.692}$ for PVA in ethylene glycol at 140°C and [η] =6.51×10^{-4} $M^{0.628}$ for PVA in water at 30°C [75]. This equation has provided a simple approach for characterising the intrinsic viscosity of a polymer and can be used for determining the Berry number (Be). Due to the relationship between intrinsic viscosity and the concentration is normalized with respect to the Berry number,

$$Be = [\eta]C \quad (2)$$

where [η] is the intrinsic viscosity and C is the solution concentration [76]. The Berry number is generally used by the researchers as a processing index for controlling t he diameter of electrospun nanofibres [77].

At a constant concentration, the morphological transition is defined from beads to beaded fibres, to complete fibres and to flat fibres with the increase of MW. When the Berry number is greater than 4 ([η]C>4), where the solution is under a semi-dilute entangled regime, the polymer chains in the solution begin to entangle with each other and the solution viscosity increases significantly. A fibrous structure could not be stabilised when the Berry number was lower than 9 ([η]C<9), the fibres exhibit a circular cross-section with a diameter between 500 nm and 1.25 Am and a bead-on-string structure will obtain, indicating the resistance of the jet to an extensional flow. A fully stabilised fibrous structure is obtained normally at [η]C>9, indicating that a minimum degree of chain entanglement is needed for producing fibrous structures. While,

the gradual shift from circular fibres to flat fibres starts at a Berry number of 12 ([η]C≥12) [68], [78].

The solution viscosity also gives the polymer a low surface tension, which is desirable in electrospinning. It has been established that the lower the surface tension, the lower the critical voltage needed for jet ejection from Taylor's cone [68].

1.5.2.2 Processing parameters

By changing the distance between the capillary tip and collection screen, the applied electric field between the tips and collector is altered and affect the formation of the fibrous membranes. Owing to the distance increase, the fibres are continually stretched and thinned within the whipping region, resulting in smaller fibre diameters [79]. Bead generation will appear if the distance is too large or too small [80]. Moreover, there is a direct impact on the fibre diameter by influencing the injection needle tip diameter and flow rate. Wang et al. reported that the fibre diameter becomes smaller with a smaller injection needle tip diameter and increased working distance [81]. In addition, Rodoplu et al. observed that a decrease in the flow rate increased the fibre diameter with smaller bead size within the nanofibre structure. A non-beaded nanofibre structure can be obtained by gradually decreasing the solution flow rate with other parameters are held constant. Yet it is necessary to increase the voltage if there is a significant decrease in flow rate in order for the electrospinning to take place [55].

Another process parameter is the type of collector (i.e. plane plate collector, rotating drum collector, edge type collector and grid type collector) that can vary the structural arrangement of electrospun fibres as randomly orientated fibrous mats, or as uniaxially aligned arrays [82]. A plane plate collector is usually used to collect randomly orientated mat. A rotating drum collector can collect either randomly orientated nanofibres or aligned nanofibres over a large surface area and uniform layer-by-layer 3D structure. Aligned and smaller diameter fibres are produced with an increase in the rotation speed of the collector [83]. Whereas, randomly orientated fibres with increasing fibre diameter are observed when the rotation speed decreased.

1.5.2.3 Ambient parameters

In addition to the effects of controlled processing and solution parameters on fibre morphology and properties, the influence of ambient parameters such as humidity, temperatures and air velocity in the electrospinning chamber were investigated. Nezarati *et al.* reported that fibre

breakage occurs at low humidity due to decreased electrostatic discharge from the jet. However, a high humidity level did not guarantee the fibres formation, it was dependent on the polymer hydrophobicity, solvent volatility and miscibility with water. Furthermore, the humidity also directly influences the number of pores on the fibre. In part, the number of surface pores is formed via vapour-induced phase separation and increased with a high evaporation rate of the highly volatile solvent at a high humidity level [80], [84].

1.5.3 Electrospun nanofibres configuration

The electrospinning is said to be highly versatile because instead of having the conventional nanofibers configuration, the electrospun nanofibers are likely to encapsulate the bioactive agents such as growth factors and drugs with a variety of configurations (**Figure 1.13**), namely co-axial (core/sheath), blend and emulsion configuration using different fabrication strategies [85], [86]. For example, the research group of Yu (2013) has produced a core/sheath nanofibers structure using the co-axial electrospinning system. The core and sheath polymer solutions were prior put into two separate syringes. Once the process of electrospinning was initiated, two polymer matrixes were then combined together and formed the core/sheath nanofibers. In the study, the model drug, ketoprofen was distributed evenly to the sheath polymer, polyvinylpyrrolidone (PVP) and the core matrix, ethyl cellulose (EC) in order to provide a biphasic drug release profiles which consisted both immediate and sustained drug release rate [87]. In addition, as outlined by Said *et al.,* it is possible to have a combination of blend and emulsion electrospinning technique to form the dual-loaded poly (ester amide) (PEA) nanofibers loaded with the fibroblast growth factor-2 (FGF2) and fibroblast growth factor-9 (FGF9). The FGF2 was blended into the PEA solution, while FGF9 was emulsified in the polymer solution. Both of the formulations were then mixed together for electrospinning. This new nanofibers configuration has shown an efficient differential release of the two growth factors in a controlled delivery strategy [88].

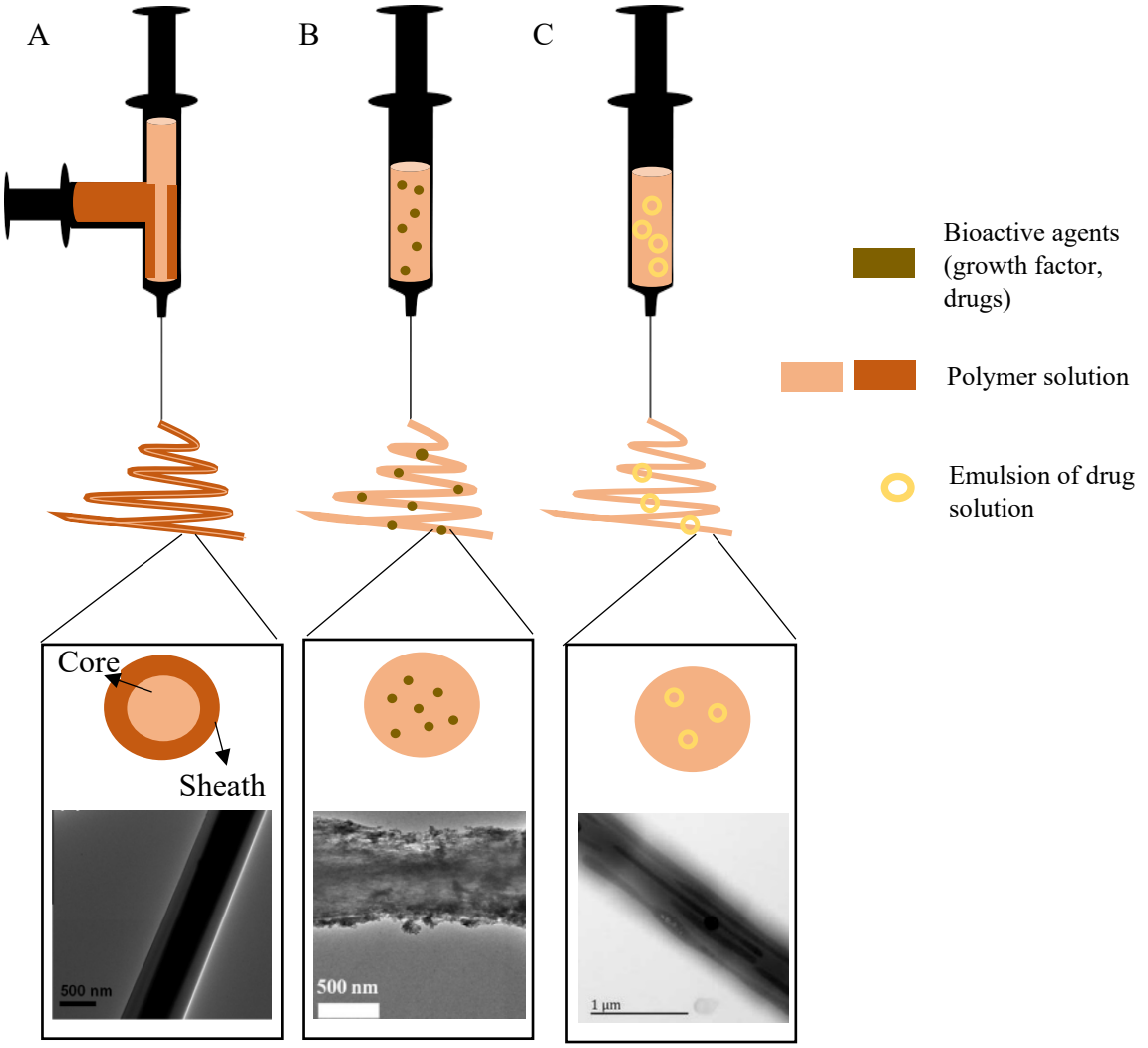

Figure 1.13: Electrospinning fabrication strategies employed to form several configurations (A) co-axial [87]**, (B) blend** [89] **and (C) emulsion** [90]**.**

1.5.4 Mass production of electrospun nanofibres

Electrospun nanofibres tend to contribute excellent control over nanofibre dimensions and alignment with lengths measuring up to kilometers as well as having an average diameter of submicrometers to tens of nanometers [52], [91], [92]. However, electrospun materials are not very cost-effective and economical. Major setback to commercialise the electrospinning products is its low production rate [93], the traditional nanofibre production is not up to speed. Furthermore, clogging of the needles a very important drawback in the conventional electrospinning mechanism which resulted in the development of free surface needleless electrospinning technique [94].

To be relevant for mass production, various types of electrospinning technologies have been developed to enable industrial level production by many dedicated companies. The advanced technology is categorised into two types: multi nozzles electrospinning and needless electrospinning. **Figure 1.14** showed several techniques used by the electrospinning equipment companies that enable to achieve high throughput nanofiber production. The electrospinning system with needleless, free liquid technology is used in some companies such as SKE Research Equipment, Elmarco, Respilon and Stellenbosch Nanofiber Company (SNC). These needleless electrospinning techniques included the Needleless Version (EF500) from SKE Research Equipment and the Needle-free Nanospider™ electrospinning technology from Elmarco by distributing spinning solution onto electrode wire to speed up the electrospinning process **(Figure 1.14a)** as well as the SNC BEST™ Ball ElectroSpinning Technology from SNC with the nanofibres produced from the thin layer of spinning solution on the surface of a ball **(Figure 1.14b)**. In addition, there are some companies such as Pardam Nano4fibers and Areka Advanced Technologies using the multiple nozzle electrospinning technology. These techniques included the Nanocentrino™ from Areka by using centrifugal forces to spin nanofibers **(Figure 1.14c)** and the Hybrid Electrospinning Technology from Inovenso **(Figure 1.14d)**.

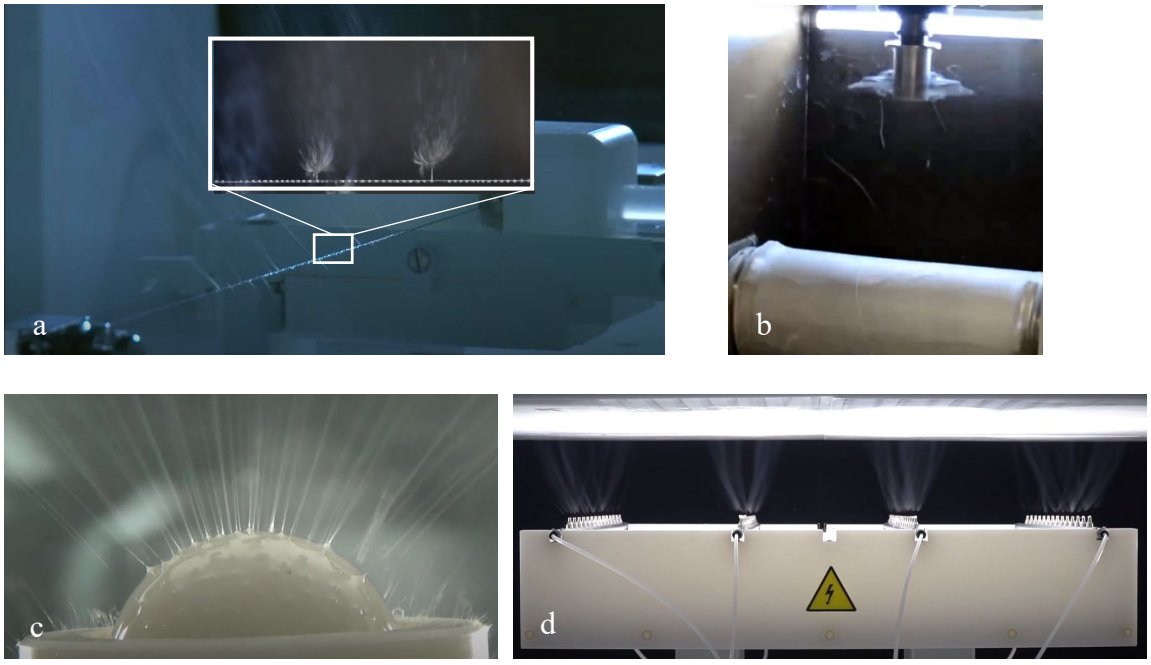

Figure 1.14: Techniques used to scale up nanofiber production line. (a) Needle-free Nanospider™ electrospinning technology, (b) SNC BEST™ Ball ElectroSpinning Technology, (c) Nanocentrino™, (d) Hybrid Electrospinning Technology.

The number of electrospun nanofibres products will be highly achievable for even diversified applications including liquid/air filtration, face masking/respiratory protective device, biomedical, laboratory tissue culture, cosmetics, fabrics, furniture and pest control, when the scaling-up of the electrospinning apparatus to commercial level units is feasible.

1.5.5 Perspective applications of electrospun hydrogels

The work in the past regarding electrospinning has mainly focused on determining suitable settings for electrospinning of various polymers and on understanding the important features of the preparation process with the purpose of gaining control of electrospun nanofibre morphology, configuration, porosity and etc. [52]. In contrast, the recent works are focused on introducing different types of organic materials (i.e. plant-based materials, biologics, nanoformulated vitamins) into hydrogels via electrospinning. Animal-based, plant-based and natural nanofibres are used for therapeutic approaches, yet plant-based materials are rarely used for electrospinning. Zhang *et al.* have analysed that there are only around a hundred publications on plant extract among all the journal articles (i.e. *Cissus quadrangularis* and Asian Panax Ginseng root) from the year 2008-2016 when compared with the total amount of papers published annually on electrospinning. The plant extracts are found to give a positive effect on the hydrophilicity and mechanical properties of nanofibres.

1.5.6 Commercial activity of electrospun nanofibers

Up to July-2020, 56,240 document results were found to be published in a basic search (article title, abstract, keywords) conducted using the Scopus database with the term “nanofibers” and 29,295 electrospinning-related published documents were found within the previous results with the term of “electrospinning”. It can be seen that nanofibers were majority produced using electrospinning technique. In addition, when come to patenting, a patent search (source: European Patent Office; term searched: “electrospinning” in title or abstract only) returned 4,789 patents had been filed around the world and with further include the term of [“electrospinning” and “nanofibers”] 886 patents were found. The Top 3 countries that contribute the highest number of patents includes China, Korean and United State. Despite the high number of patent applications related to electrospun nanofibers, the electrospun nanofibers products in the market are still considered less. The commercialised electrospun nanofibres products were mainly for liquid/air filtration, face masking/Respiratory protective device, biomedical and laboratory tissue culture applications. As seen in **Table 1.1**, there are

still require a huge effort to push the electrospun nanofibres for drug delivery applications to the market.

Table 1.2: Electrospun products available in the market produced by electrospinning for various applications.

Product	Company name and website	Country	Description	Polymer used
Liquid and air filtration				
SpurTex® MF	SPUR Nanotechnologies https://www.spur.cz/	Czech Republic	Multilayer cleanable nanostructured filtration material for microfiltration of liquids.	PU[1], PVDF[2], CA[3]
SpurTex® MF RF	SPUR Nanotechnologies https://www.spur.cz/	Czech Republic	Reinforced multilayer cleanable nanostructured filtration material for microfiltration on liquids.	PU, PVDF
RIFTELEN® N15	Filtrex and Pardam Nano4fibers joint developed https://riftelen.com/	Ireland and Czech Republic	Liquid food products filtration (desk filtration, bag and sleeve filtration, cartridge filters).	PA[4]-6
NnF MBRANE®	Pardam Nano4fibers https://www.nano4fibers.com/	Czech Republic	Polymeric nanofibrous membrane as filtration materials for water and air purification.	PVDF, PVB[5], PU, PCL[6], PAN[7], PA-6
Nanotrap™ filter	Coway http://www.coway.com/	South Korea	Household water filter.	-
Technoweb™ nanofiber	Finetex EnE http://www.ftene.com/	South Korea	Act as gas turbine filter, air pollution control, HVAC filter, automotive filter, liquid filter). Also, as face mask and window screen.	-
NanoFiber filter	AstraPool https://www.astralpool.com/	Spain	Filtration system for residential pools.	-

[1] Polyurethane
[2] Polyvinylidene fluoride
[3] Cellulose acetate
[4] Polyamide
[5] Polyvinyl butyral
[6] Polycaprolactone
[7] Polyacrylonitrile

FERENA	Koken https://www.koken-ltd.co.jp/	Japan	Air filter unit used in KOACH (an open clean room system).	Fluorine contained PVA[8] resin
Seta® nanofiber	RevolutionFibres https://www.revolutionfibres.com/	New Zealand	Air filtration (Face mask, diffuser filter).	-
Home ventilation system using SETA™ diffuser filter	HRV https://www.hrv.co.nz/	New Zealand	Home ventilation filtration.	-
Petryanov's filtering cloth	Sorbent https://en.sorbent.su/	Russia	Filtering cloth, used for fine and super fine cleaning of air and other gases of fine aerosols.	-
HIFYBER® nanofiber	Abalioglu Teknoloji http://www.hifyber.com/	Turkey	Filtration applications (gas turbine air intake filter, industrial dust collection, wire EDM filter, engine air intake filter, HVAC filter, cabin air filter, syringe filter, HEPA, facemask).	-
Mircograde NF filter	MANN+HUMMEL https://www.mann-filter.com/en/mann-filter/home/	Germany	Air Cleaner for commercial vehicles.	-
Filtriq™ non-woven membrane	Zeus https://www.zeusinc.com/	USA	Pharmaceutical filtration, aggressive liquid chemical filtration, air/gas filtration. Also used as fuel cell membranes, battery separator.	PTFE[9]
Exceed® filter	ESpin Technologies http://www.espintechnologies.com/	USA	Residential and commercial buildings filters.	-
Naked Filter	Liquidity https://nakedfilter.com/	USA	Water bottle filter.	-
Ultra-Web® Cartridge filter	Donaldson https://www.donaldson.com/en-be/	USA	Industrial dust collector.	-

[8] Polyvinyl alcohol
[9] Polytetrafluoroethylene

Filter featuring ProTura® nanofiber technology	Clark Filter https://www.parker.com/	USA	Cartridge style dust collector.	-
Filter featuring BHA® ProTura® SB Nano technology	Parker Hannifin Corporation https://www.parker.com/	USA	Cartridge style dust collector.	-
RESPILON® Window Membrane, RESPILON® Adjustable Screen	RESPILON https://www.respilon.com/	Czech Republic	Nanofiber membrane installed on window	-
Face masking/Respiratory protective device				
INOFILTER® 95/99 face mask	Inovenso https://www.inovenso.com/	Turkey	N95 and N99 three-layer respiratory masks, produced using a patented novel technology "Hybrid Electrospinning".	PVDF
BreaSAFE® ANTI-COVID-19, BreaSAFE® ACTIVE carbon	Pardam Nano4fibers https://www.nano4fibers.com/	Czech Republic	Contained active silver with antimicrobial feature in the middle nanofibers layer, reusable, non-valve respirator.	-
Smart Mask	NASK http://nask.hk/	Hong Kong, China	N95, N99 and conventional surgical bacterial killing masks.	-
Virus Killer ReSpimask® VK, Virus Killer RespiPro VK	RESPILON https://www.respilon.com/	Czech Republic	Respiratory protective equipment enriches with a layer of accelerated copper oxide.	-
Three-layer surgical face mask	LEONARDINO http://leonardino.eu/	Italy	Bacterial filtration efficiency 99.8%, start manufacturing to help Italy during the COVID19 emergency in 2020.	-
SpurTex® Nanorespirator V100 FFP2, SpurTex® VS and SpurTex® PP	SPUR Nanotechnologies https://www.spur.cz/en/	Czech Republic	3-layer or 5-layer face mask with high filtration performance nanomaterials.	PVDF

Biomedical				
Bioweb™	Zeus https://www.zeusinc.com/	USA	Scaffolding, stent encapsulation, implantable structures in the body.	PTFE
HealSmart™ Personalized Antimicrobial Dressings	PolyRemedy https://polyremedy.com/	USA	Personalized, direct-to-patient wound dressings.	HA[10]
NanoCare™	Nanofiber solutions https://nanofibersolutions.com/	USA	Advanced wound healing mesh for veterinary use.	-
NanoWhiskers™	Nanofiber solutions https://nanofibersolutions.com/	USA	Injectable, micronized nanofibers for osteoarthritis and soft-tissue repair in the veterinary field.	-
ReBOSSIS® synthetic bone	ORTHOReBIRTH https://orthorebirth.com/	Japan and USA	Biosynthetic bone scaffold, bone-void-filling material.	Silicon and PLGA[11]
AVflo™ vascular access graft	Nicast http://nicast.com/	Israel	Vascular access for hemodialysis.	PCU[12]
PK Papyrus	BIOTRONIK https://www.biotronik.com/en-gb	Germany	Non-woven electrospun nanofibers covered coronary stent.	PU
NeoDura™	MEDPRIN https://medprin.com/	Germany	Absorbable dural repair patch.	Synthetic material and porcine gelatin
ReDura™ dural patch	MEDPRIN https://medprin.com/	Germany	PLLA as dural substitute for dural defect repair.	PLLA[13]
SpinCare™	Nanomedic https://nanomedic.com/	Israel	Wound dressing for any wound shape.	Hydrogel
Laboratory tissue culture				

[10] Hyaluronic Acid
[11] Poly(lactic-co-glycolic) acid
[12] Polycarbonate-urethane
[13] Poly-L-lactic acid

BioPaper™ 3D fibrous scaffold	DiPole Materials https://www.dipolematerials.com/	USA	3D cell culture, drug screening and bioprinting.	Porcine-derived Gelatin
Cellspan™ Esophageal Implant	Biostage https://www.biostage.com/	USA	Eesophagus regeneration.	PC-PU[14]
NanoECM™, NanoAligned™, NanoHep™ cell culture plates	Nanofiber Solutions https://nanofibersolutions.com/	USA	Cell culture, cancer research, stem cell, and regenerative medicine.	PCL
Cytoweb® Sheets	ESpin Technologies http://www.espintechnologies.com/	USA	3D cell culture.	PLGA, PLLA, PDLA[15], PCL, PU
Tubular scaffold, disc scaffold	SKE Research Equipment https://www.ske.it/	Italy	3D cell culture and tissue engineering.	Silk fibroin, PCL
NBARE series	Nanofaber https://www.nanofaber.com/	Italy	3D cell culture, for R&D activities only.	PCL
Mimetix® scaffolds	Electrospinning Company https://www.electrospinning.co.uk/	United Kingdom	3D cell culture.	PLLA
Cosmetics				
actiVLayr® eye mask	RevolutionFibres https://www.revolutionfibres.com/	New Zealand	Skin care.	Marine Collagen- Type I, Hydrolysed Marine Collagen, HA
Fabrics				
Nanodream	RevolutionFibres https://www.revolutionfibres.com/	New Zealand	Pillow liner.	-
SIMWyPES®	ESpin Technologies http://www.espintechnologies.com/	USA	High performance dry wipes for removing dry dust in wood shop, paint shop, and finishing operations.	-

[14] Polycarbonate-based polyurethane
[15] Poly (D, L-lactide)

Nexture® fabrics	Finetex EnE http://www.ftene.com/	South Korea	Offer water and wind protection with a truly breathable difference. To be used for clothing and shoes.	-
Furniture				
Return focus pod featuring Phonix™	Collaboration between IQ Commercial and RevolutionFibres http://www.iqcommercial.co.nz/	New Zealand	Office partition with sound absorption function.	-
Pest control				
Bed Bug (With Pheromone Lure)	FiberTrap https://fibertrap.com/	USA	Microfiber bed bug trap.	
Nanofibers manufacturing				
Xantu.Layr®	RevolutionFibres https://www.revolutionfibres.com/	New Zealand	To be used in fibre reinforced thermoset polymer composite materials. Enhance mechanical performance of materials.	-
Wetlaid nonwoven fabrics	Hirose https://www.hirose-paper-mfg.co.jp/	Japan	To be used for medical, filter, fabric, food, daily necessities, print materials, battery separators, electronics-related materials, civil engineering construction.	Polyester, Polyolefin, PPS[16], Vinylon
NnF CERAM®	Pardam Nano4fibers https://www.nano4fibers.com/	Czech Republic	Inorganic nanofibrous powders. To be used for Li-ion batteries anode or cathode, li-ion battery/fuel cell separator, catalyst, catalyst support, photo catalyst, gas sensors, thermal insulators, metal or ceramic nano-composites, dehumidifiers, abrasives, thermal barrier coatings, filtration.	-

[16] Polyphenylene sulfide

Chapter 2
Materials and methods

2.1 Materials

PVA (Mowiol® 56-98) with molecular weight of 196,000 g/mol (98.0-98.8 mol% hydrolysed), PVA (Mowiol® 18-88) with molecular weight of 130,000 g/mol (99+% hydrolysed), PAA with molecular weight of 450,000 g/mol, ciprofloxacin (minimum purity of 98.0%), hydroxyapatite nanopowder (HAp) with a minimum purity of 90.0% and particle size lower than 200 nm and caffeine powder ReagentPlus® were purchased from Sigma-Aldrich. Anhydrous caffeine powder (MW 194.19 g/mol) was purchased from Amresco. Doxorubicin hydrochloride was purchased from Cyaman Chemical Company and Clarithromycin was purchased from Tokyo Chemical Industry Co., Ltd. Distilled water and ethanol were used as the solvents in the sample preparation. Raw propolis was collected from *Apis mellifera* hives located in Quitandinha in the state of Parana (PR), Brazil in Spring 2013 from *Baccharis uncinella* flora.

The U2OS human osteosarcoma cell line was kindly provided by the Genome Stability Lab of the National University of Ireland Galway. The NIH 3T3 Swiss mouse embryo fibroblasts cell line was bought from the American Type Culture Collection (ATCC).

2.2 Preparation of polymer solutions

Different concentration (% w/v) of PVA solutions with different MW were prepared in distilled water by heating. Dissolution was achieved by heating all type of mixtures to 75 ± 2 °C using electromagnetic stirrer till a homogenous and clear solution achieved. It usually took 1-3 h to completely dissolved the polymers. The solution was then cooled for 10 min at room temperature to remove any bubbles in the solution.

In Chapter 3, the 10 %w/v pure PVA and PVA/CAF solutions were prepared using PVA with molecular weight of 195,000. To prepare the PVA/CAF solutions, 3% of anhydrous caffeine powder (based on the weight of PVA) was added to the pure PVA solutions.

In Chapter 4, polymer solutions were prepared by dissolving PVA (MW 130,000 g/mol) in distilled water on a heater with a magnetic stirrer to prepare solutions having a concentration of 5±0.05% per weight in volume. As the polymer was completely dissolved, it was cooled down to room temperature. Drug and PAA, when appropriated, were added. Mass of drug added was 5±0.07% (%w/v), and 20±0.2% (%w/w) of PAA. As the PAA dissolved, the

temperature was increased to 50±5 °C. Thus, the hydroxyapatite was added into the necessary solutions in the amount of 5±0.5% (%w/w) of PVA. The solution was then stirred for 24 h at 600±10 rpm.

It is important to note that hydroxyapatite is a low solubility compound. Therefore, it is not completely dispersed in water. **Table 2.1** lists the reagents and their respective proportions to prepare the hydrogels studied in this work.

Table 2.1: Hydrogel solutions prepared. PVA and CIP were produced based on the volume of water used. HAp and PAA based on the amount of PVA used.

Sample	PVA (%w/v)	PAA (%w/w)	Ciprofloxacin (%v/v)	HAp (%w/w)
PVA	5.00	-	-	-
PVA-PAA	5.00	20.00	-	-
PVA-HAp	5.00	-	-	-
PVA-PAA-HAp	5.00	20.00	-	5.00
PVA-CIP	5.00	-	5.00	-
PVA-HAp-CIP	5.00	-	5.00	5.00
PVA-PAA-CIP	5.00	20.00	5.00	-
PVA-PAA-HAp-CIP	5.00	20.00	5.00	5.00

In addition, 5 %w/v pure PVA solutions with molecular weight of 195,000 g/mol were prepared. The PVA/CAF sphere was prepared by adding 3% of caffeine powder (based on the weight of PVA) into the PVA solution.

In Chapter 5, PVA (MW 195,000 g/mol) and PAA (MW 450,000 g/mol) polymeric solutions were prepared using distilled water and ethanol as illustrated in **Figure 2.1**. For PVA polymeric solution, 10 %w/v was prepared using distilled water and heated for 1.5 h. When the PVA solution was completely dissolved, ethanol was further added into the PVA solution with a ratio of 50:50 to achieve a final concentration of 5 %w/v. The solution was further stirred for 1 hour at 45 °C to prevent ethanol evaporation and to produce a homogeneous solution. Then, 3 %w/v PAA solution was prepared using ethanol and stirred for 2 h without heating.

1.5 mg/ml Doxorubicin hydrochloride (DOX) was incorporated into the PVA solution prior to electrospinning and this was labelled as PVA/DOX. While, two concentrations (2000 µM and 500 µM) of Clarithromycin (CLA) were incorporated into separate PAA solutions prior to electrospinning. The PAA solution that contained 2000 µM CLA was labelled as PAA/CLA high, while the PAA solution that contained 500 µM CLA was labelled as PAA/CLA low.

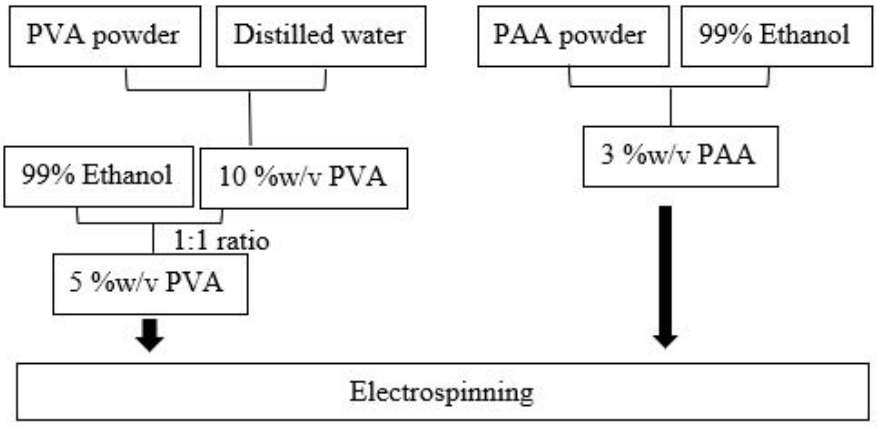

Figure 2.1: Schematic diagram of the preparation of PVA/PAA bilayer nanofibres.

In Chapter 6, 7 %(w/v) PVA solution (MW 195,000 g/mol) was prepared by heating 0.7 g PVA with 10 ml of distilled water for 3 h using electromagnetic stirrer. Four different concentration of propolis extract were used. 5 %(v/v), 10 %(v/v), 15 %(v/v) and 20 %(v/v) propolis extract based on the total volume of the polymer solution was added into the pre-cooled PVA solutions and the mixtures were then stirred overnight at 37 °C prior for electrospinning.

2.3 Solvent casting

In Chapter 3, solvent casting (SC) was performed by pipetting 1 ml of polymer solutions into 24-well plate and homogeneously spread on the surface of the wells. The samples were left at room temperature for at least 2 days and were allowed to evaporate completely before being stored or tested.

2.4 Preparation of propolis extract

Five batches propolis extract was prepared using ultrasound-assisted extraction method according to de lima *et. al*. [95]. 1 g raw propolis was grinded and mixed with 10 ml of 70 % ethanol. The mixture was then placed in an ultrasound bath for 1 hour at 70 °C. The propolis

extract was then stored in the fridge overnight to induce crystallisation of dissolved waxes. The waxes were then removed by filtration using a vacuum pump in the next day [96].

2.5 Determination of phenolic compounds in propolis extract

The propolis extract was scanned at 230-500 nm by Ultraviolet-visible (UV-VIS) spectrophotometer (Shimadzu Spectrophotometer UV-1280) triplicate. The UV- VIS spectra were recorded by diluting 1 ml of propolis extract with 100 ml of 70 % ethanol. The adsorption peak of phenolic compounds is normally located at the ultraviolet light range of 250 and 350 nm for spectrophotometric analysis [97].

2.6 Preparation of non-orientated and orientated hydrogels

In Chapter 3, a small portion of the pure PVA and PVA/CAF solution were cast into the pre-made dumbbell-shaped High Impact Polystyrene (HIPS) moulds. They were then subjected to 20 min fast freezing using liquid nitrogen (-196 ± 5 °C) and the solidified solutions were thawed for 4 h at 4 ± 2°C. Upon thawing, hydrogels were formed. This process is referred to as F/T technique. An additional uniaxial orientation was applied after each F/T cycle to produce the orientated PVA hydrogels (**Figure 2.*2***). The samples were produced with the thinnest possible configuration to refrain of obtaining two-strong orientations (x-axis and y-axis) that would interfere in the results and develop into a complex behaviour.

Table 2.*2* showed the types of samples prepared for the study. All samples with different F/T cycles and uniaxial orientation cycles (100% stretching strain per cycle) were dried at 40 ± 1 °C in Heraeus VT-5042 Vacuum Oven for 3 days. To maintain the geometry of PVA hydrogels, samples were dried using clamps in the extremities. This allowed the water to evaporate and minimizes the effect of forcing the polymer chains to deform.

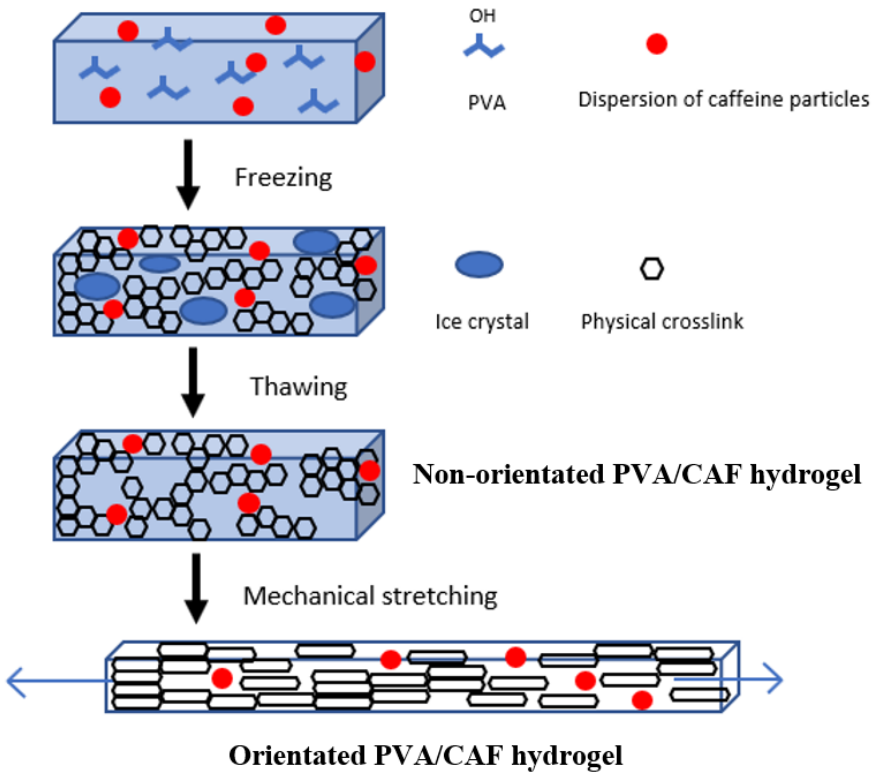

Figure 2.2: The schematic diagram of the orientated PVA/CAF hydrogel.

Table 2.2: Summary of the PVA hydrogel samples prepared.

Sample Code	Freeze-thaw cycle	Uniaxial orientation cycle (100% stretching strain)
PVA 1FT	1	0
PVA/CAF 1FT	1	0
PVA 2FT	2	0
PVA/CAF 2FT	2	0
PVA 1FT1S	1	1
PVA/CAF 1FT1S	1	1
PVA 2FT2S	2	2
PVA/CAF 2FT2S	2	2

2.7 Preparation of cryogenic spheres

The polymer solutions were dripped separately using a 100 µl micropipette into a container filled with pre-cooled ethyl acetate (AcOEt) (-80 ± 2 °C) in an ultra-low refrigerated-heating circulator (Julabo F81-ME) (**Figure 2.3**). The spheres were frozen instantaneously and kept in

AcOEt for 1 h to increase the physical crosslinking. They were removed from the circulator, placed on a petri dish and thawed in an ordinary freezer at -12 ± 2 °C for 20 min. This step was repeated three times and was labelled as a freeze cycle. After the first three freeze cycles, the spheres were then submitted to an ultra-low freezer (-80 °C ± 2) for 1 h freezing and 20 min thawing at room temperature for another three F/T cycles. This step was labelled as freeze cycle with thawing. The six F/T cycles (illustrated in **Table 2.*3***) was completed to maintain the spherical shape of the spheres. They were then submitted for drying at -57 ± 1 °C in a benchtop freeze dryer (Heto PowerDry LL3000 by Thermo Fisher Scientific) for 24 h. It was crucial that the spheres were thoroughly frozen before the drying stage started because the vacuum applied at the beginning of drying would cause any unfrozen product to "boil", altering the shape of spheres.

Finally, samples were left at 80 °C for 5 days in a vacuum oven to remove any remaining AcOEt residue.

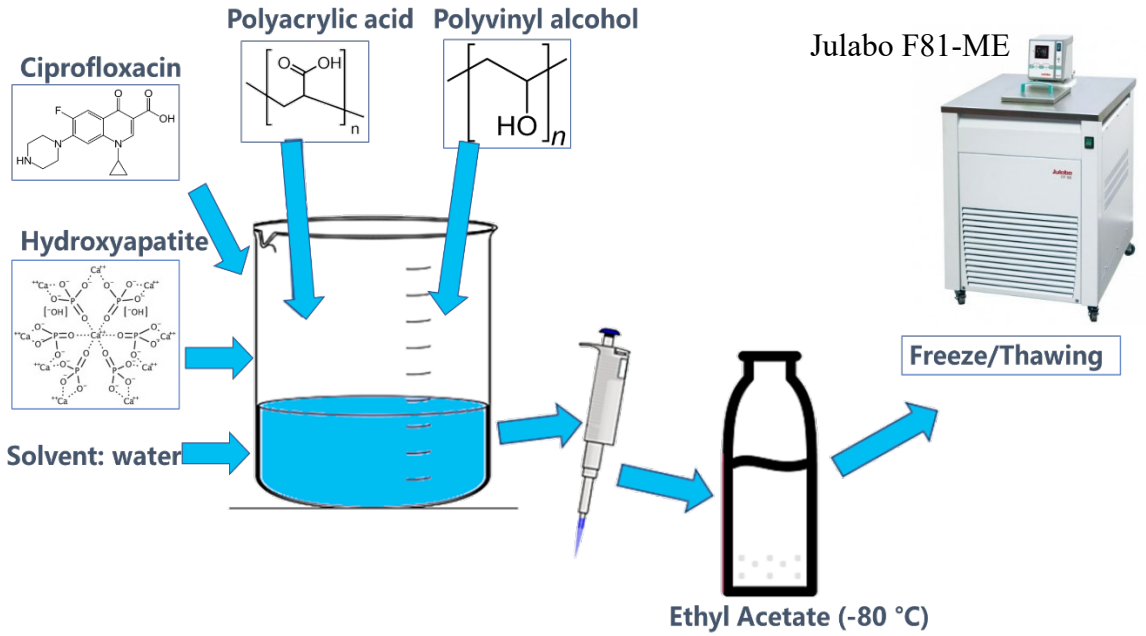

Figure 2.3: Representation of cryogenic spheres production (unscaled). After dissolving the correct materials in distilled water, they were dripped with a micropipette into a pre-cooled AcOEt, forming a sphere upon contact with the solvent, which was then followed by freeze-thawing technique.

Table 2.3: The temperature settings for each F/T cycles.

	No. of F/T cycles	Freezing temperature (°C)	Thawing temperature (°C)
Freeze cycles	1	-80	-12
	2	-80	-12
	3	-80	-12
Freeze cycles	4	-80	RT
with thawing	5	-80	RT
	6	-80	RT

* Freezing time = 1 h, thawing time = 20 min

2.8 Fabrication of electrospun nanofibres using electrospinning

In Chapter 5, a vertical electrospinning machine (Spraybase®, Ireland) was used to produce the electrospun nanofibres. Each polymeric solution was poured into a 15 ml centrifuge plastic test tube and placed inside a pressure vessel that was connected to a blunt 20 G needle via a PTFE tube. The tip of the needle was mounted at 13.5 cm vertically above a stainless-steel plate. The PVA was prepared using a voltage of 8.0 ± 0.5 kV. Conversely, the PAA nanofibres were prepared using a voltage of 10 ± 0.5 kV. Each polymeric solution was electrospun for 2 h. In order to prepare the PVA/PAA bilayer nanofibres, PAA nanofibres were directly spun onto the top of the PVA nanofibres layer (**Figure 2.4**).

The electrospun nanofibres samples (i.e. PVA, PAA and PVA/PAA bilayer) were annealed at two different temperatures, one batch at 150 °C for 40 min and another batch at 100 °C for 3 h in an oven. During the annealing process, no force was applied on the samples.

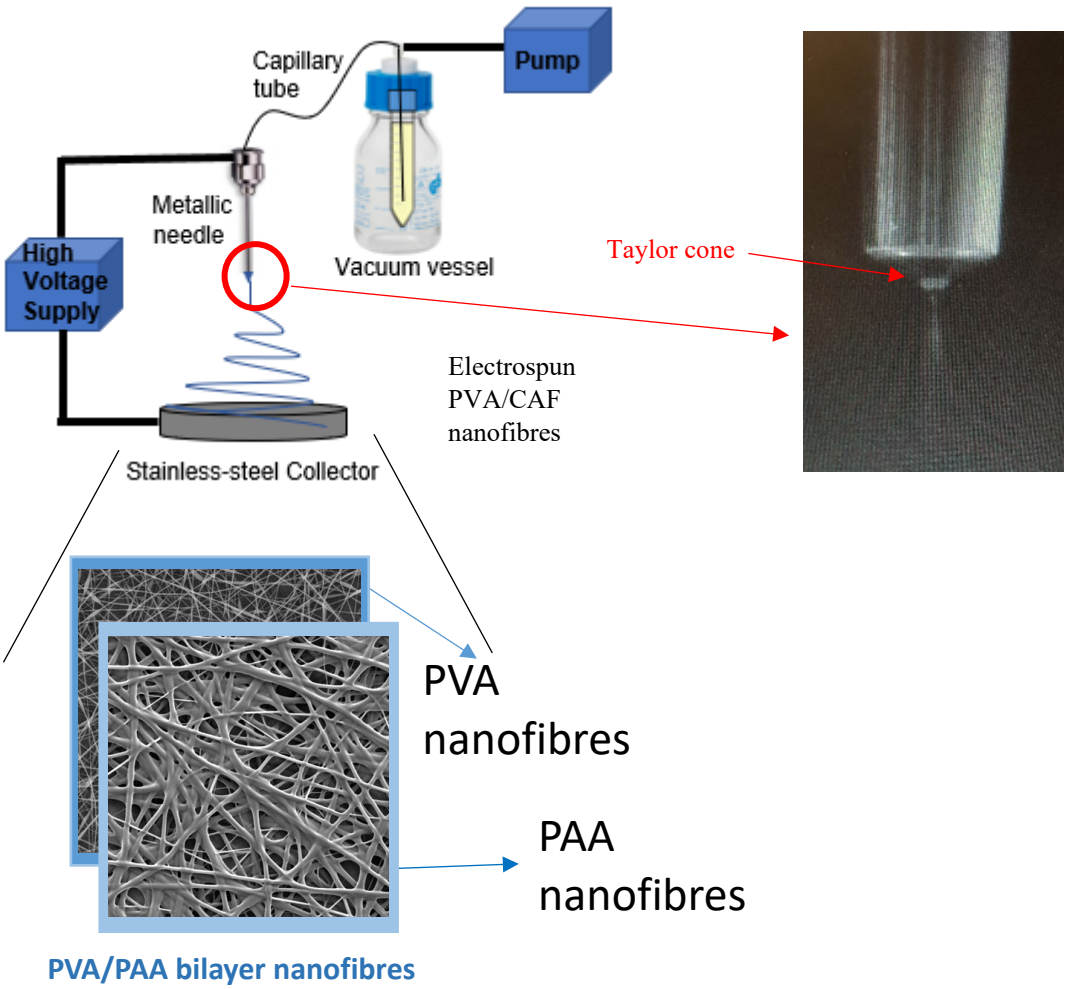

Figure 2.4: Schematic diagram of an electrospinning apparatus set up for bilayer nanofibres fabrication and showing the Taylor cone geometry during electrospinning.

In Chapter 6, a horizontal electrospinning machine (Tong Li Tech Nanofibre Electrospinning Unit, TL-Pro-BM) consists of a syringe pump attached with a syringe for controlled feeding rates, a rotating drum collector and a high voltage power supply (**Figure 2.5**). A 30 ml syringe was filled up with the PVA or PVA+propolis solution with the propolis concentration range from 5%-20%. The syringe was then connected to a blunt 22 G needle via a PTFE tube. The tip of the needle was mounted 15 cm away to the collector with the applied voltage of 22 kV. The polymer solution was delivered at a constant feeding rate of 2 ml/h. The electrospun nanofibres were collected after 9 h of electrospinning. The samples were designated as PVA as-spun and PVA+propolis as-spun nanofibres.

The freeze-thawed electrospun nanofibres were prepared by directly freezing the PVA as-spun nanofibres in liquid nitrogen (without immersing in an aqueous solution) for an hour and thawed at room temperature. The samples were designated as PVA FT and PVA+popolis FT nanofibres. All the as-spun and freeze-thawed nanofibres were stored in a desiccator and ready for testing.

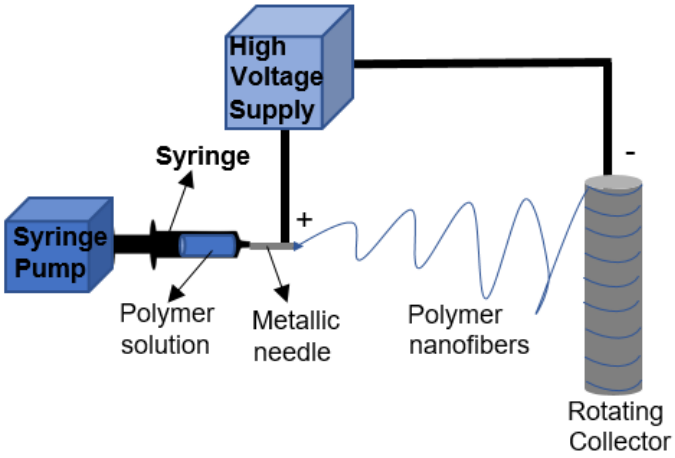

Figure 2.5: Schematic diagram of electrospinning apparatus.

2.9 Hydrogel characterisation

2.9.1 Scanning Electron Microscopy

The hydrogel samples were observed using a scanning electron microscope (SEM) (TESCAN Performance in Nanospace) with the back-scattered electron (BSE) mode (**Figure 2.6**). Prior to imaging, the samples were sputter-coated with a gold using Baltec SCD 005 for 110 s at 0.1 mBar vacuum. Images were recorded at a magnification range of 1,000 X-30,000 X.

In Chapter 3, the orientation at the cross-section of samples were observed. Prior to imaging, the samples were immersed in liquid nitrogen and broke into half to obtain cross-sectional regions.

In Chapter 4, the structure of the loaded PVA spheres cross-section and surface morphology was observed using SEM. To achieve this, the dried cryogenic spheres were immersed in liquid nitrogen and, after some time, were shattered using conventional tools in order to maintain the structural integrity of the materials. Energy dispersive X-ray (EDX) analysis was performed to confirm the elements presented in the hydrogels.

In Chapter 5, the surface and cross-section morphology of electrospun samples was observed. The diameter of the nanofibres were measured by taking 40 random readings from each sample using ImageJ software to get the mean value. While the average thickness of the PVA/PAA bilayer nanofibres were measured by taking 10 random readings at different locations of the cross section on the same image. In addition, the physical integrity behavior was examined from the changes of fibrous morphologies after swelling in pH 7.4 buffer.

In Chapter 6, the fibrous morphology of electrospun nanofibres samples were observed. The diameters of the nanofibres were measured using the image processing program, ImageJ by averaging 100 randomly selected nanofibres from the FESEM images. The structural integrity of nanofibres after swelling was also evaluated using FESEM.

2.9.2 Fourier transform infrared spectroscopy

PerkinElmer Spectrum One Fourier transform infrared spectroscopy (FTIR) (**Figure 2.7**) was used to investigate the functional groups of the hydrogel samples. The IR spectra were recorded in the spectral range of 500–4000 cm^{-1} and subsequent analysis were carried out using Spekwin32 spectroscopy software and SpectraGryph 1.2 software.

In Chapter 3, FTIR analysis was performed to investigate the existence of chemical interactions between caffeine and PVA in PVA/CAF hydrogels. In Chapter 5, FTIR analysis was performed to examine the chemical interaction of PVA and PAA electrospun nanofibres. In Chapter 6, the functional groups of propolis extract and PVA electrospun nanofibres were identified using FTIR.

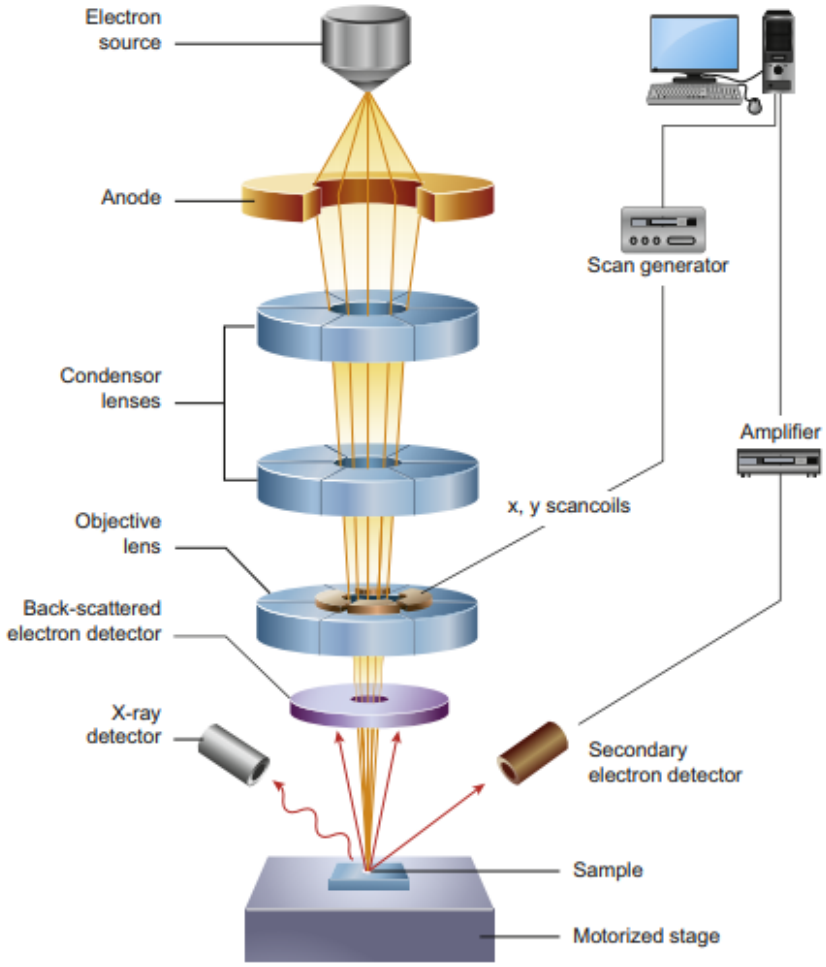

Figure 2.6 Schematic diagram of the key features of an SEM microscope [98]**.**

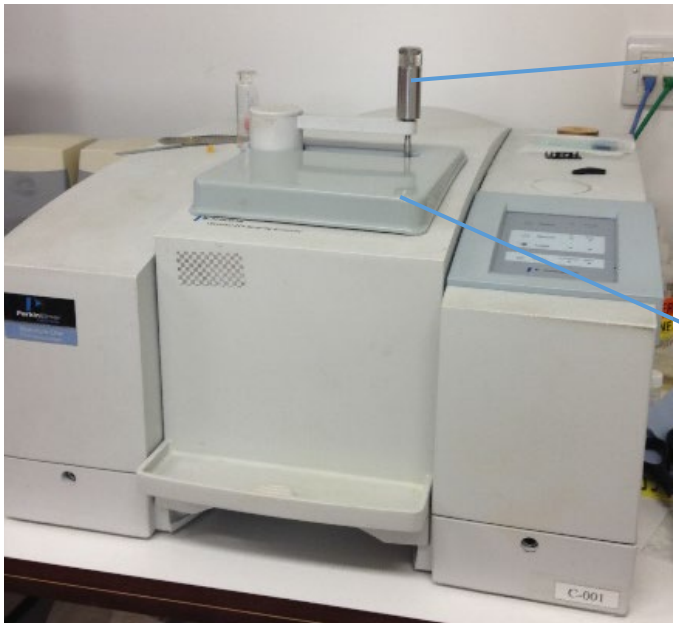

Figure 2.7: Fourier transform infrared spectroscopy.

2.9.3 Differential scanning calorimetry

For thermal analysis, differential scanning calorimetry was carried out using DSC2920 Modulated DSC from TA instruments (**Figure 2.*8***). All the samples were sealed in hermetic aluminum pans (Hermetic Pans, TA Instruments, USA) with the sample weight around 3-10 mg. The glass transition temperature and melting temperature presented in Chapter 3, a five-digit number that was automatically obtained by the equipment provider and should not be taken literally. The degree of crystallinity, X_c of the hydrogel samples was determined from the endothermic area using the following equation:

$$X_c = \Delta H_f / \Delta H_{fo}, \qquad (3)$$

where ΔHf is the measured enthalpy of fusion of the PVA hydrogel sample and ΔHfo is the thermodynamic enthalpy of fusion for 100% crystalline PVA (ΔHfo=150 J/g) [99]–[102].

In Chapter 3, one heating cycle was carried out. DSC was ramped from 20 °C to 280 °C with a heating rate of 10 °C/min under the flow of nitrogen gas. In Chapter 4, one heating cycle was carried out. DSC were ramped from 20 °C to 280 °C at 5 °C/min under the flow of nitrogen gas. In Chapter 5, a heating rate of 5 °C/min under the flow of nitrogen gas was applied to each sample. The samples were tested in 3 cycles (heating-cooling-heating cycle). In the first cycle, the sample was heated from 25 °C to 280 °C. In the second cycle, the sample was cooled in the furnace to 25 °C. In the third cycle, the sample was re-heated from 25 °C to 280 °C. In Chapter 6, two heating cycles and one cooling cycle were carried out on each sample. In each cycle, the sample was ramped from 20 °C to 250 °C with 5 °C/min heating rate and cooled down to 20 °C at the rate of 5 °C/min under the flow of nitrogen gas.

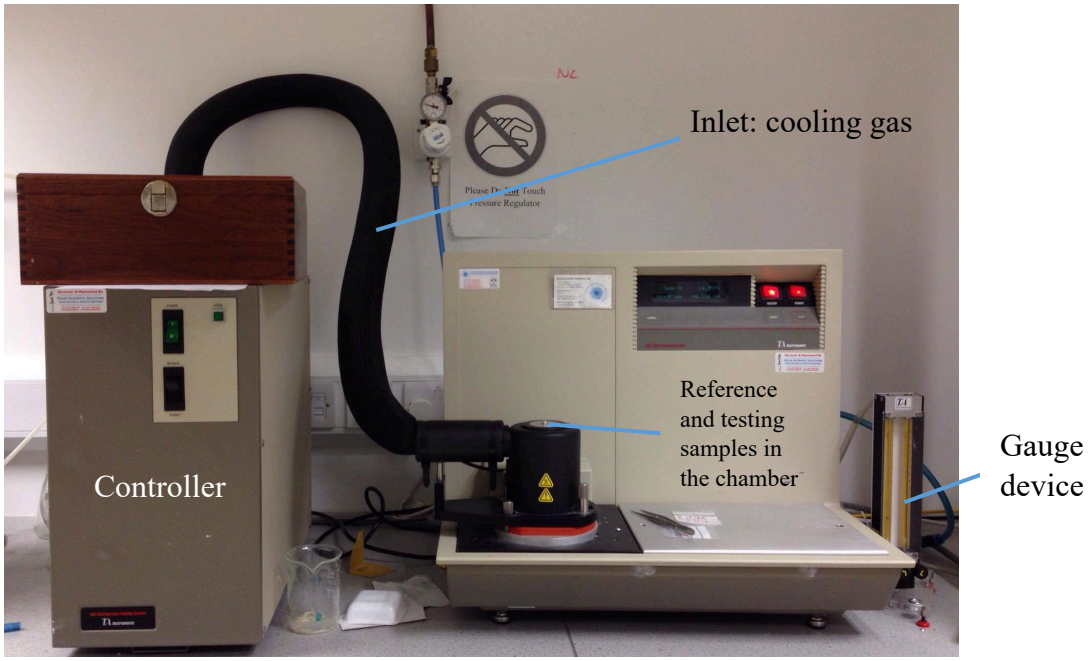

Figure 2.8: Differential scanning calorimetry.

2.9.4 Swelling behaviour

The swelling degree of the hydrogel samples (Chapter 3) and spheres (Chapter 4) was measured by immersing the dried samples in petri dishes that were filled with distilled water. In Chapter 4, in order to investigate pH responsiveness during swelling, swelling studies were also carried out at a pH of 2, 4, 6, 8 and 10, respectively. While, the electrospun PVA/PAA nanofibres (Chapter 5) and electrospun PVA/propolis nanofibres (Chapter 6) were swelled in the pH 7.4 buffer. The samples were allowed to soak at room temperature. The swollen hydrogels were removed from the water and blotted with filter paper to remove surface water. The samples were weighted and subsequently placed in water over the 24 h of soaking.

The degree of swelling was calculated using the following equation:

$$Degree\ of\ swelling = \frac{W_t - W_d}{W_d}\ x\ 100 \qquad (4)$$

where W_t is the weight of swollen hydrogels at regular intervals and W_d is the weight of dried hydrogels.

The percentage of water content of hydrogel samples was calculated by measuring the weight of swollen hydrogels at regular intervals (Wt) until the hydrogels reached the equilibrium state of swelling (weight= Ws) using the following equation:

$$water\ content\ (\%) = \frac{W_t - W_d}{W_s - W_d}\ x\ 100 \qquad (5)$$

2.9.5 Dynamic mechanical analysis

In Chapter 3, the viscoelastic behavior of the dried hydrogel samples was measured using a TA Instrument Q800 DMA with a tension mode (**Figure 2.*9***). The samples were cut into rectangular shapes (25×10 mm). They were tested at 3 °C/min heating rate with 1 Hz frequency over the temperature sweeps in a range of −80 °C to 220 °C and oscillation amplitude of 10 µm under a nitrogen atmosphere. The glass transition temperature presented in Chapter 3, a five-digit number that was automatically obtained by the equipment provider and should not be taken literally. The loss tangent, also defined as Tan Delta was obtained for each sample. It is equal to the ratio of loss modulus (G") to the storage modulus (G′).

In Chapter 5, the electrospun PVA, PAA, PVA/PAA nanofibre samples (15 x 8 mm) were analysed using a tension mode. They were tested at 5 °C/min heating rate under a nitrogen atmosphere with 1 Hz frequency and 0.1 N pre-load force. The temperature sweeps in a range of 25 °C to 160 °C.

In Chapter 6, the electrospun PVA and PVA+propolis nanofibre samples (15 x 8 mm) were analysised using a tensile mode, at a frequency of 1 Hz with 0.1 N pre-load force, and by heating from 25 °C to 200 °C of 5 °C/min.

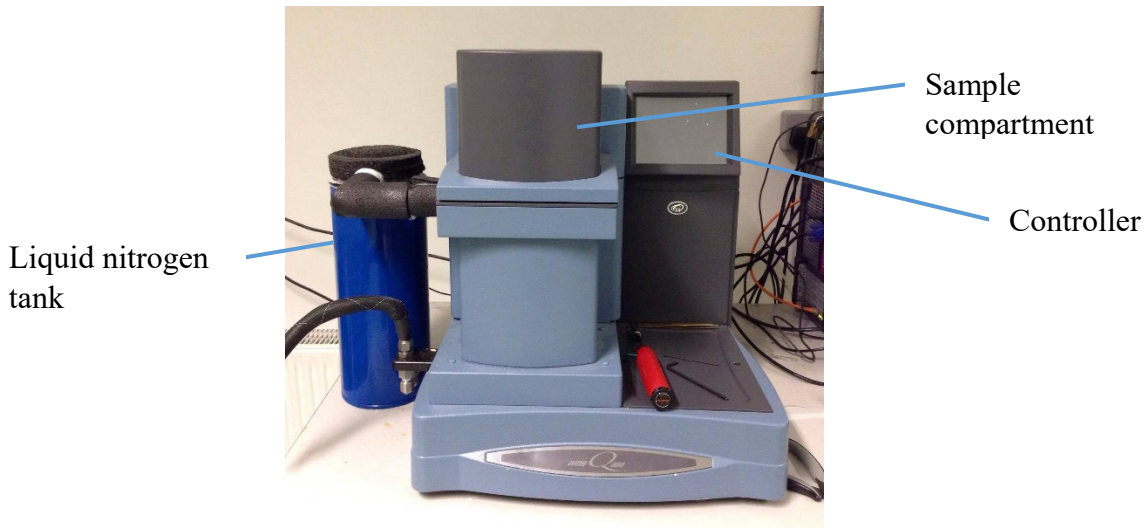

Figure 2.9: Dynamic mechanical analysis.

2.9.6 Tensile strength

In Chapter 3, a tensile test was used to evaluate the effect of the F/T cycles with uniaxial orientation on mechanical properties of the dried hydrogel samples. The test was carried out on a tabletop mechanical testing machine (Lloyd Instruments LRX material tester, AMETEK.Inc.) equipped with a gauge length of 60 mm and a drawing rate of 50 mm/min (**Figure 2.*10***). The dried hydrogel strips of 160 mm length, a width ranging between 14 and 1.5 mm and a thickness ranging between 1.5 and 0.25 mm were prepared. The dried samples were folded a little bit at the end of both sides to facilitate gripping in the mechanical testing apparatus. During the tests, the samples were stretched to break. All samples must break in the middle and not at the clamps. The mechanical test was repeated three times for each sample and the average values were used to plot the stress vs strain curves. The Young's modulus (E) of each sample was calculated by finding the maximum slope of the stress vs strain curves as followed:

$$Young's\ modulus = \frac{Stress}{Strain} = \frac{\frac{F}{A}}{\frac{\Delta L}{L_o}} \qquad (6)$$

where F is the force in Newtons (N), A is the cross-section area in m^2, ΔL is extension measured in meters and L_o is the original length measured in meters.

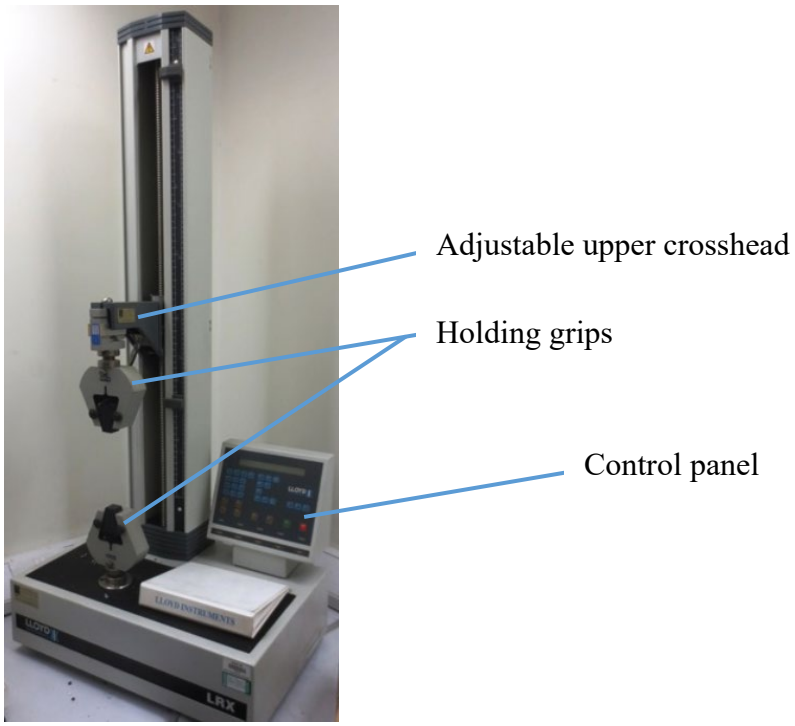

Figure 2.10: Tabletop mechanical testing machine.

2.9.7 X-ray Powder Diffraction

In Chapter 3, the X-ray diffractograms were obtained in a X'Pert MPD PRO diffractometer (PANalytical, Netherlands) with Cu Kα radiation (λ = 1.54060 Å) in the 2θ range of 10–60◦. The intensity and voltage applied were 40 mA and 40 kV.

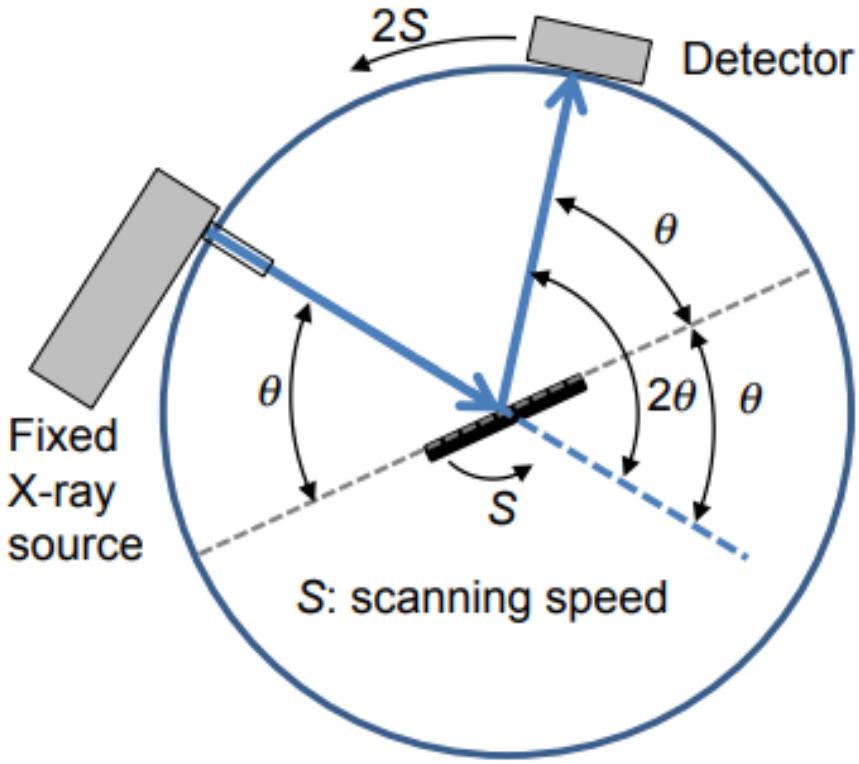

Figure 2.11: Schematic diagram of the basic principle of XRD [103]**.**

2.9.8 Drug release studies

Drug dissolution testing was evaluated using a DISTEK Model 2100B dissolution system (**Figure 2.*12***). In Chapter 3, 50 mg of the dried non-orientated and orientated PVA/CAF samples were weighed and tested in a phosphate buffer of pH 7.4 at 37±1 °C. The stir rate was set to 50 rpm with 900 ml of dissolution buffer used per vessel. The test was carried out for 60 min. 3 ml of each sample was taken every 5 min for the first 30 min and every 10 min for the next 30 min. 3 ml of dissolution buffer was replaced after each time of samples removal to maintain a sink condition. The samples were analysed using a UV/Vis spectrometer (Shimadzu Spectrophotometer UV-1280) at 273 nm with a 1 cm quartz cuvette. The concentration of caffeine release from the PVA hydrogels into the buffer was determined.

In Chapter 4, kinetics of drug release of the ciprofloxacin was evaluated through basket drug release model. Amounts of 10 mg of dried spheres were added into metallic baskets with 450 ml at 37±1 °C with a pH of 7 and a stirring rate of 50 rpm. Aliquots of 4 ml were withdrawn at different time intervals and had its absorbance measured by UV- VIS spectrometry at 322.8 nm. Furthermore, twenty dried PVA/CAF spheres with the weight around 33.42 mg were added into the metallic baskets with 450 ml pH of 7.4 buffer at 37±1 °C and a stirring rate of 100 rpm. Aliquots of 2 ml were withdrawn at different time intervals and had its absorbance measured at 273 nm.

In Chapter 5, the drug dissolution study was conducted using the rotating basket method at a speed of 100 rpm. The nanofibre samples were placed in 450 ml of phosphate buffer pH 6.5 at 37 ºC. 2 ml of sample were collected at specific time points and 2 ml of fresh buffer was replaced after each time of sample removal in order to maintain the sink condition. The amount of drug released was determined at the wavelength of 485 nm and 205 nm for Doxorubicin hydrochloride and clarithromycin, respectively using a UV/Vis Spectrophotometer.
In Chapter 6, a strip of the electrospun samples (29.8 cm x 3.0 cm) were placed in a 450 ml phosphate buffer of pH 7.4 at 37 °C with a stirring rate of 100 rpm. In order to maintain a sink condition, 3 ml of each sample was taken at specific interval and the same amount of fresh pH buffer was replaced after each time of samples removal. The taken samples were then read at 254 nm with a quartz cuvette using a UV/vis spectrometer.

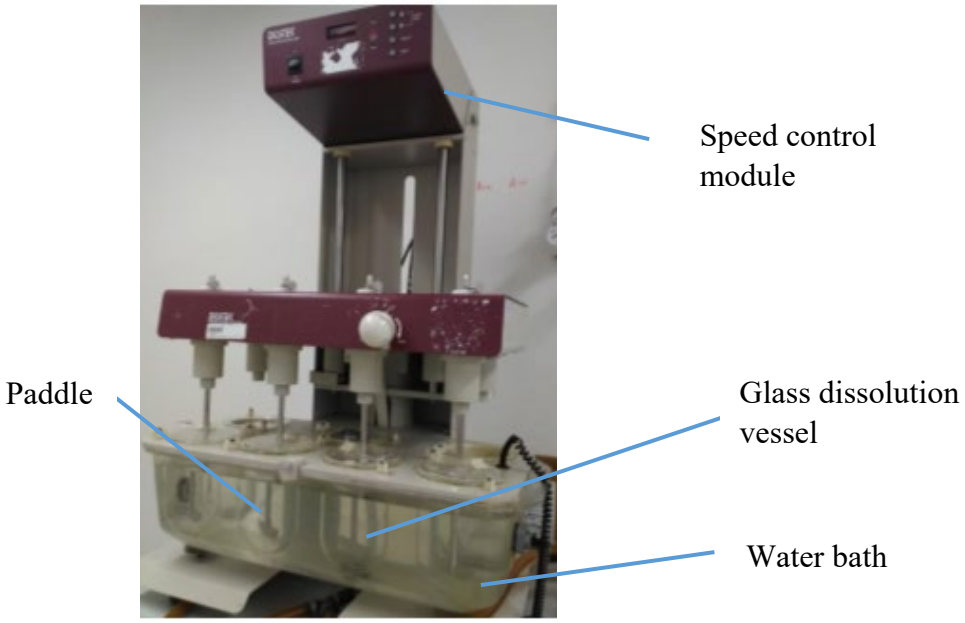

Figure 2.12: DISTEK Model 2100B dissolution system.

The dissolution profiles were evaluated using model dependent approaches such as zero-order, first-order, Higuchi, Korsmeyer-Peppas and Hixson-Crowell model. The five models were all based on different mathematical functions. The first mathematical model is called the zero-order model, which describes the drug release rate as independent of its concentration of the dissolved substance. The equation for zero-order release is as followed:

$$Q_t = Q_o + K_o t \quad (7)$$

,where Q_o is the initial amount of drug, Q_t is the cumulative amount of drug release at time "t", K is zero-order release constant and t is the time in hours. The second model is called the first-order model, which describes the drug release rate as dependence on the concentration of the dissolved substance. The equation for the first-order release is as followed:

$$LogQ_t = LogQ_o + Kt/2.303 \quad (8)$$

,where Q_t is the cumulative amount of drug release at time "t", Q_o is the initial amount of drug, K is first-order release constant and t is the time in hours. The third model is called the Higuchi model, which describes the drug release by Fick's law of diffusion [53]. The Higuchi release equation is as followed:

$$Q = K_H t^{\frac{1}{2}} \quad (9)$$

,where Q is the cumulative amount of drug release at time "t", K_H is Higuchi release constant and t is the time in hours. The fourth model is called the Korsmeyer–Peppas model and the equation is as followed:

$$\left(\frac{M_t}{M}\right) = K_m t^n \quad (10)$$

,where M_t is the amount of drug released at time "t", M is the total amount of drug in dosage form, K_m is the kinetic constant, n is the release exponent and t is the time in hours. Korsmeyer–Peppas model suggested the drug transport mechanism of the polymeric materials was controlled by more than one process according to the value of *n*. For the case of diffusional release mechanisms from polymeric films, $n \leq 0.45$ corresponds to a Fickian diffusion mechanism, $0.45 < n < 0.89$ to non-Fickian transport, $n = 0.89$ to Case II (relaxational) transport, and $n > 0.89$ to Super case II transport [104]. The fifth model is called Hixson–Crowell model, which describes the release from systems where there is a change in surface area and diameter of particles or tablets (Hixson & Crowell, 1931). The Hixson-Crowell equation is listed in the following way:

$$\sqrt[3]{W_o} - \sqrt[3]{W}_t = \kappa\, t \qquad (11)$$

where W_0 is the initial amount of caffeine, W_t is the remaining amount of drug at time t and κ (kappa) is a constant incorporating the surface volume relation [104]. The determination coefficient (R^2) of all five models were calculated and it was used as an indicator of the fitting level of the data to each model [106].

2.9.9 Disintegration and %weight loss studies

In Chapter 4, spheres containing ciprofloxacin and spheres containing caffeine were added in glass vials bottles filled with phosphate buffer pH 7 and placed in a laboratory drying oven with glass door (Salvis VC-20 vacuum oven) at 37 °C. Photographs were taken at different time points, i.e. at the beginning of the test, when the sphere is partially dissolved as well as when is fully dissolved. Spheres were photographed to visually indicate the progress of dissolution.

In Chapter 5, the unannealed and annealed PVA, PAA and PVA/PAA nanofibre samples (1 cm x 1 cm) were immersed in 5 ml of pH 7.4 buffer at room temperature. The appearance of samples was then observed at 0, 24 and 48 h. The weight loss was studied to examine the water stability of the nanofibre samples. The weight of dried samples was measured before immersed in 10 ml of pH 7.4 buffer at room temperature for 24 h. After that, the swollen samples were placed on soft paper to remove surface water and rinsed with distilled water to remove residual buffer salts. The wet samples were then dried in an oven at 37 °C until a constant weight achieved. The experiment was carried out in duplicate.

In Chapter 6, the electrospun nanofibre samples (1 cm x 1 cm) were placed in pH 7.4 buffer at room temperature for 24 h. Images of the samples were recorded after 24 h to observe the disintegration behavior. In order to evaluate the water stability of electrospun nanofibres, the weight loss study was carried by first weighing the dry samples before hydrating with distilled water for 24 h. After that, the swollen samples were placed in a freeze-dryer and dried to constant weight. The weight of re-dried samples was recorded and % weight loss was calculated. The experiment was carried out in triplicate.

2.9.10 Determination of conductivity, surface tension and viscosity of PVA and PVA+propolis solutions

In Chapter 6, the conductivity of the polymer solutions was measured using an EC 214 conductivity meter (Hanna instruments Inc., USA) at room temperature. The surface tension of the polymer solutions was determined by drop shape image analysis using goniometer at room temperature. The viscosity of the polymer solutions was measured using a rheometer (Discovery HR-1, TA instruments) with Peltier concentric cylinder at 60 °C.

2.10 *In Vitro* cytotoxicity testing

Cytotoxicity testing is useful in ensuring the biocompatibility of a medical device in accordance with ISO 10993-5: "Tests for Cytotoxicity-*In Vitro* Methods". This standard presented a number of test methods (i.e. direct contact, indirect contact and elution) designed to evaluate the cytotoxic effects of potential leachable from medical device materials. A negative cytotoxicity result indicates that a material is free of harmful chemical substances or has an insufficient quantity of them to cause acute effects under exaggerated conditions with isolated cells. Conversely, a positive cytotoxicity test result indicated that a material contains one or more toxic substances that could be of clinical importance.

2.10.1 Cell culturing

NIH 3T3 cells were cultured in Dulbecco's Modified Eagle Medium (DMEM) supplemented with 10% fetal bovine serum (FBS), 1% penicillin/streptomycin and 1% L-Glutamine at 37 °C with 5% CO_2 in a humidified incubator. The media composition was prepared as outlined in **Table 2.*4***. The medium was changed every 2 days. Once the cell monolayer was grown to 80-90% confluence in a 75 cm^2 flask, the cells were harvested by washing twice using PBS and followed by adding 5 ml trypsin-ethylenediaminetetraacetic acid (EDTA) to carry out trypsinisation and further 8 ml of fresh DMEM medium was added to inactivate trypsin-EDTA solution. Finally, the cells were centrifuged to obtain a pellet at 1500 rpm for 5 min and re-suspended in the fresh DMEM medium.

2.10.2 Subculture

When the cells have reached 80-90% confluency, the medium was removed from the plate and the monolayer was washed with PBS for twice. The monolayer was then treated with 2 ml 0.25% trypsin-EDTA solution and followed by adding 8 ml of fresh medium to deactivate the trypsin.

The cell suspension was centrifuged at 1500 rpm for 5 min to obtain a pellet of cells. The pellet was resuspended in 10 ml of fresh medium and split equally between five 75 cm^2 flasks.

Table 2.4: The composition of NIH 3T3 cell culture medium.

Component	Final concentration	Volume in ml
DMEM	-	440
FBS	10%	50
Penicillin/streptomycin	1%	5
L-Glutamine	1%	5

2.10.3 Cryopreservation of cells

In the presence of adhesion cultures, the cells needed to be 80-90% confluence before freezing down. The cell culture was treated with 2 ml 0.25% trypsin-EDTA solution and followed by adding 8 ml of fresh medium. The cell suspension was centrifuged at 1500 rpm for 5 min prior to re-suspend the pellet in 10 ml of freezing medium containing 9 ml FBS and 1ml Dimethyl sulfoxide (DMSO). 1 ml of the cell suspension was placed in each cryovial and directly put in to "Mr. Frosty" vial freezing container. The container was then placed in -80 °C freezer for at least 2 h before moving the vials to long-term storage in liquid nitrogen.

2.10.4 Reconstitution of frozen cell culture

A frozen vial that contained 1 ml cell suspension was removed from the liquid nitrogen and rapidly thawed at 37 °C. The cells were transferred to a sterile universal contained 10 ml pre-warmed DMEM medium, centrifuged at 1500 rpm for 5 min to obtain a pellet of cells. The cell pellet was re-suspended with 10 ml fresh DMEM medium. 2 ml cell suspension (1:5 split) was transferred to a 75 cm^2 flask and further 8 ml of DMEM medium was added into the flask. The cells were then incubated in a CO_2 incubator until the cell confluency reached 80%.

2.10.5 Cell counting for cell culturing

50 µl of cell suspension obtained from the subculture process was transferred into an Eppendorf tube and 100 µl of 0.2 M trypan blue was further added into the Eppendorf. The cell-contained solution was mixed by inverting several times to evenly distribute the cells. 10 µl of the solution was placed onto a haemocytometer which was covered with a glass slip. All viable cells in four

larger 1x1 mm squares were counted and the cell concentration was determined using the following equation:

$$Number\ of\ cells\ per\ mm^3 = \frac{N \times df \times 10^4}{S} \qquad (12)$$

,where *N* is the total number of cells counted in four squares, *df* is the dilution factor and *S* is the number of haemocytometer squares counted.

2.10.6 MTT assay

The MTT assay was carried out by adding 100 µl 0.1 mg/ml MTT solution into each well and incubated for 3 h in the 37 °C incubator. The MTT solution was removed and 150 µl DMSO solution was added into each well to dissolve the formazan crystals. The plate was read at 540 nm using SynergyTM HT BioTek Plate Reader. The cell viability was calculated using the following equation:

$$\frac{Abs\ @\ 540nm\ treated\ cell}{Abs\ @\ 540nm\ untreated\ cell} \times 100\% \qquad (13)$$

2.10.7 Direct contact assay

In Chapter 3, the test and control PVA and PVA/CAF hydrogel samples with 2 cm long were placed in a 6-wells plate and 2 ml of cells ($2.5x10^5$ cells/ml) were applied to the samples, incubated for 24 h at 37 °C in a CO_2 incubator. After incubation, the samples were removed and MTT assay was carried out in accordance to Section 2.10.6.

2.10.8 Elution test

In Chapter 3, the test and control PVA/CAF hydrogel samples were sterilised prior for cytotoxicity testing with Isopropanol alcohol (IPA) for 30 s, PBS for 30 s and followed by DMEM media for 30 s. The samples were then incubated in serum-supplemented DMEM medium for 24 h at 37 °C in a CO_2 incubator. 1, 5, 10 mg/ml of the hydrogel sample extracts were prepared and 200 µl of each dilution were applied to a cultured monolayer of NIH 3T3 cells ($2.5x10^5$ cells/ml) in a 96-well plate. The cells cultures were then returned to the 37 °C incubator for another 24 h. They were removed for microscopic examination on the next day and MTT assay was carried out in accordance to Section 2.10.6.

In Chapter 4, spheres were sterilised prior for cytotoxicity testing with IPA for30 s, PBS for 30 s and followed by DMEM media for 30 s. After that, the samples were incubated overnight

with DMEM. Serial dilution of sample extracts in 10000, 8000, 4000, 2000, 1000, 500, and 100 µg/ml using DMEM medium were prepared on the next day. The cytotoxicity potential of the microspheres was evaluated using an MTT colourimetric assay. 3T3 cells (1×10^4 cells/ml per well) were seeded in a 96-well plate and incubated at 37 °C and in 5% CO_2. Cells were then exposed to different concentrations, for 24 h and 48 h. After that, the medium was removed and MTT assay was carried out in accordance to Section 2.10.6.

In Chapter 5, the U2OS human osteosarcoma cell line was cultured in McCoy's 5A medium, supplemented with 10% FBS, 100 U/ml penicillin and 100 µg/ml streptomycin at 37 ºC in an incubator containing 5% CO_2. U2OS cells ($1x10^4$ cells/well) were seeded in 96-well plates and incubated for 48 h. The cells were then treated with elution samples (~8 mg nanofibres per 1 ml medium) and pure drugs samples **(Table 2.5)** for 24 h. After the treatment, the culture medium was removed and MTT assay was then carried out in accordance to Section 2.10.6.

Table 2.5: Pure drug values tested for cell viability using U2OS human osteosarcoma cell line.

Drug name	Concentration of CLA (mg/ml)	Concentration of DOX (µg/ml)
CLA H	0.374	-
CLA L	0.105	-
DOX L	-	2
DOX M	-	4
DOX H	-	8
CLA H-DOX L	0.374	2
CLA L-DOX L	0.105	2
CLA H-DOX M	0.374	4
CLA L-DOX M	0.105	4
CLA H-DOX H	0.374	8
CLA L-DOX H	0.105	8

2.10.9 Evaluation of combination drugs effect

In Chapter 5, based on the MTT results, the coefficient of drug interaction (CDI) was calculated to analyse the effects of drug combinations. The CDI value was determined as follows: CDI =AB/(A×B) [32], [33], where AB being the ratio of the drug association group (i.e. DOX+CLA) to the control group, and A or B are the ratios of the single drug group (i.e. DOX or CLA) to the control group. The CDI values of 1, < 1 or >1 express additive, synergistic or antagonistic effects, respectively. CDI value < 0.7 demonstrates strong synergism of the drug association.

2.11 Statistical analysis

The statistical difference was evaluated using Prism 5 GraphPad software (La Jolla, CA, USA) using Two-way ANOVA followed by a Dunnett's multiple comparisons test and One-way ANOVA followed by Tukey test. A P-value less than 0.05 were considered to be statistically significant. In all cases * was used for $p < 0.05$, ** for $p < 0.01$, and *** for $p < 0.001$, and **** for $p < 0.0001$. All experiments were performed at least in triplicates. Data were presented as mean ± SD for each result.

Chapter 3

The synthesis and characterisation of non-orientated and orientated physically crosslinked Polyvinyl alcohol hydrogels

3.1 Introduction

PVA is a widely used polymer material for producing hydrogel matrix. It has opened many opportunities for applications in the pharmaceutical area including drug delivery systems, regenerative medicine and tissue engineering. The numerous hydroxyl groups present on the backbone of PVA hydrogel offers the possibility of attaching drugs and cell signaling molecules, making it useful for purposes such as biologic carriers and drug carriers [17]. A biologic/drug carrier must have shown a major property of a controlled release of API within biological fluids in order to allow for optimisation of drug therapeutic abilities. However, the major concern of hydrogel is its low mechanical strength. This can be further improved by introducing crosslinks into the polymer matrix with repeated F/T cycles on the hydrogel. Freeze-thawed PVA hydrogels are thermoreversible and establish many valuable properties such as biocompatibility, high mechanical strength, viscoelasticity and swelling degree.

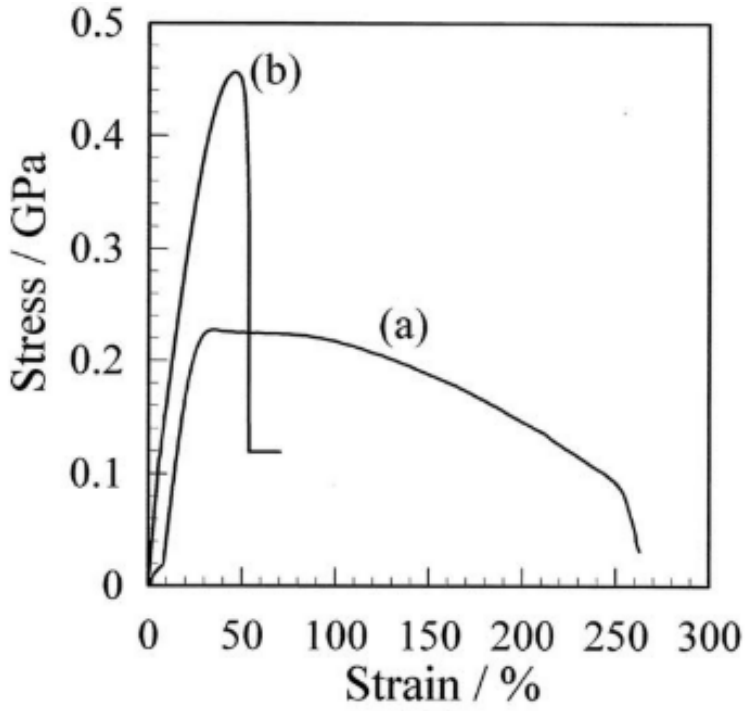

Figure 3.1: Stress–strain curves of stretched (a) 200% stretched and (b) 800% stretched PVA after annealing at 130 °C by Fukumori et. al. [107]**.**

The effect of orientation after the formation of freeze/thawed PVA films have been investigated as a function of the stretching ratio by Fukumori and Nakaoki [107], the stretched PVA after annealing at 130 °C showed that the molecular morphology of extended-chain crystals can further improve its tensile strength (**Figure 3.*1***) and Young's modulus. However, it is believed that the effect of stretching of PVA hydrogels in between freeze-thawing cycles can exhibit important parameters and physical aspects for modulation of drug delivery as well as mechanical properties. The hypothesis of this study is, as the stretching occurs the polymer chains have a tendency to align in the direction of the stretching and, in between the freeze-thawing cycles, physical crosslinking occurs throughout this orientation. In addition, the mechanical and chemical properties of PVA hydrogels are tuneable. The number of F/T cycles, temperature domain of freezing and thawing, stretching ratio and rate, concentration of PVA and drug, as well as MW of PVA can all alter the polymer structure if the aim is to analyse this behaviour [108]–[110].

For these reasons, in this study, the development of PVA hydrogels have acted as a drug carrier, while caffeine is utilised as a model drug. Caffeine is used to prepare fast-dissolving drug delivery systems due to its high water solubility [111], [112]. It is widely used as an analgesic adjuvant/mild stimulant in combination with an analgesic (e.g. paracetamol, ibuprofen, and aspirin). This type of medicines can augment their bioavailability and deliver rapid onset of action [113], [114]. The resultant PVA/CAF hydrogel samples have undergone detailed characterisation of chemical, polymer orientation, mechanical and thermal properties. A drug release study and swelling study have also undertaken and compared with the pure PVA hydrogel samples.

3.2 Result and Discussion

3.2.1 Visual inspection

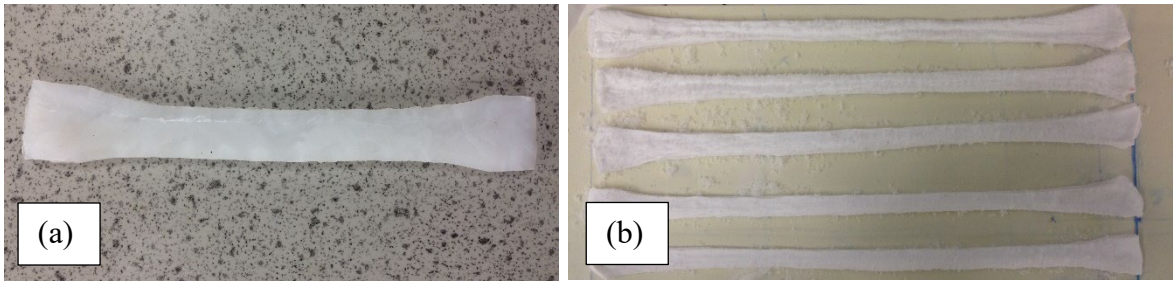

Figure 3.2: (a) Freeze-thawed PVA hydrogel before stretching, (b) Freeze-thawed PVA hydrogel after stretching.

Samples stretched (**Figure 3.*2*b**) presented a larger surface area due to the stretching mechanism but with a similar appearance to non-stretched samples (**Figure 3.*2*a**). The technique used to stretch the hydrogels was useful since no cracking or fractures in between the production (F/T cycles) of the stretched samples were detected.

It was found that maximum two complete F/T and uniaxial orientation cycles can be accomplished as the samples would be torn apart by applied forces during the third orientation cycles. This was because the water inside the hydrogel eliminated due to the formation of small crystallites that act as nucleation sites for crystallisation through a water-excluding process [107] during the repeated F/T cycles. The decrease of water content in the hydrogel would then led to the elasticity of the hydrogel decreased and sample to be broken.

3.2.2 Scanning Electron Microscopy (SEM)

The microstructure morphologies of the interior part of PVA and PVA/CAF hydrogel samples are shown in **Figure 3.3**. In these images, differences can be seen between PVA hydrogels that underwent only F/T cycles and PVA hydrogels that underwent F/T cycles with uniaxial orientations. The non-stretched samples (**Figure 3.3A-B and E-F**) presented a known morphology typical of PVA hydrogels. Small amounts of orientations were observed due to the drying mechanism to maintain its geometry. For stretched samples, it was possible to identify an increase in orientation in the morphology structure, with more cycles of stretching and F/T the orientation appeared to increase. However, when comparing the stretched samples to the non-stretched samples, non-stretched samples seem to indicate a smoother surface. Whereas stretched samples seem rougher, polymer chains are forced physically to change their direction. This occurred with the stress applied to the extremities of the stretched hydrogel as the point of forces and this results in the alignment of the chains in the direction of these points. This concept is further looked at the FTIR scans. The PVA/CAF 1FT1S and PVA/CAF 2FT2S samples have fewer orientations, being assigned to recrystallized caffeine during the drying process, as compared with the PVA 1FT1S and PVA 2FT2S samples. The formation of an amorphous dispersion of the drug in PVA hydrogels was desired for better orientation and drug dissolution. Furthermore, the alignment of these hydrogels appeared to be in a very specific direction (generally upwards in the SEM images in **Figure 3.3** and this was due to the

stretching mechanism produced, since one side was glued and the other side promoted the stretching, the chains were then aligned towards that specific point of force.

Moreover, the images also exhibited differences between pure PVA and caffeine-content PVA hydrogels. During F/T cycles, caffeine tends to form crystals in long needle-shaped [115], [116]. When compared with pure PVA hydrogel samples via SEM, the surface of caffeine-content PVA hydrogel sample (**Figure 3.3H**) was rougher. This was due to the drug crystallisation and it might have increased the crosslinks of the hydrogel system, acting as points of force against the applied force by the clamp in the drying mechanism. With more F/T cycles in PVA/CAF hydrogels exhibited a more aligned direction and it was improved with more stretching cycles.

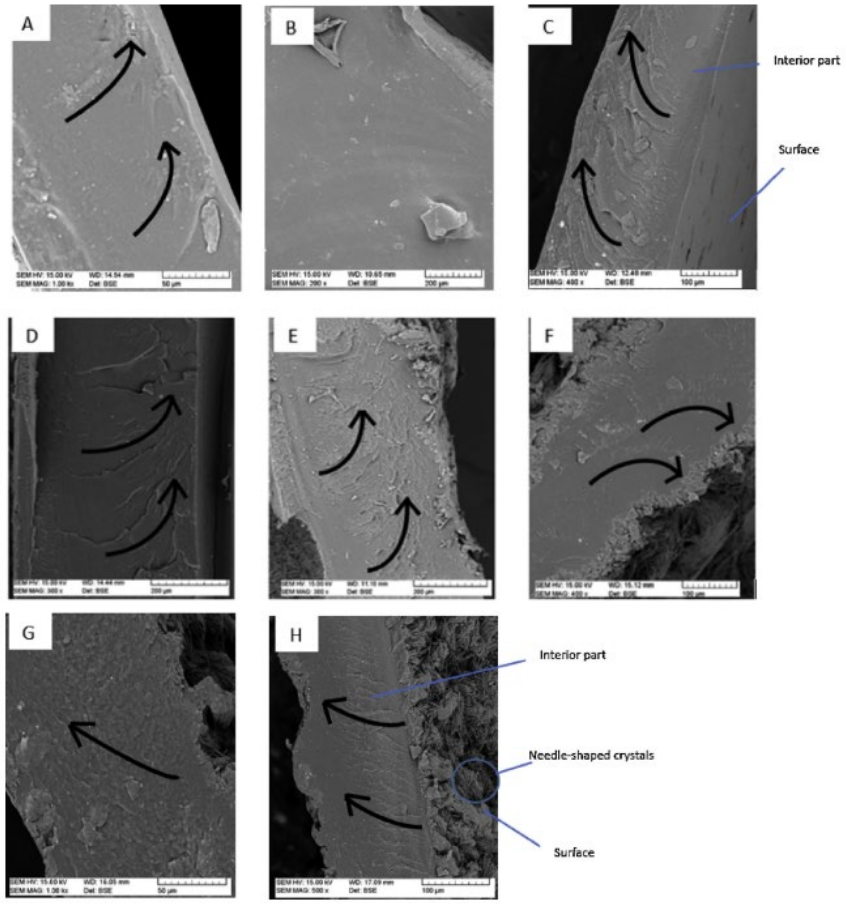

Figure 3.3: SEM micrographs of the interior part of PVA hydrogel. (A)PVA 1FT, (B) PVA 2FT, (C) PVA 1FT1S, (D) PVA 2FT2S, (E) PVA/CAF 1FT, (F) PVA/CAF 2FT, (G) PVA/CAF 1FT1S, (H) PVA/CAF 2FT2S. (*FT=Freeze-thawing cycle, S=uniaxial stretching cycle)

3.2.3 Fourier transform infrared spectroscopy (FTIR)

The FTIR spectra (**Figure 3.4**) have shown the characteristic peaks of the pure PVA and caffeine-content PVA hydrogel samples. All major peaks related to hydroxyl and acetate groups of PVA were observed. The large bands observed between 3570 and 3200 cm^{-1} [117] were linked to the stretching O–H from the intermolecular and intramolecular hydrogen bonds. The broadest band around 3300 cm^{-1} was attributed to the presence of water that was absorbed by PVA molecular chains as the orientation of chains led to a significant storage of water. In addition, the pure PVA hydrogels have broader and higher O-H peaks in comparison with PVA/CAF hydrogels. It is a fact that the peaks of the functional groups belonging to caffeine decreased and disappeared because they have been hidden by the strong and broad bond stretches of PVA hydrogel [53]. The vibrational band observed between 2850 and 3000 cm^{-1} [117] referred to the stretching C–H from alkyl groups. The peaks between 1750 and 1735 cm^{-1} [12] (region I in **Figure 3.4A**) were due to the stretching C=O from acetate group remaining from PVA. While the spectra showed two peaks in the region I in **Figure 3.4B** for the C=O stretching, which came from both acetate and carbonyl groups [118]. Furthermore, Fig. 3.3B also shown the major peaks of caffeine at 3100-3500 cm^{-1} (N-H stretching), 3000-3100 cm^{-1} (CH_3 stretching), 1400-1600 cm^{-1} (C=C stretching from aromatic ring), 1080-1360 cm^{-1} (C-N stretching) and 690-900 cm^{-1} (C-H bending & ring puckering) [118], [119]. The above data suggested that there were no physical or chemical interactions between PVA and caffeine in the hydrogel samples.

The degree of crystallinity of the hydrogels was obtained at 1141 cm^{-1} (region II in **Figure 3.4A and B**), which was further discussed in the DSC section. The presence of caffeine resulted in a broader peak at 1141 cm^{-1} due to the increase in crosslinking density caused by drug crystallisation. This was also supported by the work published by Seif and his research team, where it was shown that caffeine was a hydrophilic model drug with a high crystallisation tendency. When caffeine combined with PVA (hydrophilic polymer), it was used to form immediate release matrices [120].

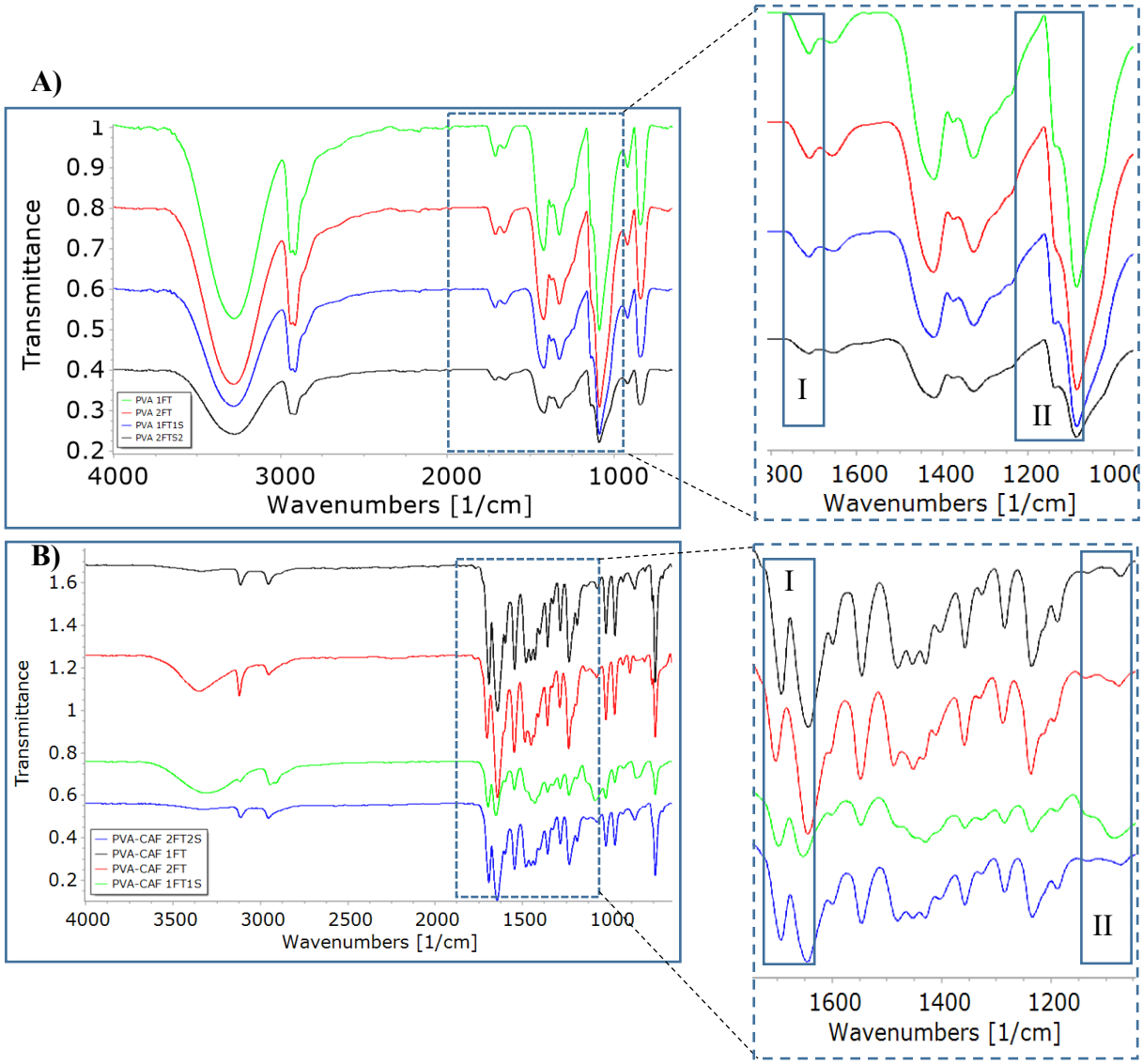

Figure 3.4: FTIR spectra of the original samples (a), PVA (b), PVA/CAF. (*CAF=caffeine)

3.2.4 Differential scanning calorimetry (DSC)

A typical DSC thermogram for a pure PVA sample exposed to repeated F/T and orientation cycles was shown in **Figure 3.5**. As seen in **Figure 3.5** and **Table 3.1**, the peak at the range of 40-64 °C, designated as the α relaxation, represents the glass transition temperature (Tg) of PVA. The Tg of the solvent cast pure PVA sample was at 64 °C and the Tg decreased to around 40 °C with the presence of F/T and orientation cycles. This low value was caused by a plasticising effect in the presence of water in the hydrogel samples and, consequently decreases the Tg [28]. While, the broad peak observed at approximately 140 °C represented the evaporation of residual water present in the samples [121], which also designated as the β

relaxation, was due to the relaxation in the PVA crystalline domains. The relatively large and sharp peak with a peak around 223 °C, represented the melting temperature (Tm) of the PVA crystalline domains [122]. Upon the increase of F/T and orientation cycles, the endothermic curve of PVA became sharper and its peak shifted to a higher temperature.

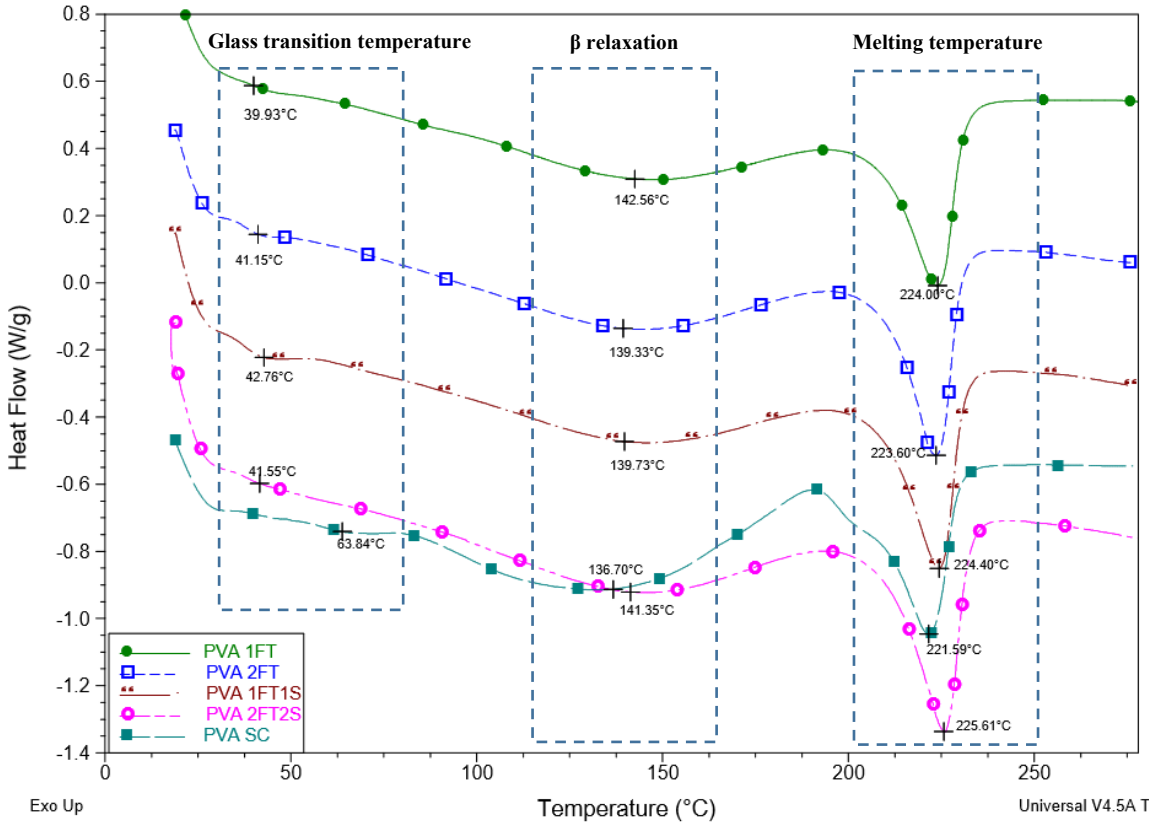

Figure 3.5: Thermal transitions in PVA samples. (*FT=freeze-thawing cycle, S=uniaxial stretching cycle, SC=solvent cast)

In another case, the effect of caffeine on the thermal transitions of PVA was showed in **Figure 3.6**. As seen in **Table 3.1**, the Tg appeared to increase with the addition of caffeine and the transitions picked up in the region of 45 to 66 °C for the PVA/CAF samples. An increase in Tg implied less chain mobility and therefore more inter- and intra-molecular hydrogen bonding contained in the PVA polymer [28]. However, the Tm was decreased from approximately 224 °C to between 215 °C and 218 °C in the presence of caffeine. The decrease seems counter-intuitive but it is explained by a study with caffeine and PET where caffeine reduces the free volume of the polymer by filling a portion of the idealized Langmuir "microvoids"[123]. This excess free volume where the caffeine is stored, decreases and further disappears when the Tg

is reached [124], then any caffeine in the PVA volume will be liberated to enrich the dissolved mode as the temperature increases and this effect produces a reduction in Tg values for the mixture compared to the neat polymer. In the case of the melting peak for caffeine, it was observed at around 236 °C [125], indicating the caffeine was not in the amorphous state.

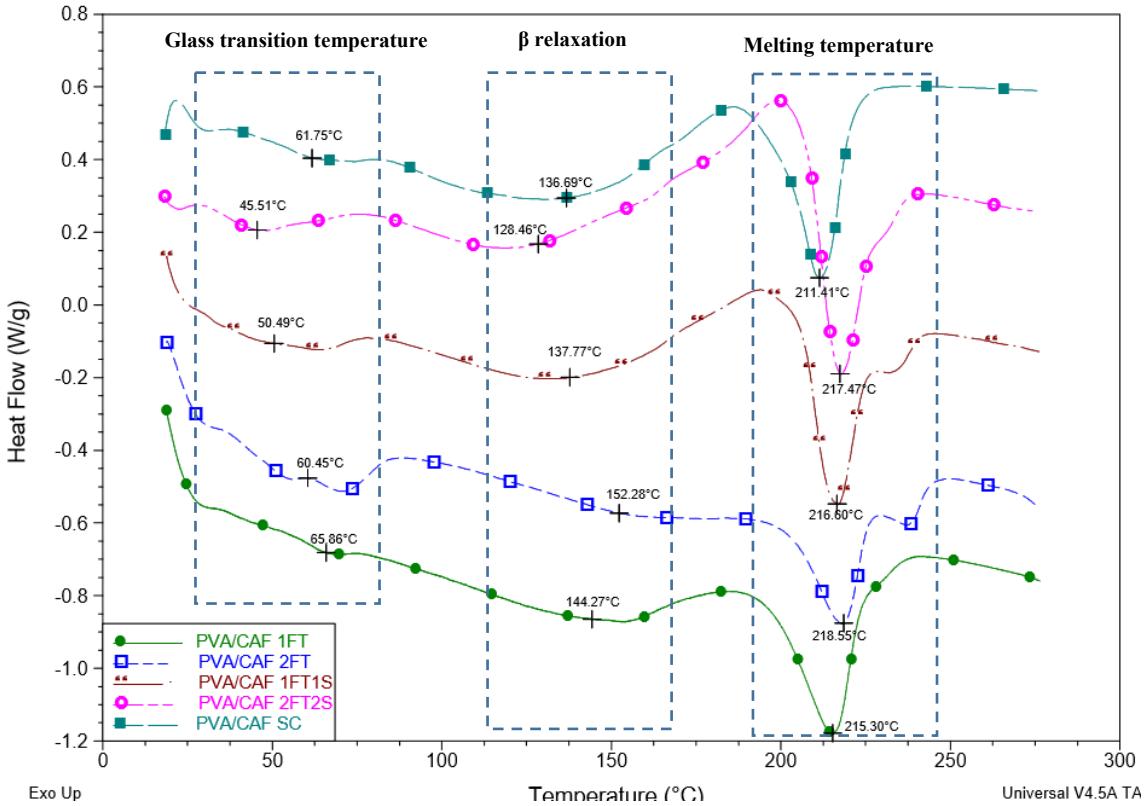

Figure 3.6: Thermal transitions in PVA/CAF samples. (*FT=freeze-thawing cycle, S=uniaxial stretching cycle, SC=solvent cast)

The degrees of crystallinity as shown in **Figure 3.7** were calculated by determining the area under the melting peak in **Figure 3.5** and **Figure 3.6**. As expected, increasing the F/T cycles leads to an increase in crystallinity. In addition, samples with stretching exhibit higher values of crystallinity compared to non-stretched samples and it further increases with more stretching. The ordered structure presented by the stretching allows more crosslinking density due to the easy arrangement of the chains; this further improves the Tg of the polymer. Furthermore, the PVA/CAF hydrogel samples have a higher degree of crystallinity in comparison to pure PVA hydrogel samples. The increase in crystallinity in PVA/CAF hydrogels is due to the caffeine is a crystalline material [53]. As the caffeine exhibited an endothermic peak around 235.5 °C (**Figure 3.6**), corresponding to crystalline caffeine melting point (Klímová & Leitner, 2012),

crystallisation of caffeine did not only occurred in PVA during F/T cycles but also in the drug itself. Studies have showed that caffeine remained in solid form at the melting point of PVA in hydrogel samples [126]. Furthermore, the increase of axial orientation has also exhibited the growth of the hydrogel crystallinity which caffeine seems to have further improved it. On the other hand, the DSC curve of the solvent casted PVA/CAF hydrogel did not show the characteristic melting peak of crystalline caffeine. This finding suggests that crystalline caffeine was converted into the amorphous state during the dissolving into water [127].

Table 3.1: The glass transition, β relaxation and melting temperatures of PVA and PVA/CAF samples. (*FT=freeze-thawing cycle, S=uniaxial stretching cycle, SC=solvent cast)

Sample	Tg (°C)	β relaxation (°C)	Tm (°C)
PVA 1FT	40	143	224
PVA 2FT	41	139	224
PVA 1FT1S	43	140	224
PVA 2FT2S	42	136	222
PVA SC	64	141	226
PVA/CAF 1FT	62	137	211
PVA/CAF 2FT	46	128	217
PVA/CAF 1FT1S	50	138	217
PVA/CAF 2FT2S	60	152	219
PVA/CAF SC	66	144	215

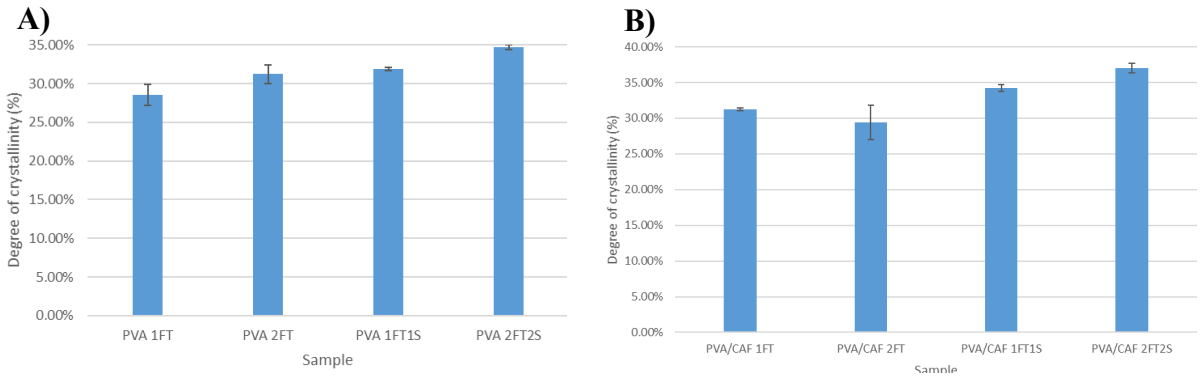

Figure 3.7: Degree of crystallinity, (A) PVA samples, (B) PVA/CAF samples. (*FT=freeze-thawing cycle, S=uniaxial stretching cycle, SC=solvent cast)

3.2.5 Swelling behaviour

Swelling characteristics, particularly the swelling degree in rehydrated pure PVA and PVA/CAF hydrogels were investigated, hydrogel samples were considered as swelling controlled-release devices. Before swelling occurs, the drug molecules were entrapped within the PVA polymer matrix and when the hydrogels absorbed water, the MW between cross-links increases and lead to polymer expansion. This essentially means that the water molecules penetrated between the polymer chains and enable the drug molecules to diffuse out of the swollen polymer networks [12], [128]. **Figure 3.8** depicted the degree of swelling and the water content (%) of the hydrogel as a function of time for pure PVA and PVA/CAF hydrogel samples. The swelling kinetics of hydrogels were estimated to variate in the number of F/T cycles and orientation cycles.

In **Figure 3.8A**, the maximum degree of swelling in 24 h for PVA 1FT, PVA 2FT, PVA 1FT1S and PVA 2FT2S are 301%, 295%, 380% and 371%, respectively. The pure PVA samples which have undergone F/T and orientation cycles have a higher swelling degree than the pure freeze-thawed samples without orientation cycles. In addition, PVA 1FT1S and PVA 2FT2S samples reached the equilibrium swelling after 24 h of soaking. Whereas PVA 1FT and PVA 2FT samples did not reach equilibrium within 24 h, both of the samples have only reached the water content of 91 % and 95 % respectively. This result can further indicate that the hydrogels with uniaxial orientation require lesser time to reach the EWC value.

In **Figure 3.8B**, PVA/CAF 1FT, PVA/CAF 2FT, PVA/CAF 1FT1S and PVA/CAF 2FT2S have the maximum degree of swelling of 287 %, 262 %, 307 % and 470 %, respectively. The PVA/CAF samples have a lower swelling degree when compared to pure PVA samples, except for the PVA/CAF 2FT2S. The low swelling values are attributed to the caffeine being a hydrophilic model drug with high crystallisation tendencies [115]; this caffeine crystallites within the PVA polymer chains leading to small size pores [129] and a decrease in swelling degree. In addition, PVA/CAF 2FT2S has the highest swelling degree of 470 % in contrast to all the PVA and PVA/CAF samples which might be caused by the crystallinity presence of caffeine and the increased number of orientation cycles applied to the hydrogel.

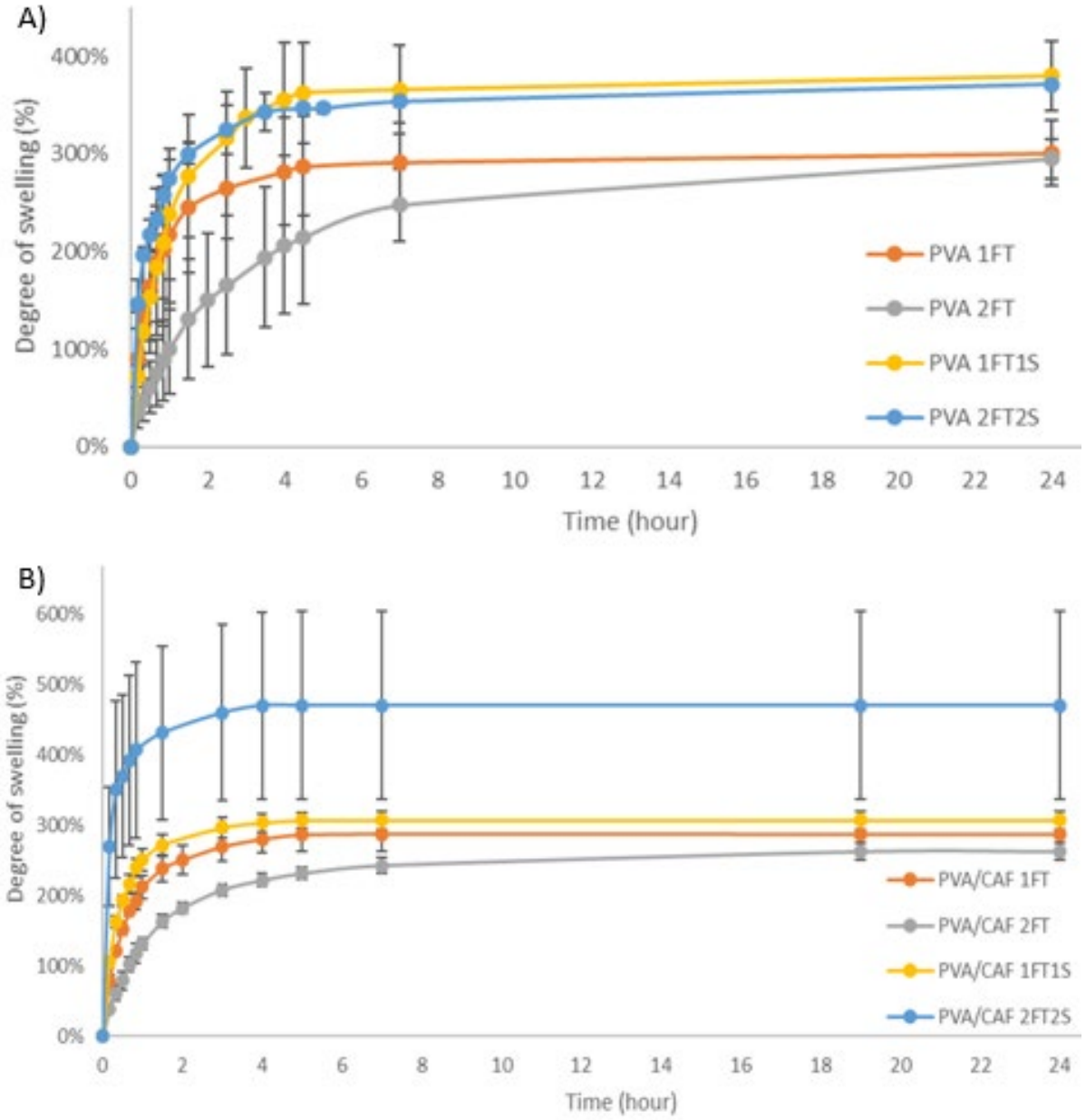

Figure 3.8: (A) Swelling degree of PVA samples, (B) Swelling degree of PVA/CAF samples.

The samples with one F/T cycle (i.e. PVA 1FT, PVA/CAF 1FT) have higher swelling degree than the samples that underwent two F/T cycles (i.e. PVA 2FT, PVA/CAF 2FT), because the degree of swelling consistently decreased with increasing numbers of F/T cycles [30]. Under the effect of orientation, the polymer chains have formed uniaxial polymer chain alignments while maintaining its structure and water content. Therefore, stretched samples gave a higher swelling degree in comparison with hydrogel samples without orientation. It is also verified that the release rate of caffeine increased with the degree of hydrogel swelling. Furthermore,

all PVA/CAF hydrogel samples have achieved an equilibrium state of swelling within 24 h. An equilibrium was achieved within 7 h for PVA/CAF 1FT, 19 h for PVA/CAF 2FT, 4.5 h for the PVA/CAF 1FT1S and 4 h for PVA/CAF 2FT2S. A reduction of time was determined to reach the EWC value within PVA/CAF samples. This confirmed that the presence of caffeine influences the swelling rate since the water can penetrate easily into the polymer network after the caffeine has dissolved into the water.

3.2.6 Dynamic mechanical analysis

From DMA measurements, the storage and loss modulus as a function of temperature was determined. The presence of a single Tg was observed in the tan δ versus temperature curves as can be seen in **Figure 3.9**. The thermogram has shown the Tg of the PVA 1FT, PVA 2FT, PVA 1FT1S and PVA 2FT2S, being 52 °C, 45°C, 48°C, and 47°C, respectively. Whereas the thermogram has shown the Tg of the PVA/CAF 1FT, PVA/CAF 2FT, PVA/CAF 1FT1S and PVA/CAF 2FT2S, being 40°C, 49°C, 49°C, and 52°C, respectively. As expected, with increasing crosslink density, this transition was slightly shifting toward higher temperatures [130]. This behaviour was due to the hydrogen bonding causing more chain stiffness and rigidity, leading to less flexibility in the PVA [131]. This property was confirmed by the tensile test. Moreover, the amount of water attained in the hydrogel was decreased with increasing crosslinking density. In general, as the water content of hydrogel decreases, the storage modulus increases and the Tg also increases [132]. The Tg data obtained from DMA are always different from that of DSC, and DMA-based Tg is more accurate [133]. While, with increasing uniaxial orientation, the transition was also shifting toward higher temperatures with a corresponding reduction in the value of tan δ. A decrease in Tan δ indicated a decrease in the phase angle δ, which meant the loss (viscous) modulus of the PVA/CAF 1FT1S and PVA/CAF 2FT2S hydrogels were lower than that of the PVA/CAF 1FT and PVA/CAF 2FT [134].

It is known that the mechanical properties of a polymer are related not only to its crystallinity (degree of crosslinking) but also to the molecular structure of its amorphous regions [135]. The height of the damping peak in the DMA curve in **Figure 3.*10*** showed the mobility of the polymer molecular chains that leads to damping of energy. The higher the peak, the less restriction there was toward the polymer chain motions [131]. As a result, the damping peak height decreases in the presence of uniaxial orientation, as the polymer chains highly packed together and the restriction for the polymer chain motions increased.

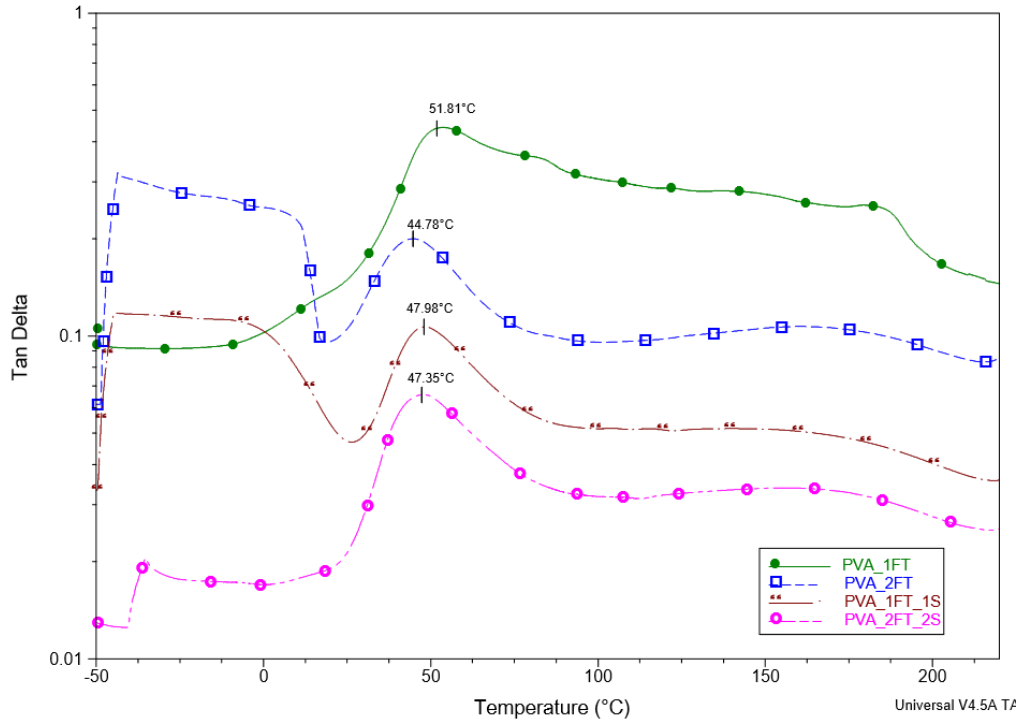

Figure 3.9: Tan δ of PVA hydrogels determined by DMA. (*FT=freeze-thawing cycle, S=uniaxial stretching cycle, SC=solvent cast)

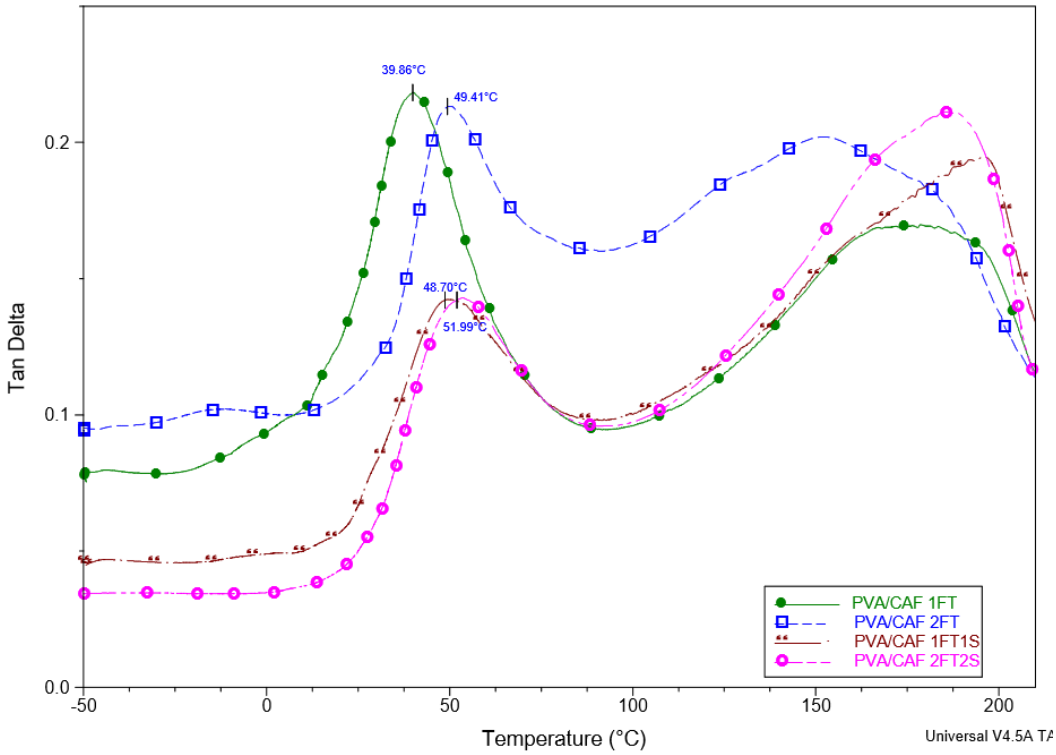

Figure 3.10: Tan δ of PVA/CAF hydrogels determined by DMA. (*FT=freeze-thawing cycle, S=uniaxial stretching cycle, SC=solvent cast)

3.2.7 Tensile strength

In the study, the tensile strain at break (ε_B) and the tensile stress at break (σ_B) were analysed. The results in both **Figure 3.11A** and **Figure 3.11B** showed that PVA and PVA/CAF hydrogel samples with two F/T cycles have the lowest tensile stress. Hydrogels behave in an elastic manner when they have lower tensile stress, so, the PVA 2FT and PVA/CAF 2FT samples were highly elastic. In contrast, when there was an addition of orientation cycles applied to the F/T samples, exhibited higher values of tensile stress. As a result, the PVA 2FT2S and PVA/CAF 2FT2S have the highest tensile stress and were very rigid which led to a decrease in the elasticity. Due to the polymer chains generated a higher degree of alignment during the orientation process, the water inside the hydrogel evaporated easily and caused the samples to become brittle, this was confirmed by the DMA results.

In **Figure 3.11A**, there was no remarkable change of tensile strains in the case of the pure PVA samples. It is likely that they have the same ratio of elongation to original length as the PVA samples have a similar percentage strain around 219%. While there was a significant difference in **Figure 3.11B** on the tensile strains. PVA/CAF 2FT2S has the lowest tensile strain and PVA/CAF 2FT has the highest tensile strain. This means PVA/CAF 2FT has higher elongation than PVA/CAF 2FT2S. El-Hadi et al. have determined that the maximum stress was always higher and the maximum elongation smaller [136]. The presence of caffeine and the effect of orientation varied the percentage strain in PVA hydrogels. The reason for the changes of tensile strength was the drug crystallisation [120]. During caffeine crystallisation, caffeine crystallites were being formed within the amorphous region of PVA. These phenomena have caused the density, crystallinity, tensile stress and Young's modulus (**Figure 3.12**) increased, and elongation at break decreased. Drug crystallisation can be restricted by fast water evaporation (e.g. electrospinning) which hindered the mobility of caffeine molecules in the hydrogels, thus exhibited the vitrification process [137]. This process gave the incorporated drug limited time to recrystallize favouring the formation of amorphous dispersions or solid solutions state [127], [137].

The Young's modulus **(Figure 3.12)** describes the stiffness of a solid material. The caffeine-content PVA hydrogel samples tend to have higher Young's modulus in comparison with pure PVA samples. In particular, the PVA/CAF hydrogels with orientation have higher Young's

modulus than pure PVA samples with orientation. The PVA/CAF 2FT2S reached the highest Young's modulus of 1462 MPA. It can be deduced that PVA hydrogels tend to increase its solidness and rigidness to undergo stretching when the number of cycles of F/T and orientation was increased, as well as drug crystallinity increases [30].

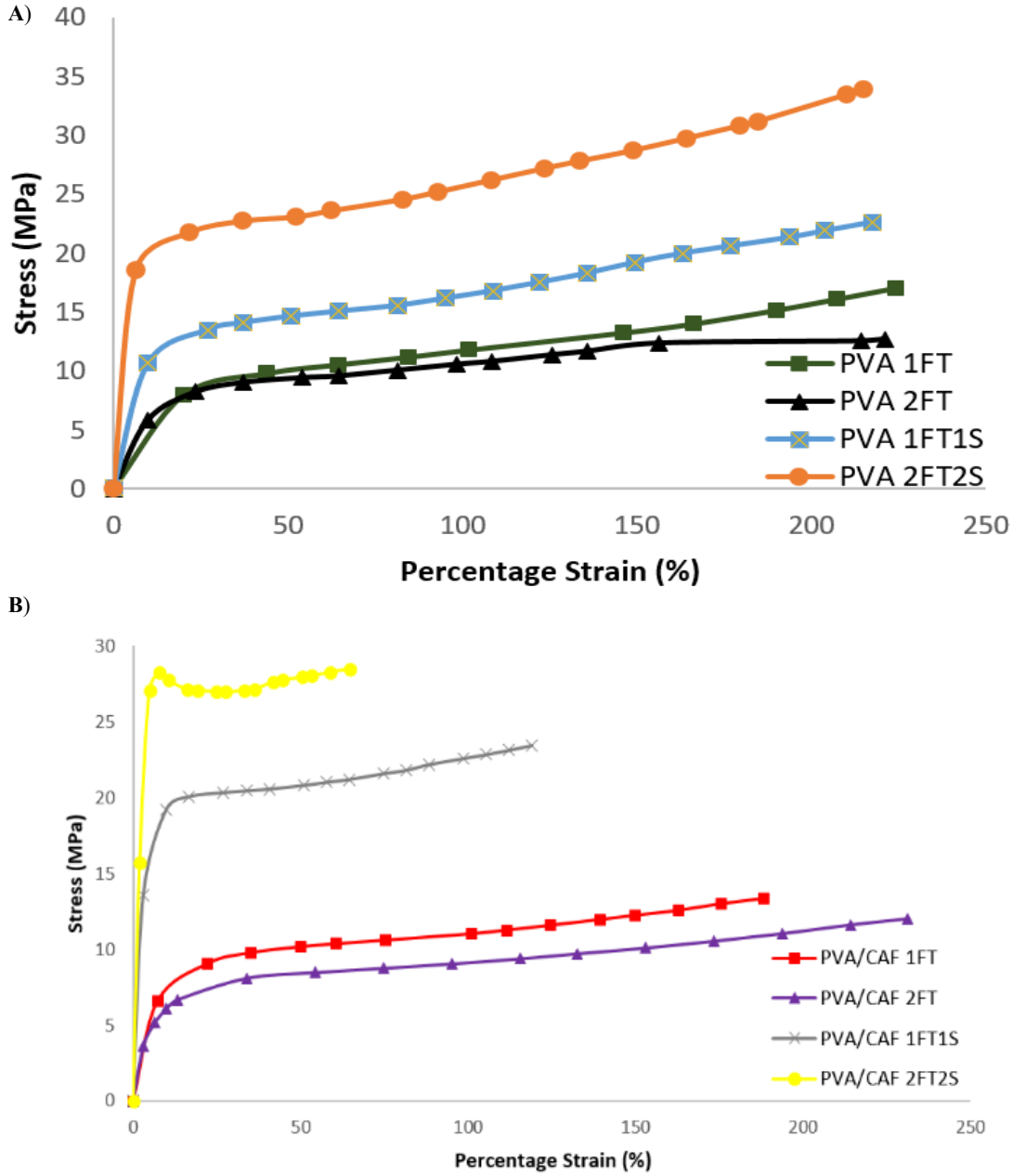

Figure 3.11: Stress vs strain curve for (A) PVA sample, (B) PVA/CAF sample. (*FT=freeze-thawing cycle, S=uniaxial stretching cycle, SC=solvent cast)

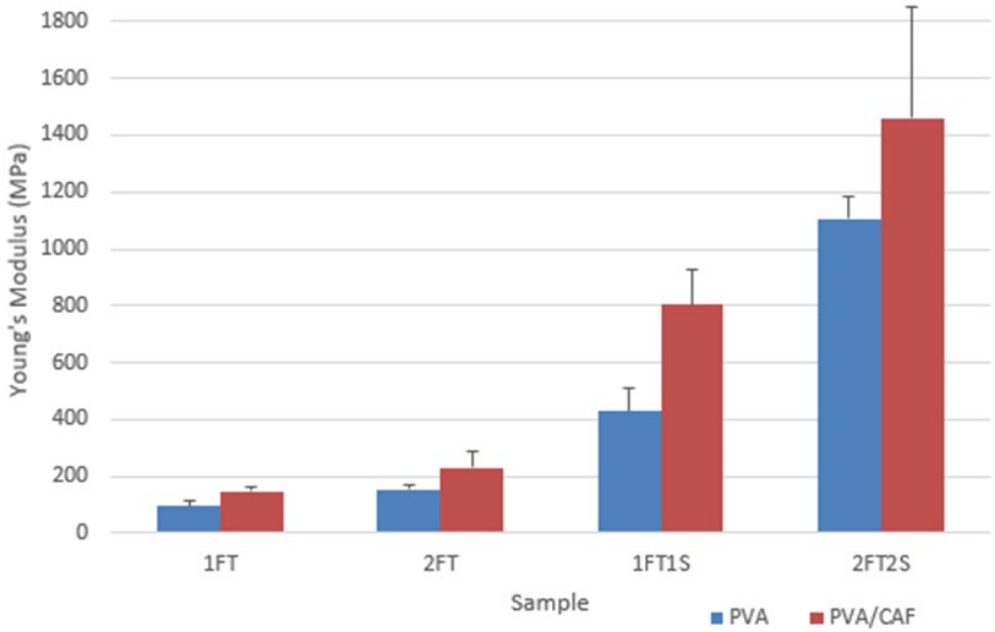

Figure 3.12: Young's modulus for PVA and PVA/CAF hydrogel samples. (*FT=freeze-thawing cycle, S=uniaxial stretching cycle, SC=solvent cast)

3.2.8 Caffeine release studies

The release profiles of caffeine-loaded PVA hydrogels was shown in **Figure 3.13**. It can be seen that there was a quick drug release at the first 10 min which followed by a slow rate of drug release. The full release of caffeine from PVA/CAF 1FT, PVA/CAF 2FT, PVA/CAF 1FT1S and PVA/CAF 2FT2S were obtained at 50 min, 60 min, 20 min and 15 min, respectively. This indicates that caffeine-loaded hydrogel samples without stretching have taken much longer to complete the drug release process. Whereas, the hydrogel samples with stretching can completely release the drug between 15 and 20 min. 80% of caffeine is released in the rate of 10.0% release/min and 20.0% release/min for PVA/CAF 1FT1S and PVA/CAF 2FT2S, respectively. This showed that the drug release rate increased with additional uniaxial orientation. In addition, the study showed an inverse correlation between the drug release rate and the degree of crosslinking resulted by F/T cycles. The hydrogel sample that undergoes a higher number of F/T cycles (i.e. PVA/CAF 2FT) has a lower caffeine release rate of 8.6% release/min when compared to PVA/CAF 1FT which has the drug release rate of 13.3% release/min at first 10 min. It can be explained by the fact that the increase of F/T cycles can cause the polymer network structure to become progressively dense and entangled [30]. The increase of crystallinity in the polymer consequently resulted in a decrease of diffusivity of PVA hydrogel and slowed down the drug release rate [138]. Hence, the introduction of uniaxial

orientation to the hydrogels can result in the polymer chains becoming increasingly aligned. These alignments encourage a rapid penetration of water into the polymer matrices that promote a remarkably fast drug release within an hour.

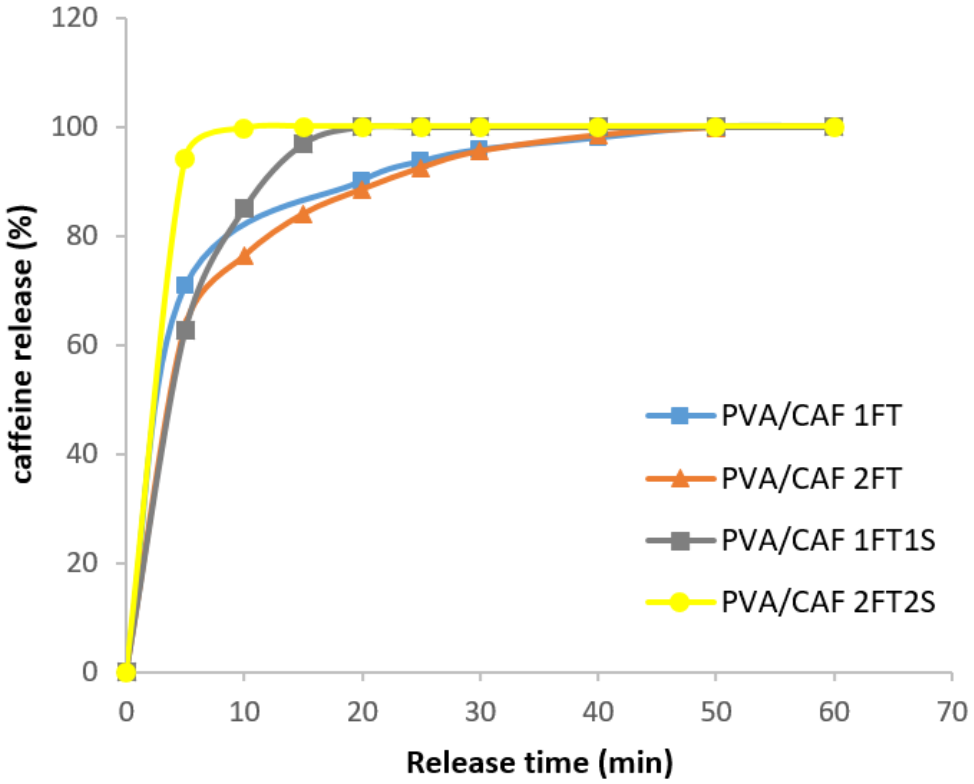

Figure 3.13: Release behaviour of caffeine from different F/T and uniaxial orientation cycles of PVA hydrogels. (*FT=freeze-thawing cycle, S=uniaxial stretching cycle, SC=solvent cast)

In the literature, a number of mathematical models have been used to interpret the drug release data and the associated release mechanism [139]. In this study, the zero-order, first-order, Higuchi Korsmeyer-Peppas and Hixson-Crowell models are used to evaluate the experimental released profile of caffeine obtained at room temperature. The determined fitting parameters (i.e. n and R^2) of all the models are listed in **Table 3.1**. In the drug release assays, it was observed that there was an initial burst effect, followed by zero-order kinetics ($R^2 = 0.9960$) for PVA/CAF 1FT and first-order kinetics ($R^2 = 0.9993$) for PVA/CAF 2FT. The differences in the release behaviour of PVA/CAF 1FT and PVA/CAF 2FT can be explained by the increase of crystallinity and denser network structure of the latter.

The drug release profile of caffeine from PVA hydrogels with orientation (i.e. PVA/CAF 1FT1S and PVA/CAF 2FT2S) have shown best fit with Hixson-Crowell model. The R^2 value for PVA/CAF 1FT1S and PVA/CAF 2FT2S was 0.9984 and 0.9904, respectively. Thus, they were related to the changes in the surface area of the hydrogels. The surface area of the orientated samples was directly proportional to the drug release rate. Due to an increase in orientation cycles, the samples surface area/volume ratio increases and it became more active, causing the drug release rate of the samples to increase. It can be deduced that the hydrogel samples with orientation were limited by the caffeine dissolution rate and not by the diffusion that might occur through the PVA polymeric matrix [140].

Although the result obtained in this work demonstrated that the release mechanism of caffeine seems to be proportional to the surface area of the oriented hydrogel, studies performed of PVA and caffeine [53], [141] suggests that the release mechanism is based on the diffusion of the entrapped caffeine to the exterior of the PVA membrane, Fickian diffusion. Although the fitting parameters for a Fickian diffusion (Higuchi model) are high for most of the polymers, i.e., they also tend to perform as a diffusion mechanism. These values decreased when the hydrogel was stretched, this was because of the preferable method of release changes because of the stress created and the aligned hydrogel produced, which is based on the surface area (Hixson-Crowell).

Table 3.2: Release behaviour of the drug-loaded PVA/caffeine hydrogels.

PVA/CAF	Zero order	First order	Higuchi	Korsmeyer-Peppas		Hixson–Crowell
	R^2	R^2	R^2	R^2	n	R^2
1FT	0.9960	0.9809	0.9808	0.9642	0.1427	0.9871
2FT	0.9800	0.9993	0.9956	0.9992	0.2564	0.9957
1FT1S	0.9696	0.9770	0.9902	0.9941	0.4020	0.9984
2FT2S	0.8033	0.9513	0.8591	0.9062	0.0579	0.9904

3.2.9 X-ray Powder Diffraction

In order to discriminate any variation in crystalline content as a result of uniaxial orientation addition to the PVA hydrogels, the XRD measurements on the PVA were carried out. As seen

in **Figure 3.14**, the first broad and high diffraction peak appeared at diffraction angles $2\theta = 20$ was corresponded to a typical crystalline atactic PVA, indicated PVA was crystalised after repeated F/T cycles and PVA polymer chains were still preserved in their semi-crystalline nature associated with the trans-planar chain conformation [142]. This might be due to the presence of strong intra-molecular hydrogen bonding in individual monomer unit of PVA and inter-molecular hydrogen bonding between its different monomer units [143]. The position of the first peak of PVA 2FT was slightly shifted to a lower value, which implied an increase in the size of the PVA crystallites. In contrast, the intensity of peaks decreased after introducing uniaxial orientation to the freeze-thawed PVA hydrogels (i.e. PVA 1FT1S and PVA 2FT2S). This showed that the PVA chains still retain their trans-planar chain conformation due to the intense intra- and intermolecular hydrogen bonding [99]. However, there was a decrease in the intensity of the doublet peaks and their peak area broadening, indicated that the crystallinity of PVA was suppressed. The second peak at diffraction angles $2\theta = 41$ was attributed to the presence of a low amount of water molecules within the PVA polymer chains [34].

XRD is also an important tool for characterizing the dispersion of caffeine in PVA hydrogel. In the case of the powder form of caffeine, it has an ordered crystalline matrix which describes the characteristic high-intensity peaks at 11.6, 11.9, 26.4 and 27.8 in the XRD [127]. As seen in **Figure 3.15**, there were high-density caffeine peaks observed around 12.0 and 24.0-28.0 as well as a low-density peak around 37.0 which depicted that the caffeine was not dispersed homogeneously in the PVA matrix and not in the amorphous form. This implied the drug was not successfully encapsulated in the hydrogel samples. Same was further supported by the DSC (**Figure 3.6**), the melting peak for caffeine at 236 °C was observed in the PVA/CAF hydrogels. When comparing the PVA and PVA/CAF samples, after integrating caffeine into PVA, the position of the peak at 20 was slightly shifted to a higher value, indicated a decrease in the size of the PVA crystallites. Furthermore, it was observed that the peak area for PVA/CAF 1FT1S and PVA/CAF 2FT2S at the diffraction peak of 41 were broader than PVA/CAF 1FT, PVA/CAF 2FT and PVA/CAF SC. It might be attributed to the PVA structural change from the lamellar structure to the microfibrillar structure associated with the lamellar break-up by strong elongational stress during uniaxial orientation [99].

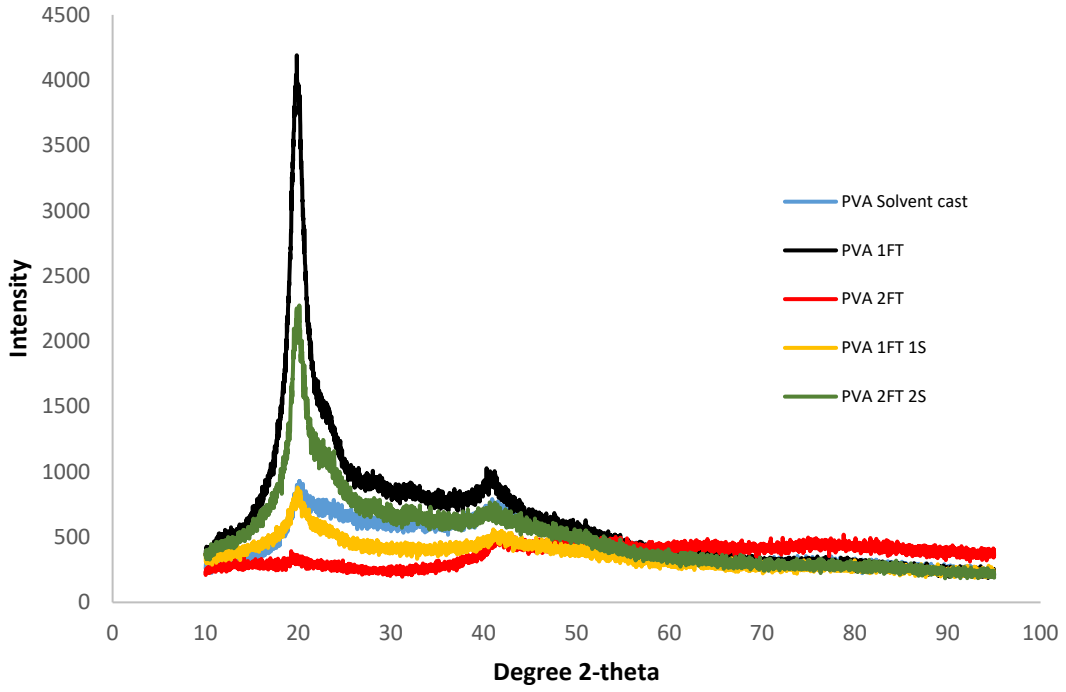

Figure 3.14: XRD for non-orientated and orientated PVA samples. (*FT=freeze-thawing cycle, S=uniaxial stretching cycle, SC=solvent cast)

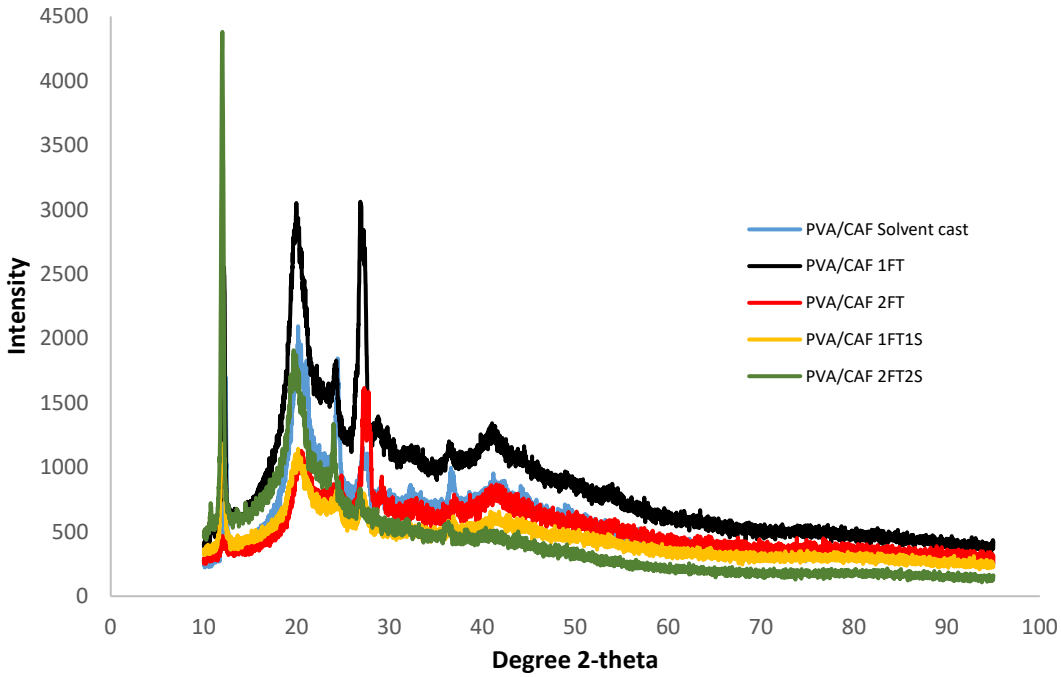

Figure 3.15: XRD for non-orientated and orientated PVA/CAF samples. (*FT=freeze-thawing cycle, S=uniaxial stretching cycle, SC=solvent cast)

3.2.10 Direct contact assay for orientated and non-orientated hydrogels

The percentage of cell viability of both pure PVA and PVA/CAF hydrogels were determined by quantifying the violet coloured formazan crystals formed during the MTT assay. It is a fact that the amount of formazan produced is directly proportional to the number of viable cells. As shown in **Figure 3.16**, the hydrogel samples were directly placed on top of cell layers and the cell viability of PVA SC, PVA 1FT, PVA 2FT, PVA 1FT1S and PVA 2FT2S were 84%, 79% and 72%, 20% and 20% respectively. It implied that when PVA SC, PVA 1FT and PVA 2FT treated with 3T3 cells, they had a non-toxic effect, according to ISO 10993-5 (2009) with cell viability being not lower than 72%. Whereas, a very low degree of cell viability was observed for the both orientated PVA samples: PVA 1FT1S and PVA 2FT2S. It was investigated that the orientated samples were not toxic as they had the same composition as PVA SC, PVA 1FT and PVA 2FT. There was a decrease in viable cells at the bottom of the wells because when the orientated hydrogels contacted with the medium, they became curve and were not able to properly sit on the wells. Therefore, it was predicted that majority of the cells might be attached on the hydrogels or still flown in the medium. When the orientated hydrogels and medium were removed, the cells were also being removed, resulting in a low percentage of viable cells on the wells. Further analysis should be carried out by analysing the orientated hydrogels on a fluorescent microscope to prove that the polymer chain alignment on the orientated hydrogels improved the cell attachment, indicated its good biocompatibility and potentially used for tissue regeneration.

All the caffeine-contented PVA samples had a very low percentage of cell viability. PVA/CAF SC, PVA/CAF 1FT, PVA/CAF 2FT, PVA/CAF 1FT1S and PVA/CAF 2FT2S had the cell viability at 15%, 16%, 14%, 20% and 10% respectively. Due to the high concentration of caffeine in the cell medium, it caused a huge cell dead in the wells. Therefore, the maximum caffeine concentration that suitable for cell growth were found out using the elution study with a varies of PVA/CAF concentrations (**Figure 3.18**). The concentrations that revealed percentage cytotoxicity of less than 28% was considered as non-cytotoxic.

3.2.11 Elution test for orientated and non-orientated hydrogels

According to **Figure 3.17,** all the PVA samples were non-toxic at 1 mg/ml. The PVA SC remained non-toxic at 5 and 10 mg/ml as it had the cell viability of 95% and 82%, respectively. The PVA 1FT also remained non-toxic at 5 and 10 mg/ml with the cell viability at 88% and

81%, respectively. However, the PVA 2FT, PVA 1FT1S and PVA 2FT2S hydrogels became toxic from the concentration of 5 and 10 mg/ml. In addition, as seen in **Figure 3.18**, the caffeine-contented PVA samples did not induce any substantial toxicity at 1 mg/ml. It was observed that PVA/CAF hydrogels should not exceed the concentration of 5 mg/ml as there was a significant decrease in cell viability at 5 mg/ml. Therefore, it can be concluded that the PVA and PVA/CAF hydrogel samples were suitable for cell proliferation at the concentration range of 1 – 4 mg/ml.

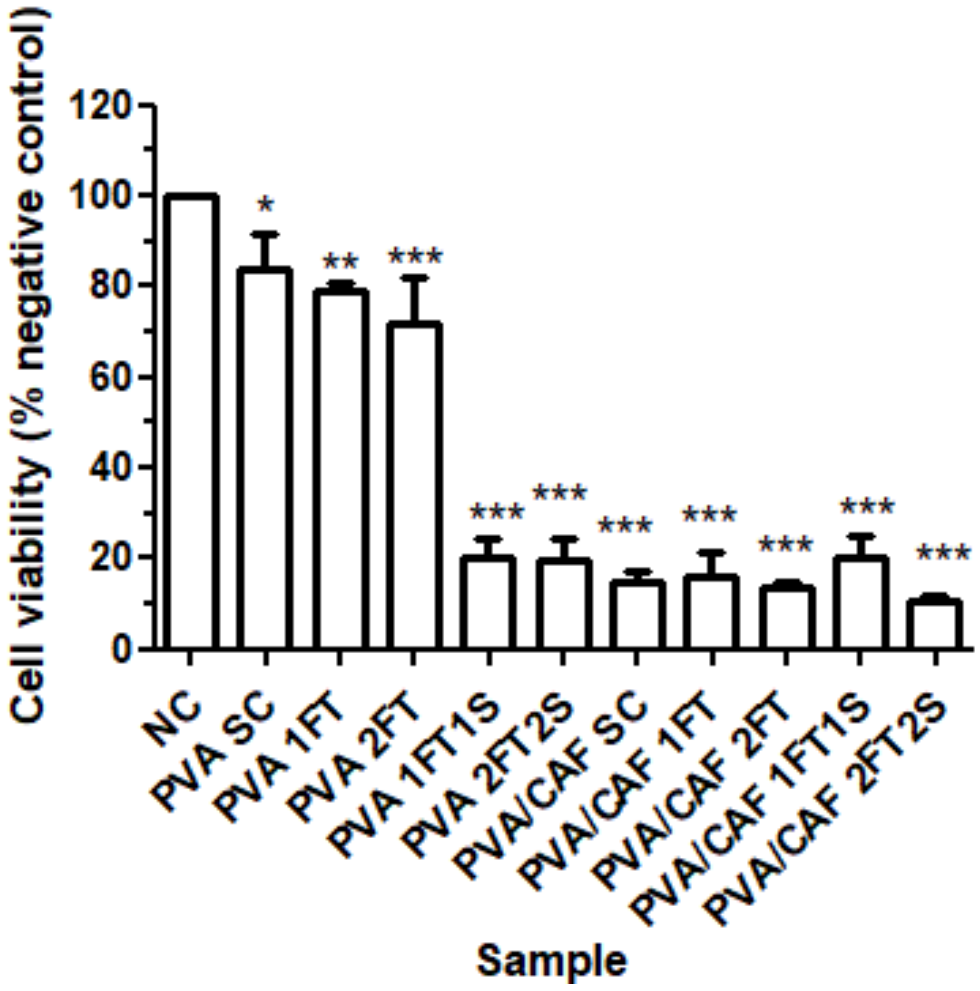

Figure 3.16: Influence of PVA and PVA/CAF hydrogels on the viability of NIH/3T3 cell line following a 24 h exposure at 37°C assessed as direct contact with MTT endpoint. It is noted that the hydrogel samples were place directly on top of cell layer during incubation. (* denotes a significant difference from the negative control).

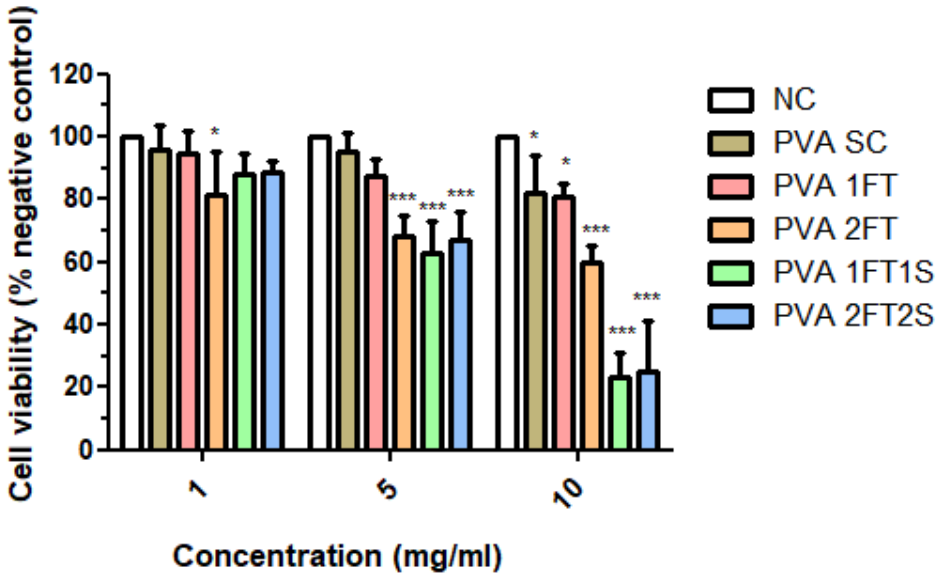

Figure 3.17: Influence of PVA hydrogels on the viability of NIH/3T3 cell line following a 24 h exposure at 37°C assessed in the elution test with MTT endpoint. The concentration refers to the hydrogel sample extracts. (* denotes a significant difference from the negative control).

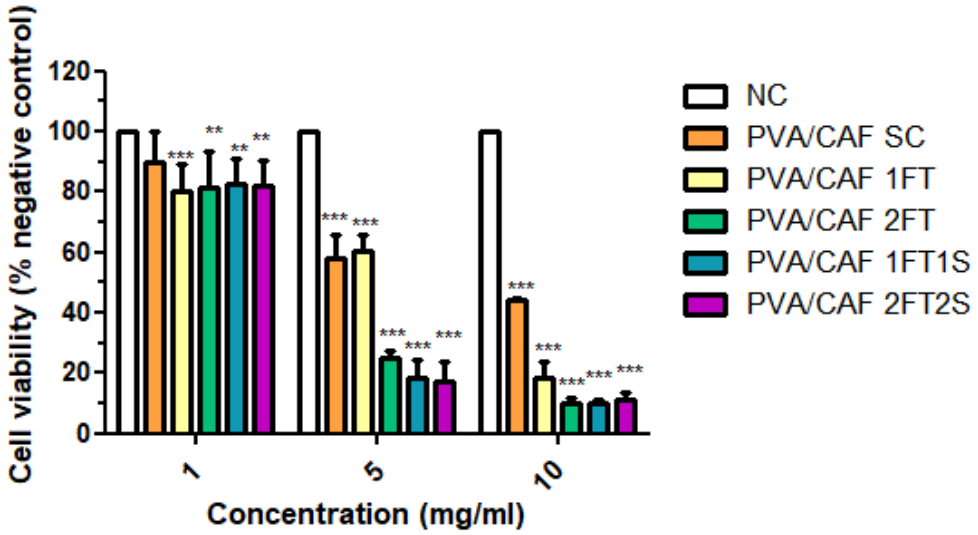

Figure 3.18: Influence of PVA/CAF hydrogels on the viability of NIH/3T3 cell line following a 24 h exposure at 37°C assessed in the elution test with MTT endpoint. The concentration refers to the hydrogel sample extracts. (* denotes a significant difference from the negative control).

3.3 Summary

A series of PVA hydrogels with or without caffeine were synthesized by combined freeze-thawing and uniaxial orientation and their properties were investigated in comparison with those without uniaxial orientation. A fixed orientation pattern was obviously observed on the SEM images of PVA 1FT1S and PVA 2FT2S hydrogels. The orientation became less obvious with the addition of CAF into the PVA hydrogel. The presence of crystallinity is determined using FTIR, DSC and XRD. The PVA and PVA/CAF with 1FT2S and 2FT2S shown an increase of crystallinity, which consequently resulted in a higher degree of swelling, tensile strength and Young's modulus. The drug release rate was also improved with a more aligned arrangement in the polymer chains of PVA hydrogels with uniaxial orientation cycles. Finally, the study indicated the orientated PVA/CAF hydrogels were non-toxic and can be served as an ideal biomaterial for drug release applications at the PVA/CAF concentration not exceeding 5 mg/ml.

Chapter 4

Synthesis and characterisation of cryogenic Polyvinyl alcohol spheres

4.1 Introduction

The efficient encapsulation of drugs including small molecules, protein and nucleic acids into an excipient such as biodegradable sphere is very important to solve some common problems such as initial burst drug release, low solubility, high potency and poor stability for better-controlled drug release. For example, the drugs especially proteins, keep internally and being protected by the degradable polymer surrounding them, the drugs can maintain their biological activity and are not easily destroyed in the body when the polymer is slowly degraded. The sphere preparation technique that we will be discussed in the following chapter has been published as a full journal paper. For the case of this study, ciprofloxacin is a pH-dependent solubility antibiotic. The drug is practically insoluble in water and crystallise at neutral pH but is soluble at an acidic pH [144]. It is believed that the poorly water soluble of ciprofloxacin can be overcome by encapsulating the drug into the PVA/PAA sphere to maximise its drug delivery efficacy [145].

The spheres can be used as the long-term applications for steady and controlled release system because it can increase patient comfort and improve patient compliance by reducing the frequency of dosage through the replacement of frequent (e.g. daily) dosages with infrequent (e.g. once per month and maybe longer) drug administration [146]. For instance, the ciprofloxacin incorporated in poly (D, L-lactide) (PLA) as a bone implant can be sustainable release for two months as illustrated by Castrol *et. al* [147]. Nevertheless, the sphere can also be used as an immediate release application as described in this study for the drug delivery.

Various techniques are available to encapsulate drugs into the biodegradable and biocompatible polymeric spheres, such as emulsification technique with water-in-oil (W/O) emulsion [148], oil-in-water (O/W) emulsion [149] or water-in-oil-in-water (W/O/W) double emulsion [150] with solvent evaporation system, phase separation [151], supercritical fluid [152], electrospraying [153] and spray drying techniques [154]. However, a new and simple technique was created to produce the sphere by directly forming the frozen sphere into a dispersing solution such as ethyl acetate (AcOEt) and chloroform at ultra-low temperature using a micropipette. In the literature, the PVA spheres are generally prepared by dipping sodium alginate over a calcium chloride solution, technically named as coacervation [155]. Therefore,

the study is aimed to use a novel technique to save the spheres preparation time and to provide a more stable drug release manner due to a better drug encapsulation efficiency.

The work demonstrated in this chapter is published by evaluating the ciprofloxacin drug releasing profile. Therefore, in order to link the work in this chapter with the previous chapter, PVA spheres containing caffeine was produced and characterised to compare with the PVA spheres containing ciprofloxacin.

4.2 Result and Discussion

4.2.1 Visual inspection

Firstly, samples produced through freezing in AcOEt the spherical shape intended (**Figure 4.1a**). As the AcOEt temperature raised (because the recipient containing the liquid was removed from the freezer at -80 °C to allow the PVA solution to be dripped into AcOEt), spheres took longer to freeze.

Despite this, at first, spheres remained separate from each other. However, as the medium temperature increased during the thawing stages, the spheres formed large agglomerates due to secondary interactions, in some cases losing the spherical shape. After the third thawing stage, some spheres could not keep the shape, indicating freeze-thaw cycles into AcOEt had to be improved for producing PVA hydrogel spheres (**Figure 4.1b**). Conversely, if the spheres were produced with freeze cycles only, i.e., freezing the solution at different temperatures followed by freeze-drying, they present a more rounded shape without aggregation on drying. However, they still present some deformities observed at the macroscopic scale (**Figure 4.1c**). The first three thawing steps were very delicate and were carried out at a lower temperature of -12 ℃ to keep the spheres at the frozen state as illustrated in **Table 2.3.**

Therefore, samples were produced by a combination of freeze cycles and thawing; samples with these modifications presented a more well-defined geometry. Freeze cycles help to maintain the shape of the sphere in the first cycles without losing its geometry which we propose is due to the minimal hydrogen bonding occurring. However, after the third freeze cycle with thawing, spheres could completely keep the shape. This demonstrated that it was a more suitable freeze-thaw method (**Figure 4.1d**) and was selected for the formulations

containing ciprofloxacin, PAA and HAp. These samples exhibited essentially the same characteristics as the spheres made of PVA only.

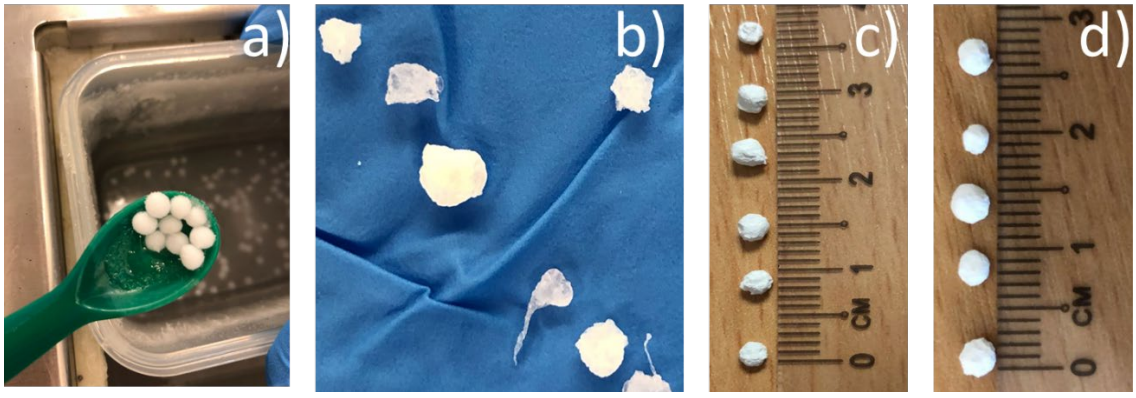

Figure 4.1: (a) Spheres frozen by the dipping method; (b) Samples after freeze-thawing and following freeze-drying; (c) Samples after freezing cycles and (d) Samples after freezing cycles and thawing following freeze-drying.

The addition of caffeine to PVA hydrogel spheres did not affect the size of sphere. Both PVA and PVA/CAF spheres were in the diameter between 2–3 mm. The research group of Soppimath reported that the use of higher molecular weight polymers could increase the size of the microspheres as well as delayed release of the drug [156]. Therefore, sphere smaller than 2 mm might be achieve by moderately lowering the molecular weight of PVA, but not too low, as it might be difficult to retain the spherical spheres.

4.2.2 Scanning Electron Microscopy (SEM)

The morphology of the hydrogels was investigated using SEM to understand the effect of freezing using the dipping method. **Figure 4.3** showed the overall cross-section of the PVA sphere. When the sphere was frozen in the pre-cooled AcOEt solution, a forced alignment of polymeric chains occurred. The sphere started to freeze from the outer part to the inner part, resulted from a fibrous structure alignment moving toward the center of the sphere.

For samples of PVA and PVA-PAA (**Figure 4.3**) it is possible to see that the samples maintained the overall spherical shape (**Figure 4.3a, d**) and upon further inspection of its surface, a porous structure was observed throughout the sample (**Figure 4.3c, f**). This porous structure can be used to create pre-defined geometries for drug delivery vehicles and allow cell

infiltration and incorporation of payloads after crosslink [157]. In the cross-section of these spheres, it was possible to observe two different morphologies within the interior of this material - a porous structure, also seen on the surface, and a fibrous pattern-like (**Figure 4.3b, e**). The fibrous structure is beneficial for cellular interaction. The overall structure comparing the addition of PAA was the presence of whiter regions on the cross-section images, which could indicate an increase in diameter of the fibrous pattern and smaller pores on the surface due to the effect of PAA.

The addition of HAp to these hydrogels **(Figure 4.4)** evidences the formation of smaller sphere sizes and decreased pore sizes. It is also possible to observe the formation of a fibrous like-structure that is slightly different from the hydrogels without HAp; these patterns had different sizes and thickness. This might be due to the interaction of HAp with the polymers. However, even on the surface of this material, it is possible to observe this spiderweb-pattern. We deduced that the technique of freeze-thawing performed here by dipping mechanism led the HAp particles to interact with the polymer chains forming this structure, which was maintained after drying by the freeze-dryer. It is interesting to note that the morphology results shown here are rather different from the ones shown in literature for freeze casting. This is due to this approach by the freeze-thawing technique before drying the samples where we obtained a porous structure rather than the conventional laminar generally found in these techniques [158], [159].

Energy dispersive X-ray analysis was applied to samples containing HAp on the regions of the fibrous pattern confirmed the presence of hydroxyapatite. **Table 4.1** presents the approximated chemical composition by weight of each sample. The calcium characteristic radiation could be identified in all of the four samples but decreasing with increasing the complexity of the formulation by adding PAA.

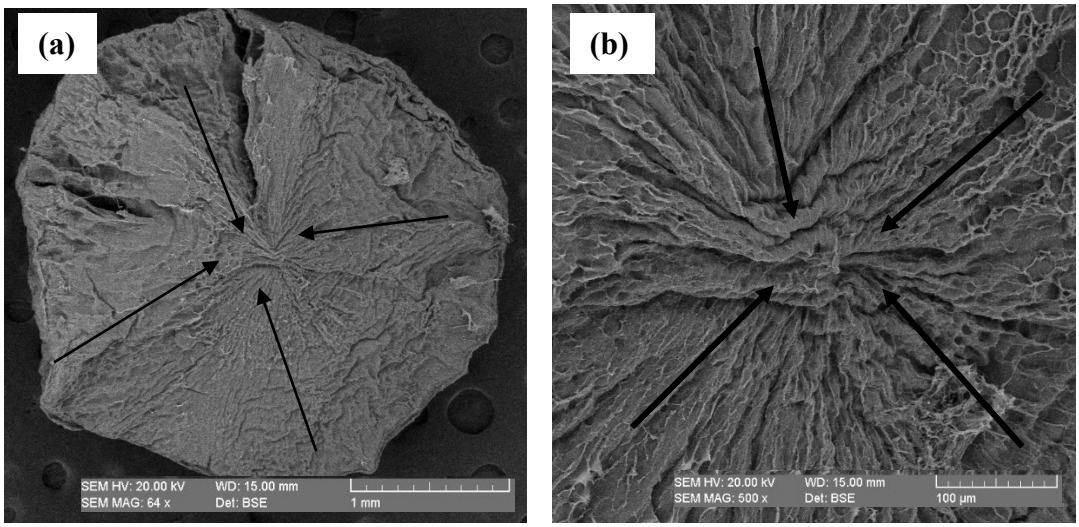

Figure 4.2: SEM images for the orientation of the cross-section of sphere after F/T.

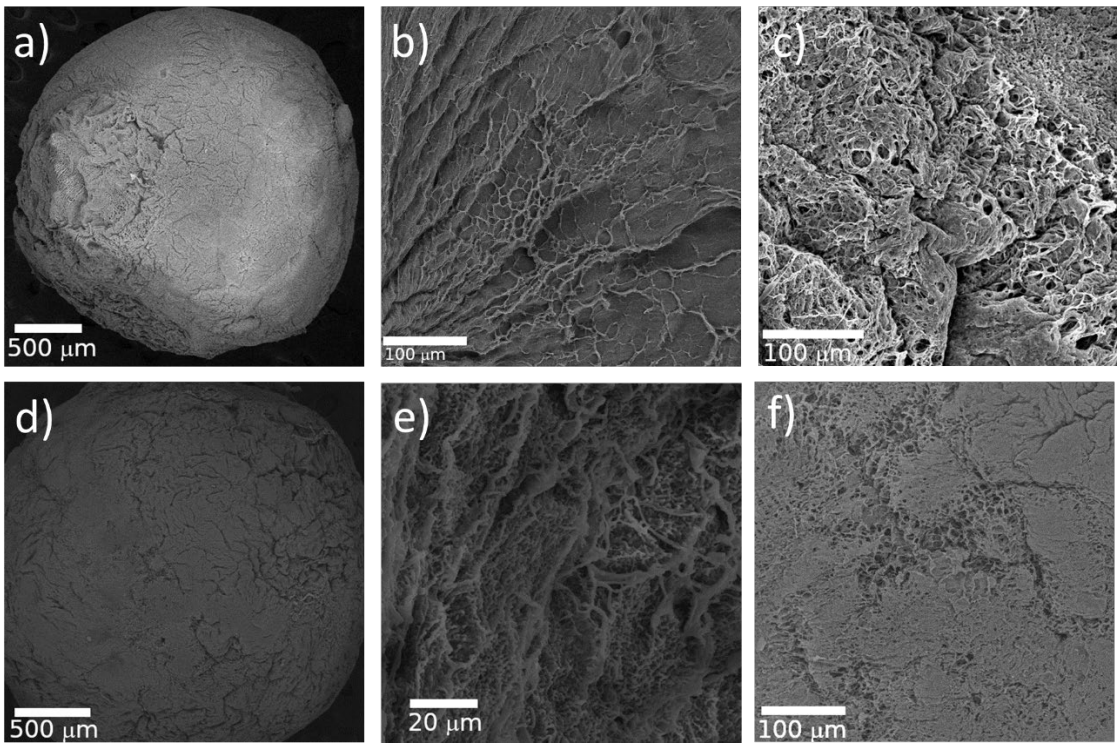

Figure 4.3: SEM images of hydrogel spheres frozen into AcOEt, the first row are PVA and second row are PVA-PAA samples; (a,d) overall image; (b,e) cross-section and (c,f) zoomed surface.

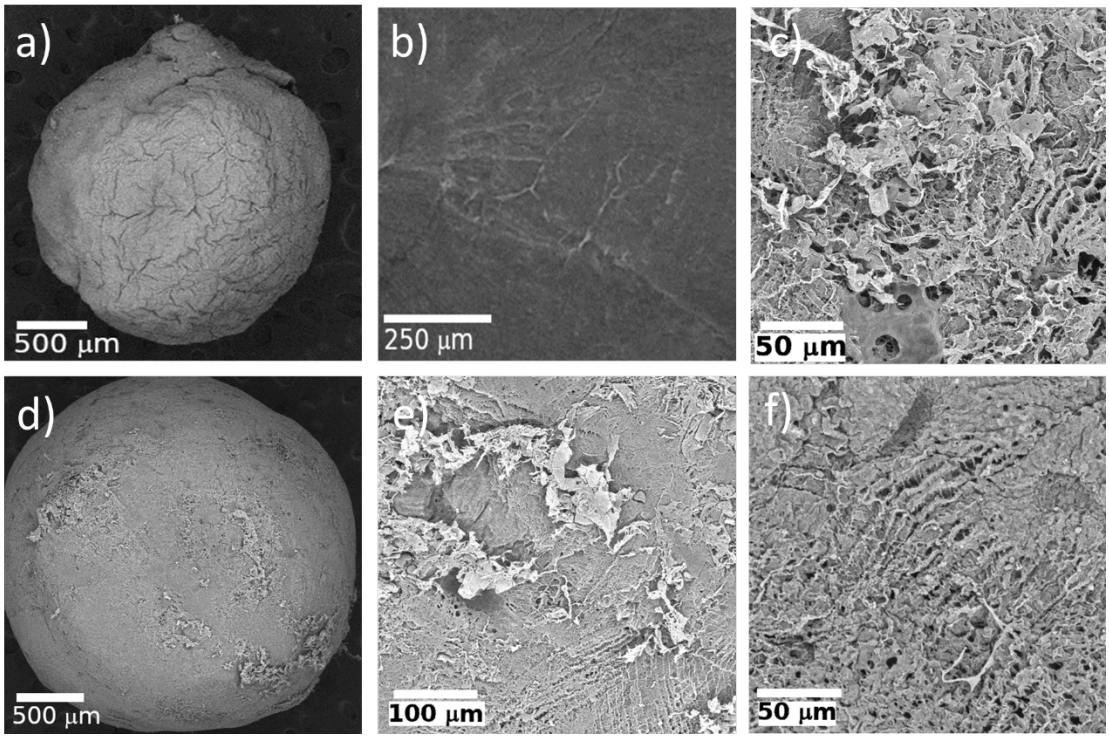

Figure 4.4: SEM images of hydrogel spheres frozen into AcOEt, first row are PVA-HAp and second row are PVA-PAA-HAp samples; (a,d) overall image; (b,e) cross-section and (c,f) zoomed surface. (*PAA=Polyacrylic acid, Hap=Hydroxyapetite)

Table 4.1:Approximated chemical composition obtained by EDX for the hydrogels investigated in this work containing HAp.

Element [%wt.]	Sample	
	PVA-Hap	PVA-PAA-HAp
C	27.02	51.45
O	38.43	44.72
P	11.79	0.33
Ca	22.76	3.50

4.2.3 Fourier transform infrared spectroscopy (FTIR)

The infrared spectra (**Figure 4.5**) show the characteristic peaks of PVA and caffeine. The PVA spectrum shows the bands at 2918 cm^{-1} (CH_2 stretching) and 2954 cm^{-1} (CH3 stretching). The very broad band around 3300 cm^{-1} is attributed to the presence of water that is absorbed by PVA molecular chains. Although the peaks of the functional groups belonging to caffeine decreased or disappeared because they have been overlapped by the strong and broad bond stretches of PVA, the main peaks of caffeine can still be identified in the PVA/CAF sphere

which included 1736 cm^{-1} and 1706 cm^{-1} (Region I) for C=O stretching of the amide group as well as 1376 cm^{-1} (Region II) for C-N amide stretches [53], [114], [160]. The above data suggested that there are no physical or chemical interactions between PVA and caffeine.

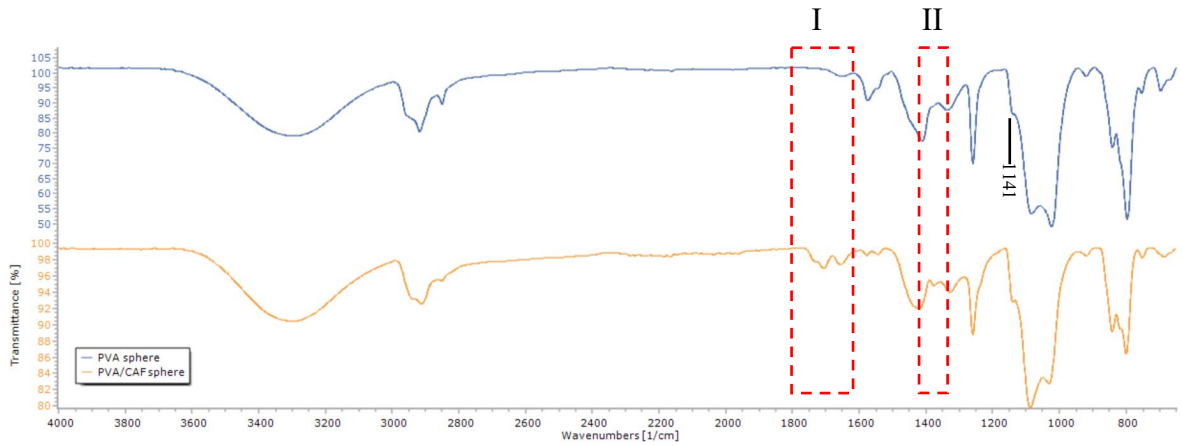

Figure 4.5: FTIR for PVA and PVA/CAF spheres.

In addition, the peak at 1141 cm^{-1} corresponding to the C-O stretching from the crystalline sequences of PVA polymeric chains were observed in both PVA and PVA/CAF spheres, is shown to be sensitive to the degree of crystallinity of PVA. This indicated that a crystalline effect occurred during freeze-thawing cycles. It is hard to determine the effect of caffeine to the degree of crystallinity in FTIR; therefore, DSC is used to further identify its crystallinity.

4.2.4 Differential scanning calorimetry (DSC)

The effect on the polymer, HAp and the drug added to the PVA hydrogel was investigated using a DSC technique. Firstly, the glass transition temperature of PVA and the α relaxation of PVA are, respectively, 84.68 °C and 63 °C. PAA is an amorphous material and has no crystalline melting peak. The PVA and CIP have melting temperatures respectively at 227.88 °C and 276.77 °C. The β-transition of the crystalline PVA domains was identified due to the relaxation of the domains in the crystalline regions. The HAp had no significant thermal transition but both PVA and PAA presented thermal degradation events.

Hydrogels studied in this work (**Figure 4.6a**) exhibits first that the incorporation of PAA decreases the melting point and increases the glass transition temperatures compared to PVA. It is known that due to the addition of PAA, the tendency of PVA to crystalize fades due to some strong H-bonding interaction between PVA and PAA in the amorphous phase, which can be seen by the broad melting peak obtained by PVA-PAA samples [161].

The addition of HAp increases the melting point of PVA and PVA-PAA samples, the effect of HAp as an addition to improve the mechanical properties of the hydrogels are known and several researchers have reported this phenomenon [162]–[164]. Conversely, when ciprofloxacin was added to the structure of these materials there is a strong decrease in the crystalline melting temperature of PVA, exhibiting the same characteristics as with samples without the drug. This decrease could be due to the interaction of the PVA and CIP; similar reports for PVA polymer have been shown [165] and for other polymers [166]. In addition, the sample containing HAp still has the highest value of PVA melting point temperature in which sample PVA-HAp-CIP exhibited the highest for samples containing the drug.

The DSC curve of caffeine powder (**Figure 4.7)** showed a melting endothermic peak at 237 ˚C. A small additional endothermic peak at around 160 ˚C was observed, attributed to the presence of a small amount of caffeine form II in the material provided [167]. Furthermore, the caffeine melting point cannot be observed in the PVA/CAF sphere, probably because the caffeine was not present as crystalline material but had been converted into an amorphous state in the sphere [114]. Although the melting temperature of PVA and PVA/CAF spheres was around 222-223 ˚C, an increase in the degree of crystallinity from 15% to 29% was identified. As stated in our previous research, caffeine has exhibited the formation of crystallite in the PVA polymer matrix [168]. However, the glass transition temperature has decreased slightly from 61 ˚C to 58 ˚C with the presence of caffeine. This may be referred to increasing in the free volume throughout amorphous regions which resulted from the physical crosslinking or crystallization process of PVA with caffeine or decreasing in hydrogel bonding in the same amorphous network [169].

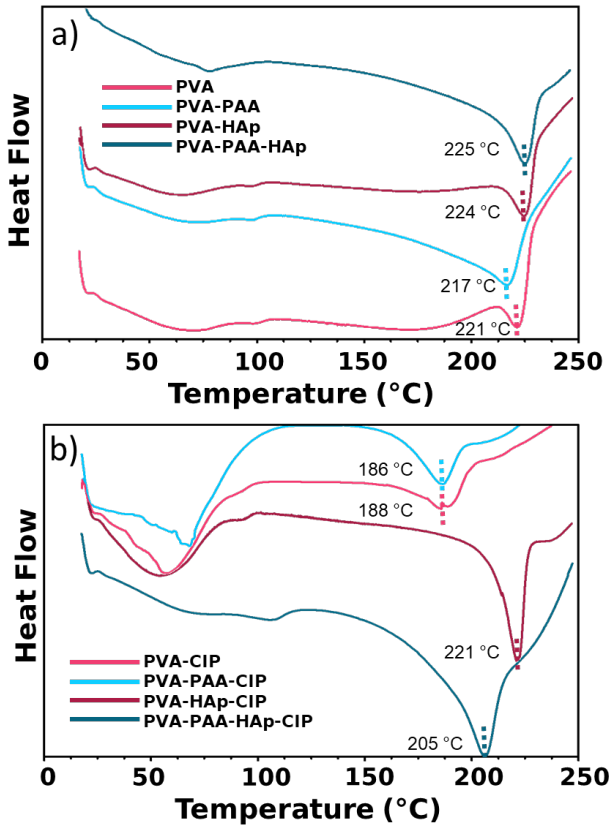

Figure 4.6: DSC to investigate the effect on Tm and Tg of PVA and PAA when adding HAp (a) and CIP (b) to the hydrogel structure – the scale of heat flow from (b) is 2x higher than (a).

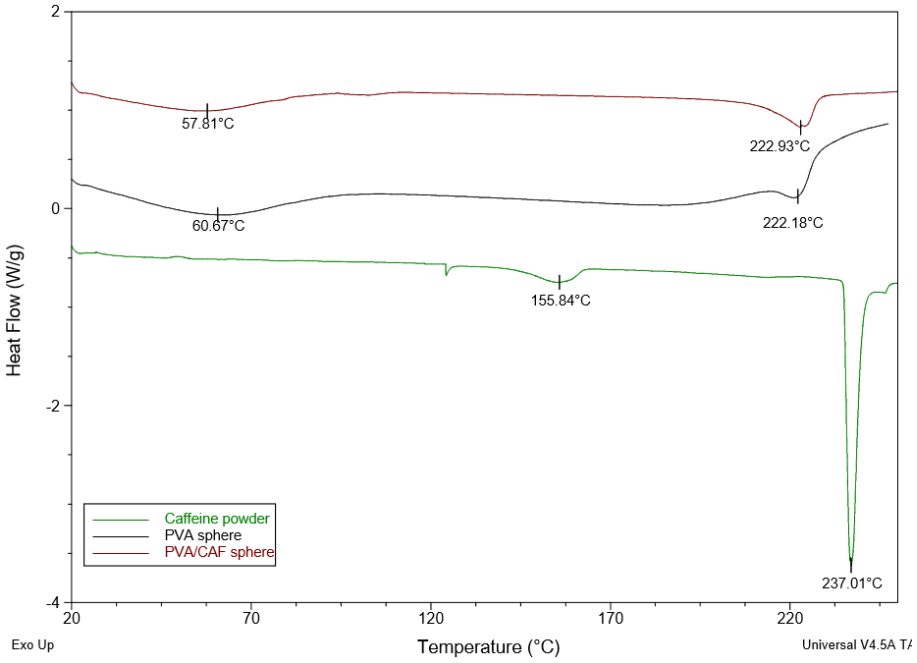

Figure 4.7: DSC for caffeine powder, PVA and PVA/CAF spheres.

237 °C

4.2.5 Swelling studies

To investigate the ability of the hydrogels for targeted drug delivery, studies on swelling were performed (**Figure 4.8**). The results elucidate the effect of the addition of PAA on increasing the swelling value due to the carboxylic acid chains. When HAp was incorporated into the structure, these values were lower for both PVA and with the addition of PAA. These results correlate with the DSC results and its morphology, leading to a more compact and resistant material. Nonetheless, the effect on PAA with the addition of HAp is still noticeable due to the increased values.

It is known that the addition of PAA to PVA can induce a pH-sensitivity in the structure of the materials. Therefore, studies at different pH were conducted. The effect of swelling of PVA is unchanged while varying the pH until the highest number investigated and is comparable to those reported in the literature [170].

Nonetheless, when adding PAA the materials, follow a somewhat linear function while increasing the pH. The effect of controlling the pH sensitivity of these materials is one requirement for biomaterials [171] and the linear function of PVA-PAA have been reported by other authors as well, though not to a wide extent shown in this work [172], [173].
The addition of HAp to the PVA also seems to exhibit a pH sensitivity though not following a linear function and swelling less than the PVA alone. When HAp was incorporated in the hydrogel with PAA the linear function is also observed while with lower swelling values. PVA hydrogel is reported to have low pH-sensitivity [12] and could have been benefited from the HAp in the structure by slightly improve its response.

When the spheres reached swelling equilibrium, they were immediately removed from the buffer solution and photographed **(Figure 4.9)**. It is possible to observe an increase in volume due to the swelling and pH sensitivity, as expected from hydrogels. It seems to follow the trend shown in swelling graphs (**Figure 4.8**). However, it is harder to perceive differences with the addition of HAp and although all components present hydroxyl groups in their chemical structures, only PVA and PAA contribute significantly to the absorption of water by hydrogen bonds [174]. The ability for pH sensitivity in the point of biomaterials is relevant is due to the

different pH values that certain body tissues have, such as the neutral pH in the intestine; also, chronic wounds have pH between 7.1 to 5.4 [175], [176].

The PVA and PVA/CAF spheres were fully swollen in 4 h with the degree of swelling of 532% and 356%, respectively. The results elucidate the addition of caffeine resulted in a decrease in the swelling value which correlated with the DSC result, which caffeine exhibited high crystallisation tendencies in the sphere, leading to a more compact and resistant material. When the spheres reached swelling equilibrium, they were immediately removed from the buffer solution and photographed **(Figure 4.10)**. Although the swelling degree of PVA sphere was significantly higher than PVA/CAF sphere, it was hard to perceive their size differences.

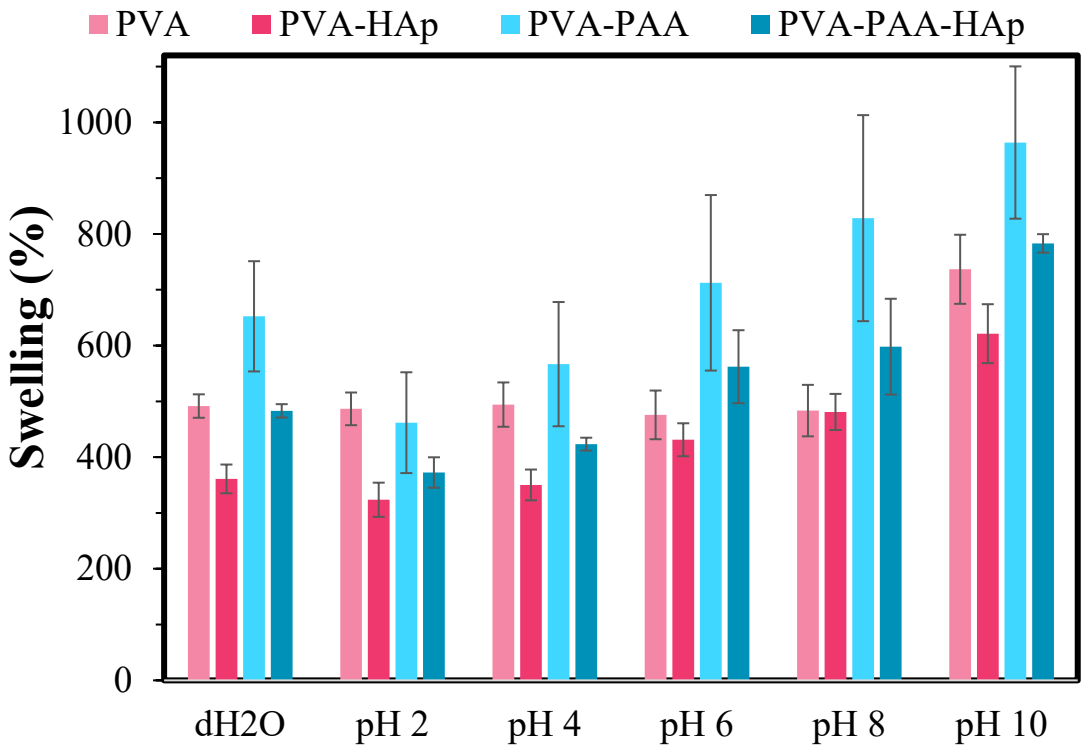

Figure 4.8: Swelling in distilled water and pH-sensitivity tests of the studied hydrogels; although PVA seems to show sensitivity towards higher pH values, they were not varied towards other pH values.

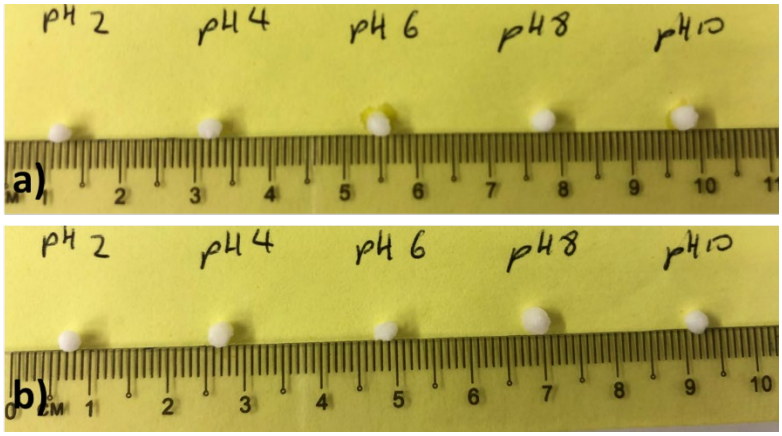

Figure 4.9: Hydrogel spheres of (a) PVA-PAA and (b) PVA-PAA-HAp after reaching equilibrium swelling at different pH values.

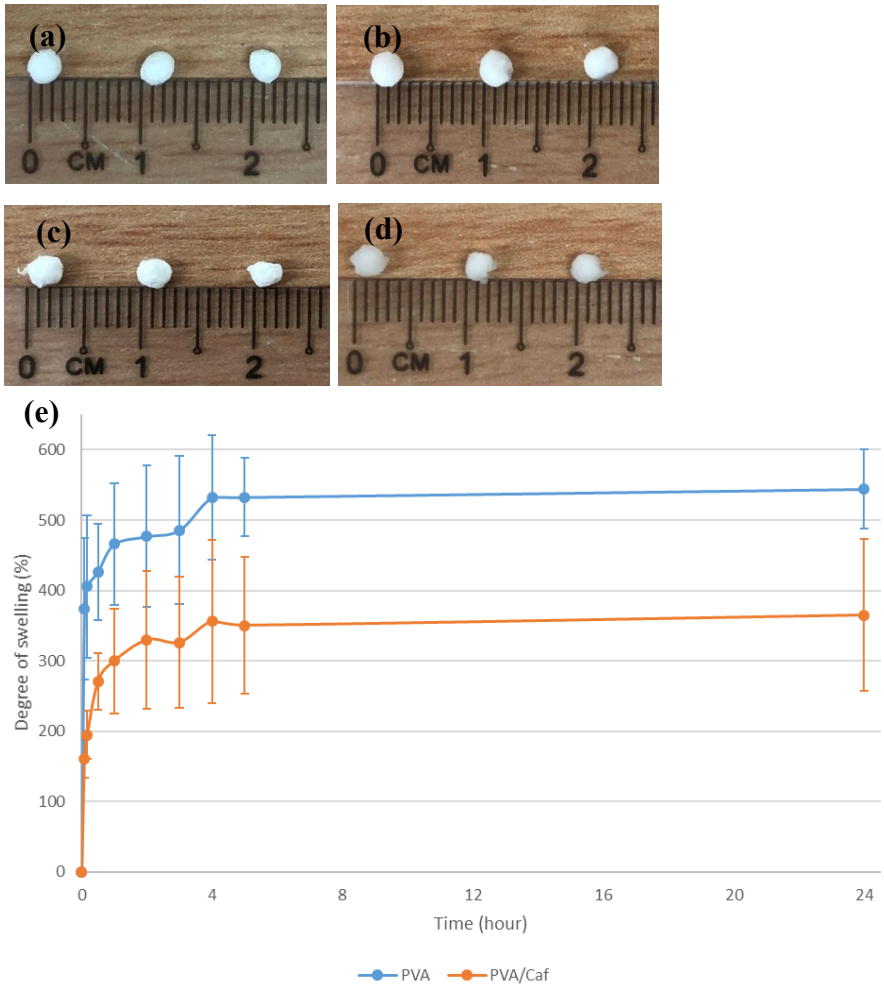

Figure 4.10: Photograph of PVA spheres (a) before swelling and (b) after swelling; PVA/CAF spheres (c) before swelling and (d) after swelling. (e) Swelling studies in pH 7.4 buffer at room temperature.

4.2.6 Drug release studies

The drug release of ciprofloxacin incorporated into the structure of the hydrogel spheres **(Figure 4.11a)** exhibits that for PVA and PVA-PAA the drug is released nearly at 30 min while when HAp was added to the structure, the drug is fully released only at 120 min for PVA-CIP and 350 min when PAA was added. In contrast, PVA-HAp hydrogels only fully release ciprofloxacin after 6 h – which is in agreement with DSC data. These results suggest that samples without HAp could be used for applications demanding drugs for immediate release. Another important result was that the PVA and PVA-PAA hydrogels dissolved at the same time that the drug was fully released, i.e., 35 min for PVA and 40 min for PVA-PAA. Hydrogels which incorporated HAp did not dissolve in the timeframe of the test. These materials maintained the integrity in swelling tests at room temperature, however, these spheres slowly dissolved at temperatures higher than 35 °C. There is a desired criteria for immediate release drug delivery system whereas it is important that the carrier should be dissolved within a short period [177], [178]. The porous structure observed by the SEM could have probably led to this fast time response delivery. Nonetheless, it is possible to modulate the profile of samples with HAp to dissolve and deliver the drug under the allowed time frame for immediate release. This can be achieved by controlling the steps on freeze-thawed mechanism, i.e., by controlling the amount of crosslinking and it could be done by either reducing the amount of cycles or the thawing time.

The entrapment efficiency of these hydrogel spheres by impregnation of ciprofloxacin reported values of 0.26 % for PVA-CIP, 0.12 % for PVA-PAA, 0.26 % for PVA-HAp and 0.24 % for PVA-PAA-HAp. These were very low values, and due to the crosslink occurring between the polymeric chain, there was not enough space for the drug to be entrapped after the hydrogel was formed; nonetheless, spheres produced by sodium alginate have reported values of impregnation of 10 % [155]. The increase in this loading was due to the different fabrication method, by coacervation. When the sphere was formed via the dipping mechanism the solution where the sphere will be formed ($CaCl_2$ for sodium alginate) will also contain the drug in a specific concentration and this mechanism may report values on the order of 90 % of entrapment efficiency [179].

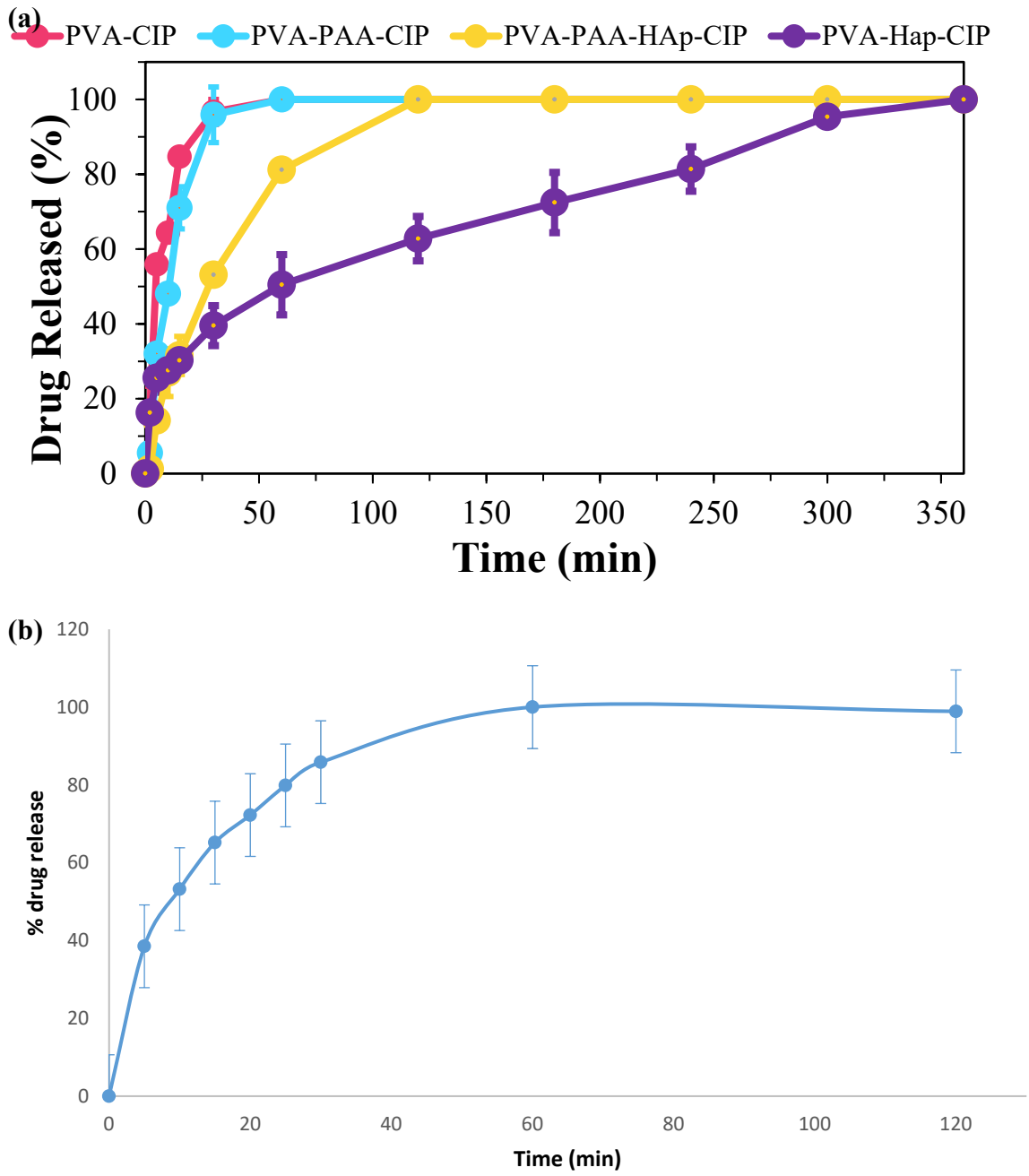

Figure 4.11: (a) Percentage of released drug in function of time for the studied samples. It is possible to observe the effect of Hap – leading to a slow release of ciprofloxacin. (b) caffeine drug release.

According to **Figure 4.11b**, the PVA/CAF sphere offered a fast drug release system. The amount of time required for complete caffeine release from the PVA/CAF sphere was within 60 min. When comparing the PVA/CIP sphere produced in our research study using the same preparation methodology [145], it is similar to the drug releasing time of PVA/CAF sphere with the ciprofloxacin fully release within 60 min (i.e. 35 min).

According to **Table 4.2**, five different drug release mechanisms was used to identify which drug release model best fit to the spheres. The PVA/CIP, PVA/PAA/CIP, PVA/PAA/HAp/CIP and PVA/CAF spheres were best fit in Hixson-Crowell release kinetic, indicated that the drug release rate is depends on the change in surface area and diameter of sphere. While, the PVA/Hap/CIP sphere is best fit in Higuchi model with the R^2 value=0.979, suggesting the CIP release by Fick's law of diffusion from the sphere.

Table 4.2: Mathematical modeling for drug dissolution profile.

	Zero-order	First-order	Higuchi	Korsmeyer-Peppas		Hixson-Crowell
	R^2	R^2	R^2	R^2	n	R^2
PVA/CIP	0.8599	0.9806	0.9663	0.9698	1.1911	0.9940
PVA/PAA/CIP	0.9450	0.9255	0.8619	0.8941	1.1908	0.9533
PVA/PAA/HAp/CIP	0.8761	0.9755	0.8807	0.9102	1.0344	0.9864
PVA/HAp/CIP	0.8650	0.8343	0.9798	0.9365	0.7585	0.8663
PVA/CAF	0.7214	0.9866	0.9565	0.8247	1.0901	0.9913

4.2.7 Disintegration studies

The cryogenic spheres containing ciprofloxacin and without HAp dissolved in the drug release tests. Therefore, these spheres were evaluated at which time it was fully dissolved (**Figure 4.12a**). For samples without HAp, it is possible to observe that the dissolution follows the drug release curve of ciprofloxacin from **Figure 4.11**. The time for the sphere to be fully dissolved matches the time for the complete release of ciprofloxacin release test. In contrast, samples containing HAp improves the structure of these hydrogels from reinforcement of intermolecular and intramolecular bonds and maintain its integrity within the time of the study. We believe the structure of the samples containing HAp was improved leading to a high crosslink polymeric network which does not led the pH 7 buffer to dissolve this material, as supported by our previous research [15].

According to **Figure 4.12b**, both PVA and PVA/CAF spheres were also not disintegrated after two weeks in pH 7.4 buffer at 37 ˚C. The spheres were sinking to the bottom of the flask when

they were fully swollen. The six F/T cycles has improved the structure of these spheres with a high crosslink polymeric network in order to maintain its integrity within the time of the study.

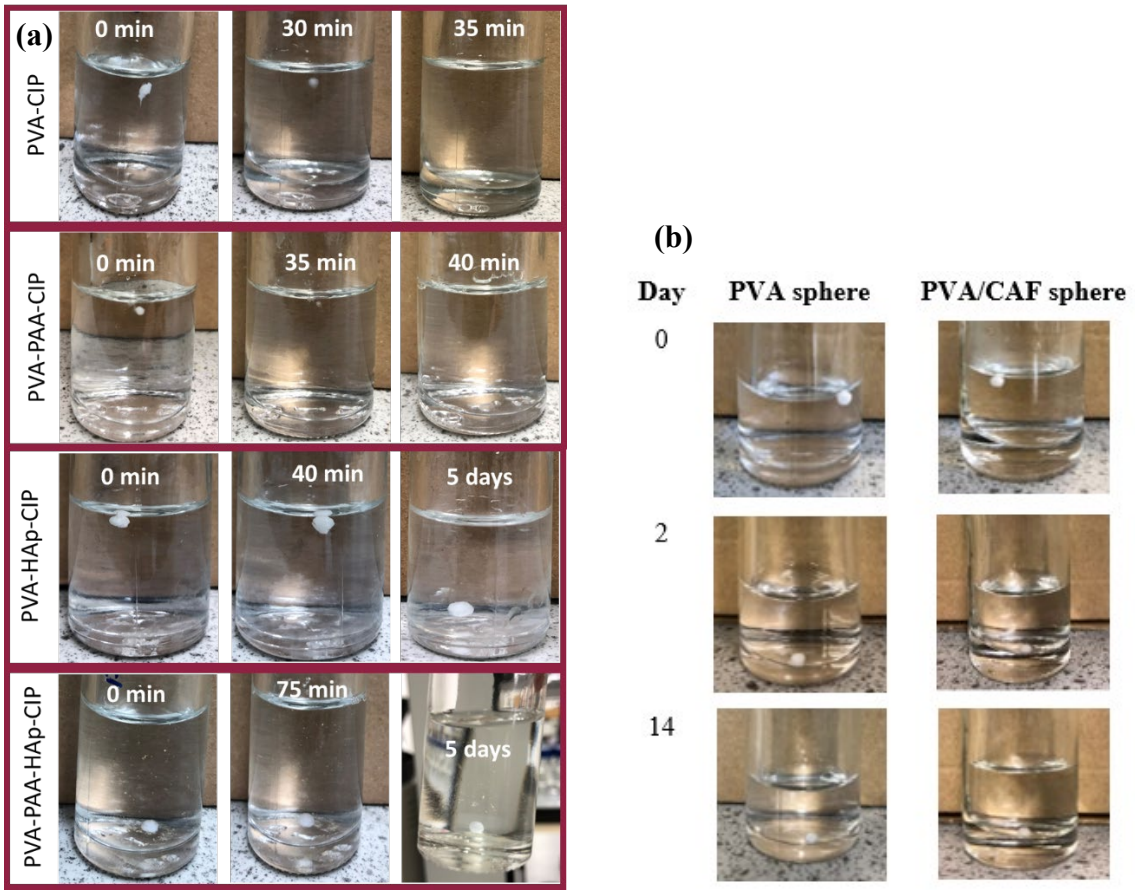

Figure 4.12: (a) Dissolution of the cryogenic spheres incorporated with ciprofloxacin. For samples without HAp, the last time measurement was performed at the point where there was no visual observation of the sphere. (b) Dissolution of the PVA and PVA/CAF spheres at 37 °C.

4.2.8 Cytotoxicity test

The results for MTT assay of NIH 3T3 cell line following a 24 h and 48 h exposure are shown in **Figure 4.13**. After the 24 h exposition, it was possible to observe that all spheres presented to be non-toxic (cell viability > 72%) in all concentrations of sphere sample elution extracts. Furthermore, after the 3T3 cell line being exposed for 2 days, it can be observed that there was an increase in cell viability for most of the samples and still exhibiting a non-toxic profile. It is also observed that the PVA and PVA/CAF spheres presented to be non-toxic with the cell viability of 78% and 84%, respectively **(Figure 4.14)**.

Although, sphere samples were produced with AcOEt – that is known to be toxic for specific concentrations (i.e. oral median lethal dose (LD50) in rats =10100 mg/kg body weight [180]), the procedure performed in this work shows that any remaining solvent in the hydrogel sphere was not effective to decrease the cellular viability. It is worth mentioning that although these spheres produced via a droplet method using AcOEt as solvent to form the cryogenic spheres upon impact, it was only chosen due to the easy access to this compound from our lab, nonetheless it is possible to use any other solvent that can freeze below the temperatures studied in this work and that could have lower toxicity values.

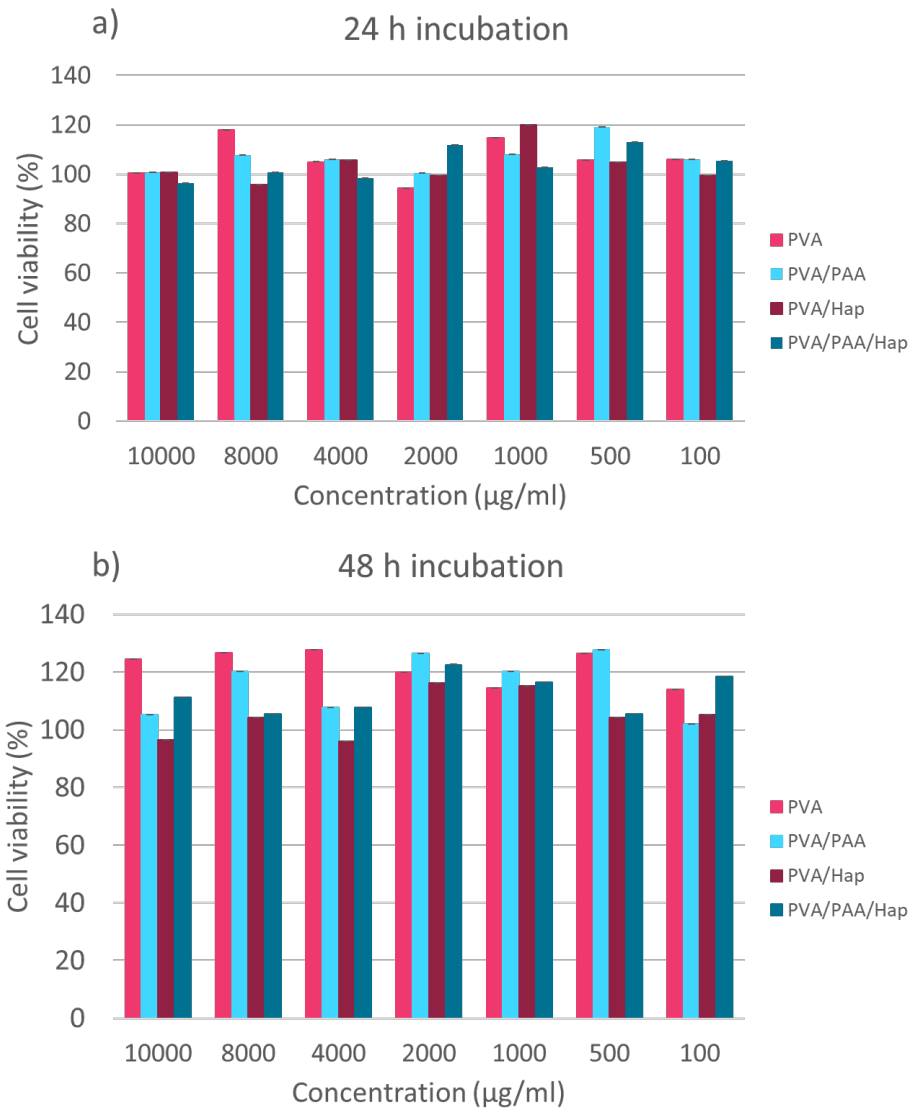

Figure 4.13: Cell viability tests of the studied hydrogels on NIH 3T3 cells after (a) 24 h and after (b) 48 h.

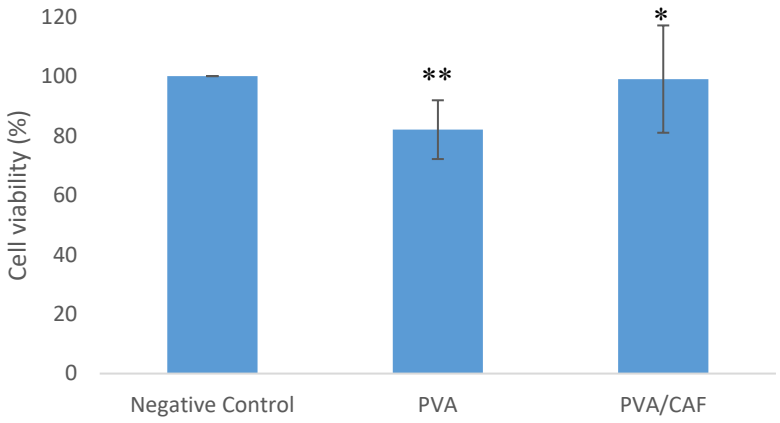

Figure 4.14: Percentage viability of 3T3 cells after (a) 24 h exposure. (* denotes a significant difference from the negative control).

4.3 Summary

In the present study, hydrogels for the immediate release of ciprofloxacin for osteomyelitis treatment was reported. Hydrogels were produced with different formulations of poly (vinyl alcohol), poly (acrylic acid), ciprofloxacin and hydroxyapatite in aqueous solutions and shaped into spheres by dispensing liquid droplets into ethyl acetate at low temperature (-80 °C) following by formation of hydrogels by freeze and thawing cycles. Samples were able to maintain a spherical shape after the freeze-thawing cycles technique described. The cross-section of these samples revealed different internal structures, depending on the components incorporated into the PVA.

In addition, EDX exhibited quantities of Ca and P into these hydrogels due to the HAp incorporated. These materials modified the melting point and the glass transition temperature of PVA and also led to a pH sensitivity, which improved by the addition of poly acrylic(acid). Hydrogels were able to immediately release ciprofloxacin under 60 min and dissolves under 1 h for samples without Hap. In addition, the immediate release of caffeine from the PVA/CAF spheres within 60 min, which best fit in Hixson-Crowell release kinetic was reported. Finally, these samples presented to be non-toxic from cellular viability tests against NIH 3T3 cell line while also increasing the cellular activity after 2 days. It is believed that this material can be used as a support for biomaterials intended as load bearing which can be incorporated by the technique proposed herein.

Chapter 5

Synthesis and characterisation of electrospun Polyvinyl alcohol/Polyacrylic acid bilayer nanofibres

5.1 Introduction

Nanofibres are used in a wide range of biomedical and industrial applications including wound healing [181], biosensor [182], water filtration [183], and food packaging [184]. Within the various techniques to produce continuous nanofibres, electrospinning stands out as a versatile technique. Our lab has used this technique in a number of applications such as brain implant [185], wound dressing [186], bone implant and drug delivery. A wide variety of aqueous polymer solutions such as polyvinyl alcohol (PVA), polyacrylic acid (PAA), poly (2,-hydroxyethyl methacrylate) (PHEMA) and poly(N-isopropyl acrylamide) (PNIPAAm) can be used for electrospinning [187], which directly relates to the fibres properties and can be modified using crosslinking agents in order to confer specific characteristic and, in many cases, SMART configurations [188]. In this study, PVA and PAA were chosen to fabricate a bilayer electrospun nanofibre as they present as a well-formed cross-linked hydrophilic polymer structure, which can retain large amounts of water and biological fluids [145]. Moreover, the PVA/PAA bilayer nanofibres exhibit the heterogenous properties from both PVA (i.e. biocompatible, biodegradable, water soluble, and non-carcinogenic) and PAA (i.e. pH-sensitive) [189].

The strong interaction of inter-polymer hydrogen bonding between PVA and PAA results in a completely miscible blend [190]. PVA/PAA is therefore, commonly used for producing wound dressings [191], adsorbents for wastewater treatment [192], solid polymer electrolytes for the alkaline batteries and other electrochemical systems [193]. Although the combination of PVA and PAA nanofibres via electrospinning have been extensively studied [191], [194]–[197], the concept of producing bilayer electrospun nanofibres with PVA and PAA is of potential interest in the synthesis of novel hydrogel-based nanofibres. Moreover, the PVA/PAA bilayer hydrogels were investigated before [35], [198], [199] but not in the form of polymeric nanofibres.

Our group has previously produced a bilayer hydrogel consisting of PVA and PAA on a macroscale, in which we demonstrated that both physical crosslinks between two different hydrogels compositions occurs after freeze-thawing, resulting double the theophylline drug releasing time from the bilayer PVA/PAA hydrogel with high molecular weight of PAA within 4 h when comparing with the PVA single layer hydrogel [200]. Further research in this study

has allowed us to optimise the assembly of PVA/PAA bilayer hydrogel in nanoscale utilising electrospinning with the potential to be used for dual drug delivery applications. Researchers have already produced bilayer electrospun nanofibres with different polymers for either single or dual drug delivery. For example, bilayer poly (lactic-co-glycolic acid) (PLGA) scaffolds 3 containing vascular endothelial growth factor (VEGF) and platelet-derived growth factor (PDGF) in separated layer revealed that the release of VEGF was faster than PDGF as the VEGF contained PLGA layer was degraded faster than PDGF contained PLGA layer [201].

Previous works have highlighted the potential usage of a bilayer electrospun membrane for drug delivery and for mechanical improvement of polymeric nanofibres [202]–[204]. Within these various studies, stands out the incorporation of microparticles loaded with drug, or nanofibres, within a bilayer which is further heat-annealed in order to assemble this membrane [205]. Moreover, studies have also shown that it is possible to use different polymers in this bilayer, in order to present a hydrophobic and hydrophilic side, so as to present a preferential drug release, particularly in the hydrophilic facet [206]. However, the study of a dual drug delivery using this technique was not yet thoroughly evaluated, particularly if these different hydrophobic-hydrophilic sides were incorporated with synergetic drugs so as to understand their potential improvement in the drug release.

Thermal treatment is proposed to be a viable method to enhance the tensile strength, thermal stability and water stability [207], [208] of biomaterials due to the crystallisation and crosslinking in the polymer matrix. As reported by Park et. al., the water stability of electrospun PVA/PAA nanofibres prepared by blending the PVA solution with the PAA solution at PAA weight fraction=0.5 were dramatically enhanced through heat treatment with conserved fibrous morphology [196]. However, the study of two distinct layers combining together (i.e. PVA/PAA bilayer) for drug delivery and tissue engineering has not been investigated yet.

Therefore, the unannealed and annealed PVA, PAA and PVA/PAA bilayer electrospun nanofibres prepared in this study were subjected to several tests included FESEM, FTIR, DSC, DMA, water contact angle, disintegration, swelling and weight loss studies. In this work, doxorubicin hydrochloride was incorporated in this synthesized membrane in order to be used for the osteosarcoma treatment. Previous works presented the effectiveness of using PVA microspheres for doxorubicin release [209], presenting high cytotoxicity against osteosarcoma

cells [210]. In order to prove the effectiveness of a dual drug delivery system using this membrane, clarithromycin was added in order to, hypothetically, obtain a synergetic enhancement of doxorubicin efficacy. This was suggested since a recent work related that this occurs for MCF7 cells, breast cancer cells [211].

5.2 Result and Discussion

5.2.1 The thermal annealing temperature and time

The prepared PVA/PAA bilayer electrospun nanofibres were physically crosslinked through thermal annealing. The crosslinking effectiveness of the PVA/PAA nanofibres can be influenced by annealing depending on the temperature [212], length of annealing time and the molecular weight of PAA or PVA [213]. **Figure 5.1** exhibits a visual macroscopic observation of the nanofibres prepared at different annealing temperatures and annealing time. As seen in **Figure 5.1(**Error! Reference source not found.**I)**, the electrospun nanofibres were decomposed from white to slightly yellowish at 150 °C. Furthermore, the sample became harder and crispy. In fact, the degraded nanofibre showed a brownish or yellowish colour [213]. Therefore, nanofibre samples annealed at 150 °C with mild degradation were not tested in the study.

Nanofibre samples annealed at 100 °C for 3 h as showed in **Figure 5.1(II)**, also demonstrated by Zeng *et. al.* [213], retained the same colour before annealing **Figure 5.1(III)** which was white in colour with no degradation were subjected for further analysis. Although the nanofibres annealed at 100 °C were slightly transparent when compared to the unannealed nanofibres, their structure was both remained to be flexible.

5.2.2 FESEM results

As shown in **Figure 5.1a-d**, the PVA nanofibres and PAA nanofibres in PVA/PAA bilayer nanofibres were randomly aligned. PVA solutions are normally prepared using distilled water. However, production of ultrafine nanofibres using water as solvent is hardly achievable due to its low conductivity and high surface tension of water which requires high voltage in order to obtain a stable jet and it might exceed the electric breakdown threshold of the surrounding gaseous medium, air in such cases, producing a corona discharge [214]. Therefore, it is important to be aware that the content of ethanol presented in polymer solutions could lower the surface tension and form a stable Taylor cone that gradually modify the morphology of nanofibres from beaded-nanofibres to ultrafine-nanofibres [215]. As reported by Zhang *et. al.*,

the ethanol/water ratio of less than 5:95 in PVA solution can speed up the solvent evaporation rate as the jet travel through the air and what is reached through the collector is only smooth nanofibres [216]. In our work, the ethanol/water ratio was increased up to a 50:50 ratio, the formation of non-beaded nanofibres was achieved and yet the diameter of nanofibres were not uniform. The addition of high amount ethanol has heavily decreased the surface tension of the electrospinning solutions which led to instable liquid jet formation and non-uniform fibre size.

Interestingly, the FESEM images revealed changes in the diameter of PVA and PAA nanofibres as well as the thickness of the PVA/PAA bilayer after thermal annealing process. Before annealing, the average diameter of PVA nanofibres **(Figure 5.1a)** and PAA nanofibres **(Figure 5.1c)** was 341±220 nm and 437±188 nm, respectively. After annealing, the average diameter of PVA nanofibres **(Figure 5.1b)** and PAA nanofibres **(Figure 5.1d)** was increased to 464±152 nm and 611±166 nm, respectively. There is no significant difference between unannealed PVA nanofibres and annealed PVA nanofibres; while there is a significant difference ($p < 0.001$) between unannealed PAA nanofibres and annealed PAA nanofibres. It is suggested that the diameter of nanofibres increased due to the nanofibres released stress during heating and caused the polymer chains orientated in axial, followed by expanding in the horizontal direction. It is possible that the thinnest fibres may present a different behaviour when under annealing, since it surpasses the glass transition of the polymer. Therefore, it is possible that agglomeration of finer fibre occurred. Nonetheless, these values were not statistically significant different between annealed and non-annealed. Previous works also reported an increase in diameter of the annealed poly (vinyl pyrrolidone) (PVP) nanofibres when a slow heating rate (i.e. 1, 3, 4 °C/min) is performed, which was attributed to the nucleation process [217], [218].

In contrast, as seen on the cross-section morphology of the PVA/PAA bilayer nanofibres, the thickness of the PVA/PAA bilayer nanofibres decreased after annealing, with the thickness of 279±27 µm and 169±18 µm for the unannealed **(Figure 5.1e)** and annealed PVA/PAA bilayer **(Figure 5.1f)**, respectively. The annealed bilayer nanofibres were remained to be two discrete layers and yet the two layers were "glued" together, leaving less spaces between the nanofibre layers. Moreover, the thermal annealing induced the *in situ* fibre-fibre fusion (interfibre bonding) [219]. This fusion can be observed by looking at the sharp vertex formed by overlapped nanofibres which became rounded, as indicated by the arrows in **Figure 5.1d**.

Furthermore, the mechanical properties of nanofibres can be enhanced with an increase of interfibre bonding.

Figure 5.2 showed the surface morphology of electrospun nanofibres after swollen in pH 7.4 buffer for 48 h. Although all the swollen nanofibres were destroyed, the annealed bilayer PVA/PAA nanofibres retained a porous structure which is due to the heat-annealing treatment. The unannealed and annealed PAA nanofibres were completely dissolved after 48 h. Thus, there was no SEM images for swollen PAA nanofibres.

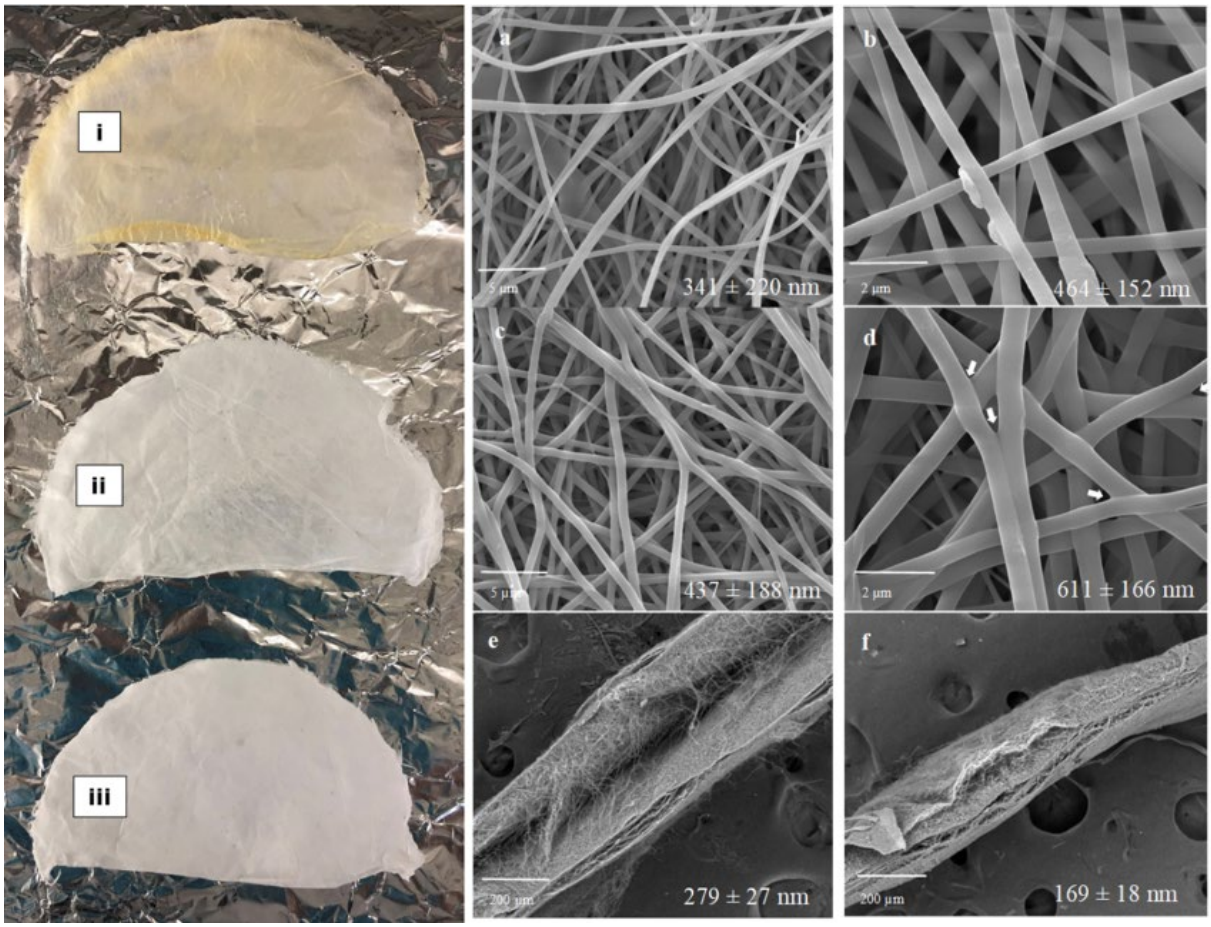

Figure 5.1: PVA nanofibre sample annealed (I) at 150 °C with slightly degradation, (II) at 100 °C and (III) without annealing. The surface morphology of (a) Unannealed PVA/PAA bilayer (PVA surface), (b) Annealed PVA/PAA bilayer (PVA surface), (c) Unannealed PVA/PAA bilayer (PAA surface), and (d) Annealed PVA/PAA bilayer (PAA surface). The cross-section morphology of (e) Unannealed PVA/PAA bilayer, and (f) Annealed PVA/PAA bilayer.

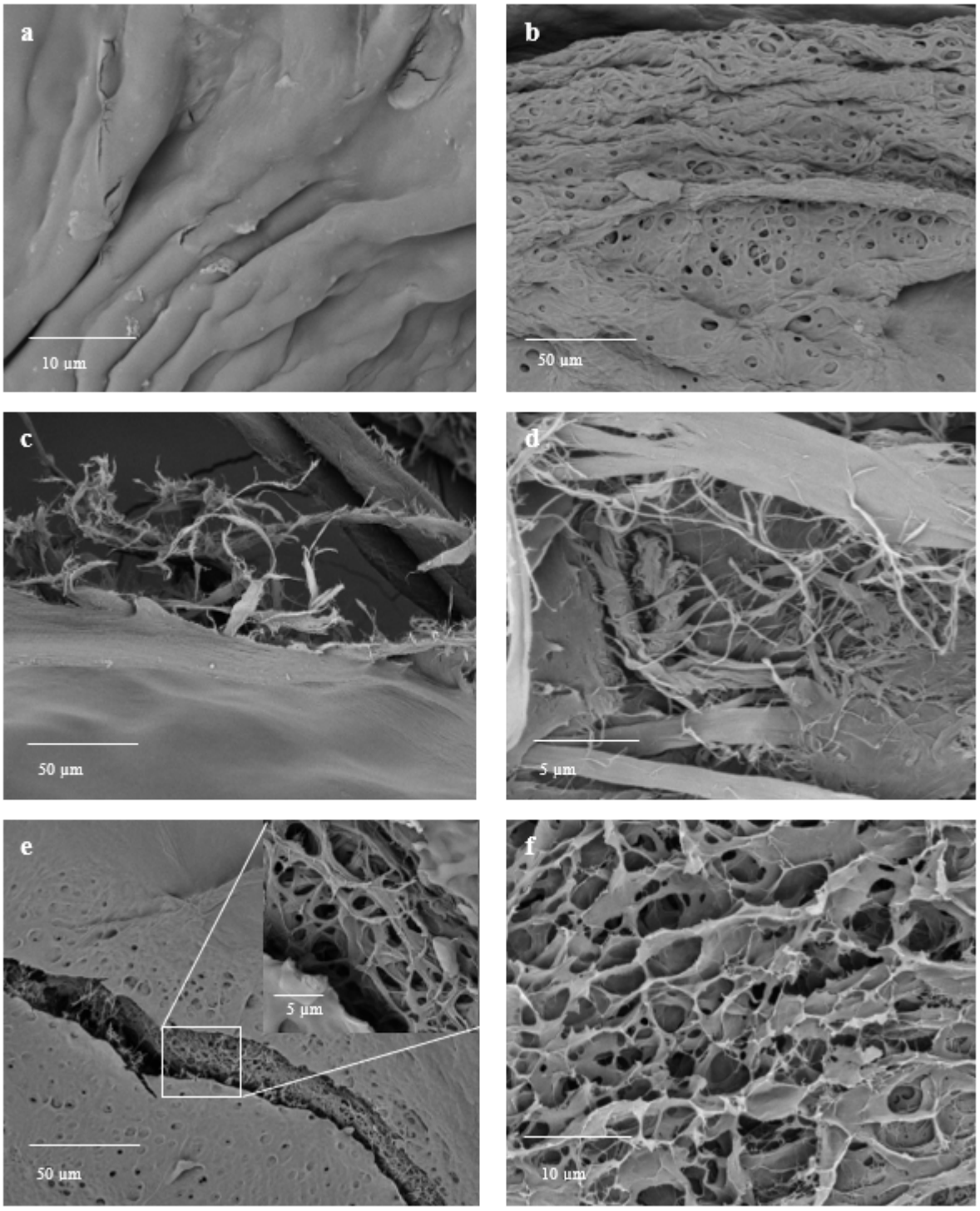

Figure 5.2: Electrospun nanofibres after swollen in pH 7.4 buffer for 48 h, (a) Unannealed PVA, (b) Annealed PVA, (c) Unannealed PVA/PAA bilayer (PVA surface), (d) Unannealed PVA/PAA bilayer (PAA surface), (e) Annealed PVA/PAA bilayer (PVA surface) and (f) Annealed PVA/PAA bilayer (PAA surface).

5.2.3 FTIR results

The major absorption bands of PVA and PAA were identified in the FTIR spectrum (**Figure 5.3**). The characteristic peaks of unannealed and annealed PVA (**Figure 5.3a and Figure 5.3b**) which included the peak around 3290 cm^{-1} for O-H stretching, 2943 and 2911 cm^{-1} for C-H stretching of alkyl group, 1431 cm^{-1} for C-H bending in CH_2 groups, 1266 cm^{-1} for C-O stretching, 1141 cm^{-1} for C-O-C stretching, 1092 cm^{-1} for C-O stretching, 920 cm^{-1} for C-H stretching and 838 cm^{-1} for C-C stretching [95]. When comparing unannealed PVA with annealed PVA, there was an extra peak at 1141 cm^{-1} on the annealed PVA spectra, which represented the crystalline sensitive band [220]. The PVA crystallisation is caused by the thermal annealing treatment.

Furthermore, the major absorption bands of unannealed and annealed PAA (**Figure 5.3e and Figure 5.3f**) included the peaks around 3506 cm^{-1} for free O-H group, 3138 cm^{-1} for bonded O-H group, 2943 cm^{-1} for C-H stretching, 1704 cm^{-1} for C=O stretching of carbonyl group, 1453 cm^{-1} for C-H bending in CH_2 groups, 1414 cm^{-1} for C–O–H bending, 1236 cm^{-1} for C-O stretching, 1171 cm^{-1} for C-O stretching, 907 cm^{-1} for C-O symmetric stretching and 803 cm^{-1} for CH_2 rocking [221], [222].

It is very difficult to identify the overlapping of PVA and PAA dominant peaks on the obtained spectra of the unannealed and annealed PVA/PAA bilayer nanofibres. This might be due to the bilayer nanofibres being too thick to determine the dominant peaks of the PAA surface when testing the PVA surface or vice versa. It can be concluded that the PVA and PAA did not completely blend together after annealing, two discrete layers were still remained. Therefore, both PVA surface and PAA surface of the unannealed and annealed PVA/PAA bilayer nanofibres were analysed separately.

On the PVA surface of the PVA/PAA bilayer, the degree of PVA crystallinity in the annealed PVA/PAA bilayer nanofibres (**Figure 5.3d)** has increased when compared to the unannealed PVA/PAA bilayer (**Figure 5.3c)**. It is supported by the sharper peak at 1141 cm^{-1} assigned to C-O-C stretching and C-C stretching. This result is similar to the result obtained from pure PVA nanofibres spectra.

It is possible that an esterification occurred from ester crosslinking, with presence of hydroxyl groups (-OH) of PVA molecules and carboxyl groups (C=O) from PAA molecules as

previously reported [198]. On the PAA surface of the PVA/PAA bilayer, the peaks at 1522 cm^{-1} and 1541 cm^{-1} (as indicated by the red region) were observed on both unannealed (**Figure 5.3g)** and annealed (**Figure 5.3h)** PVA/PAA bilayer, suggesting a shift peak from the band of 1610-1560 cm^{-1} assigned to -COO^{-} [223]. Moreover, the annealed PVA/PAA bilayer (**Figure 5.3h)** showed a peak at 1636 cm^{-1} (as indicated by the red region) assigned to C=O from ester crosslinking [224].

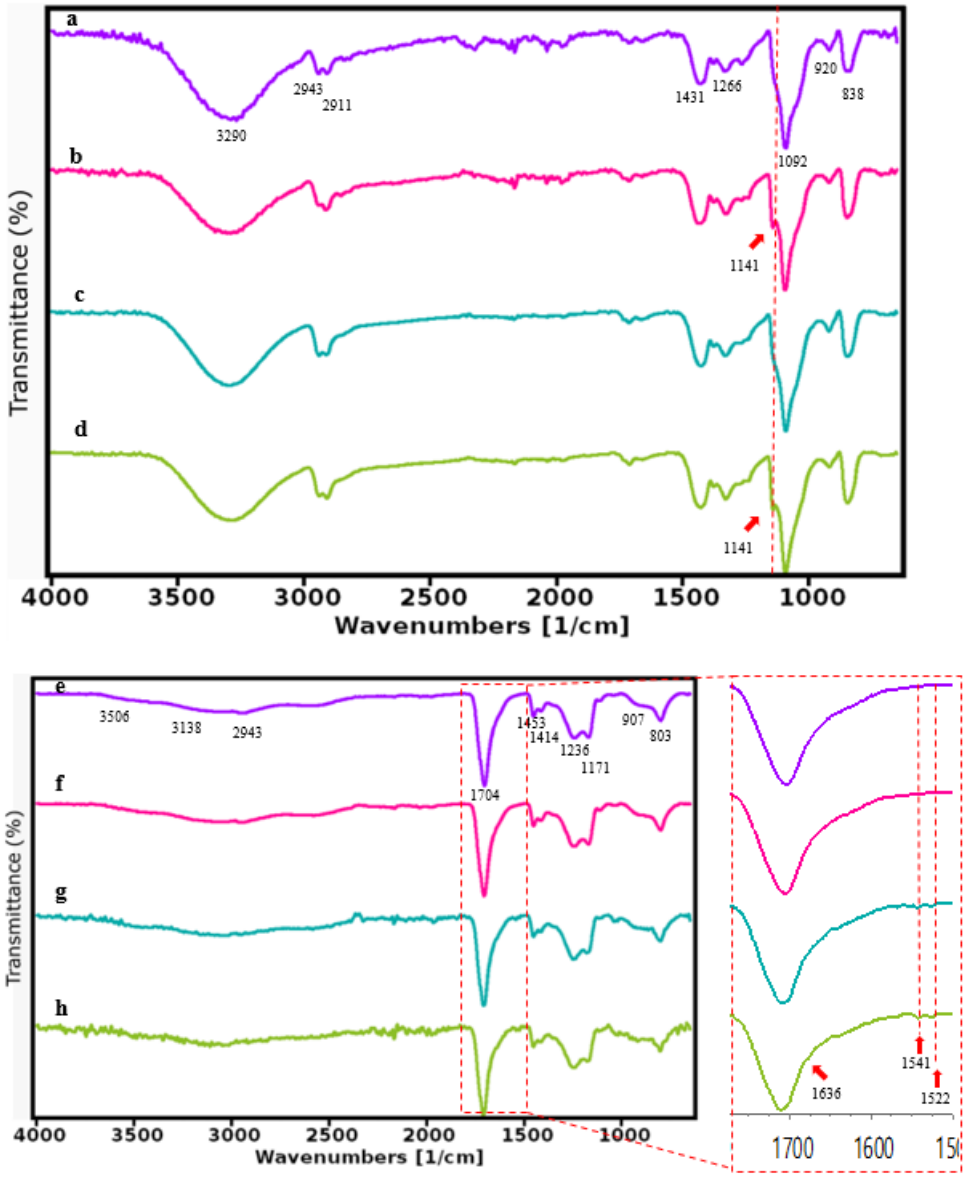

Figure 5.3: FTIR result of the electrospun nanofibres: (a) Unannealed PVA, (b) Annealed PVA, (c) Unannealed PVA/PAA (PVA surface), (d) Annealed PVA/PAA (PVA surface), (e) Unannealed PAA, (f) Annealed PAA, (g) Unannealed PVA/PAA (PAA surface), (h) Annealed PVA/PAA (PAA surface).

5.2.4 DSC results

The glass transition temperature (Tg) and melting temperature (Tm) of the pure PVA, pure PAA and PVA/PAA bilayer nanofibres before and after annealing were identified from the DSC thermographs and illustrated in **Figure 5.4a**. As reported by Samprasit *et al.*, the absence of endothermic and exothermic peaks below 100 °C, indicates the low moisture contents of the substances [225]. Therefore, the endothermic peaks observed in the temperature range of 41-53 °C attributed to the evaporation of adsorbed water in the samples [226]. Moreover, all the heat flow curves upon the cooling cycle and second heating cycle of each sample were a flat shape. The flat shape was caused by the rupture of ionic clusters of the sample around 250 °C at the first heating cycle and hence the polymer morphology is no longer possible to be recovered [227]. Therefore, the Tg and Tm of each sample were determined on the first heating cycle.

The Tg values decreased significantly from 132 °C to 86 °C in pure PVA nanofibres after annealing. It might be because annealing caused the relaxation of polymer chains and rearranged the crystallites into a crystal lattice, an effect seen for annealed starch [228]. In contrast, the Tg of pure PAA nanofibres increased from 102 °C to 120 °C after annealing because of the formation of strong covalent bonds in the anhydrides attributed by crosslinking that limited the segmental motions of the polymer chains [229]. In contrast to the pure PVA nanofibres, the Tg was not affected in the PVA/PAA bilayer nanofibres, the Tg was between 119 °C to 121 °C.

The endothermic melting peak of unannealed and annealed pure PVA were around 222 °C-223 °C and the crystallinity increased from 45% to 75% after annealing. While the pure PAA nanofibres showed no melting peak because it is amorphous [27]. For the unannealed and annealed PVA/PAA bilayer nanofibres, the Tm was the same at 221 °C. The PVA/PAA bilayer nanofibres had 27% and 30% crystallinity before and after annealing, respectively. This is similar to the result of Chen *et. al.* [207], annealing promoted the formation of crystallites of the PVA/PAA nanofibres.

5.2.5 DMA

The dynamic of the glass transition temperature in nanofibres samples was remeasured using DMA as the sensitivity of DMA is higher than that by DSC. As illustrated in **Figure 5.4b**, the Tg of unannealed pure PVA nanofibres was 110 °C. While the annealed pure PVA nanofibres exhibited two peaks at 84 °C and 131 °C. The first peak at 84 °C is called the α_a relaxation peak, it represents the glass transition temperature; the second peak at 131 °C is called the β_c relaxation peak, it is due to the relaxation in the PVA crystalline domains [122]. The results for pure PVA nanofibre samples were similar to DSC.

Furthermore, as illustrated in **Figure 5.4c**, the Tg of unannealed and annealed pure PAA nanofibres was found around 135 °C and 134 °C, respectively. The results were similar to the result reported by Garza *et. al.*, the centrifugally spun PAA nanofibres were found to have a Tg at 135.73 °C in DSC analysis [230]. By looking at the tan delta curve, there was a large drop after Tg in the pure PAA nanofibres, this might be due to the large shift of polymer chains and dehydration of adjacent carboxylic group for anhydrides formation [230].

As seen in **Figure 5.4d**, the unannealed PVA/PAA bilayer nanofibre sample has the Tg around 136 °C. A sudden drop of Tan delta to 0 was observed after Tg, suggested the transition of glassy region to the fluid region was increased for the unannealed PVA/PAA bilayer nanofibre sample. While the annealed PVA/PAA bilayer nanofibres sample has a Tg at 140 °C, and a βc relaxation peak at 154 °C. Therefore, the crosslinking reaction increased the Tg values of samples annealed characteristic of ester linkage and provided an improved mechanical property to these samples.

The variation of storage modulus in term of elasticity of PVA, PAA and PVA/PAA bilayer nanofibres are also determined using DMA. The unannealed PVA nanofibres has a storage modulus of ~219 MPa. After annealing, the PVA nanofibres showed the highest storage modulus at ~1380 MPa. It is directly related to the degree of crosslinking. Thus, the annealed PVA nanofibres has the highest degree of crosslinking, which supported by the DSC result. The storage modulus of unannealed and annealed PAA nanofibres are ~200 MP and ~132 MPa, respectively. Moreover, the unannealed and annealed PVA/PAA bilayer nanofibres have the lowest values of storage modulus of ~95 MPa and ~87 MPa, respectively. Due to the presence of PAA in the bilayer nanofibres, the storage modulus decreased, the stiffness of the materials decreased.

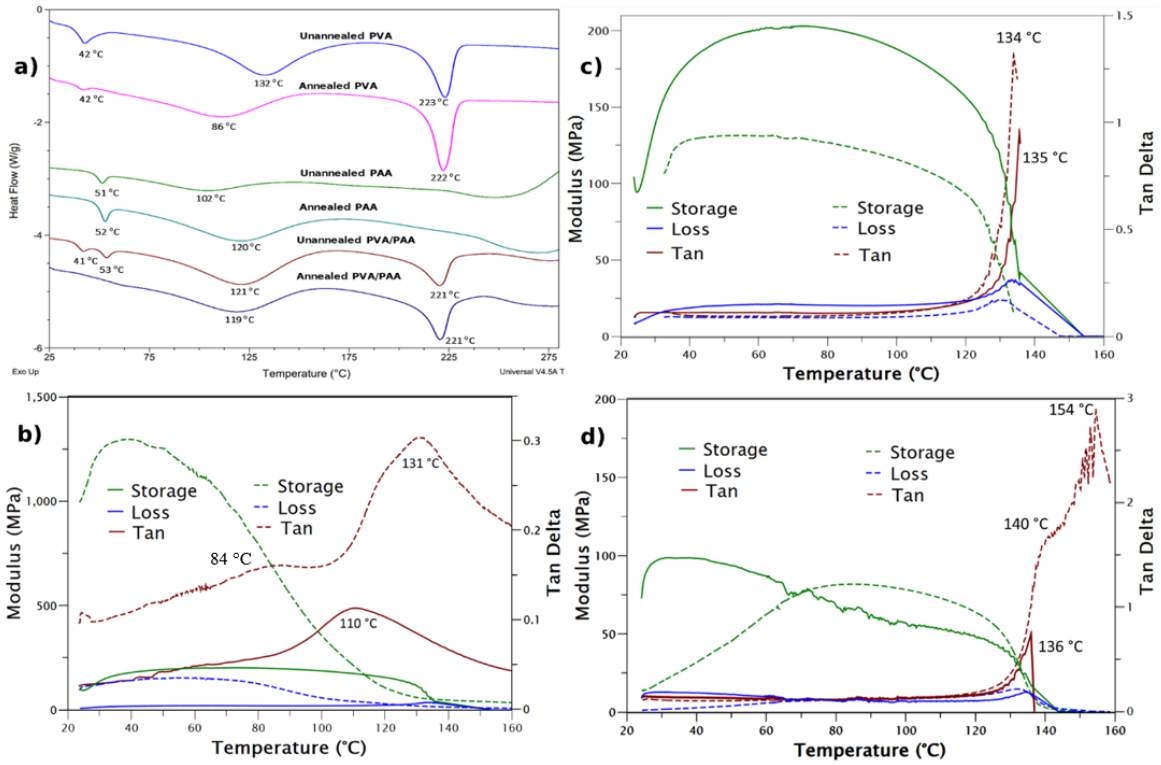

Figure 5.4: (a) DSC thermographs of the nanofibre samples. DMA spectra for (b) PVA, (c) PAA and (d) PVA/PAA bilayer nanofibre samples (Solid line represented unannealed samples; dashed line represented annealed samples).

5.2.6 Water contact angle

Water contact angle is the most straightforward method to measure the wettability property of a solid surface. The hydrophilicity increases with lower water contact angle. The PVA/PAA bilayer nanofibres are produced by a layer of pure PVA nanofibres and a layer of pure PAA nanofibres. It is proposed that the PVA and PAA were not melted and formed a blend after thermal annealing. As illustrated in **Figure 5.1e-f**, the annealed bilayer nanofibres sample still remained as two discrete layers. Therefore, the hydrophilicity was tested on both surfaces (i.e. PVA surface and PAA surface) of the PVA/PAA bilayer nanofibres.

Figure 5.5 shows that the surface wettability of PAA nanofibres was better than PVA nanofibres. On the PVA/PAA bilayer nanofibres, it can be seen that the contact angles of PAA surface (unannealed: 0°; annealed: 23°) were lower than the PVA surface (unannealed: 51°;

annealed: 67°). This indicated the PVA/PAA bilayer nanofibres were more hydrophilic when the water contacted on the PAA surface of the bilayer nanofibres. Moreover, the unannealed samples displayed a higher degree of hydrophilicity when compared to the annealed samples. The PAA surface of unannealed PVA/PAA nanofibres demonstrated a vanishing contact angle $\theta=0°$ within 27 seconds, indicated a super-hydrophilic wetting behaviour which can be attested to the hydrophilic group (C=O group). It can be concluded that the degree of hydrophilicity is related to the thermal annealing treatment and also depends on the type of polymers, in this case both PVA and PAA.

In addition, it is observed that the PVA surface of the bilayer nanofibre has the highest contact angle (67°) after annealing, suggesting a significant decrease in hydrophilicity of the corresponding surface of PVA from the PVA/PAA bilayer nanofibres. An increase water stability of annealed PVA/PAA bilayer nanofibres could be caused by the increase in average diameter of nanofibres after annealing. Furthermore, it could be caused by the formation of hydrophobic ester groups within the PVA and PAA molecules and the physical crosslinking network among small crystals of PVA during annealing process [208], [213], [231].

Overall, there are significant difference of these samples [i.e. unannealed PAA ($p < 0.0001$), annealed PAA ($p < 0.0001$), annealed PVA/PAA bilayer (PVA surface) ($p < 0.01$), unannealed PVA/PAA bilayer (PAA surface) ($p < 0.0001$), annealed PVA/PAA bilayer (PAA surface) ($p < 0.0001$)] when comparing with the unannealed PVA nanofibres.

5.2.7 Swelling and weight loss studies

As shown in **Figure 5.6b**, the nanofibres have a very fast swelling rate, all the samples have achieved full swelling within 1 mi and reached the plateau in 60 min. The unannealed PVA, PAA and PVA/PAA bilayer nanofibres have a maximum swelling degree of 930%, 257% and 637%, respectively. Furthermore, the results showed a lower swelling ratio in the annealed samples. The annealed PVA, PAA and PVA/PAA bilayer nanofibre samples have a maximum swelling degree of 613%, 199% and 437%, respectively. For pure PVA nanofibres, such decrease of the swelling degree after thermal annealing treatment is influenced by the increase of PVA crosslinking density, i.e., the decrease of the polymer network free volume and subsequently decreased the polymer to swell in the buffer. For PVA/PAA bilayer nanofibres, PAA is used as a crosslinking agent and esterification crosslinking occurred during thermal

annealing treatment. The decrease in swelling ratio of annealed PVA/PAA sample expected to influence by the presence of PAA, indicating the crosslinking density was further increased by the esterification reaction [198], [231].

It should be also taken into account that the thermal annealing influences the hydrophilicity of the nanofibres (**Figure 5.5**), and, consequently, contributes to the swelling ability of the nanofibres [232]. After the nanofibres were fully hydrated, the swelling index started to decrease due to the disintegration of nanofibres into the pH 7.4 buffer. The unannealed and annealed PVA and PVA/PAA nanofibres were partially disintegrated and reached equilibrium within 60 min. However, the unannealed and annealed PAA started to degrade at 7 min and 13 min, respectively (**Figure 5.5b)**. Although the annealing process did not improve the water stability of pure PAA nanofibres, the complete degradation of pure PAA nanofibres are extended from 15 min to 30 min.

Regarding the water stability of PVA/PAA bilayer nanofibres, due to the high-water solubility of PVA and PAA, the % weight loss of unannealed PVA and PVA/PAA bilayer nanofibres was 78% and 74%, respectively. However, after annealing, the % weight loss of annealed PVA and PVA/PAA bilayer nanofibres has decreased to 40% and 67%, respectively. The water stability of annealed PVA/PAA bilayer nanofibres was slightly improved. These swelling and degradation characteristics of nanofibres are of potential in order to modulate a complex dual delivery with two different poor solubility drugs on the bilayer nanofibres so as to improve the drug release profile.

5.2.8 Disintegration test

Same sizes of unannealed and annealed PVA, PAA and PVA/PAA bilayer nanofibres were immersed in the pH 7.4 buffer. As seen in **Figure 5.6a**, the nanofibres curled and shrunk once they contacted with the buffer. The PVA and PVA/PAA nanofibres with and without annealing were not completely disintegrated after 48 h of buffer immersion at room temperature. In contrast, the unannealed and annealed PAA nanofibres were dissolved within 30 min as mentioned in the swelling test. Hence, the PAA nanofibre layer on the unannealed and annealed PVA/PAA bilayer nanofibres might be completely disintegrated and only the PVA nanofibre layer was left after 48 h.

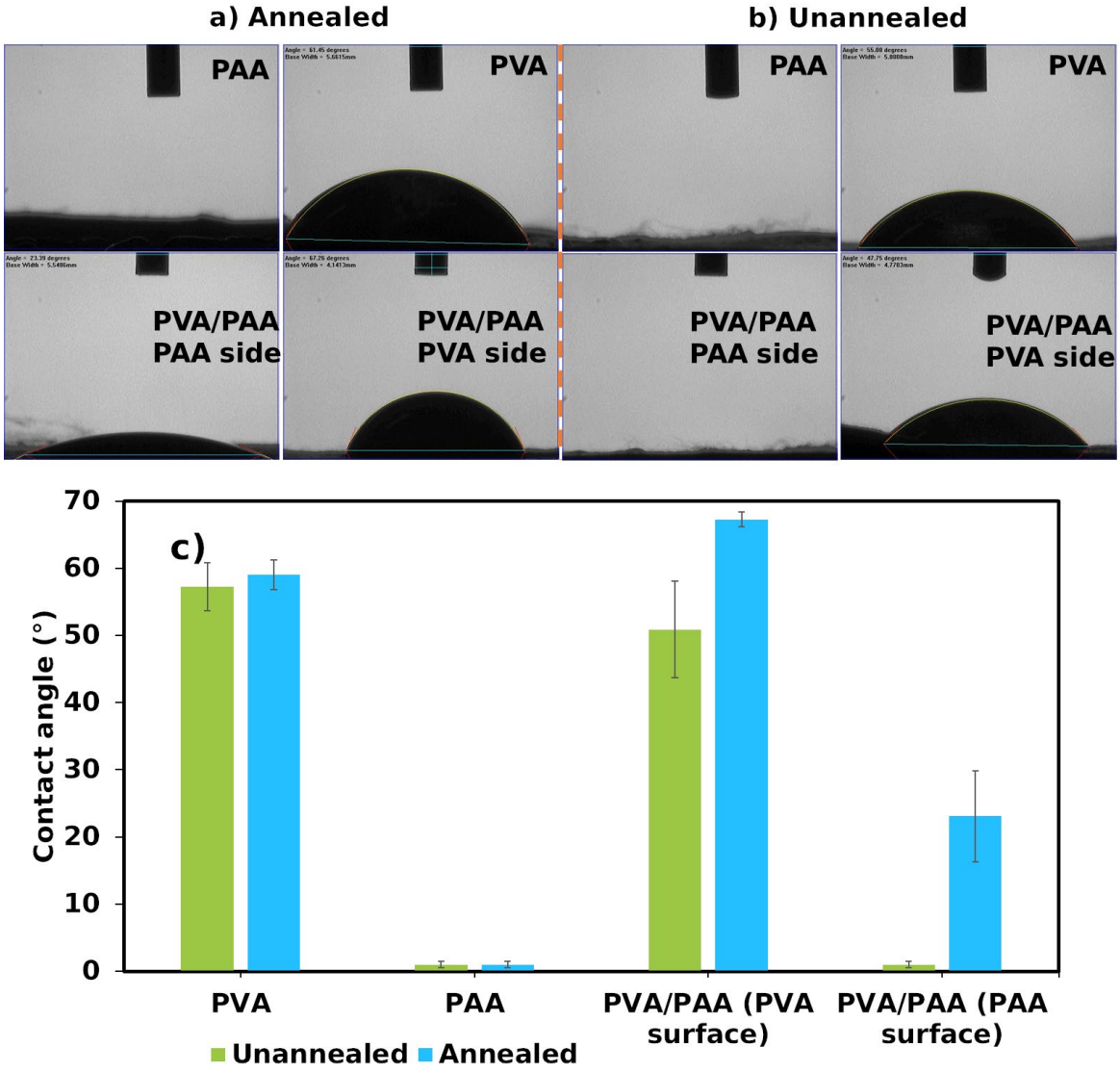

Figure 5.5: Images of water droplet on (a) annealed nanofibre samples, and (b) unannealed nanofibre samples at 27 seconds. (c) contact angle measurement of electrospun nanofibre samples.

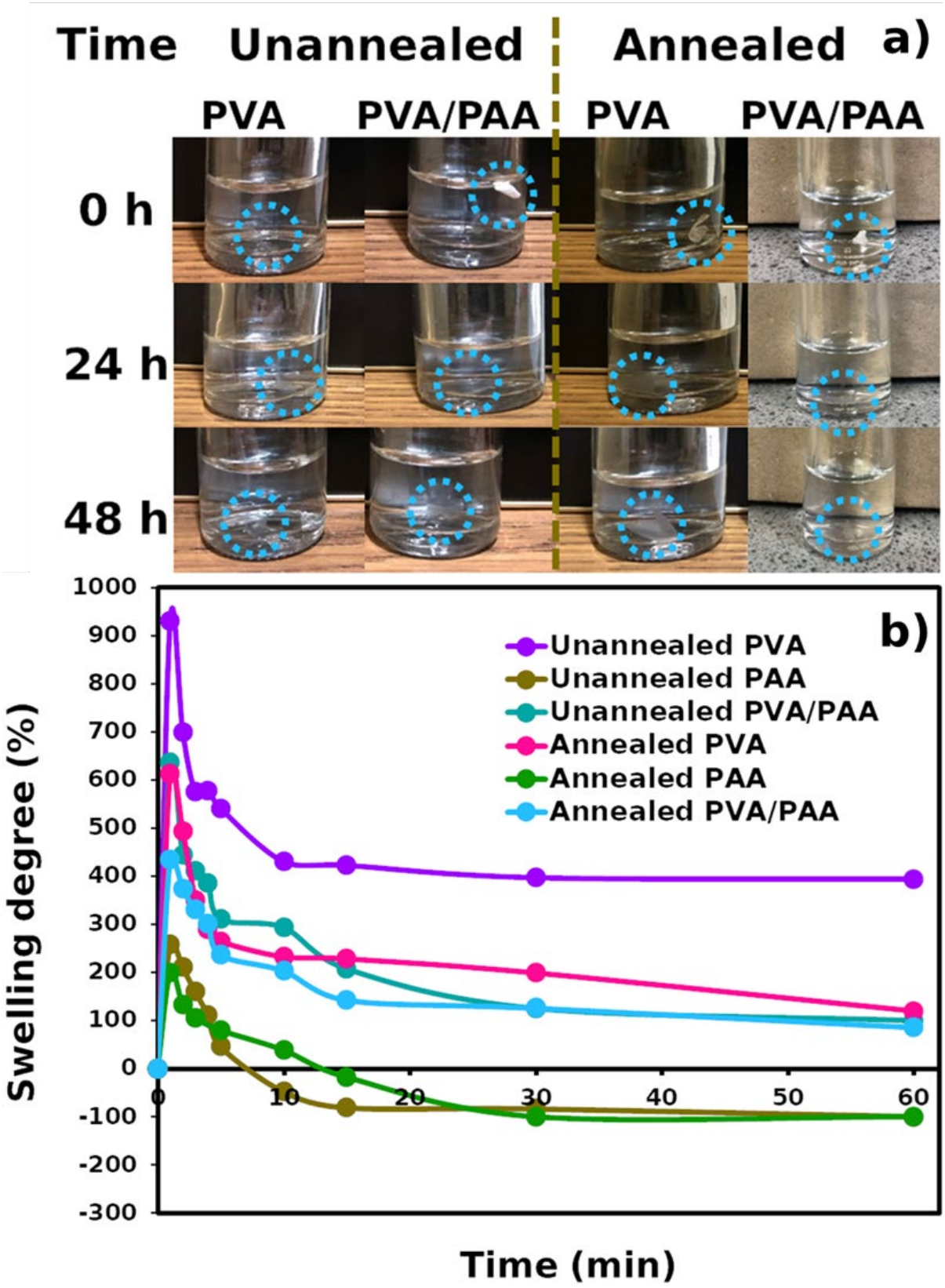

Figure 5.6: (a) Disintegration studies, (b) Swelling and degradation characteristic of unannealed and annealed PVA, PAA and PVA/PAA bilayer nanofibres.

5.2.9 *In vitro* drug dissolution study

The drug release of the antibiotic (CLA in **Figure 5.7b**, as clarithromycin) is steadily released, achieving 100% after 24 h. When the bilayer is used for this drug, there seems to be a slow release rate attributed to the crosslink between layers that better entrap this drug.

However, no significant variation is seen with heat-annealing in the release rate for pure PAA, since this drug was incorporated into the PAA, and this polymer readily dissolves under water; therefore, it expected that the annealing would weakly affect this rate. It is also interesting to notice that, even though the PAA is readily dissolved, there is a slower drug release rate for annealed bilayer both for a high and lower dosages of this drug. Since the interaction between the polymer and the drug changed after heating and it forms an assemble structure, it is possible that the crosslink, evidenced by the FTIR section, retained part of the drug at the interface of both films and this behavior occurred.

According to **Table 5.1**, unannealed and annealed PVA/DOX+PAA/CLA high bilayer nanofibres best fit in Korsmeyer-Peppas drug releasing model with the R^2 value of 0.9398 and 0.9254, respectively. The n exponent was 0.7907 ($0.45 < n < 0.89$) for unannealed PVA/DOX+PAA/CLA high bilayer nanofibres, indicating the CLA released by non-Fickian transport. While, annealed PVA/DOX+PAA/CLA high bilayer nanofibres with the n exponent = 1.0427 ($n > 0.89$) obeyed the Super case II transport method. This occurs when the sorption process is completely controlled by stress-induced relaxations [233], [234].It is further explained that the speed of buffer diffusion is much higher, resulted in an acceleration of buffer penetration and followed by tension and breaking of the nanofibres [234]. Furthermore, only unannealed PVA/DOX+PAA/CLA low bilayer nanofibres best fit in zero-order drug release model, suggesting the drug release rate as independent of its concentration of the dissolved substance. The remaining nanofibres best fit in first-order drug release model, indicating the drug release rate as dependence on the concentration of the dissolved substance.

When doxorubicin hydrochloride (DOX) is used, the pure PVA presents a very slow-release rate, and it further decreases with annealing. In addition, it seems that it reaches constant values after 24 h. Nonetheless, when a bilayer is used for releasing this drug, there seems to be a steady release rate, but it also reaches low maximum dosages at 24 h (2% drug release). This is a very good indication that the drug will be slow released with non-harmful dosages. Doxorubicin hydrochloride is very toxic and controlling the rate of this drug is very important for any

targeted application. Although, no further values after 24 h were made, it is possible that the drug will continue being delivered based on the profile of the release curve.

Table 5.1: Mathematical modelling of drug releasing profile for clarithromycin.

	Zero order	First order	Higuchi	Korsmeyer-Peppas		Hixson-Crowell
	R^2	R^2	R^2	R^2	n	R^2
Unannealed PAA/**CLA** high	0.5616	0.9286	0.7884	0.7323	0.6508	0.8707
Annealed PAA/**CLA** high	0.6078	0.8884	0.8270	0.8164	0.6193	0.8404
Unannealed PAA/**CLA** low	0.5839	0.9691	0.8572	0.9106	0.8312	0.9317
Annealed PAA/**CLA** low	0.5230	0.945	0.8281	0.9103	0.625	0.9031
Unannealed PVA/DOX+PAA/**CLA** high	0.5253	0.8887	0.7998	0.9398	0.7907	0.8581
Annealed PVA/DOX+PAA/**CLA** high	0.4805	0.9248	0.7741	0.9254	1.0427	0.865
Unannealed PVA/DOX+PAA/**CLA** low	0.9898	0.7731	0.9643	0.9762	0.8481	0.8441
Annealed PVA/DOX+PAA/**CLA** low	0.7108	0.9988	0.929	0.9401	0.7676	0.987

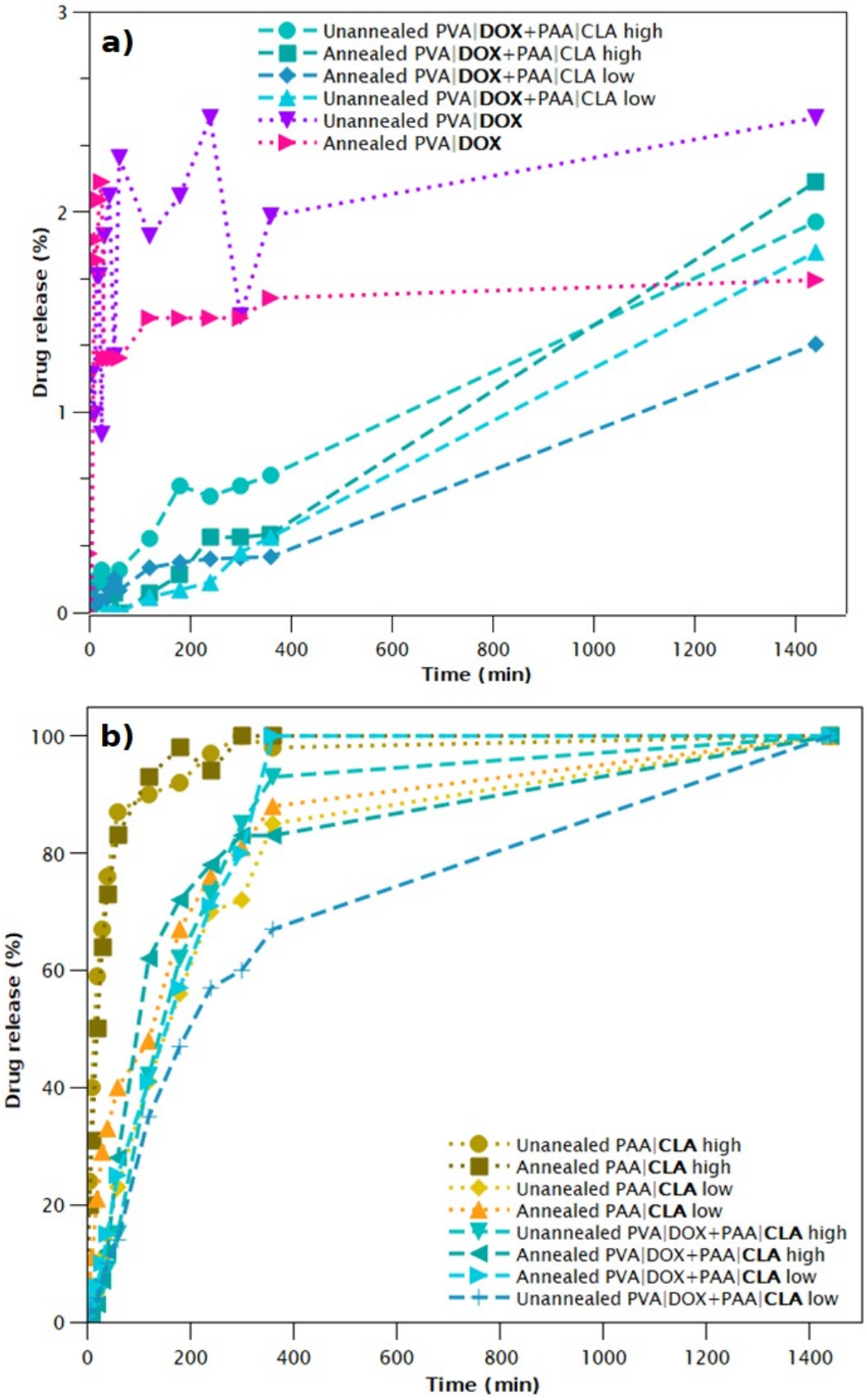

Figure 5.7: Drug dissolution studies of (a) CLA and (b) DOX from the electrospun nanofibre samples. Bold character in the legend of each figure indicates the drug that is being studied.

5.2.10 Cell proliferation inhibition studies

The human osteosarcoma U2OS cell line was used to investigate the effect of DOX with or without CLA as it is reported that this antibiotic presents a synergism effect when used together with DOX in MCF7 breast cancer cells. Therefore, it is hypothesised that DOX and CLA also may present synergism against osteosarcoma cell line. Primarily the pure drugs of CLA and DOX were tested against the U2OS cells but also in conjunction using various dosages of both drugs. It can be seen in **Figure 5.8a** that most concentrations slightly decreased the cell viability with a mean of 30%, even the DOX dosages studied herein were not able to fully inhibit these cells. However, when both drugs (DOX+CLA) are used in conjunction two specific dosage inhibited more than 40% cell growth, which was the CLA H+DOX M and CLA H+DOX H. Regarding their synergism, CLA H+DOX M presenting a value of 0.9 (CDI <1) indicating this specific dosage gave a synergism effect. In this case, 0.374 mg/ml of CLA and 4 μg/ml of DOX. However, the CDI value of CLA H+DOX H was 1.2 (CDI >1) showed that this drug combination has an antagonistic effect. While the other drug combinations of CLA H+DOX L, CLA L+DOX L, CLA L+DOX M and CLA L+DOX H showed a synergism effect with the CDI values of 0.9, 0.8, 0.8 and 0.9, respectively. Therefore, this result showed that the combination of both drugs can also be used for the treatment of osteosarcoma.

When these drugs were incorporated into the electrospun membrane, their values further increased the cell inhibition from up to 90% **(Figure 5.8b)**; however, it is possible that these values may be masked by the PAA, which in this work indicates that it is extremely harmful for these cells. It is possible that the dissolution of the PAA creates an acidic environment, and the cells cannot proliferate, so the neutralisation used for the pure PAA was inadequate. Nonetheless, membranes with pure DOX exhibited a decrease in the cell inhibition when thermal treatment was performed, presenting a statistically significant difference and this may be related to their drug release behavior where higher dosages was obtained with unannealed samples. The CDI values for the bilayer nanofibres containing DOX and CLA were all greater than 1, indicating an antagonistic effect. Thus, the concentration of DOX and CLA in the bilayer nanofibres has to be further modulated.

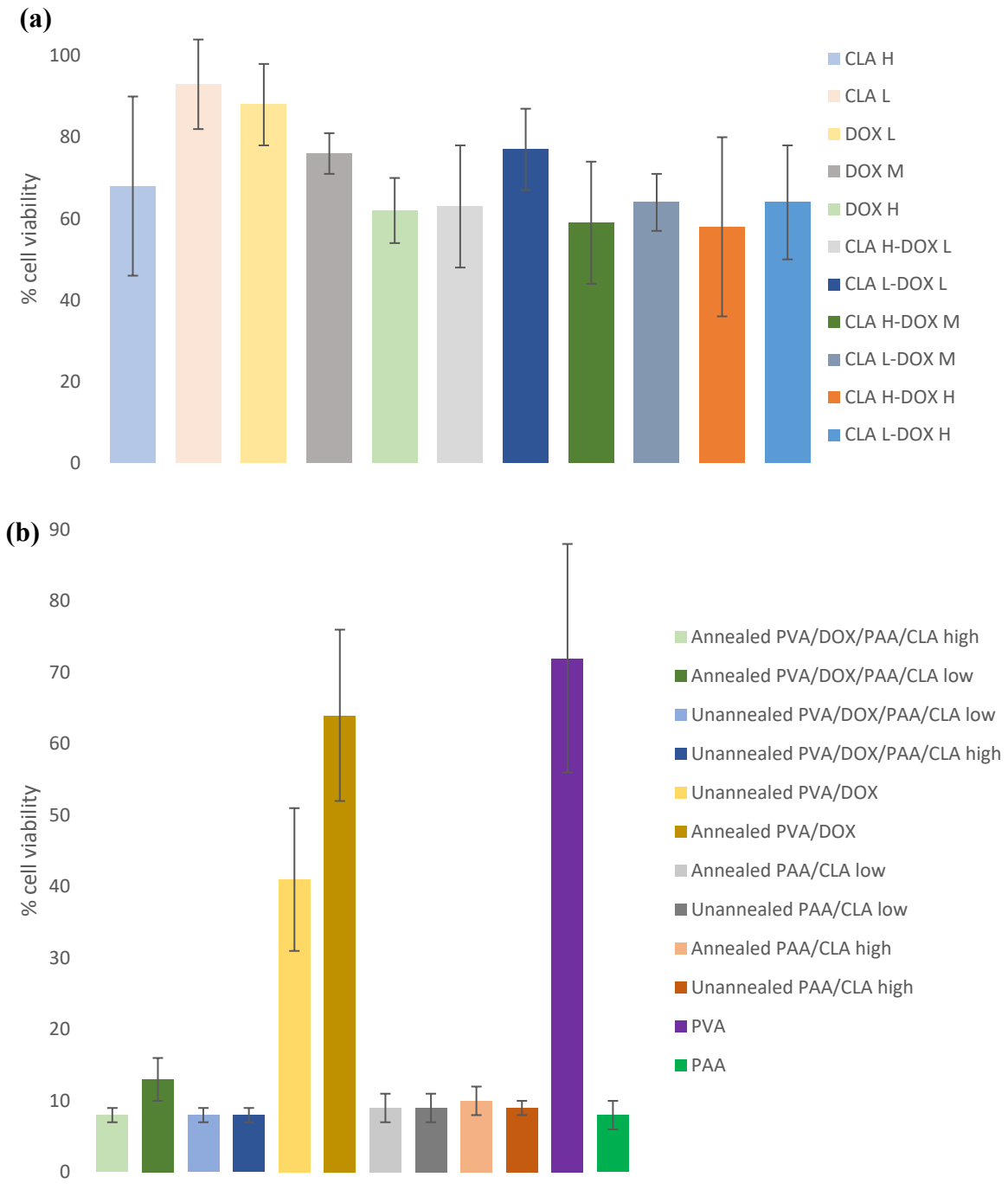

Figure 5.8: Osteosarcoma U2OS cell cytotoxicity values against (a) pure and combined clarithromycin and doxorubicin effects at various dosages and (b) membrane loaded drugs.

5.3 Summary

In summary, the PVA/PAA bilayer nanofibres were successfully prepared using electrospinning technology and thermal annealing treatment. Only the annealed nanofibres at

100 °C for 3 h without variation on colour tone from white, proving to be non-degraded nanofibres were analysed. The morphology, diameter and thickness of the nanofibres samples were characterised by FESEM. The results showed an increase of average diameter of annealed PVA and PAA nanofibres, but a decrease in thickness in annealed PVA/PAA bilayer nanofibres. Moreover, the crystallinity of the annealed PVA/PAA bilayer nanofibres have increased, indicating the increase of physical crosslinking within the PVA/PAA polymer matrix during the annealing process. The impact of PAA on the hydrophilic property of the PVA was described. There was a difference in degree of hydrophilicity of the nanofibre surfaces of PVA and PAA. The PAA nanofibre layer had a higher hydrophilicity than PVA nanofibre layer. The annealed bilayer nanofibres can be considered as a potential to be used in modelling drug release especially for dual drug delivery, whereby biologically relevant drug molecules can be incorporated into the polymer solution prior to electrospinning. Further work would be useful to increase the crosslinking density by changing the temperatures and time of annealing. The combined effect of clarithromycin and doxorubicin proves that a synergetic enhance cytotoxicity against osteosarcoma cell line occurs and it may be improved with the bilayer electrospun bilayer. However, the PAA needs to be further evaluated towards their safety of usage. Nonetheless a fast and slow release-rate can be achieved using this membrane for any targeted application and this works provides the advantage of a different surface hydrophilicity that could be modulated for drug release rate of two different drugs on PVA/PAA bilayer nanofibres.

Chapter 6

Synthesis and characterisation of freeze-thawed electrospun Polyvinyl alcohol nanofibres

6.1 Introduction

Electrospinning is one of the foremost nanotechnology applications with high flexibility and versatility to fabricate polymer fibres encapsulated with drug with the diameters in nanometres range. By adjusting the parameters of electrospinning such as polymer parameter, solution parameter, ambient parameter and the processing conditions, the morphology and diameter of the electrospun nanofibres can be further tailored [66]. Furthermore, the use of nanotechnology in drug delivery system can enhance bioavailability, stability and solubility of drugs [235]. In this case, the incorporation of propolis extract by directly dissolving it into the PVA solution resulted in the bioactive molecules are better encapsulated in the PVA nanofibres.

Because of PVA does not have any fundamental antimicrobial property, it has acted as a drug nanocarrier with higher surface wettability, biocompatible and controlled drug release in medical device materials for pharmaceutical applications. While, propolis extract was being selected as the active pharmaceutical ingredient (API). As propolis extract contains abundant phenolic compounds and flavonoids that have the antimicrobial, anti-inflammatory [95], [236], anticancer [237] and antioxidant [238] activities, it can decrease hospital infections which caused by the Gram positive bacteria (e.g. *Staphylococcus aureus*) and the Gram negative bacteria (e.g. Enterobacter species and *Escherichia coli*) [239]. Due to these great properties, propolis extract is widely used for wound healing. Nevertheless, propolis extract promote cell growth by lowering the concentration to a certain threshold [240]. In addition, every individual propolis has a difference in the chemical compositions (e.g. caffeic acid, cumaric acid, ferulic acid etc.), which depend on several factors such as the flora in the part of country where it is collected, the season that propolis is produced, the selection of extraction solvent and extraction methods [241], [242].

Propolis extract has been incorporated within the PVA polymer as hydrogels [95], [236] and nanofibres [239], [243]–[246] prepared using different molecular weight and concentration of PVA as well as different concentration of propolis extract by many researchers to study their drug releasing profile. For example, the freeze-thawed PVA/propolis extract hydrogels have the drug release more than 6 h to 24 h [95], [236]. Furthermore, the heat treated electrospun PVA/propolis extract nanofibres performed a sustained release for at least 90 h [243]. The

electrospun PVA/propolis extract nanofibres without applying any further treatment has a complete release in 15 min [244] . Nevertheless, study on freeze-thawing (FT) PVA electrospun nanofibres containing propolis extract has not been investigated yet.

Previous work has been producing a dual layer PVA patch by pouring PVA solution on top of PVA electrospun nanofibres and underwent FT [247]. The freeze-thawed PVA hydrogel containing PVA nanofibres showed an increase of swelling ratio. Moreover, PVA contained glutaraldehyde (GA) as a chemical crosslinker was electrospun and followed by immersing in an aqueous solution for FT [248]. The freeze-thawed PVA/GA showed an increase of tensile strength compared to pristine nanofibres. In addition, glycerol (Gly) was added to PVA solution prior to electrospinning to form physical crosslinking and followed by three FT cycles, which led to stability in water [249]. Both of the freeze-thawed PVA nanofibres previously mentioned have contained a chemical reagent (e.g. GA, GLY) to increase the crystallinity of nanofibres and drug release studies were not yet evaluated. Therefore, this study aims to fabricate PVA nanofibres without using any reagents and also carry out the FT process without immersing the nanofibres into aqueous solution to avoid the release of propolis extract during the FT cycle.

The chemical, thermal, mechanical and swelling properties as well as the drug releasing behaviour of PVA as-spun and freeze-thawed PVA electrospun nanofibres encapsulated with ethanolic propolis extract are comprehensively studied. The freeze-thawed PVA nanofibres are not limited to be used as wound dressings, they have the potential to be used in a variety of biomedical applications including therapeutics and regenerative medicine which need a bi-phasic drug delivery system.

6.2 Result and Discussion

6.2.1 Phenolic compounds in propolis extract

Ultrasonic extraction method was employed because this method can shorten the extraction times significantly and offer the best extraction yields of phenolic compounds contained in the Brazilian propolis extract. According to a previous study, the propolis/ethanol ratio of 1:10 with a minimum of 30 min ultrasonication gave the highest amount of phenolics than other extraction methods such as maceration extraction and microwave assisted extraction [250]. In addition, 70% ethanol is the most effective solvent for extraction as this specific concentration

of ethanol can strongly inhibited microbial growth and had the greatest antioxidant activity [251].

Figure 6.1 presented the λ max of the phenolic compounds in five batches of propolis extract at $1x10^4$ g/ml. The curve of Batch 2 and Batch 3 were hardly observed as they were overlapped with Batch 4. It showed that the propolis extracts had a λ max around 254 nm. Hence, the wavelength of 254 nm was used to determine the propolis concentration during the drug release studies.

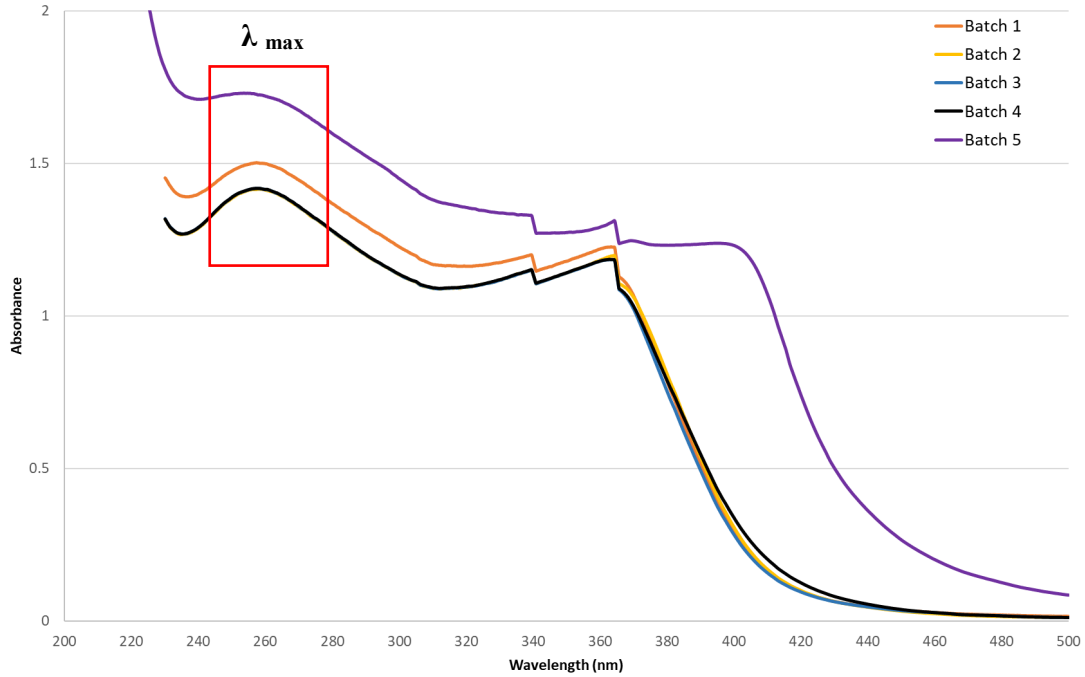

Figure 6.1: UV spectra for propolis extract using ultrasound extraction method.

6.2.2 FESEM

The FESEM revealed that all the electrospun nanofibres samples were not uniform and beads were found within the nanofibres. As illustrated by the diameter distribution graphs in **Figure 6.2**, the average diameter of pure PVA as-spun, PVA+5% propolis as-spun, PVA+10% propolis as-spun, PVA+15% propolis as-spun and PVA+20% propolis as-spun nanofibres was 142±57 nm, 176±50 nm, 161 ±52 nm, 161 ±54 nm and 160±74 nm, respectively. Furthermore, the average diameter of pure PVA FT, PVA+5% propolis FT, PVA+10% propolis FT, PVA+15% propolis FT and PVA+20% propolis FT nanofibres was 148±62 nm, 142±44 nm, 137 ±40 nm, 190 ±51 nm and 171±61 nm, respectively. When comparing the nanofibres in the same propolis concentration before and after freeze-thawing, there are significant difference between PVA+5%

propolis as-spun and PVA+5% propolis FT nanofibres as well as between PVA+15% propolis as-spun and PVA+15% propolis FT nanofibres. The diameter distribution of nanofibres are showed in **Figure 6.3**.

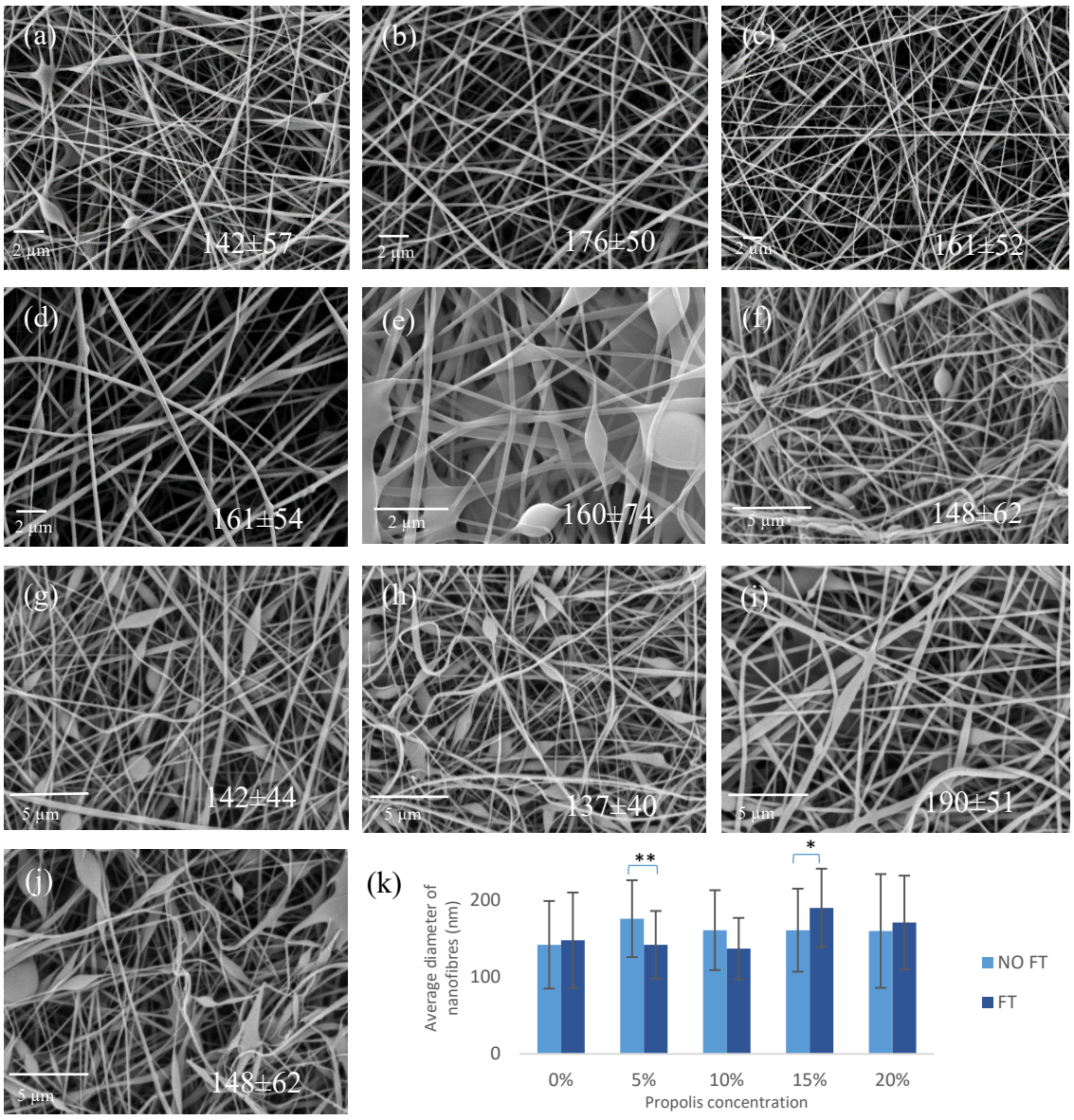

Figure 6.2: Surface morphology of (a) PVA as-spun, (b) PVA+5% propolis as-spun, (c) PVA+10% propolis as-spun, (d) PVA+15% propolis as-spun, (e) PVA+20% propolis as-spun, (f) PVA FT, (g) PVA+5% propolis FT, (h) PVA+10% propolis FT, (i) PVA+15% propolis FT, (j) PVA+20% propolis FT electrospun nanofibres samples, (k) average diameter of all samples.

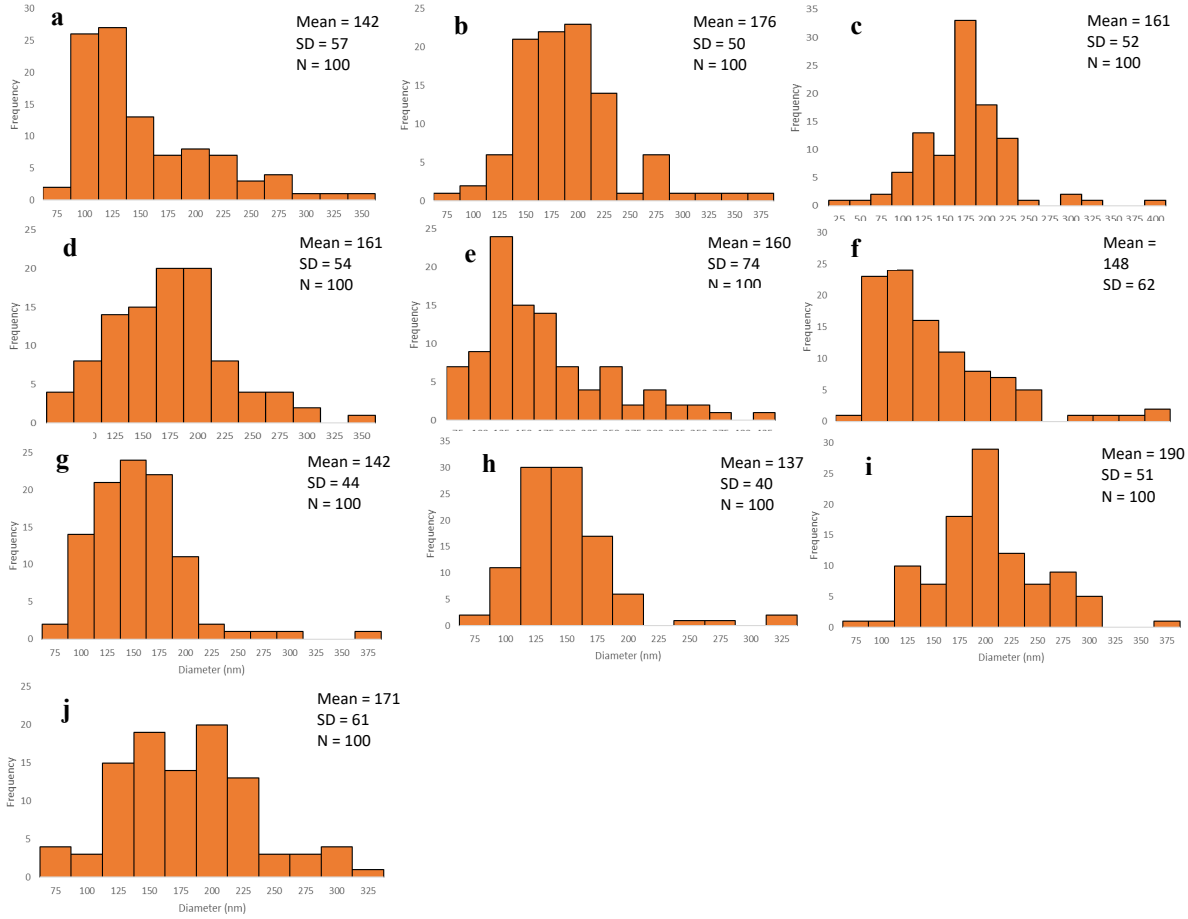

Figure 6.3: Diameter distribution of (a) PVA, (b) PVA+5% propolis, (c) PVA+10% propolis, (d) PVA+15% propolis, (e) PVA+20% propolis, (f) PVA FT, (g) PVA+5% propolis FT, (h) PVA+10% propolis FT, (i) PVA+15% propolis FT, (j) PVA+20% propolis FT electrospun nanofibres samples.

6.2.3 Conductivity, surface tension and viscosity of PVA and PVA+propolis solutions

The physiochemical properties included conductivity, surface tension and viscosity of PVA and PVA+propolis polymer solutions are the important solution parameters that could affect the morphology and diameter of the produced nanofibres. According to **Figure 6.4a**, the surface tension of the polymer solutions decreased from 72 mN/m to 52 mN/m with increasing propolis extract concentration, resulting an increase formation of beaded nanofibres. As reported by Liu *et. al.*, the number of beads on the nanofibres increased with a lower surface tension [252]. Therefore, an increase of PVA concentration higher than 7 %(w/v) should help to increase the surface tension and leading to fewer beads.

In contrast, the conductivity (**Figure 6.4a)** of the polymer solutions increased with an increase of propolis extract concentration. The increasing conductivity was probably resulted from the nature of chemical compounds with many hydroxyl groups (i.e. flavonoids, amino acids, phenolic acids) in the propolis extract [243]. Electrical conductivity directly influences the build-up of an electrostatic repulsion force that is critical to initiate jetting [253], higher charges level giving higher elongation forces and thus smaller diameter can be created. The conductivity of PVA+propolis polymer solutions at 167-234 μS/cm fabricated the nanofibres with the diameter ranging from 137-190 nm.

The viscosity **(Figure 6.4b)** of the polymer solutions also increased with an increase concentration of propolis extract, though a lower viscosity reading was observed for PVA+10% propolis solution. As reported by de Lima *et.al.* (2018), the balance of viscosity is very crucial, a low viscosity excludes the formation of continuous fibres and cannot resist the bead formation during electrospinning [254]. Even though the viscosity has increased in PVA+propolis polymer solutions up to 0.49 Pa.s, it was not high enough to form smooth nanofibres. Previous works showed that viscosity greater than 1.00 Pa.s have successfully fabricated smooth and non-beaded PVA/propolis nanofibres. For example, Zeighampour *et. al*. using 8 %w/v PVA solution (MW 72,000 g/mol, distilled water as solvent) containing 40% propolis extract had a viscosity of 1.024 Pa.s have produced uniform and non-beaded nanofibres [243]. Chawalinee *et. al.* also produced non-beaded nanofibres using 10 %w/v PVA (MW 85,000-146,000g/mol, distilled water as solvent) containing 2%(w/v) propolis extract with a viscosity of 1.613 Pa.s [255].

As the solution parameters in electrospinning is highly related to each other, the surface tension, conductivity and viscosity have to be considered together in order to fabricate the desired nanofibres.

(a) Sample	Conductivity (µS/cm)	Surface tension (mN/m)
PVA	92±11	71.99±1.06
PVA+5% propolis	167±23	56.14±1.03
PVA+10% propolis	184±5	54.32±1.06
PVA+15% propolis	212±23	54.18±0.66
PVA+20% propolis	234±1	51.89±0.73

(b)

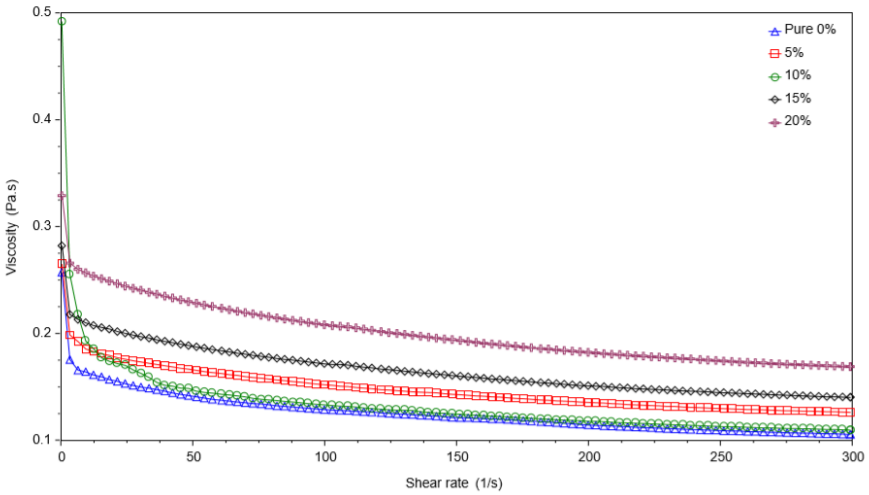

Figure 6.4: (a) Conductivity and surface tension of electrospinning solution. (b) Viscosity of PVA, PVA+5% propolis, PVA+10% propolis, PVA+15% propolis and PVA+20% propolis solutions.

6.2.4 FTIR analysis

Since the propolis extract is an alcoholic extract, the characteristic bands of ethanol can be found in propolis extract. The FTIR of ethanolic propolis extract (**Figure 6.5**) showed the broad band at 3600 cm^{-1} - 3100 cm^{-1} related to O-H stretching and O-H wagging (hydroxyl group of phenolic compounds) [236], [256]. The three peaks between 2976 cm^{-1} and 2899 cm^{-1} were assigned to the aliphatic and aromatic C-H stretching [256]. The peaks around 2359 cm^{-1}, 2133 cm^{-1} and 1922 cm^{-1} attributed to O=C=O, C=C=O and C=C=C groups, respectively. The peaks on the band at 1454 cm^{-1} - 1274 cm^{-1} would be related to O-H bending [256]. The band at 1088 cm^{-1} and 1048 cm^{-1} would be due to C-O stretching of ester groups [236], [256]. In addition, propolis extract had confirmed the presence of abundant phenolic compounds, mainly flavonoids and aromatic acids [239]. Therefore, aromatic bands were also identified in the spectra. The band at 1651 cm^{-1} corresponding to the double bond (C=C group) adsorptions and was shown by most six-membered aromatic rings systems [256]. The band at 1274 cm^{-1} would be related to the C-O groups of polyols and ester groups of flavonoids [236]. The band at 880 cm^{-1} would be due to aromatic ring ($R_2C=CH_2$ group) vibration and Meta-disubstituted benzene

ring [256]. All the bands stated above was found to be similar to the Brazilian propolis described in the other study [257].

As can be seen from **Figure 6.6a**, all major peaks of PVA related to hydroxyl and acetate groups were all identified, which included band at 3304 cm^{-1} for O-H stretching; band at 2944 cm^{-1} and 2910 cm^{-1} for C-H stretching of alkyl groups; band at 1713 cm^{-1} for C=O stretching of unhydrolysed acetate groups and C=C stretching; band at 1432 cm^{-1} for bending, wagging, in plane (C-H in CH_2 groups) stretching (C-O-C) of unhydrolysed acetate groups, in plane (O-H); band at 1377 cm^{-1} for coupling of in plane (O-H), wagging (C-H); band at 1335 cm^{-1} for bending (CH+OH), fan and twist (-CH_2-); band at 1264 cm^{-1} and 1237 cm^{-1} for C-C stretching, fan and twist (-CH_2-); band at 1141 cm^{-1} for C-O-C stretching, C-C stretching; band at 1092 cm^{-1} for C-O stretching, O-H bending; band at 920 cm^{-1} for stretching (bending out of plane) (O-H); band at 850 cm^{-1} for stretching, pendular C-C [95], [236].

Furthermore, the propolis bands were overlapped with the PVA bands because it is observed that the peak at 3745 cm^{-1} (Region I) was only found on PVA+propolis as-spun and FT nanofibres, attributed to O-H stretching of alcohol group. The propolis peaks at Region II were found to be getting sharper in as-spun nanofibres when the concentration of propolis extract increased in **Figure 6.6a**. Surprisingly, there was no changes observed at Region II from the PVA+propolis FT nanofibres in **Figure 6.6Error! Reference source not found.b**. The freeze-thawing process might be breaking down the accumulated double bonds in PVA+propolis FT nanofibres.

The FTIR analysis has also been widely used to study the crystallisation behaviour of PVA. It is worth to mention that the crystalline sensitive band, 1141 cm^{-1} which is related to either the C-O stretching vibrations in C-OH groups of the crystalline polymer or the C-C stretching vibrations on the same side of the carbon chain in the crystalline phase [243], [258], was found in all as-spun and FT samples. It can be explained that there is an intermolecular interaction of C-OH groups between the PVA and propolis in the crystalline phase.

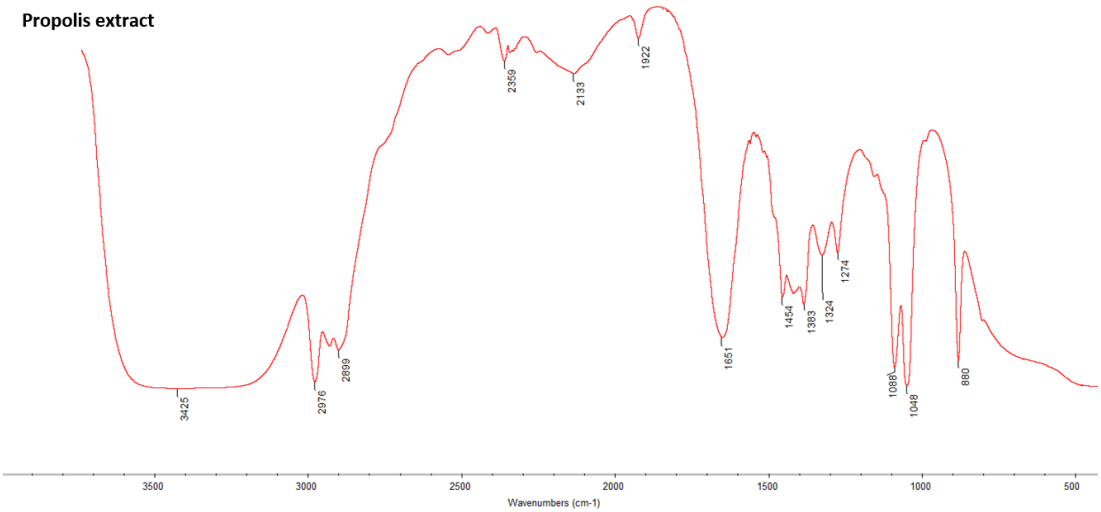

Figure 6.5: FTIR for ethanolic propolis extract.

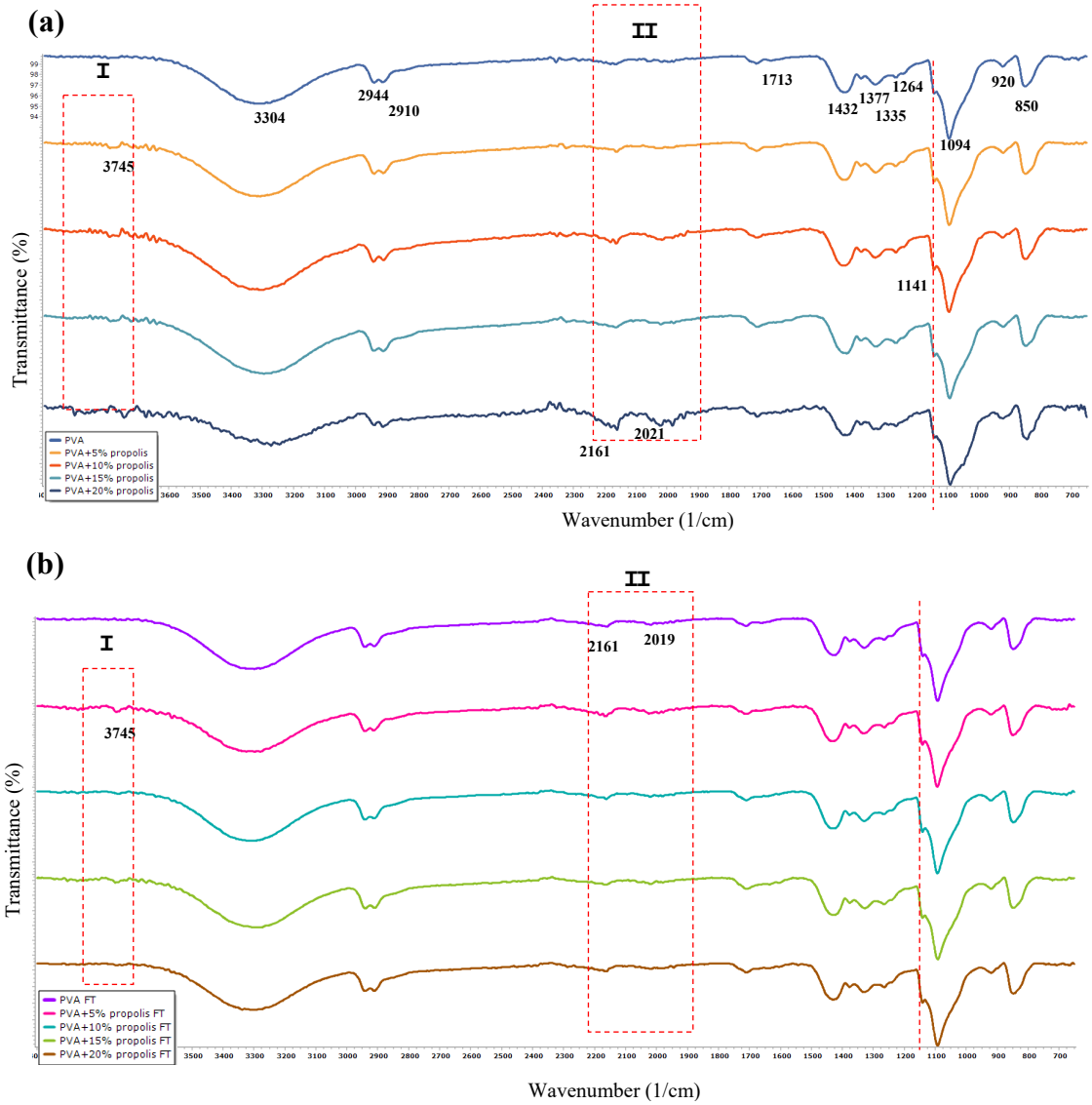

Figure 6.6: FTIR spectra for PVA and PVA+propolis (a) as-spun nanofibres and (b) FT nanofibres.

6.2.5 DSC analysis

In **Figure 6.7**, the spectra of the PVA+propolis as-spun and FT nanofibres were shifted to the left when compared to the neat PVA as-spun and FT nanofibres, indicating the melting temperature (Tm) were decreased with the increase of propolis extract amount in PVA nanofibres. It is also noticed that the degree of crystallinity decreased as the concentration of propolis increased. PVA as-spun, PVA FT, PVA+5% propolis as-spun, PVA+5% propolis FT, PVA+10% propolis as-spun, PVA+10% propolis FT and PVA+20% propolis as-spun showed the degree of crystallinity of 27%, 25%, 32%, 30%, 21%, 15% and 18% respectively. This is supported by the study performed by Oliveira *et. al.*, the propolis extract weaken the movement of PVA polymer chains and hinder the chains packing followed by inhibiting crystals growth with increased amounts of propolis in the samples [236]. Even with the introduction of FT, the degree of crystallinity and Tm did not increase. The FT process may be inducing the relaxation of the chains instead of modifying them in a way that it increases the Tm. Previous works reported that the increase of propolis extract might homogenously mixed in the PVA nanofibres in an amorphous state, consequently lowering the degree of crystallinity [243]. As seen in **Figure 6.7**, the PVA+15% propolis as-spun and FT nanofibres as well as PVA+20% propolis FT showed no melting peaks indicating the nanofibres were in a completely amorphous state. Since there are many alcohols or phenolics chains, they might weaken the PVA-PVA binding ability and prefer to align with propolis.

6.2.6 DMA analysis

As seen in **Figure 6.8**, all the curve of FT nanofibres was shifted to the right, indicating the Tg of FT nanofibres was higher than as-spun nanofibres. This might be due to the rearrangement of the non-bounded or loosely bounded PVA polymer chains to form a better orientation and increase the resistance to degradation. The FT process has enhanced the thermal properties of nanofibres.

The stiffness of the nanofibres can also be determined in DMA by looking at the storage modulus. The storage modulus of PVA+propolis as-spun nanofibres increased from 60 MPa (PVA+5% propolis as-spun), 90 MPa (PVA+10% propolis as-spun), 100 MPa (PVA+15% propolis as-spun), to 115 MPa (PVA+20% propolis as-spun), indicating the stiffness of PVA+propolis nanofibres increased when the amount of propolis increased. Same condition

happened on PVA+propolis FT nanofibres, the storage modulus of PVA+5% propolis FT, PVA+10% propolis FT, PVA+15% propolis FT and PVA+20% propolis FT was 60 MPa, 60 MPa, 195 MPa and 85 MPa, respectively. It is noticed that all FT nanofibres was lower than as-spun nanofibres, suggesting a decrease of the stiffness of FT nanofibres, except for the PVA+15% propolis FT nanofibres. The FT process might be inducing the relaxation of the PVA chains instead of making them stronger. While the PVA+15% propolis FT has the highest storage modulus of 195 MPa, the propolis extract at the concentration of 15% has some way induced a stronger interaction with PVA polymer chains.

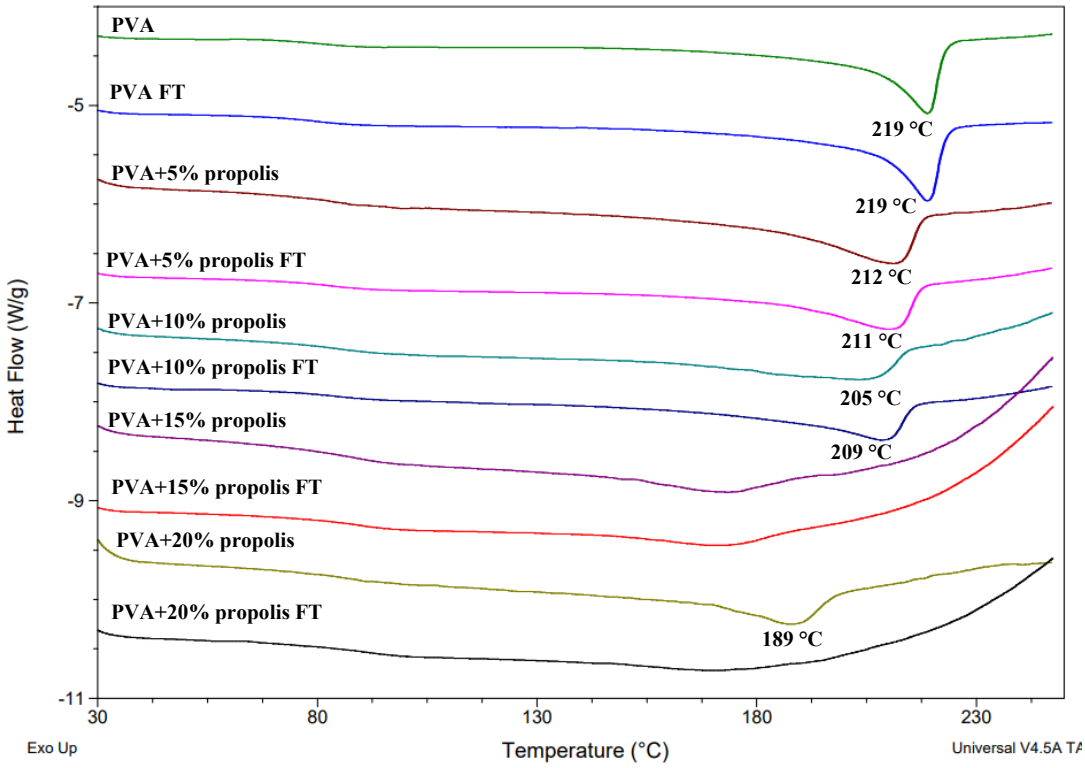

Figure 6.7: DSC of electrospun nanofibres at second heating cycle.

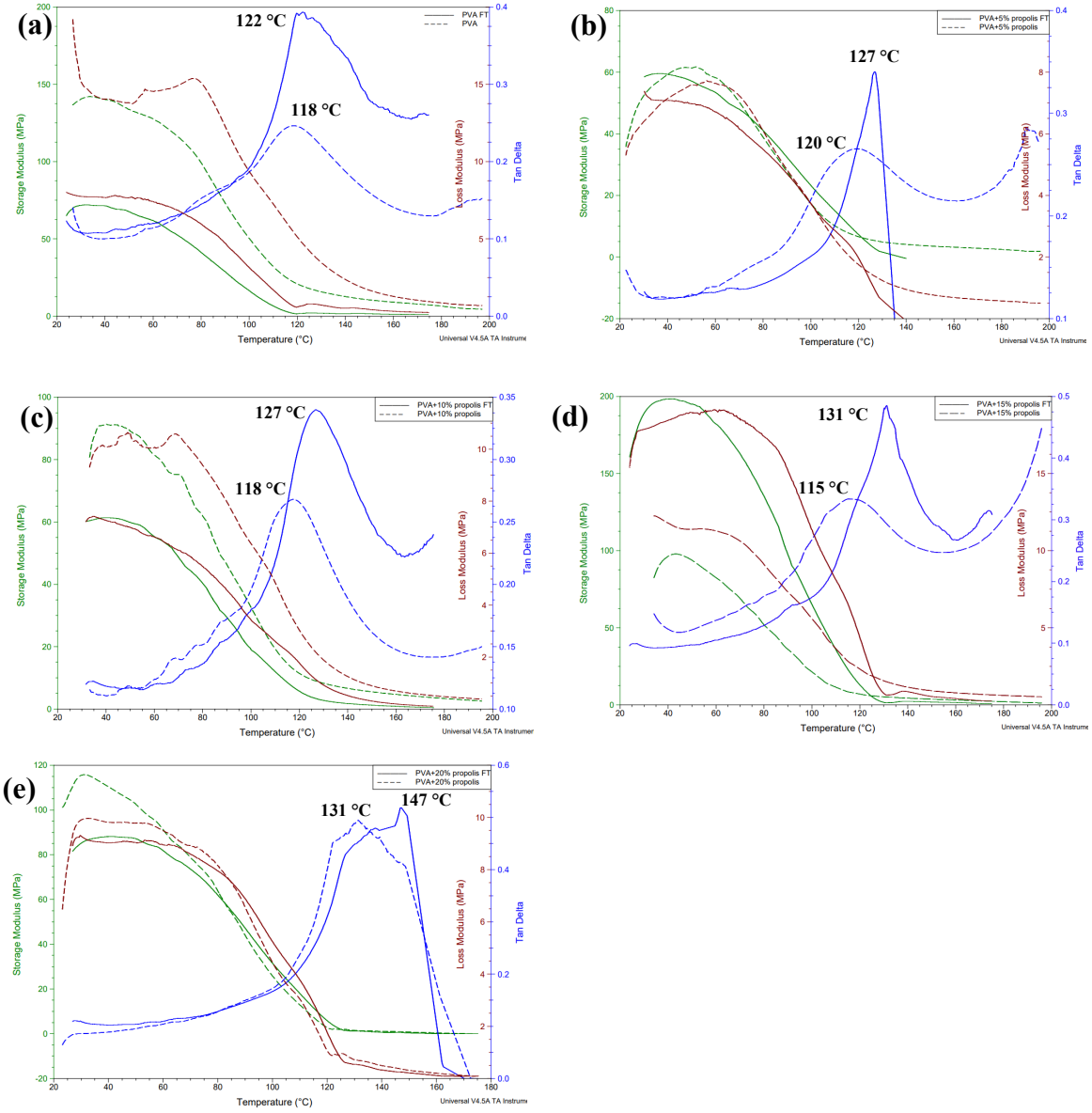

Figure 6.8: DMA spectra for as-spun and FT nanofibres. (a) PVA, (b) PVA+5% propolis, (c) PVA+10% propolis, (d) PVA+15% propolis, and (e) PVA+20% propolis. (Dash line designated as as-spun nanofibres, solid line designated as FT nanofibres)

6.2.7 Water contact angle

As shown in **Figure 6.9,** all the electrospun nanofibres samples were considered as hydrophilic because the water contact angles were all below 90°. There is a significant difference between pure PVA and PVA+propolis nanofibres. It is apparent from **Figure 6.9** that the hydrophilicity is significantly increased with the presence of propolis extract. Furthermore, the hydrophilicity is increased with an increase concentration of propolis extract in the PVA nanofibres, as result

of its good wettability. Interestingly, the water contact angle of PVA+propolis FT nanofibres containing 5%-15% propolis extract remained around 40° and PVA+20% propolis FT dropped slightly to 30°. The PVA+propolis FT nanofibres were slightly resist to water.

This hydrophilic characteristic of both PVA+propolis as-spun and FT nanofibres is extremely useful for medical haemostatic and drug delivery applications. Therefore, the PVA+propolis electrospun nanofibres prepared in this work have the potential to be produced as wound dressing materials.

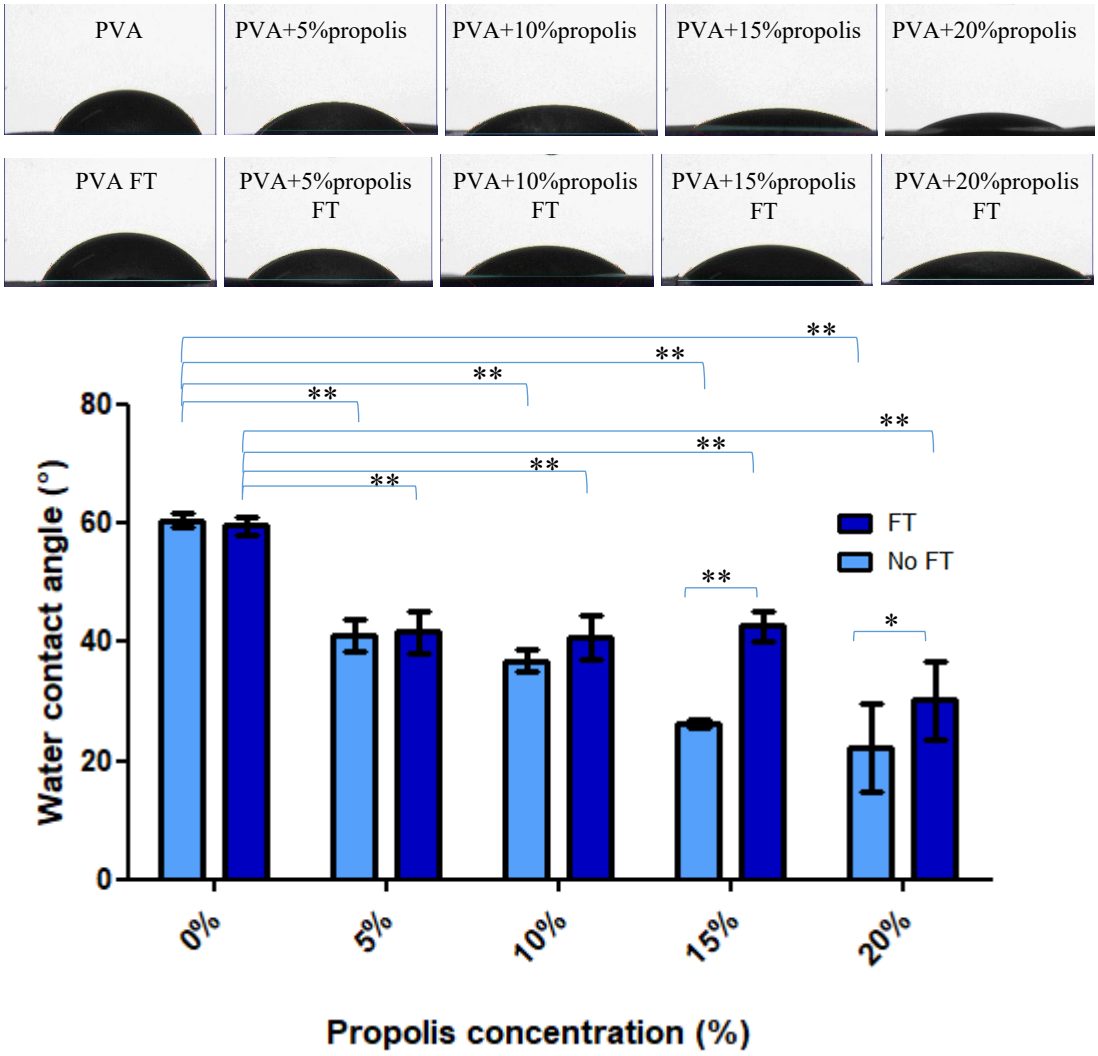

Figure 6.9: Water contact angle of the PVA and PVA+propolis electropsun nanofibres with and without freeze-thawed at 25 seconds.

6.2.8 Swelling study

As shown in **Figure 6.10**, it is observed that the swelling of as-spun and FT nanofibres happened in the first 1-2 min of immersion. The maximum swelling degree of as-spun electrospun nanofibres was 511% for PVA as-spun, 616% for PVA+5% propolis as-spun, 515% for PVA+10% propolis as-spun, 419% for PVA+15% propolis as-spun and 352% for PVA+20% propolis as-spun nanofibres. It is noticed that the swelling degree of as-spun electrospun nanofibres decreased as the propolis extract concentration increased. While the maximum swelling degree of freeze-thawed electrospun nanofibres was 405% for PVA FT, 433% for PVA+5% propolis FT, 499% for PVA+10% propolis FT, 445% for PVA+15% propolis FT and 527% for PVA+20% propolis FT nanofibres.

The swelling degree of PVA FT, PVA+5% propolis FT and PVA+10% propolis decreased when compared to PVA as-spun, PVA+5% propolis as-spun and PVA+10% propolis as-spun, respectively. Normally, the swelling degree is influenced by the number of FT cycles as FT caused an increase of physical crosslinking and resulted in a decrease of swelling degree [247]. However, in this case, the formation of crystalline decreased when FT applied as mentioned in DSC. Thus, it might be possible that the non-bounded or loosely bounded PVA chains were rearranged during FT and a better orientation was formed to hinder the mobility of polymer chain, which led to lower swelling degree. In contrast, the swelling degree of PVA+15% propolis FT and PVA+20% propolis FT increased when compared to the PVA+15% propolis as-spun and PVA+20% propolis as-spun nanofibres. This might be due to the amorphous state of PVA+15% propolis FT and PVA+20% propolis FT, as mentioned in DSC, exhibited greater swelling ability.

After the first 1-2 min, the swelling curves started to descend, indicating the degradation of nanofibres was happening [259]. All the swelling curves have the same trend which presented a well structural stability of the nanofibres. The electrospun nanofibres underwent fast weight loss during the first 30 min. Over longer immersion times, the weight loss of electrospun nanofibres was slowed down remarkably, reaching a plateau after approximately 180 min.

Moreover, the final swelling degree of freeze-thawed nanofibres after 300 min was higher than the as-spun nanofibres, except for the PVA+15% propolis FT sample. This is suggested that the PVA+propolis nanofibres underwent FT process resulted in a decrease in weight loss.

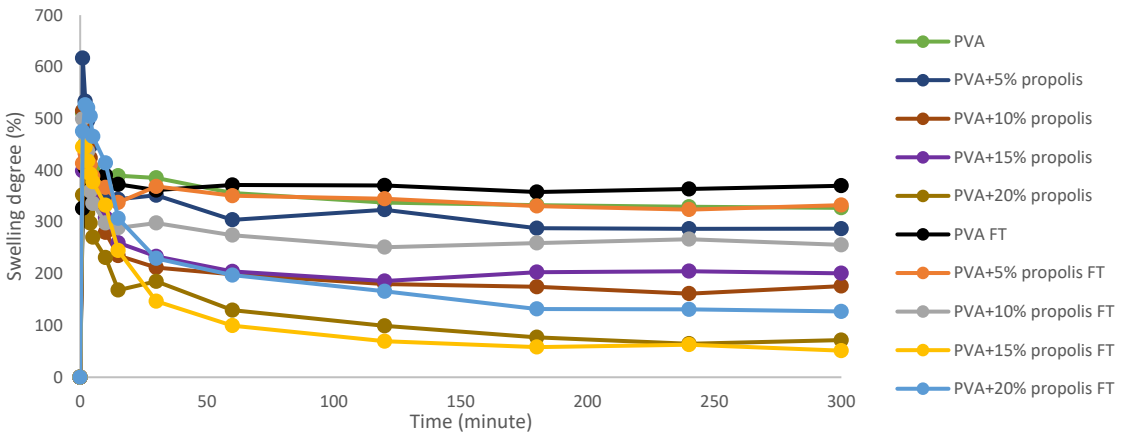

Figure 6.10: Swelling degree of electrospun nanofibres in 5 h. Maximum swelling degree reached in 1-2 min.

6.2.9 Disintegration and weight loss studies

The disintegration behaviours of electrospun nanofibres was tested by immersing in pH 7.4 buffer. As can be seen in **Figure 6.11A**, the as-spun and FT electrospun nanofibres (1 cm x 1 cm) experienced a different degree of shrinkage when they hydrated. It is observed that the nanofibres did not fully disintegrate after 24 h of immersion. The pure PVA as-spun and FT nanofibres have superior integrity. The better quality of crystalline structure and the strong hydrogen bonding interactions between the PVA matrix may be responsible for this observation. However, with the presence of propolis, the size and the colour of PVA+propolis as-spun and FT nanofibres became smaller and more yellowish with increase concentration of propolis. As explained by other study, propolis could be a physical barrier to PVA chains packing [236] which resulted in partial disintegration. The appearance of PVA+propolis FT nanofibres have the same tendency in PVA+propolis as-spun nanofibres after 24 h of immersion.

The weight loss study **(Figure 6.11B)** showed the water stability ability of as-spun and FT nanofibres. It is noticed that the % weight loss increased as the amount of propolis increased. Unfortunately, there are no significant difference in weight loss before and after FT. The FT method applied on the electrospun nanofibres has no effect on inhibiting the disintegration.

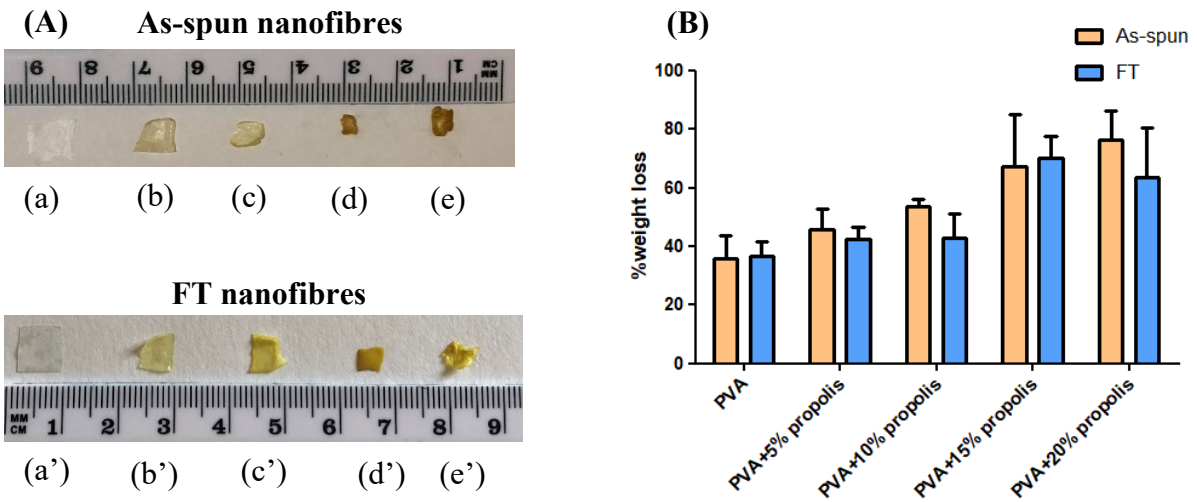

Figure 6.11: (A) Photographs of as-spun and FT electrospun nanofibres after immersing in pH 7.4 buffer for 24 h. (a, a') PVA, (b, b') PVA+5% propolis, (c, c') PVA+ 10% propolis, (d, d') PVA+ 15% propolis, (e, e') PVA+ 20% propolis. (B) % weight loss studies.

6.2.10 Drug dissolution study

The *in vitro* release behavior of the PVA+propolis as-spun and PVA+propolis FT nanofibres were showed in **Figure 6.12**. An initial burst drug release was observed in first 30 min and followed by a much slower release, indicating the PVA+propolis as-spun and FT nanofibres have a biphasic release profile. The rapid drug release might be attributed to the high hydrophilicity of the nanofibres or the weakly bound propolis to the PVA nanofibres. The drug releasing rate tend to became faster as the concentration of propolis increased. However, the most surprising aspect of the data is the drug releasing rate of PVA+20% propolis as-spun nanofibres were significant slower among all the PVA+ propolis as-spun nanofibres; also, same condition happened on PVA+20% propolis FT nanofibres. This might be due to the high concentration of propolis extract has interacted more with the PVA chains which led to slower release.

Accumulated release at 24 h was 79% for PVA+5% propolis as-spun, 93% for PVA+5% propolis FT, 75% for PVA+10% propolis as-spun, 81% for PVA+10% propolis FT, 86% for PVA+15% propolis as-spun, 98% for PVA+15% propolis FT, 69% for PVA+20% propolis as-spun and 61% for PVA+20% propolis FT nanofibres. Overall, it is observed that the freeze-thawed PVA+ propolis nanofibres have a higher accumulated release in 24 h.

The drug release behaviour of PVA+propolis as-spun and FT electrospun nanofibres was predicted based on a few mathematical models including zero order, first order, Hixson-crowell, Higuchi and Korsmeyer-Peppas. The correlation coefficients (R^2) were calculated based on the kinetic release showed in **Table 6.1**. It is noted that the closest value of the correlation coefficient to one will be selected as the best fit model of the release mechanism. All the PVA+propolis as-spun and FT nanofibres, except for the PVA+5% propolis FT nanofibres, were best fit with the Korsmeyer-Peppas model with the *n* exponent ≤ 0.5 [234], indicating Fickian diffusion makes the predominant contribution to release of propolis extract from the PVA nanofibres. In addition, the diffusion of propolis extract from the PVA nanofibres was much greater than the process of polymeric chain relaxation [234]. The PVA+5% propolis FT nanofibres sample was found to be best fit in first order release kinetics (R^2=0.9415), indicating the propolis release was directly proportional to the concentration of propolis.

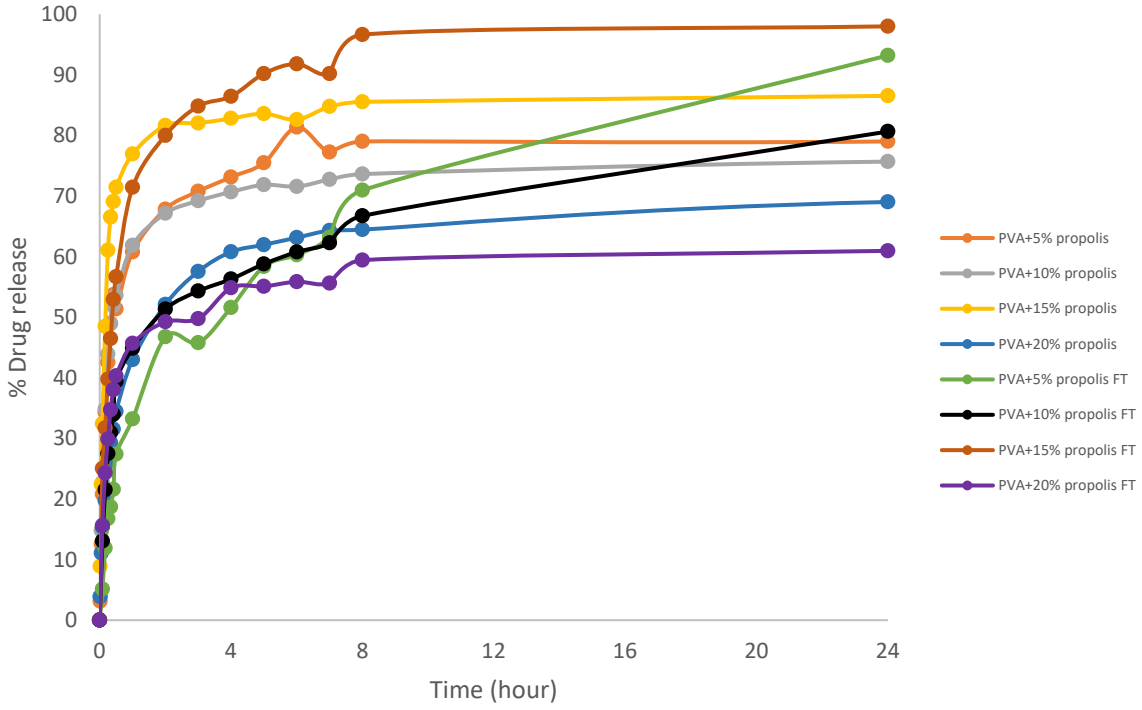

Figure 6.12: % drug release of PVA+propolis nanofibres samples with and without freeze-thawed.

Table 6.1: Drug release kinetics of PVA+propolis electrospun nanofibres samples with and without freeze-thawed.

	Sample	Zero order	First order	Hixson-Crowell	Higuchi	Korsmeyer-Peppas	
		R^2	R^2	R^2	R^2	R^2	n
As-spun	PVA+5% propolis	0.5991	0.7843	0.7286	0.7857	0.8625	0.2330
	PVA+10% propolis	0.5167	0.6728	0.6229	0.7155	0.8375	0.2036
	PVA+15% propolis	0.3844	0.6017	0.5284	0.6369	0.7362	0.1521
	PVA+20% propolis	0.7314	0.8250	0.8328	0.9192	0.9636	0.3065
FT	PVA+5% propolis	0.8655	0.9415	0.9207	0.8655	0.9329	0.4775
	PVA+10% propolis	0.7078	0.8250	0.7884	0.7078	0.9111	0.2940
	PVA+15% propolis	0.6695	0.9107	0.8489	0.6695	0.9347	0.2755
	PVA+20% propolis	0.5951	0.7038	0.6687	0.5951	0.8669	0.2321

6.3 Summary

The electrospun PVA+propolis nanofibres had distinctive advantage for burst drug release in the first 30 min and followed by a slower drug release up to 2-8 h. The results showed that the PVA+propolis FT nanofibres have a slower drug releasing rate when compared to PVA+propolis as-spun nanofibres. These electrospun nanofibres showed that the nanotechnology has enormous potential to be applied to the production of hydrogels in a novel and innovative manner with the properties tailored for specific conditions such as rapid drug release to the targeted site at a high drug content once administration and keep release for another few hours. Although the degree of crystallinity and Tm decreased when the propolis concentration increased, and the FT process further induce the PVA chains relaxation resulted in forming a PVA+propolis nanofibres in homogenously state, the water contact angle study showed improve water resistance ability in PVA+propolis FT nanofibres. Furthermore, the Tg of FT nanofibres was higher than as-spun nanofibres, suggesting the FT process enhanced the thermal properties of PVA+propolis nanofibres. The PVA+15% propolis FT nanofibres sample was the most rigid sample as this sample has the highest storage modulus of 195 MPa among all the as-spun and FT nanofibres.

Chapter 7
Conclusion

Novel PVA hydrogels with difference sizes range and with different APIs were successfully developed for drug delivery applications in this thesis. Freeze-thawing and thermal annealing methods proved to be effective in increasing the physical crosslinking of PVA hydrogels. Furthermore, in order to improve the drug encapsulation, the surface area of PVA hydrogels was increased by decreasing the size of hydrogel from centi-, micro-, to nano- meter. As the PVA hydrogels became smaller, the drugs releasing time became longer. Moreover, the PVA hydrogels were considered to be biocompatible as they were non-toxic to NIH 3T3 fibroblast cells.

Chapter 3: Preparation of orientated and freeze-thawed PVA hydrogels

A series of PVA hydrogels with or without caffeine which were synthesized by combined freeze-thawing and uniaxial orientation and their properties were investigated in comparison with those without uniaxial orientation. The degree of crystallinity, degree of swelling, tensile strength and Young's modulus of the orientated PVA/CAF hydrogel samples were higher than pure orientated PVA hydrogels. These positive results were attributed to the aligned oriented chains that occurred in between the freeze-thawing, a more aligned PVA hydrogel has been produced with increase number of F/T cycles. The incorporation of caffeine in the aligned hydrogel structure presented a Hixson-Crowell drug release mechanism and this rapid caffeine release in 15-20 min resulted from the aligned PVA polymer chains that were formed by the physical orientation method. The PVA/CAF hydrogels were found to be non-toxic to NIH 3T3 cells.

Chapter 4: Preparation of freeze-thawed PVA spheres

The formation of PVA spheres in the pre-cooled AcOEt (-80 °C) solution using a micropipette following by six freeze and thawing cycles was successfully accomplished. Although the samples were able to maintain a spherical shape, the desired diameter (<1 micrometer) of the spheres was not achieved as the prepared spheres were range between 2-3 mm in diameter. Future work may incorporate a powder spray device to replace the micropipette for optimising the size of the spheres.

The PVA/CIP and PVA/PAA/CIP spheres were able to immediately release ciprofloxacin and fully dissolved under 60 min for osteomyelitis treatment. In addition, the immediate release of caffeine from the PVA/CAF spheres was achieved within 60 min. The PVA/CIP,

PVA/PAA/CIP and PVA/CAF spheres were best fit in Hixson-Crowell release kinetic. The spheres were also non-toxic to NIH 3T3 cells.

Chapter 5: Preparation of thermal annealed PVA/PAA bilayer nanofibres

Nanomedicine and nanotechnology are transforming society's approach to medicine and biomedical science. However, as in every material science technology, there are three distinct interrelated aspects: the applications, the process and the material. The applications are diverse for electrospinning and include wound healing, bone regeneration and tissue engineering. PVA electrospun materials have remarkable properties in terms of biocompatibility and this combined with the developments in the electrospinning process will lead to a rapidly growing area. Hence, it has driven the research on developing novel PVA electrospun nanofibres in this thesis.

The PVA/PAA bilayer electrospun nanofibres containing clarithromycin and doxorubicin hydrochloride were successfully prepared using thermal annealing and electrospinning technology for osteosarcoma treatment. The annealed bilayer nanofibres can be considered as a potential to be used in modelling drug release especially for dual drug delivery. The combined effect of clarithromycin and doxorubicin hydrochloride proves that a synergetic enhance cytotoxicity against U2SO osteosarcoma cell line occurs and it may be improved with the bilayer electrospun nanofibres. A fast (100% CLA released in 24 h) and slow (2% DOX released in 24 h) release-rate can be achieved using this bilayer membrane.

Chapter 6: Preparation of freeze-thawed PVA nanofibres

The physiochemical properties included conductivity, surface tension and viscosity of PVA and PVA+propolis polymer solutions are the important solution parameters that could affect the morphology and diameter of the produced nanofibres. Beaded nanofibres were fabricated with the given polymer solutions. Therefore, an increase of PVA concentration higher than 7 %(w/v) should help to increase the surface tension and leading to fewer beads or smooth nanofibres. Moreover, the glass transition temperature and water contact angle of FT nanofibres was higher than as-spun nanofibres, suggesting the FT process enhanced the thermal properties and water resistance ability of PVA+propolis nanofibres.

The PVA+propolis electrospun nanofibres had a distinctive advantage for burst drug release in the first 30 min and followed by a slower drug release up to 2-8 h. The results showed that the

PVA+propolis FT nanofibres have a slower drug releasing rate when compared to PVA+propolis as-spun nanofibres. Majority of the PVA+propolis as-spun and FT nanofibres were best fit with the Korsmeyer-Peppas model.

Summary

Overall, these PVA hydrogels have the potential for use in a variety of biomedical applications, especially in the biomedical area. Utilising PVA as the base polymer, has a number of advantages in that a biocompatible hydrogel can be formed without the use of chemical crosslinkers. This functionality can be further exploited if the core process is modified and this was the approach undertaken in this thesis.

The study of the PVA hydrogels undertaken have been extensive, different geometries, processes and APIs have been incorporated in a number of novel ways including orientation, dipping and electrospinning. The release of the APIs has been modelled and the results fit with literature. The research detailed has scientific merit as the approach outlined in the thesis has demonstrated how the properties can be modified and tailored. Comprehensive characterisation underpins the scientific approach and future work can build on further modification and optimisation for biomedical and nanotechnology applications.

Finally, the advancement of this tunable PVA hydrogels is potential to be manufacture as new commercialable products. Furthermore, PVA hydrogel as hydrophilic polymer structure is capable of retaining large amounts of water similar to soft tissue, while remaining structurally stable with a high capacity for the permeation and diffusion of molecules in terms of mimicking the *in vivo* environment compared with current commercial technological approaches.

Future work

Further attempts to analyse the produced hydrogels using thermogravimetric analysis (TGA) and Raman spectroscopy could prove beneficial to the work detailed in the research. The thermal stability of hydrogels can be evaluated by TGA, while the Raman investigations could further characterise the molecular chain conformations and crystallisation of PVA and the APIs.

Future research should be devoted to the development of core-shell nanofibres or nanoparticles using co-axial electrospinning or electrospraying technology. Compared to conventional electrospinning and electrospraying, co-axial electrospinning and electrospraying is highly tunable and can precisely control the location of the APIs within the core as well as an increase of drug loading capacity can be achieved. Although different type of water-soluble and poorly water-soluble drugs have been studied in this thesis, the delivery of proteins or peptides (e.g. neuroglobin) from PVA hydrogels have not yet been investigated. Due to their high molecular size, they are not able to cross plasma membranes, hence not penetrating through the blood-brain barrier. It is believed that this novel approach by incorporating proteins/peptides in core-shell PVA nanoparticles could prove an important area for future research.

References

[1] E. Chiellini, A. Corti, S. D'Antone, and R. Solaro, *Biodegradation of poly (vinyl alcohol) based materials*, vol. 28, no. 6. 2003.

[2] M. A. Huha and J. A. Lewis, "Polymer Effects on the Chemorheological and Drying Behavior of Alumina–Poly(vinyl alcohol) Gelcasting Suspensions," *J. Am. Ceram. Soc.*, vol. 83, no. 8, pp. 1957–63, 2000.

[3] T. Wang, M. Turhan, and S. Gunasekaran, "Selected properties of pH-sensitive, biodegradable chitosan-poly(vinyl alcohol) hydrogel," *Polym. Int.*, 2004, doi: 10.1002/pi.1461.

[4] N. H. A. Ngadiman, M. Y. Noordin, D. Kurniawan, A. Idris, and A. S. A. Shakir, "Influence of Polyvinyl Alcohol Molecular Weight on the Electrospun Nanofiber Mechanical Properties," *Procedia Manuf.*, vol. 2, no. February, pp. 568–572, 2015, doi: 10.1016/j.promfg.2015.07.098.

[5] J. Zanela, A. P. Bilck, M. Casagrande, M. V. E. Grossmann, and F. Yamashita, "Polyvinyl alcohol (PVA) molecular weight and extrusion temperature in starch/PVA biodegradable sheets," *Polímeros*, vol. 28, no. 3, pp. 256–265, 2018, doi: 10.1590/0104-1428.03417.

[6] G. Joshi and S. M. Pawde, "Effect of molecular weight on dielectric properties of polyvinyl alcohol films," *J. Appl. Polym. Sci.*, vol. 102, no. 2, pp. 1014–1016, 2006, doi: 10.1002/app.24062.

[7] A. D. Jenkins, P. Kratochvíl, R. F. T. Stepto, and U. W. Suter, "Glossary of Basic Terms in Polymer Science," *Pure Appl. Chem.*, vol. 68, no. 8, p. 2291, 1996.

[8] W. S. Ha, W. S. Lyoo, and Y. K. Choi, "Poly(vinyl alcohol) microfibrillar short fiber and its preparative method," 1995.

[9] M. L. Oyen, "Mechanical characterisation of hydrogel materials," *Int. Mater. Rev.*, vol. 59, no. 1, pp. 44–59, 2014.

[10] F. dos S. Campos, D. L. Cassimiro, M. S. Crespi, A. E. Almeida, and M. P. D. Gremião, "Preparation and characterisation of Dextran-70 hydrogel for controlled release of praziquantel," *Brazilian J. Pharm. Sci.*, vol. 49, no. 1, pp. 75–83, 2013.

[11] S. L. Bassner and E. H. Klingenberg, "Using poly(vinyl alcohol) as a binder," *Am. Ceram. Soc. Bull.*, vol. 77, no. 6, pp. 71–75, 1998.

[12] H. S. Mansur, C. M. Sadahira, A. N. Souza, and A. A. P. Mansur, "FTIR spectroscopy characterization of poly (vinyl alcohol) hydrogel with different hydrolysis degree and chemically crosslinked with glutaraldehyde," *Mater. Sci. Eng.*, vol. 28, no. 4, pp. 539–548, 2008.

[13] K. S. Saxena, "Polyvinyl Alcohol (PVA)," *Int. J. Toxicol.*, vol. 1, no. 3, pp. 3–5, 2004, doi: 10.1016/j.jvir.2010.09.018.

[14] M. Bercea, S. Morariu, and D. Rusu, "In situ gelation of aqueous solutions of entangled poly(vinyl alcohol)," *Soft Matter*, vol. 9, p. 1244, 2013.

[15] P. Hong, J. Chen, H. Wu, Hong, Chen, and Wu, "Solvent effect on structural change of poly(vinyl alcohol) physical gels," *J. Appl. Polym. Sci.*, vol. 69, no. 12, pp. 2477–2486, 1998, doi: 10.1002/(SICI)1097-4628(19980919)69:12<2477::AID-APP19>3.3.CO;2-2.

[16] J. Hensey, “An Investigation of PVA/PAA Hydrogel Compounds,” Athlone Institute of Technology, 2004.

[17] S. J. Bryant, K. A. Davis-Arehart, N. Luo, R. K. Shoemaker, J. A. Arthur, and K. S. Anseth, “Synthesis and characterization of photopolymerised multifunctional hydrogels: water-soluble poly(vinyl alcohol) and chondroitin sulfate macromers for chondrocyte encapsulation,” *Macromolecules*, vol. 37, no. 18, pp. 6726–33, 2004.

[18] S. H. Hyon, W. I. Cha, and Y. Ikada, “Preparation of transparent poly(vinyl alcohol) hydrogel,” *Polym. Bull.*, vol. 22, no. 2, pp. 119–122, 1989.

[19] J. K. Li, N. Wang, and X. S. Wu, “Poly(vinyl alcohol) nanoparticles prepared by freezing-thawing process for protein/peptide drug delivery,” *J. Control. Release*, vol. 56, no. 1–3, pp. 117–126, 1998.

[20] N. Chirani, H. Yahia, L. Gritsch, F. L. Motta, S. Chirani, and S. Faré, “History and Applications of Hydrogels,” *J. Biomed. Sci.*, vol. 4, no. 2, pp. 13–23, 2015.

[21] W. E. Hennink and C. F. van Nostrum, “Novel crosslinking methods to design hydrogels,” *Adv. Drug Deliv. Rev.*, vol. 64, pp. 223–236, 2012.

[22] S. R. Raghavan and J. F. Douglas, “The conundrum of gel formation by molecular nanofibers, wormlike micelles, and filamentous proteins: gelation without cross-links?,” *Soft Matter*, vol. 8, no. 33, pp. 8539–8546, 2012, doi: 10.1039/c2sm25107h.

[23] H. Zhang, F. Zhang, and J. Wu, “Physically crosslinked hydrogels from polysaccharides prepared by freeze-thaw technique,” *React. Funct. Polym.*, vol. 73, no. 7, pp. 923–928, 2013, doi: 10.1016/j.reactfunctpolym.2012.12.014.

[24] N. A. Peppas, “Turbidimetric Studies of Aqueous Polyvinyl-Alcohol) Solutions,” *Makromol. Chemie-Macromolecular Chem. Phys.*, vol. 176, no. 11, pp. 3433–3440, 1975, doi: 10.1002/macp.1975.021761125.

[25] F. Yokoyama, I. Masada, K. Shimamura, T. Ikawa, and K. Monobe, “Morphology and structure of highly elastic poly(vinyl alcohol) hydrogel preparaed by repeated freezing and melting,” *Colloid Polym Sci*, vol. 264, no. 7, pp. 595–601, 1986.

[26] C. M. Hassan and N. a Peppas, “Structure and Applications of Poly (vinyl alcohol) Hydrogels Produced by Conventional Crosslinking or by Freezing / Thawing Methods,” *Adv. Polym. Sci.*, vol. 153, pp. 37–65, 2000, doi: 10.1007/3-540-46414-X_2.

[27] M. J. D. Nugent and C. L. Higginbotham, “Investigation of the influence of freeze-thaw processing on the properties of polyvinyl alcohol/polyacrylic acid complexes,” *J. Mater. Sci.*, vol. 41, no. 8, pp. 2393–2404, 2006, doi: 10.1007/s10853-006-7075-9.

[28] M. J. D. Nugent, A. Hanley, P. T. Tomkins, and C. L. Higginbotham, “Investigation of a novel freeze-thaw process for the production of drug delivery hydrogels,” *J. Mater. Sci. Mater. Med.*, vol. 16, no. 12, pp. 1149–1158, 2005.

[29] C. M. Hassan, J. H. Ward, and N. A. Peppas, “Modeling of crystal dissolution of poly(vinyl alcohol) gels produced by freezing/thawing processes,” *Polymer (Guildf).*, vol. 41, no. 18, pp. 6729–6739, 2000, doi: 10.1016/S0032-3861(00)00031-8.

[30] U. Fumio, Y. Hiroshi, N. Kumiko, N. Sachihiko, S. Kenji, and M. Yasunori, “Swelling and mechanical properties of poly(vinyl alcohol) hydrogels,” *Int. J. Pharm.*, vol. 58,

no. 2, pp. 135–142, 1990.

[31] Biopharma Process Systems Ltd., “Misconceptions in Freeze Drying,” 2014. .

[32] L. Zhang, J. Zhao, J. Zhu, C. He, and H. Wang, “Anisotropic tough poly(vinyl alcohol) hydrogels,” *Soft Matter*, vol. 8, p. 10439, 2012, doi: 10.1039/c2sm26102b.

[33] J. L. Holloway, A. M. Lowman, and G. R. Palmese, “The role of crystallization and phase separation in the formation of physically cross-linked PVA hydrogels,” *Soft Matter*, vol. 9, no. 3, pp. 826–833, 2013, doi: 10.1039/C2SM26763B.

[34] F. Ricciardi, R.; Finizia, A.; Rosa, C.; Lauprêtre, “X-ray Diffraction Analysis of Poly (vinyl alcohol) Hydrogels , Obtained by Freezing and Thawing Techniques,” *Macromolecules*, vol. 37, pp. 1921–1927, 2004, doi: 10.1021/ma035663q.

[35] M. J. D. Nugent and C. L. Higginbotham, “Preparation of a novel freeze thawed poly(vinyl alcohol) composite hydrogel for drug delivery applications,” *Eur. J. Pharm. Biopharm.*, vol. 67, no. 2, pp. 377–386, 2007, doi: 10.1016/j.ejpb.2007.02.014.

[36] M. G. Cascone, L. Lazzeri, E. Sparvoli, M. Scatena, L. P. Serino, and S. Danti, “Morphological evaluation of bioartificial hydrogels as potential tissue engineering scaffolds,” *J. Mater. Sci. Mater. Med.*, vol. 15, no. 12, pp. 1309–1313, 2004, doi: 10.1007/s10856-004-5739-z.

[37] S. Choi and J. Kim, “Designed fabrication of super-stiff, anisotropic hybrid hydrogels via linear remodeling of polymer networks and subsequent crosslinking,” *J. Mater. Chem. B*, vol. 3, no. 8, pp. 1479–1483, 2015, doi: 10.1039/c4tb01852d.

[38] S. Zhang *et al.*, “Creating polymer hydrogel microfibres with internal alignment via electrical and mechanical stretching,” *Biomaterials*, vol. 35, no. 10, pp. 3243–3251, 2014.

[39] J. Wang, G. Liu, J. Chen, B. Zhao, and P. Zhu, “Synthesis of biocompatible hydroxyapatite using chitosan oligosaccharide as a template,” *Materials (Basel).*, vol. 8, no. 12, pp. 8097–8105, 2015, doi: 10.3390/ma8125440.

[40] U. O. and Y. H. S.-H. Hyon, W.-I. Cha, Y. Ikada, M. Kita, *Proceedings of The Third World Biomaterials Congress*, vol. 3:536. 1988.

[41] M. J. Mc Gann, C. L. Higginbotham, L. M. Geever, and M. J. D. Nugent, “The synthesis of novel pH-sensitive poly(vinyl alcohol) composite hydrogels using a freeze/thaw process for biomedical applications,” *Int. J. Pharm.*, vol. 372, no. 1–2, pp. 154–161, 2009, doi: 10.1016/j.ijpharm.2009.01.008.

[42] C. L. Bell and N. A. Peppas, “Biomedical membranes from hydrogels and interpolymer complexes,” *Adv. Polym. Sci.*, vol. 122, pp. 126–177, 1995.

[43] M. Z. Ramakrishna S, Fujihara K, Teo W, Lim T, *An Introduction to Electrospinning and Nanofibers*. New Jersey: World Scientific, 2005.

[44] E. Sapountzi, M. Braiek, J. F. Chateaux, N. Jaffrezic-Renault, and F. Lagarde, “Recent advances in electrospun nanofiber interfaces for biosensing devices,” *Sensors (Switzerland)*, vol. 17, no. 8, 2017, doi: 10.3390/s17081887.

[45] N. Zhang *et al.*, “Electrospun TiO 2 nanofiber-based cell capture assay for detecting circulating tumor cells from colorectal and gastric cancer patients,” *Adv. Mater.*, vol.

24, no. 20, pp. 2756–2760, 2012, doi: 10.1002/adma.201200155.

[46] J. H. Park, S. Lee, J. H. Kim, K. Park, K. Kim, and I. C. Kwon, “Polymeric nanomedicine for cancer therapy,” *Prog. Polym. Sci.*, vol. 33, no. 1, pp. 113–137, 2008, doi: 10.1016/j.progpolymsci.2007.09.003.

[47] I. Armentano, M. Dottori, E. Fortunati, S. Mattioli, and J. M. Kenny, “Biodegradable polymer matrix nanocomposites for tissue engineering: A review,” *Polym. Degrad. Stab.*, vol. 95, no. 11, pp. 2126–2146, 2010, doi: 10.1016/j.polymdegradstab.2010.06.007.

[48] E. Kostakova, E. Zemanova, P. Mikes, J. Soukupova, H. Matheisova, and K. Klouda, “Electrospinning and Electrospraying of Polymer Solutions with Spherical Fullerenes,” *Nanocon 2012, 4th Int. Conf.*, pp. 435–439, 2012.

[49] N. Tucker, J. Stanger, M. Staiger, H. Razzaq, and K. Hofman, “The History of the Science and Technology of Electrospinning from 1600 to 1995.,” *J. Eng. Fiber. Fabr.*, vol. 7, pp. 63–73, 2012, [Online]. Available: http://search.ebscohost.com/login.aspx?direct=true&profile=ehost&scope=site&authtype=crawler&jrnl=15589250&AN=82858886&h=UtG5q+tUVjvz8MblBT1qQ8N1movMQ2sTD17Z2flGZJNPnoLkRlnQSSDUKNCSLEKdCjisYNfIXKh0RSIxURHETg==&crl=c.

[50] W. J. Morton, “Method of Dispersing Fluids,” 1902.

[51] M. Zafar, S. Najeeb, Z. Khurshid, M. Vazirzadeh, and S. Zohaib, “Potential of Electrospun Nanofibers for Biomedical and Dental Applications,” pp. 1–21, 2016, doi: 10.3390/ma9020073.

[52] A. Frenot and I. S. Chronakis, “Polymer nanofibers assembled by electrospinning,” *Curr. Opin. Colloid Interface Sci.*, vol. 8, no. 1, pp. 64–75, 2003, doi: 10.1016/S1359-0294.

[53] X. Li, M. A. Kanjwal, L. Lin, and I. S. Chronakis, “Electrospun polyvinyl-alcohol nanofibers as oral fast-dissolving delivery system of caffeine and riboflavin,” *Colloids Surfaces B Biointerfaces*, vol. 103, pp. 182–188, 2013.

[54] S. J. Reinholt, a Sonnenfeldt, a Naik, M. W. Frey, and a J. Baeumner, “Developing new materials for paper-based diagnostics using electrospun nanofibers.,” *Anal. Bioanal. Chem.*, pp. 3297–3304, 2013, doi: 10.1007/s00216-013-7372-5.

[55] D. Rodoplu and M. Mutlu, “Effects of electrospinning setup and process parameters on nanofiber morphology intended for the modification of quartz crystal microbalance surfaces,” *J. Eng. Fiber. Fabr.*, vol. 7, no. 2, pp. 118–123, 2012.

[56] N. Bhardwaj and S. C. Kundu, “Electrospinning: A fascinating fiber fabrication technique,” *Biotechnol. Adv.*, vol. 28, no. 3, pp. 325–347, 2010, doi: 10.1016/j.biotechadv.2010.01.004.

[57] M. Yunmin, L. Yuanyuan, C. Haiping, and H. Qingxi, “Application and Analysis of Biological Electrospray in Tissue Engineering.,” *Open Biomed. Eng. J.*, vol. 9, pp. 133–7, 2015, doi: 10.2174/1874120701509010133.

[58] G. B. C. Cardoso, A. B. Machado-Silva, M. Sabino, A. R. Santos, and C. A. C. Zavaglia, “Novel hybrid membrane of chitosan/poly (ε-caprolactone) for tissue engineering,” *Biomatter*, vol. 4, no. April, pp. 1–9, 2014, doi: 10.4161/biom.29508.

[59] O. Karaman, C. Celik, and A. S. Urkmez, “Self-Assembled Biomimetic Scaffolds for Bone Tissue Engineering,” in *Emerging Research on Bioinspired Materials Engineering*, 1st ed., M. Bououdina, Ed. Hershey: IGI Global, 2016, pp. 104–132.

[60] M. G. Raucci *et al.*, “Antimicrobial ionic liquids in bioactive sol-gel hydroxyapatite for bone tissue engineering,” *Front. Bioeng. Biotechnol.*, vol. 4, 2016, doi: 10.3389/conf.FBIOE.2016.01.00578.

[61] G. Ghersi *et al.*, “PLLA Scaffold via TIPS for Bone Tissue Engineering,” vol. 49, pp. 301–306, 2016, doi: 10.3303/CET1649051.

[62] J. Erben *et al.*, “The combination of meltblown and electrospinning for bone tissue engineering,” *Mater. Lett.*, vol. 143, no. January, pp. 172–176, 2015, doi: 10.1016/j.matlet.2014.12.100.

[63] L. Cui, N. Zhang, W. Cui, P. Zhang, and X. Chen, “A Novel Nano/Micro-Fibrous Scaffold by Melt-Spinning Method for Bone Tissue Engineering,” *J. Bionic Eng.*, vol. 12, no. 1, pp. 117–128, 2015, doi: 10.1016/S1672-6529(14)60106-2.

[64] T. Subbiah, G. S. Bhat, R. W. Tock, S. Parameswaran, and S. S. Ramkumar, “Electrospinning of nanofibers,” *J. Appl. Polym. Sci.*, vol. 96, no. 2, pp. 557–569, 2005, doi: 10.1002/app.21481.

[65] G. G. De Lima *et al.*, “Synthesis and characterization of electrospun PVA scaffolds for bone tissue engineering,” 2017.

[66] B. S. Chee, G. G. De Lima, D. Devine, and M. J.D.Nugent, *Electrospun hydrogels composites for bone tissue engineering*. Elsevier Inc., 2018.

[67] Z. M. Huang, Y. Z. Zhang, M. Kotaki, and S. Ramakrishna, “A review on polymer nanofibers by electrospinning and their applications in nanocomposites,” *Compos. Sci. Technol.*, vol. 63, no. 15, pp. 2223–2253, 2003, doi: 10.1016/S0266-3538(03)00178-7.

[68] A. Koski, K. Yim, and S. Shivkumar, “Effect of molecular weight on fibrous PVA produced by electrospinning,” *Mater. Lett.*, vol. 58, no. 3–4, pp. 493–497, 2004, doi: 10.1016/S0167-577X(03)00532-9.

[69] S. L. Shenoy, W. D. Bates, H. L. Frisch, and G. E. Wnek, “Role of chain entanglements on fiber formation during electrospinning of polymer solutions: Good solvent, non-specific polymer-polymer interaction limit,” *Polymer (Guildf).*, vol. 46, no. 10, pp. 3372–3384, 2005, doi: 10.1016/j.polymer.2005.03.011.

[70] A. Moreira *et al.*, “Protein encapsulation by electrospinning and electrospraying,” *J. Control. Release*, vol. 329, no. July 2020, pp. 1172–1197, 2021, doi: 10.1016/j.jconrel.2020.10.046.

[71] B. Zhang, X. Yan, H.-W. He, M. Yu, X. Ning, and Y.-Z. Long, “Solvent-free electrospinning: opportunities and challenges,” *Polym. Chem.*, vol. 8, no. 2, pp. 333–352, 2017, doi: 10.1039/C6PY01898J.

[72] W. Graessley, “The Entanglement Concept in Polymer Rheology,” *Adv. Polym. Sci.*, vol. 16, p. 179, 1974.

[73] F. John D, *Viscoelastic properties of polymers*, 3rd ed. New York: Wiley, 1980.

[74] C. Tanford, “Physical chemistry of macromolecules,” *J. Polym. Sci.*, vol. 62, no. 173,

pp. S22–S23, 1961.

[75] J. C. J. F. Tacx, H. M. Schoffeleers, A. G. M. Brands, and L. Teuwen, “Dissolution behavior and solution properties of polyvinylalcohol as determined by viscometry and light scattering in DMSO, ethyleneglycol and water,” *Polymer (Guildf).*, vol. 41, no. 3, pp. 947–957, 2000, doi: 10.1016/S0032-3861(99)00220-7.

[76] P. Gupta, C. Elkins, T. E. Long, and G. L. Wilkes, “Electrospinning of linear homopolymers of poly(methyl methacrylate): Exploring relationships between fiber formation, viscosity, molecular weight and concentration in a good solvent,” *Polymer (Guildf).*, vol. 46, no. 13, pp. 4799–4810, 2005, doi: 10.1016/j.polymer.2005.04.021.

[77] K. Nasouri, A. M. Shoushtari, and A. Kaflou, “Investigation of polyacrylonitrile electrospun nanofibres morphology as a function of polymer concentration, viscosity and Berry number,” *Micro Nano Lett.*, vol. 7, no. 5, p. 423, 2012, doi: 10.1049/mnl.2012.0054.

[78] J. Tao and S. Shivkumar, “Molecular weight dependent structural regimes during the electrospinning of PVA,” *Mater. Lett.*, vol. 61, no. 11–12, pp. 2325–2328, 2007, doi: 10.1016/j.matlet.2006.09.004.

[79] M. Cells and H. Hall, “Tuning Electrospinning Parameters for Production of 3D-Fiber-Fleeces With Increased Porosity for Soft Tissue Engineering Applications,” vol. 21, pp. 286–303, 2011.

[80] M. Zhu *et al.*, “Electrospun Nanofibers Membranes for Effective Air Filtration,” *Macromol. Mater. Eng.*, vol. 302, no. 1, p. 1600353, 2016, doi: 10.1002/mame.201600353.

[81] M. Wang and H. W. Tong, “Effects of processing parameters on the morphology and size of electrospun PHBV micro- And nano-fibers,” *Key Eng. Mater.*, vol. 334-335 II, p. 1233, 2007, doi: 10.4028/www.scientific.net/KEM.334-335.1233.

[82] W. Cui, Y. Zhou, and J. Chang, “Electrospun nanofibrous materials for tissue engineering and drug delivery,” *Sci. Technol. Adv. Mater.*, vol. 11, no. 1, p. 014108, 2010, doi: 10.1088/1468-6996/11/1/014108.

[83] A. Becker, H. Zernetsch, M. Mueller, and B. Glasmacher, “A novel coaxial nozzle for in-process adjustment of electrospun scaffolds’ fiber diameter,” *Curr. Dir. Biomed. Eng.*, vol. 1, no. 1, pp. 104–107, 2015, doi: 10.1515/cdbme-2015-0027.

[84] R. M. Nezarati, M. B. Eifert, and E. Cosgriff-Hernandez, “Effects of Humidity and Solution Viscosity on Electrospun Fiber Morphology,” *Tissue Eng. Part C Methods*, vol. 19, no. 10, pp. 810–819, 2013, doi: 10.1089/ten.tec.2012.0671.

[85] N. Nikmaram *et al.*, “Emulsion-based systems for fabrication of electrospun nanofibers: Food, pharmaceutical and biomedical applications,” *RSC Adv.*, vol. 7, no. 46, pp. 28951–28964, 2017, doi: 10.1039/c7ra00179g.

[86] K. A. Rieger, N. P. Birch, and J. D. Schiffman, “Designing Electrospun Nanofiber Mats to Promote Wound Healing – A Review,” *J. Mater. Chem. B*, vol. 1, no. 36, pp. 4531–4541, 2013.

[87] D. G. Yu, X. Wang, X. Y. Li, W. Chian, Y. Li, and Y. Z. Liao, “Electrospun biphasic drug release polyvinylpyrrolidone/ethyl cellulose core/sheath nanofibers,” *Acta Biomater.*, vol. 9, no. 3, pp. 5665–5672, 2013, doi: 10.1016/j.actbio.2012.10.021.

[88] S. S. Said, C. O'Neil, H. Yin, Z. Nong, J. G. Pickering, and K. Mequanint, "Concurrent and Sustained Delivery of FGF2 and FGF9 from Electrospun Poly(ester amide) Fibrous Mats for Therapeutic Angiogenesis," *Tissue Eng Part A*, vol. 22, no. 7–8, pp. 584–596, 2016, doi: 10.1089/ten.tea.2015.0493.

[89] F. A. Sheikh, M. A. Kanjwal, S. Saran, W. J. Chung, and H. Kim, "Polyurethane nanofibers containing copper nanoparticles as future materials," *Appl. Surf. Sci.*, vol. 257, no. 7, pp. 3020–3026, 2011, doi: 10.1016/j.apsusc.2010.10.110.

[90] X. Chen *et al.*, "Electrospun poly(l-lactic acid-co-ε-caprolactone) fibers loaded with heparin and vascular endothelial growth factor to improve blood compatibility and endothelial progenitor cell proliferation," *Colloids Surfaces B Biointerfaces*, vol. 128, pp. 106–114, 2015, doi: 10.1016/j.colsurfb.2015.02.023.

[91] S. J. Lee, S. H. Oh, J. Liu, S. Soker, A. Atala, and J. J. Yoo, "The use of thermal treatments to enhance the mechanical properties of electrospun poly(epsilon-caprolactone) scaffolds.," *Biomaterials*, vol. 29, no. 10. pp. 1422–30, 2008, doi: 10.1016/j.biomaterials.2007.11.024.

[92] R. Sridhar, R. Lakshminarayanan, K. Madhaiyan, V. Amutha Barathi, K. H. C. Lim, and S. Ramakrishna, "Electrosprayed nanoparticles and electrospun nanofibers based on natural materials: applications in tissue regeneration, drug delivery and pharmaceuticals," *Chem. Soc. Rev.*, vol. 44, pp. 790–814, 2015, doi: 10.1039/c4cs00226a.

[93] D. Han and A. J. Steckl, "Coaxial Electrospinning Formation of Complex Polymer Fibers and their Applications," *Chempluschem*, vol. 84, no. 10, pp. 1453–1497, 2019, doi: 10.1002/cplu.201900281.

[94] R. Ramakrishnan *et al.*, "Needleless electrospinning technology - An entrepreneurial perspective," *Indian J. Sci. Technol.*, vol. 9, no. 15, 2016, doi: 10.17485/ijst/2016/v9i15/91538.

[95] G. G. De Lima, R. O. De Souza, A. D. Bozzi, M. A. Poplawska, D. M. Devine, and M. J. D. Nugent, "Extraction Method Plays Critical Role in Antibacterial Activity of Propolis-loaded Hydrogels," *J. Pharm. Sci.*, vol. 105, no. 3, pp. 1248–1257, 2016, doi: 10.1016/j.xphs.2015.12.027.

[96] I. B. S. Cunha *et al.*, "Factors that influence the yield and composition of Brazilian propolis extracts," *J. Braz. Chem. Soc.*, vol. 15, no. 6, pp. 964–970, 2004, doi: 10.1590/S0103-50532004000600026.

[97] T. J. Mabry, K. R. Markham, and M. B. Thomas, *The Ultraviolet Spectra of Flavones and Flavonols*. Berlin Heidelberg: Springer, 1970.

[98] B. J. Inkson, "Scanning Electron Microscopy (SEM) and Transmission Electron Microscopy (TEM) for Materials Characterization," in *Materials Characterization Using Nondestructive Evaluation (NDE) Methods*, Sheffield, United Kingdom: Elsevier Ltd, 2016, pp. 17–43.

[99] G.-M. Kim, A. S. Asran, G. H. Michler, P. Simon, and J.-S. Kim, "Electrospun PVA/HAp nanocomposite nanofibers: biomimetics of mineralized hard tissues at a lower level of complexity.," *Bioinspir. Biomim.*, vol. 3, no. 4, pp. 1–12, 2008.

[100] R. Ricciardi, F. Auriemma, C. Gaillet, C. De Rosa, and F. Lauprêtre, "Investigation of

the crystallinity of freeze/thaw poly(vinyl alcohol) hydrogels by different techniques," *Macromolecules*, vol. 37, no. 25, pp. 9510–9516, 2004, doi: 10.1021/ma048418v.

[101] P. J. Willcox *et al.*, "Microstructure of poly(vinyl alcohol) hydrogels produced by freeze/thaw cycling," *J. Polym. Sci. Part B Polym. Phys.*, vol. 37, no. 24, pp. 3438–3454, 1999.

[102] J. E. Mark, *Physical Properties of Polymers Handbook*. Woodbury, NY: American Institute of Physics Press, 1996.

[103] J. Epp, *X-Ray Diffraction (XRD) Techniques for Materials Characterization*. Elsevier Ltd, 2016.

[104] S. Dash, P. N. Murthy, L. Nath, and P. Chowdhury, "Kinetic modeling on drug release from controlled drug delivery systems.," *Acta Pol. Pharm.*, vol. 67, no. 3, pp. 217–23, 2010.

[105] A. W. Hixson and J. H. Crowell, "Dependence of Reaction Velocity upon Surface and Agitation: III—Experimental Procedure in Study of Agitation," *Ind. Eng. Chem.*, vol. 23, no. 10, pp. 1160–1168, 1931.

[106] X. Chen *et al.*, "Astragaloside IV-loaded nanoparticle-enriched hydrogel induces wound healing and anti-scar activity through topical delivery," *Int. J. Pharm.*, vol. 447, no. 1–2, pp. 171–181, 2013, doi: 10.1016/j.ijpharm.2013.02.054.

[107] T. Fukumori and T. Nakaoki, "High strength poly(vinyl alcohol) films obtained by drying and then stretching freeze/thaw cycled gel," *J. Appl. Polym. Sci.*, vol. 132, no. 1, pp. 1–7, 2014, doi: 10.1002/app.41318.

[108] S. Gupta, S. Goswami, and A. Sinha, "A combined effect of freeze--thaw cycles and polymer concentration on the structure and mechanical properties of transparent PVA gels," *Biomed. Mater.*, vol. 7, no. 1, p. 015006, 2012.

[109] E. A. Kamoun, X. Chen, M. S. Mohy Eldin, and E. R. S. Kenawy, "Crosslinked poly(vinyl alcohol) hydrogels for wound dressing applications: A review of remarkably blended polymers," *Arab. J. Chem.*, vol. 8, no. 1, pp. 1–14, 2015.

[110] S. K. Sharma and A. Misra, "The effect of stretching conditions on properties of amorphous polyethylene terephthalate film," *J. Appl. Polym. Sci.*, vol. 34, no. 6, pp. 2231–2247, 1987, doi: 10.1002/app.1987.070340615.

[111] A. Goyanes, M. Kobayashi, R. Martínez-Pacheco, S. Gaisford, and A. W. Basit, "Fused-filament 3D printing of drug products: Microstructure analysis and drug release characteristics of PVA-based caplets," *Int. J. Pharm.*, vol. 514, no. 1, pp. 290–295, 2016.

[112] S. Bahrainian, M. Abbaspour, M. Kouchak, and P. Taghavi Moghadam, "A Review on Fast Dissolving Systems: From Tablets to Nanofibers," *Jundishapur J. Nat. Pharm. Prod.*, vol. 12, no. 2, p. e34267, 2017.

[113] C. J. Derry, S. Derry, and R. A. Moore, "Caffeine as an analgesic adjuvant for acute pain in adults," *Cochrane Database Syst. Rev.*, vol. 14, no. 3, pp. 1–47, 2012, doi: 10.1002/14651858.CD009281.pub3.

[114] U. E. Illangakoon *et al.*, "Fast dissolving paracetamol/caffeine nanofibers prepared by electrospinning," *Int. J. Pharm.*, vol. 477, no. 1–2, pp. 369–379, 2014.

[115] V. Garsuch and J. Breitkreutz, “Novel analytical methods for the characterization of oral wafers,” *Eur. J. Pharm. Biopharm.*, vol. 73, no. 1, pp. 195–201, 2009.

[116] M. D. Eddieston and W. Jones, “Formation of tubular crystals of pharmaceutical compounds,” *Cryst. Growth Des.*, vol. 10, no. 1, pp. 365–370, 2010.

[117] E. F. dos Reis *et al.*, “Synthesis and characterization of poly (vinyl alcohol) hydrogels and hybrids for rMPB70 protein adsorption,” *Mater. Res.*, vol. 9, no. 2, pp. 185–191, 2006.

[118] R. M. Silverstein, G. C. Bassler, and T. C. Morrill, *Spectrometric Identification of Organic Compounds*, 4th ed. New York: John Wiley and Sons, 1981.

[119] W. Reusch, “Infrared Spectroscopy,” *Michigan State University*, 2013. https://www2.chemistry.msu.edu/faculty/reusch/virttxtjml/spectrpy/infrared/infrared.htm.

[120] S. Seif, L. Franzen, and M. Windbergs, “Overcoming drug crystallization in electrospun fibers - Elucidating key parameters and developing strategies for drug delivery,” *Int. J. Pharm.*, vol. 478, no. 1, pp. 390–397, 2015.

[121] C. M. Hassan and N. A. Peppas, “Structure and morphology of freeze/thawed PVA hydrogels,” *Macromolecules*, vol. 33, no. 7, pp. 2472–2479, 2000.

[122] J. S. Park, J. W. Park, and E. Ruckenstein, “Thermal and dynamic mechanical analysis of PVA/MC blend hydrogels,” *Polymer (Guildf).*, vol. 42, no. 9, pp. 4271–4280, 2001.

[123] S. K. Burgessa, J. S. Lee, C. R. Mubarak, R. M. Kriegel, and W. J. Korosa, “Caffeine antiplasticization of amorphous poly(ethylene terephthalate): Effects on gas transport, thermal, and mechanical properties,” *Polymer (Guildf).*, vol. 65, pp. 33–44, 2015.

[124] J. S. Lee, J. Leisen, R. P. Choudhury, R. M.Kriegel, H. W.Beckham, and W. J.Korosa, “Antiplasticization-based enhancement of poly(ethylene terephthalate) barrier properties,” *Polymer (Guildf).*, vol. 53, no. 1, pp. 213–222, 2012.

[125] K. Klímová and J. Leitner, “DSC study and phase diagrams calculation of binary systems of paracetamol,” *Thermochim. Acta*, vol. 550, no. 2, pp. 59–64, 2012.

[126] A. Goyanes *et al.*, “3D Printing of Medicines: Engineering Novel Oral Devices with Unique Design and Drug Release Characteristics,” *Mol. Pharm.*, vol. 12, no. 11, pp. 4077–4084, 2015, doi: 10.1021/acs.molpharmaceut.5b00510.

[127] H. W. Kwak, H. Woo, I. C. Kim, and K. H. Lee, “Fish gelatin nanofibers prevent drug crystallization and enable ultrafast delivery,” *RSC Adv.*, vol. 7, no. 64, pp. 40411–40417, 2017, doi: 10.1039/c7ra06433k.

[128] P. Weiss, A. Fatimi, J. Guicheux, and C. Vinatier, “Biomedical Applications of Hydrogels Handbook,” *Business*, vol. c, pp. 247–268, 2010.

[129] F. S. Matty, M. T. Sultan, and A. K. Amine, “Swelling Behavior of Cross-link PVA with Glutaraldehyde,” *Ibn Al-Haitham J. Pure Appl. Sci.*, vol. 28, no. 2, 2015.

[130] S. Deb, Q. Mary, and M. E. Road, “Dynamic mechanical characterization of hydrogel blends of poly (vinyl alcohol-vinyl acetate) with poly (acrylic acid) or poly (vinyl pyrrolidone),” *J. Mater. Sci. Med.*, vol. 7, pp. 349–353, 1996.

[131] A. Karimi and W. M. A. W. Daud, “Harmless Hydrogels Based on PVA/Na1-MMT

Nanocomposites for Biomedical Applications: Fabrication and Characterization," *Polym. Compos.*, vol. 38, no. 6, pp. 1135–1143, 2017.

[132] J. V Cauich-Rodriguez, S. Deb, and R. Smith, "Effect of cross-linking agents on the dynamic mechanical properties of hydrogel blends of poly(acrylic acid)- poly(viny1 alcohol-vinyl acetate)," *Biomoterids*, vol. 17, no. 23, pp. 2259–2264, 1996.

[133] C.-C. Yang, Y.-J. Lee, and M. Jen, "Direct methanol fuel cell (DMFC) based on PVA/MMT composite polymer membranes," *J. Power Sources*, vol. 188, no. 1, pp. 30–37, 2009.

[134] L. Li *et al.*, "Effect of water state and polymer chain motion on the mechanical properties of a bacterial cellulose and polyvinyl alcohol (BC/PVA) hydrogel," *RSC Adv.*, vol. 5, no. 32, pp. 25525–25531, 2015.

[135] T. Fukumori and T. Nakaoki, "Significant Improvement of Mechanical Properties for Polyvinyl Alcohol Film Prepared from Freeze/Thaw Cycled Gel.," *Open J. Org. Polym. Mater.*, vol. 3, no. 110–116, pp. 110–116, 2013.

[136] A. El-Hadi, R. Schnabel, E. Straube, G. Müller, and S. Henning, "Correlation between degree of crystallinity, morphology, glass temperature, mechanical properties and biodegradation of poly (3-hydroxyalkanoate) PHAs and their blends," *Polym. Test.*, vol. 21, no. 6, pp. 665–674, 2002, doi: 10.1016/S0142-9418(01)00142-8.

[137] G. Verreck *et al.*, "Incorporation of drugs in an amorphous state into electrospun nanofibers composed of a water-insoluble, nonbiodegradable polymer," *J. Control. Release*, vol. 92, no. 3, pp. 349–360, 2003, doi: 10.1016/S0168-3659(03)00342-0.

[138] J. C. Fu, D. L. Moyer, and C. Hagemeier, "Effect of comonomer ratio on hydrocortisone diffusion from sustained-release composite capsules," *J. Biomed. Mater. Res.*, vol. 12, no. 3, pp. 249–254, 1978.

[139] K. Asghar, M. Qasim, G. Dharmapuri, and D. Das, "Investigation on a smart nanocarrier with a mesoporous magnetic core and thermo-responsive shell for co-delivery of doxorubicin and curcumin: a new approach towards combination therapy of cancer," *RSC Adv.*, vol. 7, no. 46, pp. 28802–28818, 2017.

[140] H. K. Shaikh, R. V. Kshirsagar, and S. G. Patil, "Mathematical models for drug release characterization: A review," *World J. Pharm. Pharm. Sci.*, vol. 13, no. 3, pp. 123–133, 2010.

[141] K. Morimotol, A. Nagayasu, S. Fukanoki, K. Morisaka, and Y. Ikada, "Evaluation of Polyvinyl Alcohol Hydrogel as Sustained-Release Vehicle for Transdermal Sytem of Bunitrolol-HCL," *Drug Dev. Ind. Pharm.*, vol. 16, no. 1, pp. 13–29, 1990.

[142] C. W. Bunn, "Crystal Structure of Polyvinyl Alcohol," *Nat. Publ. Gr.*, vol. 161, pp. 707–709, 1948, doi: 10.1038/162680a0.

[143] S. Mahendia, A. K. Tomar, R. P. Chahal, P. Goyal, and S. Kumar, "Optical and structural properties of poly(vinyl alcohol) films embedded with citrate-stabilized gold nanoparticles," *J. Phys. D. Appl. Phys.*, vol. 44, no. 20, 2011, doi: 10.1088/0022-3727/44/20/205105.

[144] M. A. Al-Omar, "Ciprofloxacin: Physical Profile," *Profiles Drug Subst. Excipients Relat. Methodol.*, vol. 31, pp. 163–178, 2005, doi: 10.1016/S0000-0000(00)00000-0.

[145] G. G. de Lima *et al.*, “The production of a novel poly(vinyl alcohol) hydrogel cryogenic spheres for immediate release using a droplet system,” *Biomed. Phys. Eng. Express*, vol. 5, p. 045017, 2019.

[146] K. K. Kim and D. W. Pack, “Microspheres for Drug Delivery,” *BioMEMS Biomed. Nanotechnol.*, pp. 19–50, 2006, doi: 10.1007/978-0-387-25842-3_2.

[147] C. Castro, C. Évora, M. Baro, I. Soriano, and E. Sánchez, “Two-month ciprofloxacin implants for multibacterial bone infections,” *Eur. J. Pharm. Biopharm.*, vol. 60, no. 3, pp. 401–406, 2005, doi: 10.1016/j.ejpb.2005.02.005.

[148] M. Trotta, D. Chirio, R. Cavalli, and E. Peira, “Hydrophilic microspheres from water-in-oil emulsions by the water diffusion technique,” *Pharm. Res.*, vol. 21, no. 8, pp. 1445–1449, 2004, doi: 10.1023/B:PHAM.0000036919.94865.57.

[149] J. L. Maia, M. H. A. Santana, and M. I. Ré, “The effect of some processing conditions on the characteristics of biodegradable microspheres obtained by an emulsion solvent evaporation process,” *Brazilian J. Chem. Eng.*, vol. 21, no. 1, pp. 1–12, 2004, doi: 10.1590/S0104-66322004000100002.

[150] F. Tao Meng, G. Hui Ma, W. Qiu, and Z. Guo Su, “W / O / W double emulsion technique using ethyl acetate as organic solvent: effects of its diffusion rate on the characteristics of microparticles,” *J. Control. Release*, vol. 91, pp. 407–416, 2003, doi: 10.1016/S0168-3659(03)00273-6.

[151] X. Wang, T. Yucel, Q. Lu, X. Hu, and D. L. Kaplan, “Silk Nanospheres and Microspheres from Silk/PVA Blend Films for Drug Delivery,” *Eur. Cells Mater.*, vol. 31, no. 6, pp. 1025–1035, 2010, doi: 10.1016/j.biomaterials.2009.11.002.Silk.

[152] R. K. Kankala, Y. S. Zhang, S. Bin Wang, C. H. Lee, and A. Z. Chen, “Supercritical Fluid Technology: An Emphasis on Drug Delivery and Related Biomedical Applications,” *Adv. Healthc. Mater.*, vol. 6, no. 16, 2017, doi: 10.1002/adhm.201700433.

[153] L. Zhang, J. Huang, T. Si, and R. X. Xu, “Coaxial electrospray of microparticles and nanoparticles for biomedical applications,” *Expert Rev. Med. Devices*, vol. 9, no. 6, pp. 595–612, 2012, doi: 10.1586/erd.12.58.

[154] D. Ë. Ermis and A. Yu, “Preparation of spray-dried microspheres of indomethacin and examination of the effects of coating on dissolution rates,” vol. 16, no. 3, 1999.

[155] L. Lacerda, A. L. Parize, V. Fávere, M. C. M. Laranjeira, and H. K. Stulzer, “Development and evaluation of pH-sensitive sodium alginate/chitosan microparticles containing the antituberculosis drug rifampicin,” *Mater. Sci. Eng. C*, vol. 39, pp. 161–167, Jun. 2014, doi: 10.1016/j.msec.2014.01.054.

[156] K. S. Soppimath and T. M. Aminabhavi, “Ethyl acetate as a dispersing solvent in the production of poly(DL-lactide-co-glycolide) microspheres: Effect of process parameters and polymer type,” *J. Microencapsul.*, vol. 19, no. 3, pp. 281–292, 2002, doi: 10.1080/02652040110105319.

[157] J. Li and D. J. Mooney, “Designing hydrogels for controlled drug delivery,” *Nat. Rev. Mater.*, vol. 1, no. 12, p. 16071, 2016.

[158] J. Wang, Q. Gong, D. Zhuang, and J. Liang, “Chemical vapor infiltration tailored hierarchical porous CNTs/C composite spheres fabricated by freeze casting and their

adsorption properties," *RSC Adv.*, vol. 5, no. 22, pp. 16870–16877, 2015.

[159] Q. Cheng, C. Huang, and A. P. Tomsia, "Freeze casting for assembling bioinspired structural materials," *Adv. Mater.*, vol. 29, no. 45, p. 1703155, 2017.

[160] E. B. Division and T. Nadu, "Biodegradation of Caffeine by Trichosporon asahii Isolated from Caffeine Contaminated Soil," *Int. J. Eng. Sci. Technol.*, vol. 3, no. 11, pp. 7988–7997, 2011.

[161] J. Jose, F. Shehzad, and M. a. Al-Harthi, "Preparation method and physical, mechanical, thermal characterization of poly(vinyl alcohol)/poly(acrylic acid) blends," *Polym. Bull.*, vol. 71, pp. 2787–2802, 2014, doi: 10.1007/s00289-014-1221-3.

[162] J. A. Killion *et al.*, "Hydrogel/bioactive glass composites for bone regeneration applications: Synthesis and characterisation," *Mater. Sci. Eng. C*, vol. 33, no. 7, pp. 4203–4212, Oct. 2013, doi: 10.1016/j.msec.2013.06.013.

[163] G. G. de Lima, L. Campos, A. Junqueira, D. M. Devine, and M. J. D. Nugent, "A novel pH-sensitive ceramic-hydrogel for biomedical applications," *Polym. Adv. Technol.*, vol. 26, no. 12, pp. 1439–1446, 2015, doi: 10.1002/pat.3593.

[164] A. Anitha *et al.*, "Chitin and chitosan in selected biomedical applications," *Prog. Polym. Sci.*, vol. 39, no. 9, pp. 1644–1667, Sep. 2014, doi: 10.1016/j.progpolymsci.2014.02.008.

[165] S. S. Sana and V. K. N. Boya, "Poly (vinyl alcohol)/poly (acrylamide-co-diallyldimethyl ammonium chloride) semi-IPN hydrogels for ciprofloxacin hydrochloride drug delivery," *IET nanobiotechnology*, vol. 11, no. 1, pp. 52–56, 2016.

[166] H. Abdelkader and H. F. Mansour, "Comparative studies for ciprofloxacin hydrochloride pre-formed gels and thermally triggered (in situ) gels: in vitro and in vivo appraisal using a bacterial keratitis model in rabbits," *Pharm. Dev. Technol.*, vol. 20, no. 4, pp. 410–416, 2015.

[167] S. Hubert *et al.*, "Process induced transformations during tablet manufacturing: Phase transition analysis of caffeine using DSC and low frequency micro-Raman spectroscopy," *Int. J. Pharm.*, vol. 420, no. 1, pp. 76–83, 2011, doi: 10.1016/j.ijpharm.2011.08.028.

[168] B. S. Chee, G. G. de Lima, D. M. Devine, and M. J. D. Nugent, "Investigation of the effects of orientation on freeze/thawed Polyvinyl alcohol hydrogel properties," *Mater. Today Commun.*, vol. 17, no. March, pp. 82–93, 2018, doi: 10.1016/j.mtcomm.2018.08.005.

[169] E. R. Kenawy, E. A. Kamoun, M. S. Mohy Eldin, and M. A. El-Meligy, "Physically crosslinked poly(vinyl alcohol)-hydroxyethyl starch blend hydrogel membranes: Synthesis and characterization for biomedical applications," *Arab. J. Chem.*, vol. 7, no. 3, pp. 372–380, 2014, doi: 10.1016/j.arabjc.2013.05.026.

[170] A. C. Wenceslau, F. G. dos Santos, É. R. F. Ramos, C. V. Nakamura, A. F. Rubira, and E. C. Muniz, "Thermo- and pH-sensitive IPN hydrogels based on PNIPAAm and PVA-Ma networks with LCST tailored close to human body temperature," *Mater. Sci. Eng. C*, vol. 32, no. 5, pp. 1259–1265, Jul. 2012, doi: 10.1016/j.msec.2012.04.001.

[171] Y. Qiu and K. Park, "Environment-sensitive hydrogels for drug delivery," *Adv. Drug Deliv. Rev.*, vol. 64, pp. 49–60, Dec. 2012, doi: 10.1016/j.addr.2012.09.024.

[172] S. M. M. Quintero, R. V. Ponce F, M. Cremona, a. L. C. Triques, a. R. d'Almeida, and a. M. B. Braga, "Swelling and morphological properties of poly(vinyl alcohol) (PVA) and poly(acrylic acid) (PAA) hydrogels in solution with high salt concentration," *Polymer (Guildf).*, vol. 51, no. 4, pp. 953–958, Feb. 2010, doi: 10.1016/j.polymer.2009.12.016.

[173] J. Tavakoli, S. Mirzaei, and Y. Tang, "Cost-effective double-layer hydrogel composites for wound dressing applications," *Polymers (Basel).*, vol. 10, no. 3, 2018, doi: 10.3390/polym10030305.

[174] E. Caló, L. Ballamy, and V. V Khutoryanskiy, "Hydrogels in Wound Management," *Hydrogels Des. Synth. Appl. Drug Deliv. Regen. Med.*, p. 128, 2018.

[175] D. Schmaljohann, "Thermo-and pH-responsive polymers in drug delivery," *Adv. Drug Deliv. Rev.*, vol. 58, no. 15, pp. 1655–1670, 2006.

[176] G. Goetten de Lima, S. Halligan, L. Geever, M. Dalton, C. McConville, and M. J. D. Nugent, "Controlled release of poorly soluble active ingredients from bioresorbable polymers," in *Bioresorbable Polymers*, 1ed ed., D. Devine, Ed. Berlin, Boston: De Gruyter, 2019, pp. 47–68.

[177] B. Neeraj, K. Abhishek, C. Abhilash, C. Rubia, and B. Rajni, "A review on immediate release drug delivery system," *Int. Res. J. Pharm. Appl. Sci.*, vol. 4, no. 1, pp. 78–80, 2014.

[178] A. Gupta, A. K. Mishra, V. Gupta, P. Bansal, R. Singh, and A. K. Singh, "Recent trends of fast dissolving tablet-An overview of formulation technology," *Int. J. Pharm. Biol. Arch.*, vol. 1, no. 1, pp. 1–10, 2010.

[179] M. de Matos, B. D. Mattos, B. L. Tardy, O. J. Rojas, and W. L. E. Magalhães, "Use of Biogenic Silica in Porous Alginate Matrices for Sustainable Fertilization with Tailored Nutrient Delivery," *ACS Sustain. Chem. Eng.*, vol. 6, no. 2, pp. 2716–2723, 2018.

[180] GermanResearchFoundation, "Ethyl acetate," in *The MAK-Collection for Occupational Health and Safety*, Wiley-VCH Verlag GmbH & Co. KGaA, 2012.

[181] J. Wang, V. Planz, B. Vukosavljevic, and M. Windbergs, "Multifunctional electrospun nanofibers for wound application – Novel insights into the control of drug release and antimicrobial activity," *Eur. J. Pharm. Biopharm.*, vol. 129, pp. 175–183, 2018, doi: 10.1016/j.ejpb.2018.05.035.

[182] A. M. Al-Dhahebi, S. C. B. Gopinath, and M. S. M. Saheed, "Graphene impregnated electrospun nanofiber sensing materials: a comprehensive overview on bridging laboratory set-up to industry," *Nano Converg.*, vol. 7, no. 1, 2020, doi: 10.1186/s40580-020-00237-4.

[183] S. P. Sundaran, C. R. Reshmi, P. Sagitha, O. Manaf, and A. Sujith, "Multifunctional graphene oxide loaded nanofibrous membrane for removal of dyes and coliform from water," *J. Environ. Manage.*, vol. 240, pp. 494–503, 2019, doi: 10.1016/j.jenvman.2019.03.105.

[184] M. Arkoun, F. Daigle, R. A. Holley, M. C. Heuzey, and A. Ajji, "Chitosan-based nanofibers as bioactive meat packaging materials," *Packag. Technol. Sci.*, vol. 31, no. 4, pp. 185–195, 2018, doi: 10.1002/pts.2366.

[185] L. Steffens *et al.*, "Electrospun PVA-Dacarbazine nanofibers as a novel nano brain-

implant for treatment of glioblastoma: in silico and in vitro characterization," *Eur. J. Pharm. Sci.*, vol. 143, p. 105183, 2020, doi: 10.1016/j.ejps.2019.105183.

[186] L. S. Reinhardt *et al.*, "Plantago australis Hydroethanolic Extract-Loaded Formulations: Promising Dressings for Wound Healing," *Rev. Bras. Farmacogn.*, vol. 31, pp. 91–101, 2021, doi: 10.1007/s43450-021-00126-9.

[187] W. A. Laftah, S. Hashim, and A. N. Ibrahim, "Polymer hydrogels: A review," *Polym. - Plast. Technol. Eng.*, vol. 50, no. 14, pp. 1475–1486, 2011, doi: 10.1080/03602559.2011.593082.

[188] H. L. Lim, Y. Hwang, M. Kar, and S. Varghese, "Smart hydrogels as functional biomimetic systems," *Biomater. Sci.*, vol. 2, no. 5, pp. 603–618, 2014, doi: 10.1039/c3bm60288e.

[189] M. Rizwan *et al.*, "pH Sensitive Hydrogels in Drug Delivery : Brief History , Properties , Swelling , and Release Mechanism , Material Selection and Applications," *Polymers (Basel).*, vol. 9, no. 12, p. 137, 2017, doi: 10.3390/polym9040137.

[190] Q. Chena, H. Kurosub, L. Mab, and M. Matsuo, "Elongation-induced phase separation of poly(vinyl alcohol)/ poly(acrylic-acid) blends as studied by 13 C CP/MAS NMR and wide-angle x-ray diffraction," *Polymer (Guildf).*, vol. 43, no. 4, pp. 1203–1206, 2002, doi: 10.1016/S0032-3861(01)00690-5.

[191] H. Serinçay *et al.*, "PVA/PAA-Based Antibacterial Wound Dressing Material with Aloe Vera," *Polym. - Plast. Technol. Eng.*, vol. 52, no. 13, pp. 1308–1315, 2013, doi: 10.1080/03602559.2013.814671.

[192] J. A. Park, J. K. Kang, S. C. Lee, and S. B. Kim, "Electrospun poly(acrylic acid)/poly(vinyl alcohol) nanofibrous adsorbents for Cu(ii) removal from industrial plating wastewater," *RSC Adv.*, vol. 7, no. 29, pp. 18075–18084, 2017, doi: 10.1039/c7ra01362k.

[193] G. M. Wu, S. J. Lin, and C. C. Yang, "Preparation and characterization of PVA/PAA membranes for solid polymer electrolytes," *J. Memb. Sci.*, vol. 275, no. 1–2, pp. 127–133, 2006, doi: 10.1016/j.memsci.2005.09.012.

[194] Z. J. Chang, X. H. Jin, J. Zeng, T. Y. Song, and J. Zhang, "High photocatalytic activity of covalent grafting of phthalocyanines on crosslinked electrospun PVA/PAA nanofibers," *Mater. Sci. Forum*, vol. 848, pp. 419–424, 2016, doi: 10.4028/www.scientific.net/MSF.848.419.

[195] J. Yun, J. S. Im, Y.-S. Lee, and H.-I. Kim, "Electro-responsive transdermal drug delivery behavior of PVA/PAA/MWCNT nanofibers," *Eur. Polym. J.*, vol. 47, no. 10, pp. 1893–1902, 2011, doi: 10.1016/j.eurpolymj.2011.07.024.

[196] J. C. Park *et al.*, "Electrospun poly(vinyl alcohol) nanofibers: Effects of degree of hydrolysis and enhanced water stability," *Polym. J.*, vol. 42, no. 3, pp. 273–276, 2010, doi: 10.1038/pj.2009.340.

[197] J. A. Park, S. C. Lee, and S. B. Kim, "Synthesis of dual-functionalized poly(vinyl alcohol)/poly(acrylic acid) electrospun nanofibers with enzyme and copper ion for enhancing anti-biofouling activities," *J. Mater. Sci.*, vol. 54, no. 13, pp. 9969–9982, 2019, doi: 10.1007/s10853-019-03578-6.

[198] H. Lee, R. Mensire, R. E. Cohen, and M. F. Rubner, "Strategies for Hydrogen Bonding

Based Layer-by-Layer Assembly of Poly (vinyl alcohol) with Weak Polyacids," *Macromolecules*, vol. 45, pp. 347–355, 2012, doi: 10.1021/ma202092w.

[199] T. Liu *et al.*, "Super-strong and tough poly(vinyl alcohol)/poly(acrylic acid) hydrogels reinforced by hydrogen bonding," *J. Mater. Chem. B*, vol. 6, pp. 8105–8114, 2018, doi: 10.1039/C8TB02556H.

[200] G. G. de Lima *et al.*, "Composite cryogels for dual drug delivery and enhanced mechanical properties," *Polym. Compos.*, vol. 39, no. July 2019, pp. E210–E220, 2018, doi: 10.1002/pc.24450.

[201] Y. Zhou, Q. Zhao, and M. Wang, "Dual release of VEGF and PDGF from emulsion electrospun bilayer scaffolds consisting of orthogonally aligned nanofibers for gastrointestinal tract regeneration," *MRS Commun.*, vol. 9, no. 3, pp. 1098–1104, 2019, doi: 10.1557/mrc.2019.104.

[202] F. Amini, D. Semnani, S. Karbasi, and S. N. Banitaba, "A novel bilayer drug-loaded wound dressing of PVDF and PHB/Chitosan nanofibers applicable for post-surgical ulcers," *Int. J. Polym. Mater. Polym. Biomater.*, vol. 68, no. 13, pp. 772–777, 2019, doi: 10.1080/00914037.2018.1506982.

[203] W. Li, X. Tan, T. Luo, Y. Shi, Y. Yang, and L. Liu, "Preparation and characterization of electrospun PLA/PU bilayer nanofibrous membranes for controlled drug release applications," *Integr. Ferroelectr.*, vol. 179, no. 1, pp. 104–119, 2017, doi: 10.1080/10584587.2017.1331113.

[204] H. E. Colley *et al.*, "Pre-clinical evaluation of novel mucoadhesive bilayer patches for local delivery of clobetasol-17-propionate to the oral mucosa," *Biomaterials*, vol. 178, pp. 134–146, 2018, doi: 10.1016/j.biomaterials.2018.06.009.

[205] D. H. Kim *et al.*, "Biocompatibility and bioactivity of an FGF-loaded microsphere-based bilayer delivery system," *Acta Biomater.*, vol. 111, pp. 341–348, 2020, doi: 10.1016/j.actbio.2020.04.048.

[206] N. Lavielle, A. Hébraud, L. Thöny-Meyer, R. M. Rossi, and G. Schlatter, "3D Composite Assemblies of Microparticles and Nanofibers for Tailored Wettability and Controlled Drug Delivery," *Macromol. Mater. Eng.*, vol. 302, no. 8, pp. 1–8, 2017, doi: 10.1002/mame.201600458.

[207] K. Chen, G. Chen, S. Wei, X. Yang, D. Zhang, and L. Xu, "Preparation and property of high strength and low friction PVA-HA/PAA composite hydrogel using annealing treatment," *Mater. Sci. Eng. C*, vol. 91, pp. 579–588, 2018, doi: 10.1016/j.msec.2018.05.080.

[208] K. Kumeta, I. Nagashima, S. Matsui, and K. Mizoguchi, "Crosslinking reaction of poly(vinyl alcohol) with poly(acrylic acid) (PAA) by heat treatment: Effect of neutralization of PAA," *J. Appl. Polym. Sci.*, vol. 90, no. 9, pp. 2420–2427, 2003, doi: 10.1002/app.12910.

[209] B. Cerroni, E. Chiessi, S. Margheritelli, L. Oddo, and G. Paradossi, "Polymer shelled microparticles for a targeted doxorubicin delivery in cancer therapy," *Biomacromolecules*, vol. 12, no. 3, pp. 593–601, 2011, doi: 10.1021/bm101207k.

[210] S. Ghosh *et al.*, "Development and physicochemical characterization of doxorubicin-encapsulated hydroxyapatite–polyvinyl alcohol nanocomposite for repair of

osteosarcoma-affected bone tissues," *Comptes Rendus Chim.*, vol. 22, no. 1, pp. 46–57, 2019, doi: 10.1016/j.crci.2018.10.005.

[211] N. Amani, M. Shokrzadeh, and F. Shaki, "Clarithromycin effectively enhances doxorubicin-induced cytotoxicity and apoptosis in MCF7 cells through dysregulation of autophagy," *Adv. Med. Sci.*, vol. 65, no. 2, pp. 235–243, 2020, doi: 10.1016/j.advms.2020.03.002.

[212] T. A. W. Wijanarko, A. Kusumaatmaja, Chotimah, Roto, and K. Triyana, "Effect of heat treatment on morphology and crystallinity of electrospun Poly(vinyl alcohol) nanofibers," *AIP Conf. Proc.*, vol. 1755, no. July 2016, 2016, doi: 10.1063/1.4958583.

[213] J. Zeng, H. Hou, J. H. Wendorff, and A. Greiner, "Electrospun poly(vinyl alcohol)/poly(acrylic acid) fibres with excellent water-stability," *E-Polymers*, vol. 078, 2004, doi: 10.1515/epoly.2004.4.1.899.

[214] B. Felice, M. P. Prabhakaran, M. Zamani, A. P. Rodríguez, and S. Ramakrishna, "Electrosprayed poly(vinyl alcohol) particles: Preparation and evaluation of their drug release profile," *Polym. Int.*, vol. 64, no. 12, pp. 1722–1732, 2015, doi: 10.1002/pi.4972.

[215] H. Fong, I. Chun, and D. H. Reneker, "Beaded nanofibers formed during electrospinning," *Polymer (Guildf).*, vol. 40, no. 16, pp. 4585–4592, 1999, doi: 10.1016/S0032-3861(99)00068-3.

[216] C. Zhang, X. Yuan, L. Wu, Y. Han, and J. Sheng, "Study on morphology of electrospun poly(vinyl alcohol) mats," *Eur. Polym. J.*, vol. 41, no. 3, pp. 423–432, 2005, doi: 10.1016/j.eurpolymj.2004.10.027.

[217] S. Kumari, L. K. Pradhan, L. Kumar, M. K. Manglam, and M. Kar, "Effect of Annealing Temperature on Morphology and Magnetic Properties of Cobalt Ferrite Nanofibers," *Mater. Res. Express*, vol. 6, no. 12, 2019.

[218] W. Pan, Z. Ma, J. Liu, Q. Liu, and J. Wang, "Effect of heating rate on morphology and structure of CoFe 2O4 nanofibers," *Mater. Lett.*, vol. 65, no. 21–22, pp. 3269–3271, 2011, doi: 10.1016/j.matlet.2011.06.102.

[219] Z. Wang *et al.*, "Effect of thermal annealing on mechanical properties of polyelectrolyte complex nanofiber membranes," *Fibers Polym.*, vol. 15, no. 7, pp. 1406–1413, 2014, doi: 10.1007/s12221-014-1406-2.

[220] I. M. Jipa *et al.*, "Potassium sorbate release from poly(vinyl alcohol)-bacterial cellulose films," *Chem. Pap.*, vol. 66, no. 2, pp. 138–143, 2012, doi: 10.2478/s11696-011-0068-4.

[221] W. Kam, C. W. Liew, J. Y. Lim, and S. Ramesh, "Electrical, structural, and thermal studies of antimony trioxide-doped poly(acrylic acid)-based composite polymer electrolytes," *Ionics (Kiel).*, vol. 20, no. 5, pp. 665–674, 2014, doi: 10.1007/s11581-013-1012-0.

[222] A. Aytimur and I. Uslu, "Promising Materials for Wound Dressing: PVA/PAA/PVP Electrospun Nanofibers," *Polym. - Plast. Technol. Eng.*, vol. 53, no. 7, pp. 655–660, 2014, doi: 10.1080/03602559.2013.874031.

[223] J. S. Gaffney, N. A. Marley, and D. E. Jones, "Fourier Transform Infrared (FTIR) Spectroscopy," *Charact. Mater.*, 2012, doi: 10.1016/c2009-0-22072-1.

[224] W. DH and F. I., “Infrared spectra,” in *Spectroscopic Methods in Organic Chemistry*, 6th ed., London: McGraw-Hill Higher Education, 2008.

[225] W. Samprasit, P. Akkaramongkolporn, T. Ngawhirunpat, T. Rojanarata, R. Kaomongkolgit, and P. Opanasopit, “Fast releasing oral electrospun PVP/CD nanofiber mats of taste-masked meloxicam,” *Int. J. Pharm.*, vol. 487, no. 1–2, pp. 213–222, 2015, doi: 10.1016/j.ijpharm.2015.04.044.

[226] N. D. Gavrilova, I. A. Malyshkina, E. E. Makhaeva, V. K. Novik, and A. V. Vorobiev, “Dielectric relaxation anomalies in polyacrylic acid and their relationship with ‘critical’ points of water,” *Ferroelectrics*, vol. 504, no. 1, pp. 3–14, 2016, doi: 10.1080/00150193.2016.1238284.

[227] S. Mollá and V. Compañ, “Polyvinyl alcohol nanofiber reinforced Nafion membranes for fuel cell applications,” *J. Memb. Sci.*, vol. 372, no. 1–2, pp. 191–200, 2011, doi: 10.1016/j.memsci.2011.02.001.

[228] X. Zhu, X. Du, X. Chen, J. Hu, X. Zhou, and L. Guo, “Determining the effects of annealing time on the glass transition temperature of Pueraria lobata (Willd.) Ohwi starch,” *Int. J. Food Sci. Technol.*, vol. 53, no. 1, pp. 43–49, 2018, doi: 10.1111/ijfs.13518.

[229] Y. Park *et al.*, “Crosslinking effect on thermal conductivity of electrospun poly(acrylic acid) nanofibers,” *Polymers (Basel).*, vol. 11, no. 5, pp. 1–13, 2019, doi: 10.3390/polym11050858.

[230] D. De la Garza, F. De Santiago, L. Materon, M. Chipara, and M. Alcoutlabi, “Fabrication and characterization of centrifugally spun poly(acrylic acid) nanofibers,” *J. Appl. Polym. Sci.*, vol. 136, no. 19, pp. 1–9, 2019, doi: 10.1002/app.47480.

[231] M. Lim, D. Kim, and J. Seo, “Enhanced oxygen-barrier and water-resistance properties of poly(vinyl alcohol) blended with poly(acrylic acid) for packaging applications,” *Polym. Int.*, vol. 65, no. 4, pp. 400–406, 2016, doi: 10.1002/pi.5068.

[232] E. Rynkowska, K. Fatyeyeva, S. Marais, J. Kujawa, and W. Kujawski, “Chemically and Thermally Crosslinked PVA-Based Membranes: Effect on Swelling and Transport Behavior,” *Polymers (Basel).*, vol. 11, p. 1799, 2019.

[233] C. H. M. Jacques, H. B. Hopfenberg, and V. Stannett, “Super Case II Transport of Organic Vapors in Glassy Polymers,” *Am Chem Soc, Div Org Coatings Plast Chem1974*, vol. 34, no. 1, pp. 452–456, 1974.

[234] M. L. Bruschi, “Mathematical models of drug release,” in *Strategies to Modify the Drug Release from Pharmaceutical Systems*, M. L. Bruschi, Ed. Woodhead Publishing, 2015, pp. 63–86.

[235] T. Gunasekaran, T. Haile, T. Nigusse, and M. D. Dhanaraju, “Nanotechnology: An effective tool for enhancing bioavailability and bioactivity of phytomedicine,” *Asian Pac. J. Trop. Biomed.*, vol. 4, no. Suppl 1, pp. S1–S7, 2014, doi: 10.12980/APJTB.4.2014C980.

[236] R. N. Oliveira *et al.*, “PVA hydrogels loaded with a Brazilian propolis for burn wound healing applications,” *J. Appl. Polym. Sci.*, vol. 132, no. 25, 2015, doi: 10.1002/app.42129.

[237] Y. Ishida *et al.*, “Anticancer Activity in Honeybee Propolis: Functional Insights to the

Role of Caffeic Acid Phenethyl Ester and Its Complex With γ-Cyclodextrin," *Integr. Cancer Ther.*, vol. 17, no. 3, pp. 867–873, 2018, doi: 10.1177/1534735417753545.

[238] P. Premratanachai and C. Chanchao, "Review of the anticancer activities of bee products," *Asian Pac. J. Trop. Biomed.*, vol. 4, no. 5, pp. 337–344, 2014, doi: 10.12980/apjtb.4.2014c1262.

[239] H. Kübra Arikan and H. Hale Aygun, "Propolis Extract-PVA Nanocomposites of Textile Design: Antimicrobial Effect on Gram Positive and Negative Bacterias," *Int. J. Sec. Metab. Res. Artic. J.*, vol. 4, no. 1, pp. 218–224, 2017, doi: 10.21448/ijsm.371563.

[240] C. Shi Fung, H. Mohamad, S. Hashim, A. Htun, and A. Ahmad, "Proliferative Effect of Malaysian Propolis on Stem Cells from Human Exfoliated Deciduous Teeth: An In vitro Study," *Br. J. Pharm. Res.*, vol. 8, no. 1, pp. 1–8, 2015, doi: 10.9734/bjpr/2015/19918.

[241] J. M. Sforcin, A. Fernandes, C. A. M. Lopes, V. Bankova, and S. R. C. Funari, "Seasonal effect on Brazilian propolis antibacterial activity," *J. Ethnopharmacol.*, vol. 73, no. 1–2, pp. 243–249, 2000, doi: 10.1016/S0378-8741(00)00320-2.

[242] A. Aygun, *Effects of Propolis on Eggshell*. Elsevier Inc., 2017.

[243] F. Zeighampour, F. Alihosseini, M. Morshed, and A. A. Rahimi, "Comparison of prolonged antibacterial activity and release profile of propolis-incorporated PVA nanofibrous mat, microfibrous mat, and film," *J. Appl. Polym. Sci.*, vol. 135, no. 6, pp. 1–13, 2018, doi: 10.1002/app.45794.

[244] E. Adomavičiūtė, S. Stanys, M. Žilius, and V. Briedis, "Formation and analysis of electrospun nonwoven mats from bicomponent PVA/aqueous propolis nano-microfibres," *Fibres Text. East. Eur.*, vol. 23, no. 5, pp. 35–41, 2015, doi: 10.5604/12303666.1161754.

[245] C. Thapakorn, C. Nilrattanakoon, D. Pimpan, B. Vongsak, and N. Charernsriwilaiwat, "In vitro antioxidant activity of electrospun polyvinyl alcohol nanofiber mats containing stingless bees' propolis extracts," *Thai J. Pharm. Sci.*, vol. 40, pp. 61–64, 2016.

[246] T. B. Alberti, D. S. Coelho, M. de Prá, M. Maraschin, and B. Veleirinho, "Electrospun PVA nanoscaffolds associated with propolis nanoparticles with wound healing activity," *J. Mater. Sci.*, 2020, doi: 10.1007/s10853-020-04502-z.

[247] S. Sa'adon, S. I. Abd Razak, A. E. Ismail, and K. Fakhruddin, "Fabrication of Dual Layer Polyvinyl Alcohol Transdermal Patch: Effect of Freezing-Thawing Cycles on Morphological and Swelling Ability," *Procedia Comput. Sci.*, vol. 158, pp. 51–57, 2019, doi: 10.1016/j.procs.2019.09.027.

[248] H. Lee *et al.*, "Enhancement of mechanical properties of polymeric nanofibers by controlling crystallization behavior using a simple freezing/thawing process," *RSC Adv.*, vol. 7, no. 69, pp. 43994–44000, 2017, doi: 10.1039/c7ra06545k.

[249] Y. Nagakawa, M. Kato, S. I. Suye, and S. Fujita, "Fabrication of tough, anisotropic, chemical-crosslinker-free poly(vinyl alcohol) nanofibrous cryogels: Via electrospinning," *RSC Adv.*, vol. 10, no. 62, pp. 38045–38054, 2020, doi: 10.1039/d0ra07322a.

[250] B. Trusheva, D. Trunkova, and V. Bankova, "Different extraction methods of

biologically active components from propolis; a preliminary study," *Chem. Cent. J.*, vol. 1, no. 1, pp. 1–4, 2007, doi: 10.1186/1752-153X-1-13.

[251] Y. K. Park and M. Ikegaki, "Preparation of Water and Ethanolic Extracts of Propolis and Evaluation of the Preparations," *Biosci. Biotechnol. Biochem.*, vol. 62, no. 11, pp. 2230–2232, 1998, doi: 10.1271/bbb.62.2230.

[252] Y. Liu, J.-H. He, J. Yu, and H. Zeng, "Controlling numbers and sizes of beads in electrospun nanofibers," *Polym. Int.*, vol. 57, pp. 632–636, 2008, doi: 10.1002/pi.

[253] M. He, B. Zhang, Y. Dou, G. Yin, Y. Cui, and X. Chen, "Fabrication and characterization of electrospun feather keratin/poly(vinyl alcohol) composite nanofibers," *RSC Adv.*, vol. 7, no. 16, pp. 9854–9861, 2017, doi: 10.1039/c6ra25009b.

[254] G. G. de Lima, S. Lyons, D. M. Devine, and M. J. D. Nugent, "Electrospinning of Hydrogels for Biomedical Applications," in *Hydrogels*, Springer Singapore, 2018, pp. 219–258.

[255] C. Asawahame, K. Sutjarittangtham, S. Eitssayeam, Y. Tragoolpua, B. Sirithunyalug, and J. Sirithunyalug, "Formation of orally fast dissolving fibers containing propolis by electrospinning technique," *Chiang Mai J. Sci.*, vol. 42, no. 2, pp. 469–480, 2015.

[256] I. Fleming and D. Williams, *Spectroscopic Methods in Organic Chemistry*, 7th ed. Springer International Publishing, 2019.

[257] R. N. Oliveira *et al.*, "FTIR analysis and quantification of phenols and flavonoids of five commercially available plants extracts used in wound healing," *Matéria (Rio Janeiro)*, vol. 21, no. 3, pp. 767–779, 2016, doi: 10.1590/S1517-707620160003.0072.

[258] O. N. Tretinnikov and S. A. Zagorskaya, "Determination of the degree of crystallinity of poly(Vinyl alcohol) by ftir spectroscopy," *J. Appl. Spectrosc.*, vol. 79, no. 4, pp. 521–526, 2012, doi: 10.1007/s10812-012-9634-y.

[259] B. Sarker *et al.*, "Evaluation of fibroblasts adhesion and proliferation on alginate-gelatin crosslinked hydrogel," *PLoS One*, vol. 9, no. 9, 2014, doi: 10.1371/journal.pone.0107952.

Appendix 1: List of Publications

Journal paper

1. **B. S. Chee**, G. G. de Lima, D. M. Devine, and M. J. D. Nugent, "Investigation of the effects of orientation on freeze/thawed Polyvinyl alcohol hydrogel properties," Materials Today Communications, vol. 17, pp. 82–93, 2018.
2. L. Steffens Reinhardt, **B. S. Chee**, Z. Cao, D. Jaqueline Moura and M. J. D. Nugent, "Freeze-thaw electrospun PVA-dacarbazine nanoparticles: preparation, characterization and anticancer evaluation," International Journal of Polymeric Materials and Polymeric Biomaterials, 2019.
3. G. G. de Lima, **B. S. Chee** and et al., "A tough and novel dual-response PAA/P(NiPAAM-co-PEGDMA) IPN hydrogels with ceramics by photopolymerization for consolidation of bone fragments following fracture," Biomedical Materials, 2019.
4. G. G. de Lima, **B. S. Chee** and et al., "The production of a novel poly (vinyl alcohol) hydrogel cryogenic spheres for immediate release using a droplet system," Biomedical Physics & Engineering Express, vol. 5, pp. 045017, 2019.
5. B. L. Pereira, G. Beilner, C. M. Lepienski, E. S. Szameitat, **B. S. Chee** and et. al. "Oxide coating containing apatite formed on Ti-25Nb-25Ta alloy treated by Two-Step Plasma Electrolytic Oxidation" Surface and Coatings Technology, pp.125224, 2019.
6. G. G. de Lima, R. R. C. Barbosa, M. P. de Andrade Santos, **B. S. Chee**, W. L. E. Magalhães, D. M. Devine and M. J. D. Nugent, "Effect of unidirectional freezing using a thermal camera on polyvinyl (alcohol) for aligned porous cryogels" Quantitative InfraRed Thermography Journal, 2020.
7. M. Aliabadi, **B. S. Chee**, M. Matos, Y. J. Cortese, M. J. D. Nugent, T. A. M. de Lima, W. L. E. Magalhães and G. G. de Lima, "Yerba Mate Extract in Microfibrillated Cellulose and Corn Starch Films as a Potential Wound Healing Bandage", Polymers, vol. 12, 2020.
8. B. L. Pereira, C. M. Lepienskia, V. Seba, G. Hobold, P. Soares, **B. S. Chee**, P. A. B. Kuroda, E. S. Szameitat, L. L. dos Santos, C. R. Grandini, M. Nugent, "Titanium-Niobium (Ti-xNb) Alloys with High Nb Amounts for Applications in Biomaterials", Materials Research. 23(6), e20200405, 2020.
9. M. Bandeira, **B. S. Chee**, R. Frassini, M. Nugent, M. Giovanela, M. Roesch-Ely, J.d.S. Crespo, D.M. Devine, "Antimicrobial PAA/PAH Electrospun Fibre Containing Green Synthesized Zinc Oxide Nanoparticles for Wound Healing", Materials, vol.14, pp. 2889, 2021.
10. M. Aliabadi, **B. S. Chee**, M. Matos, Y. J. Cortese, M. J. D. Nugent, T. A. M. Lima, W. L. E. Magalhães, G. G. Lima & M. D. Firouzabadi, "Microfibrillated cellulose films containing chitosan and tannic acid for wound healing applications Micro fibrillated cellulose films containing chitosan and tannic acid for wound healing applications", Journal of Materials Science: Materials in Medicine, Vol. 32, 2021.
11. G. G. de Lima, E. L. de S. Júnior, B. B. Aggio, E. M. de M. Filho, **B. S. Chee**, F. A. de S. Segundo, M. B. Fournet, D. M. Devine, W. L. E. Magalhães, M. J. C. de Sá, "Nanocellulose for peripheral nerve regeneration in rabbits using citric acid as crosslinker with chitosan and freeze/thawed PVA", Biomedical Materials, 2021.
12. V. Seba, G. G. de Lima, B. L. Pereira, G. Silva, L. S. Reinhardt, P. R. Arantes, **B. S. Chee**, M. B. dos Santos, S. C. França, L. O. Regasini, A. L. Fachin, Z. Cao, M. J. D. Nugent, M. Marins, "Development, characterization and cell viability inhibition of PVA spheres loaded with Doxorubicin and 4'-amino-1-Naphthyl-Chalcone (D14) for osteosarcoma", Polymers, 2021.

13. **B. S. Chee**, G. G. de Lima, T. A. M. de Lima, V. Seba, C. Lemarquis, B. L. Pereira, M. Bandeira, Z. Cao, M. Nugent, "Effect of thermal annealing on a bilayer polyvinyl alcohol - polyacrylic acid electrospun hydrogel nanofibers loaded with doxorubicin and clarithromycin for a synergism effect against osteosarcoma cells", Materials Today Chemistry, 2021.

Conference Proceeding

1. G. G. de Lima, V. F. Moritz, **B. S. Chee**, B. V. Staal, D. M. Devine, M. J. D. Nugent, "Synthesis and Characterization of Poly (vinyl alcohol) Hydrogel Cryogenic Spheres for Biomedical Applications" Orthopaedic Proceedings Vol. 100-B, No. SUPP_14, 2018.

Book Chapter

1. **B. S. Chee**, G. G. De Lima, D. Devine, and M. J. D. Nugent, "Electrospun hydrogels composites for bone tissue engineering", Applications of Nanocomposite Materials in Orthopedics, Elsevier Inc., 2018, pp. 39–70.
2. **B. S. Chee** and M. J. D. Nugent," Electrospun natural polysaccharide for biomedical application", Polysaccharides in Drug Delivery and Biomedical Applications, Elsevier Inc., 2019, pp 589-612.
3. V. Seba, G. Silva, **B. S. Chee**, J. G. Henn, G. G. de Lima, Z. Cao, M. M. and M. J. D. Nugent, "Stimuli-responsive biopolymeric systems for drug delivery to cancer cells" Tailor-Made and Functionalized Biopolymer Systems for Drug Delivery and Biomedical Applications, Woodhead Publishing, 2021.